The effect of reactive oxygen species on monocytes and macrophages

Dissertation

zur Erlangung des Grades „Doktor der Naturwissenschaften“

am Fachbereich Biologie
der Johannes Gutenberg-Universität Mainz

vorgelegt von

Viviane Ponath

geboren am 06.09.1987 in Bonn

Mainz 2017

Dekan: [redacted]

1. Berichterstatter: [redacted]

2. Berichterstatter: [redacted]

Table of Contents

Abstract

The myeloid immune system is the first line of defence against infections. The acute inflammatory response encompasses the recruitment of immune cells to the site of inflammation, the production of cytokines, phagocytosis of foreign material and the release of reactive oxygen species (ROS) to kill pathogens. The latter is accomplished by the NADPH oxidase which generates superoxide anions from molecular oxygen and releases them against pathogens.

Previously, it was shown that monocytes, but not macrophages and dendritic cells (DCs), lack the DNA repair proteins XRCC1, ligase IIIα and PARP-1 which are required for the efficient repair of damaged DNA bases and single-strand breaks (SSBs) during base excision repair (BER). In addition, the double-strand break repair protein DNA-PKcs is also not expressed (Bauer et al. 2011; Briegert and Kaina 2007). The attenuated BER and non-homologous end-joining pathways sensitise monocytes to DNA oxidising and alkylating agents while DNA repair competent macrophages and DCs are resistant.

As ROS are potent genotoxins, it was addressed whether the oxidative burst of myeloid cells led to DNA damage in the ROS-producing cells (auto-intoxication). It was shown that phorbol 12-myristate 13-acetate (PMA) can stimulate the NADPH oxidase via upstream activation of the protein kinase C. PMA-mediated stimulation of myeloid immune cells, *i.e.* granulocytes, macrophages and monocytes, led to an increase in intracellular ROS levels. The extracellular ROS burst was detected using a chemiluminescence-based assay. In contrast to T lymphocytes, myeloid immune cells produced massive ROS in a time-dependent manner. It was shown that monocytes, but not macrophages are killed by their own ROS; following PMA treatment and triggering the oxidative burst, cells exhibited oxidative DNA damage and SSB formation followed by cell death. Surviving monocytes were unable to differentiate into macrophages. Furthermore, it was shown that ROS from adjacent cells were also strong enough to damage monocytes (so called 'killing *in trans*'). Co-culture experiments with stimulated macrophages or granulocytes and unstimulated monocytes led to DNA damage in monocytes, subsequent activation of the DNA damage response and ultimately monocytic cell death. DNA repair competent macrophages were resistant and did not die. These findings strengthen the hypothesis that the BER-defect of monocytes functions as a regulatory feedback loop in the acute immune response by removing monocytes from the site of inflammation and thus dampening the immune reaction.

The analysis of the regulation of the BER protein XRCC1 in monocytes and macrophages was another aspect of this work. It was shown that the demethylation inhibitor 2-hydroxy-glutarate led to an attenuated XRCC1 signal during cytokine-induced differentiation into macrophages. However, the XRCC1 promoter analysis showed no differential methylation pattern between the two cell types. Using a reverse chromatin immunoprecipitation assay coupled with mass spectrometry, potential transcription factors responsible for XRCC1 expression were screened for. Promising candidates were CTCF and AP-1 factors, which were also found by *in silico* analysis of the promoters of PARP-1, DNA-PK and ligase IIIα.

The findings of DNA repair defects in monocytes were extended to neutrophilic granulocytes. It was shown that neutrophils also display severe defects in DNA repair affecting BER and double-strand break repair. Similar to monocytes they do not express XRCC1, PARP-1 and ligase IIIα. Furthermore, DNA damage signalling factors like ATM, p53 and γH2AX were also not detectable. The data indicate a lineage-specific phenomenon.

Zusammenfassung

Das myeloische Immunsystem ist die erste Abwehr bei Infektionen. Die akute Entzündungsreaktion umfasst die Rekrutierung von Immunzellen zum Entzündungsherd, die Zytokin-Produktion, die Phagozytose vom Fremdmaterial und die Freisetzung von reaktiven Sauerstoffspezies (ROS), um Pathogene abzutöten. Letzteres wird durch die NADPH-Oxidase vermittelt, die Superoxid-Anionen aus molekularem Sauerstoff generiert und gegen Pathogene freisetzt.

Frühere Studien haben gezeigt, dass den Monozyten – nicht aber den Makrophagen oder dendritische Zellen (DC) – die DNA-Reparaturproteine XRCC1, Ligase IIIα und PARP-1 fehlen, welche für die effiziente Basen-Exzisionsreparatur (BER) bei geschädigten DNA-Basen und Einzelstrangbrüchen (ESB) notwendig sind. Des Weiteren wird das Doppelstrangbruch-Reparaturprotein DNA-PKcs nicht exprimiert. (Bauer et al. 2011; Briegert and Kaina 2007). Die beeinträchtigte BER und nicht-homologe Endverknüpfung sensitivieren Monozyten gegenüber oxidierenden und alkylierenden Substanzen, während DNA-reparaturkompetente Makrophagen und DC resistent sind.

Da ROS stark genotoxisch sind, wurde untersucht, ob der *‚oxidative burst‘* myeloischer Zellen in den Produzenten zu DNA-Schäden führt (Autointoxikation). Es wurde gezeigt, das Phorbol-12-Myristat 13-Acetat (PMA) die NADPH-Oxidase mittels Aktivierung der Proteinkinase C stimuliert. PMA-vermittelte Stimulation der myeloischen Immunzellen, *i.e.* Granulozyten, Monozyten und Makrophagen, führte zu einem Anstieg an intrazellulären ROS. Der extrazelluläre *‚burst‘* wurde über einen Chemilumineszenz-Ansatz gemessen. Im Gegensatz zu T Lymphozyten, produzieren myeloische Immunzellen viel ROS in einer Zeit-Wirkungsbeziehung. Es wurde gezeigt, dass Monozyten, nicht aber Makrophagen, durch ihre eigenen ROS getötet werden; der durch PMA-Behandlung ausgelöste *‚oxidative burst‘* führte in Monozyten zu oxidativen DNA-Schäden und ESB, gefolgt von Zelltod. Die überlebenden Monozyten konnten nicht mehr zu Makrophagen ausdifferenzieren. Zusätzlich konnte gezeigt werden, dass ROS von benachbarten Zellen stark genug waren, um Monozyten zu schädigen (sog. *killing in trans*). Co-Kulturexperimente mit aktivierten Makrophagen oder Granulozyten mit nicht-aktivierten Monozyten führten zu DNA-Schäden in Monozyten, der Aktivierung ihrer DNA-Schadensantwort und letztlich zum monozytären Zelltod. DNA-reparaturkompetente Makrophagen waren resistent und starben nicht. Die Ergebnisse untermauern die Hypothese, dass der monozytäre BER-Defekt eine negative Rückkopplungsschleife in der akuten Immunantwort ist, indem er die Monozyten vom Entzündungsherd entfernt und damit die Immunreaktion abschwächt.

Ein weiterer Teil dieser Arbeit betraf die Analyse der Regulation des BER-Proteins XRCC1 in Monozyten und Makrophagen. Es wurde gezeigt, dass der Demethylierungsinhibitor 2-Hydroxyglutarat zu einem abgeschwächten XRCC1-Signal während der Zytokin-vermittelten Ausdifferenzierung zu Makrophagen führte. Die XRCC1-Promoteranalyse zeigte jedoch keine Unterschiede im Methylierungsgrad der beiden Zelltypen. Mittels reverser Chromatin-Immunpräzipitation und anschließender Massenspektrometrie wurden potentielle Transkriptionsfaktoren verantwortlich für die XRCC1-Expression gesucht. Vielversprechende Kandidaten waren CTCF und AP-1-Faktoren, die auch in der *in silico*-Analyse der Promotoren von PARP-1, DNA-PK und Ligase IIIα gefunden wurden.

Die Erkenntnisse über DNA-Reparaturdefekte in Monozyten wurden auf neutrophile Granulozyten ausgeweitet. Neutrophile wiesen massive Defekte in ihrer DNA-Reparatur, besonders BER und Doppelstrangbruchreparatur, auf. Ähnlich den Monozyten wurden XRCC1, PARP-1 und Ligase IIIα nicht exprimiert. Des Weiteren konnten DNA-Schadensantwortproteine wie ATM, p53 oder γH2AX nicht detektiert werden. Die Daten lassen ein Abstammungslinie-bedingtes Phänomen vermuten.

1 Introduction

1.1 The immune system

The human immune system consists of cellular and soluble components that recognise and eliminate foreign particles and abnormal cells. Most pathogens enter the organism via the mucosa (*e.g.* in the gastrointestinal tract, the lungs or the urogenital tract) as the skin is a very effective barrier and cannot be penetrated easily. Non-cellular, or humoral, immunity is mediated by soluble factors like antibodies, complement proteins, acute phase proteins (*e.g.* C-reactive protein) and many other peptides (*e.g.* defensins, opsonins, lysozyme, etc.) (Rink *et al.* 2015). The cellular immune system is organised in a hierarchy and originates from a haematopoietic stem cell (HSC). Asymmetric cell division of a HSC leads to the two main branches of the cellular immune system: the myeloid and lymphoid immune cells (Fig. 1). The innate or myeloid immune system elicits the acute inflammatory response involving systemic vasodilation, vascular leakage, and leukocyte emigration at the site of injury in order to kill pathogens (Mittal *et al.* 2014). The adaptive, or lymphoid, immune system develops an immunological memory that allows for a rapid and effective response to previously encountered pathogens – the basis for vaccination (Flajnik and Kasahara 2010).

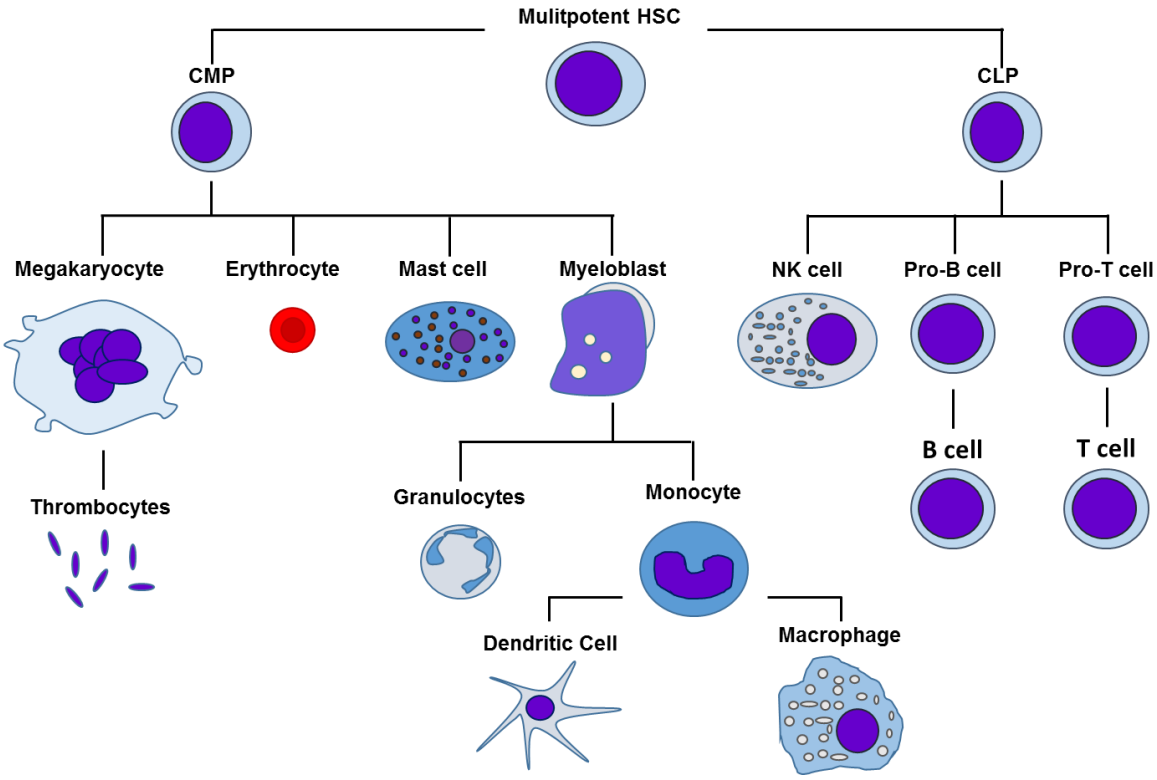

Fig. 1: Hierarchy of the haematopoietic system
In the bone marrow, multipotent haematopoietic stem cells (HSCs) divide asymmetrically and give rise to myeloid and lymphoid progenitor cells – the two branches of the cellular immune system. The common myeloid progenitor (CMP) divides and generates specialised cells serving functions in oxygen transport (erythrocytes), blood clotting (thrombocytes), allergic reaction (mast cells) and the innate immune response via myeloblast-derived immune cells (i.e. granulocytes, monocytes and monocyte-derived macrophages and dendritic cells). The common lymphoid progenitor (CLP) divides and forms adaptive immune cells, i.e. mainly B cells and T cells. NK cells, although derived from the CLP, are part of the innate immune system as they recognise abnormal cells and kill them in the absence of antigen-specific receptors.

Haematopoiesis, the generation of blood cells, is a continuous process throughout life as many blood cells are short-lived and need to be replaced. The multipotent HSCs are located in the bone marrow where they reside in “niches” that allow them to maintain their capacity for “self-renewal” while also allowing for dividing asymmetrically (Fig. 1). Daughter cells are exposed to colony-stimulating factors (CSFs) and other cytokines, *e.g.* interleukins (IL) and interferons (IFN) that commit them to a certain lineage, *i.e.* the myeloid lineage with megakaryocytic, granulocytic and monocytic progenitors or the lymphoid lineage with Natural Killer (NK), B and T cell progenitors (Robb 2007). Furthermore, the myeloid lineage is also responsible for blood clotting and oxygen transport as they generate the progenitor cells for thrombocytes and erythrocytes respectively.

Terminally differentiated immune cells reside in the blood, tissue and lymph system. Many of them can be distinguished by their morphology and staining properties, *e.g.* Giemsa staining of blood films. This is not the case for progenitor cells and different subsets of T cells, *i.e.* T helper cells, cytotoxic T cells and regulatory T cells. Instead, they are distinguished by their characteristic expression of various “cluster of differentiation” (CD) markers. CD markers are glycoproteins and glycolipids that often act as ligands or receptors to cells (Zola *et al.* 2007). They are distinctive for different leukocyte subpopulations and are therefore used for immunophenotyping. For example, cytotoxic T cells express CD8, a transmembrane glycoprotein that is a co-receptor for the T cell receptor and recognises the major histocompatibility complex class I (MHC I) (Daniels *et al.* 2001). T helper cells on the other hand express CD4, a transmembrane glycoprotein that interacts with MHC class II (MHC II) (Vignali *et al.* 1993). The differential CD marker expression facilitates the analysis of blood samples and is extensively used in the lab.

In the following sections, the innate and adaptive immune system and their respective cells will be described in more detail.

1.1.1 The innate immune system

The innate immune system evolved around 500-600 million years ago along with multi-cellular organisms and it pre-dates the adaptive immune system (Rink *et al.* 2015). It consists of phagocytes that ingest (“phagocytose”) foreign particles and then degrades them. The main players are granulocytes, monocytes, macrophages and dendritic cells. The innate immune system does not develop a memory, but it is able to recognise pathogen-associated molecular patterns (PAMPs) via pattern recognition receptors (PRRs). PAMPs are highly conserved domains expressed in viruses, bacteria, protozoa, and fungi but not in vertebrates. Lipopolysaccharides (LPS), lipoteichoic acid, flagellin, and peptidoglycans are prototypical molecules for PRRs. Danger-associated molecular patterns (DAMPs), also known as alarmins, like dsDNA, dsRNA and uric acid crystals are also targets for PRRs as they do not occur freely in the body and are a sign of cellular stress and tissue injury (Jounai *et al.* 2012; Kawai and Akira 2007). Examples of PRRs are Toll-like receptors (TLRs), c-type lectin receptors and cytoplasmic NOD-like receptors (NLRs). PRR activation leads to a signal transduction that activates nuclear factor κB (NF-κB) which leads to the release of pro-inflammatory cytokines. Those recruit more immune cells to the site of infection and initiate the acute immune response. The immune defence includes the release of reactive oxygen species (ROS) that damage and kill pathogens and the phagocytosis of pathogens with their subsequent breakdown in the presence of oxidants and digesting enzymes (*i.e.* proteases, lipases, nucleases, etc.). Microbial molecules are

processed for antigen-presentation for the adaptive immune cells in order to develop a memory. Prototypical cells for the acute inflammatory response are monocytes, macrophages, dendritic cells and neutrophilic granulocytes.

Monocytes:

Monocytes, together with macrophages and dendritic cells (DCs), are mononuclear phagocytes that play a crucial role in tissue homeostasis and innate immunity. They originate in the bone marrow from a CMP shared with neutrophils (Fig. 1). They enter the bloodstream where they account for 3 – 8 % of all circulating leukocytes in humans and move to the periphery where they can migrate into the tissue. Depending on the local growth factors, cytokines and microbial molecules, they differentiate into tissue-resident macrophages or DCs. Pro-inflammatory cytokines can recruit monocytes to sites of infection where they assist in host defence and tissue-remodelling (Godon *et al.* 2008). However, an accumulation of monocytes can also aggravate and promote the progression of inflammatory diseases like atherosclerosis, arthritis and diabetes mellitus (see section 1.2.3) (Parihar *et al.* 2010).

Upon inflammation, monocytes differentiate into “inflammatory” or recruited macrophages that are involved in the host defence as they clear apoptotic cells and debris at the damage site (Jakubzick *et al.* 2017). Upon infection, especially pulmonary or dermal infections, monocytes carry microbial antigens to local lymph nodes where they either differentiate into DCs or transfer the loaded antigen to local DCs that present it to passing T and B cells (Shi and Pamer 2011). Monocytes express PRRs like TLR4 in combination with CD14 (for LPS), TLR2 (for lipoteichoic acid) and c-type lectin receptors (for microbial carbohydrates) (Hoving *et al.* 2014) that recognise PAMPs and DAMPs and thus induce pro-inflammatory cytokines like IL-1, IL-6, tumour necrosis factor α (TNF-α) and tissue-remodelling factors like transforming growth factor β (TGF-β). Under non-inflammatory conditions, monocytes are short-lived immune cells that undergo apoptosis spontaneously. In response to differentiation-initiating factors like CSFs, apoptosis is suppressed and the cells undergo differentiation into long-living macrophages and DCs (Parihar *et al.* 2010).

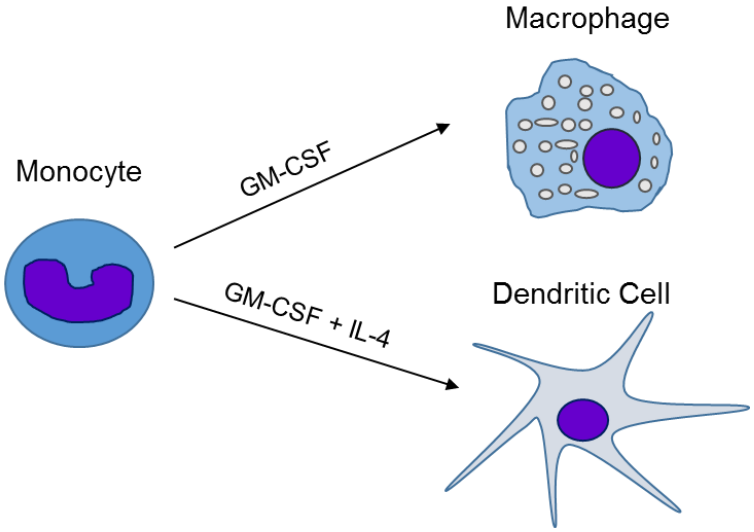

Fig. 2: Cytokine-induced differentiation of monocyte into macrophages and DCs
Monocytes isolated from buffy coats or fresh blood can be differentiated into macrophages by adding GM-CSF and subsequent incubation of the cells for six days. DCs are generated by adding GM-CSF and IL-4 at days 0, 3 and 6 over the course of eight days. Macrophages adhere to the plate and show an elongated, spindle-like shape. DCs are suspension cells.

In vitro, monocytes can be differentiated into macrophages over the course of six days by adding macrophage CSF (M-CSF) or granulocyte/macrophage CSF (GM-CSF) (Fig. 2). *In vivo*, the rate of differentiation is postulated to be quicker (Jakubzick *et al.* 2017). Monocyte-derived DCs are generated in the presence of GM-CSF and IL-4 (Gordon and Taylor 2005). They are still immature DCs (iDCs) that require further stimuli to become mature DCs, *e.g.* LPS, TNF-α, IL-1β, IL-6, IFNα and IFNγ (Castiello *et al.* 2011).

Macrophages:

Macrophages are ubiquitously found in the body. As Kupffer cells in the liver, alveolar macrophages in the lung, microglia in the brain or osteoclasts in the bone, macrophages are omnipresent and support tissue homeostasis. They are heterogeneous in appearance and function. Therefore, macrophages are often categorised as M1, classically-activated pro-inflammatory macrophages and M2, alternatively-activated, anti-inflammatory macrophages. The M1 type, activated by IFNγ ± LPS, is known to release oxidants and pro-inflammatory cytokines like IL-1, IL-6 and TNF-α whereas the M2 type, activated by IL-4, is mainly involved in tissue-repair and releases anti-inflammatory factors like IL-4, IL-10, IL-13 and TGF-β, Vascular Endothelial Growth Factor (VEGF) and Epidermal Growth Factor (EGF). Depending on local growth factors and cytokines the differences between these two types of macrophages is often transient.

Tissue-resident macrophages play an important role in tissue homeostasis, as they phagocytose cell debris and apoptotic cells in their surroundings. They release cytokines like IL-1, IL-6 and TNF-α which promote the infiltration of neutrophils in an acute immune response upon infection. They also release IL-12 and IL-18 to activate NK cells which in turn produce anti-viral IFNγ (Chung *et al.* 2007). In addition, they produce anti-inflammatory IL-10 which downregulates the pro-inflammatory cytokine action and thus dampens the immune response (Groen *et al.* 2015). Afterwards, they remove spent neutrophils and apoptotic cells, thereby effectively resolving the inflammation site and enabling wound healing. They promote angiogenesis via the release of VEGF, fibroblast proliferation via platelet-derived growth factor (PDGF) and extracellular matrix synthesis by releasing growth factors that promote protein biosynthesis and cell proliferation (Koh and DiPietro 2011).

Macrophages are long-living cells with lifespans ranging from months to years and it was shown that they can replenish themselves by local replication rather than differentiation of recruited monocytes (Parihar *et al.* 2010; Gordon and Plűddemann 2013). Similar to DCs they can phagocytose foreign particles and present their antigens to CD4+ T helper cells and CD8+ cytotoxic T cells via their MHC complexes, thus recruiting the adaptive immune system in the host defence (Mantegazza *et al.* 2013).

During inflammation, monocytes can differentiate into recruited, inflammatory macrophages (M1 type) which accumulate at the site of infection. Here, they phagocytose microbes as well as spent neutrophils, they release pro-inflammatory cytokines, *e.g.* IL-1, IL-6 and TNF-α, to recruit more immune cells, and they produce oxidants to damage and kill pathogens. Similar to neutrophils and monocytes, macrophages express NADPH oxidase which produces ROS as a defence mechanism against microbes. They generate superoxide anions ($O_2^{\cdot-}$) which they release in an explosive “respiratory burst” into the direction of pathogens (see section 1.2.2). Furthermore, other reactive oxygen and nitrogen species like H_2O_2, $OH^{\cdot}$, NO and peroxynitrite are released that damage microbial biomolecules like proteins, lipids and DNA. Under conditions of chronic inflammation, macrophages and

monocytes are contributing factors to the progression of inflammatory diseases (see section 1.2.3). Continuous pro-inflammatory signalling leads to elevated oxidant levels and a diminished production of anti-inflammatory cytokines and tissue-remodelling factors which then promote cell and tissue dysfunction.

Dendritic cells

Dendritic cells (DCs) bridge the innate and the adaptive immune system. They are professional antigen-presenting cells (APC) which take up foreign material, process its fragments and presents them to CD4+ T helper cells and CD8+ cytotoxic T cells via their MHC molecules (see section 1.1.4). They are crucial in distinguishing "self" from "non-self" for the adaptive immune system. They have to detect pathogens as well as aberrant cells, *i.e.* cancer cells, while simultaneously being tolerant towards healthy cells. DCs take up foreign material by different mechanisms, including receptor-mediated endocytosis, pinocytosis and phagocytosis. During the process of phagocytosis, large particles are engulfed in phagosomes which subsequently fuse with lysosomes to form phagolysosomes (Mantegazza *et al.* 2013). Macromolecules of pathogenic origin are processed by proteases before they are loaded onto MHC I and II molecules. In lymphoid tissues, DCs present the MHC-peptide complex on their plasma membrane surface to passing T cells (Broeke *et al.* 2013), thereby activating the adaptive immune system and promoting memory-mediated immunity. They also mediate immunological tolerance to self-antigens, thereby reducing the risk of autoimmunity (Banchereau and Steinman 1998).

Furthermore, DCs play an important role in cancer immunotherapy. This anti-cancer therapy attempts to vaccinate DCs with tumour-specific antigens in order to stimulate the patient's T cell killing response towards cancer. *Ex vivo,* monocytes are differentiated into DCs which are then exposed to tumour-specific material derived from the cancer patient. The DCs phagocytose the material and processes it for antigen-presentation. The now mature DCs are then injected into the patient where they display the tumour-antigens to T cells resulting in tumour-specific cytotoxic T lymphocytes (Palucka and Banchereau 2012).

In vitro, immature DCs (iDCs) can be generated from monocytes by adding GM-CSF and IL-4 followed by incubating the cells for eight days while refreshing the cytokine cocktail after three and six days. Maturation of DCs can be achieved when the cells are incubated with LPS, TNF-α, IL-1β or other cytokines (Castiello *et al.* 2011).

Granulocytes

The group of granulocytes comprises neutrophilic, basophilic and eosinophilic granulocytes. Their names are based on their staining properties in immunohistochemistry. 1 – 5 % of peripheral blood cells are eosinophils and together with basophils (~1 %) they are involved in the defence against parasites, *e.g.* helminths, that are too large to be ingested by macrophages or neutrophils (Janeway 2001). Due to their histamine production basophils are also involved in allergic reactions like hayfever, asthma and anaphylactic shock. Neutrophilic granulocytes (neutrophils) are by far the most prevalent cell type (~95 % of granulocytes). They account for 55 – 75 % of all leukocytes and they are constantly replenished in very high numbers even under steady-state conditions (1 - 2 x 10^{11} cells/day) (Rink *et al.* 2015). Exposed to life-threatening infections, *e.g.* sepsis, 'emergency'

granulopoiesis occurs leading to a marked increase in the production of neutrophils from myeloid progenitor cells (Manz and Boettcher 2014).

Neutrophils are primed for apoptotic cell death and have a very short lifespan ranging from 6 h to 8 h (Simon and Kim 2010; Summers *et al.* 2010; Pillay *et al.* 2010). They undergo phagocytosis-induced cell death (PICD) by macrophages mainly in the liver, the spleen and the bone marrow (Kolaczkowska and Kubes 2013). The induction of cell death can be delayed in the presence of certain cytokines (*e.g.* GM-CSF and Granulocyte-CSF, G-CSF) or pathogenic molecules like LPS. They activate the phosphatidylinositol-3-kinase (PI3K) / Akt pathway which phosphorylates caspase-9 and inhibits Bcl-2-associated X protein (Bax) association at the mitochondria for the induction of the intrinsic apoptosis pathway (see section 1.3.3) (McCracken and Allen 2014).

Neutrophils are essential for the acute inflammatory reaction. Resident cells at the site of infection or inflammation release chemokines like IL-8 (CXCL8), macrophage inflammatory protein 2 (MIP-2, CXCL2) and KC (CXCL1) to recruit neutrophils. They arrive quickly at the damage site and immediately initiate their anti-microbial functions. In a process called degranulation, they release high amounts of ROS, oxidants and microbiocidal molecules into the extracellular space (ECS) to damage pathogens. Furthermore, they phagocytose foreign material. Another important defence pathway is a process called NETosis (neutrophil extracellular trap, NET). Neutrophils eject their genomic DNA and lytic enzymes into the ECS, thereby trapping bacteria. Stuck to the DNA, enzymes like elastase, permeability increasing protein, cathepsin G, proteinase 3 and myeloperoxidase are in close vicinity to pathogens and effectively kill them. The spent neutrophil is removed from the site of inflammation by macrophages. Interestingly, NETosis cannot occur in patients with chronic granulomatous disease (CGD) as they are impaired in ROS production by NADPH oxidase, see section 1.2.2 (Papayannopoulos and Zychlinsky 2009).

Neutrophils serve as the primary defence against infections. Consequently, patients suffering from neutropenia are susceptible to develop life-threatening infections (neutropenic sepsis).

1.1.2 GM-CSF- and M-CSF-matured macrophages

As mentioned above, macrophages are very heterogeneous in their function and they are often categorised as either pro- or anti-inflammatory. Classically activated M1 type macrophages display a pro-inflammatory cytokine profile. Alternatively activated M2 type macrophages have an anti-inflammatory cytokine profile. The maturation of monocytes into macrophages can be induced by different cytokines. GM-CSF and M-CSF are the most prevalent cytokines used to differentiate monocytes *in vitro*. Both cytokines have a wide range of functions including survival, activation, differentiation, and mobilisation. They induce some common recognition patterns but also lead to differentially expressed genes in macrophages.

M-CSF is ubiquitously and constitutively expressed by a variety of cells like endothelial cells, fibroblasts, osteoblasts, smooth muscle cells, and macrophages (Ushach and Zlotnik 2016). Under resting conditions, it is detectable in the blood at ~10 ng/ml. It is commonly used in *in vitro* studies to induce differentiation of bone marrow cells into macrophages. The M-CSF-induced signalling is triggered when it binds to its type III tyrosine kinase transmembrane receptor colony stimulating factor 1 (CSF1R). Upon M-CSF binding the receptor dimerises, autophosphorylates and activates PI3K / AKT, the extracellular signal-

regulated kinases (ERK), and the phospholipase C pathways which subsequently lead to the nuclear localisation of transcription factor Sp1. Mutations in the CSF1R are associated with acute myeloid leukaemia and myelodysplastic syndromes (Ushach and Zlotnik 2016). M-CSF-generated macrophages are often used as a model for tissue-macrophages that feature a more anti-inflammatory cytokine profile (*e.g.* expression of IL-10 and chemokine (C-C motif) ligand 2, CCL2) and show M2 type characteristics (Lacey *et al.* 2012). In the presence of IFNγ or LPS, M-CSF-generated macrophages can be polarised towards the M1 type and in the presence of IL-4 to the M2 type (Jaguin *et al.* 2013).

GM-CSF, also known as colony stimulating factor 2 (CSF2), is a glycoprotein that binds to the GM-CSF receptor (CSF2R). Unlike M-CSF, which is continuously produced, GM-CSF is released by cells during an inflammatory response or under pathologic conditions. It is required for the maturation of alveolar macrophages (Ushach and Zlotnik 2016). Studies in GM-CSF-deficient mice showed impaired reproductive capacity, lung pathologies (so-called alveolar proteinosis due to functionally-deficient alveolar macrophages) and a reduced long-term survival. They did not display defects in their steady-state haematopoiesis and peripheral blood counts (Manz and Boettcher 2014).

The CSF2R is a member of the class I cytokine receptor family which dimerises when the ligand binds. It does not have intrinsic tyrosine kinase activity and thus associates with the tyrosine kinase Janus kinase 2 (Jak2) which leads to transphosphorylation. This initiates the intracellular signalling cascade via the Jak2 / signal transducer and activator of transcription 5 (STAT5), PI3K and the ERK / mitogen-activated protein kinase (MAPK) pathways (Hercus *et al.* 2009). GM-CSF-generated macrophages have a pro-inflammatory cytokine and chemokine profile (*e.g.* TNF-α, IL-6, IL-1β, CCL22, CCL1 and CCL5). GM-CSF-generated macrophages show strong phagocytic activity and are excellent APC for T and B cells. In combination with IL-4, GM-CSF-exposure of monocytes leads to the generation of monocyte-derived DCs. Lacey *et al.* compared the gene expression profiles of GM-CSF- and M-CSF-generated macrophages. They differentially express certain cytokines, especially if they were primed with LPS. Then, GM-CSF-macrophages showed a more dramatic production in a time-dependent manner of TNF-α, IL-1β, IL-8 and IL-12p40 (Jaguin *et al.* 2013). However, compared to monocytes, both sets of macrophages produce higher amounts of cytokines and chemokines.

1.1.3 The acute inflammatory response

Tissue necrosis by trauma, foreign material like dirt or splinters, or infections are stimuli for acute inflammation. The encounter with a bacterial molecule like LPS can initiate an acute inflammatory response. LPS, an important component of the outer membrane of Gram-negative bacteria, is bound by soluble LPS-binding protein (LBP) and shuttled to the TLR4 which is in complex with CD14, a glycosylphosphatidylinositol-anchored protein highly expressed in monocytes and macrophages (Lu *et al.* 2008). This complex activates a signal transduction pathway that leads to the activation of NFκB-induced pro-inflammatory cytokines. Thus, the acute immune response is initiated as pro-inflammatory mediators like IL-1β, TNF-α, IL-6 and monocyte chemoattractant protein 1 (MCP-1) are released and attract neutrophils and monocytes to the site of infection. The cells are recruited to the endothelium and in a multi-step process of tethering, rolling, adhesion, crawling, and transmigration immune cells (mainly neutrophils) enter the infected tissue. There, they initiate their phagocytic function and kill microbes. They release ROS (see section 1.2.2)

and proteases that damage microbes, they opsonise foreign particles to facilitate phagocytosis for macrophages and they secrete additional vasoactive and pro-inflammatory mediators like histamine, prostaglandins, platelet-activating factors, bradykinin and thrombin that increase vascular permeability which in turn leads to fluid accumulation (oedema) and leukocyte extravasation (Kumar *et al.* 2013). After successful elimination of the pathogen, macrophages phagocytose spent neutrophils and cell debris and help to repair the damaged tissue by releasing tissue-remodelling factors like transforming TGF-β, VEGF and EGF. The whole process occurs over a period of minutes, hours or days and is normally controlled and self-limiting.

If the inflammatory site is not resolved properly, chronic inflammation can occur. Many diseases are associated with and progress under chronic inflammatory conditions, *e.g.* arthritis, autoimmune diseases, diabetes, cancer, and neurodegenerative disorders like Alzheimer's or Parkinson's. Characteristic features of chronic inflammation are elevated oxidant levels, pro-inflammatory mediator signalling and an infiltration of monocytes/macrophages into the tissue, resulting in tissue remodelling leading to a loss of function due to fibrosis (Kumar *et al.* 2013) (see section 1.2.3).

1.1.4 The adaptive immune system

The adaptive or acquired immune system is composed of highly specialised T and B lymphocytes that are able to develop an immunological memory after encountering a pathogen. Unlike myeloid immune cells that recognise PAMPs and DAMPs, lymphoid cells recognise specific antigens and efficiently eliminate pathogens, infected and aberrant cells. The antigens are presented on the surface of professional APC, namely DCs who bridge the innate and the adaptive immune system. APC take up foreign material via macropinocytosis, receptor-mediated phagocytosis, or as a host during viral infection. The antigens can be presented by MHC I or MHC II molecules. MHC I comprises the endogenous pathway when DCs are infected by viruses. Viral proteins are processed by the proteasome and they are presented on the cell surface by MHC I to activate CD8+ cytotoxic T cells (CTL) which then mediate the induction of apoptosis. The exogenous or endosomal pathway processes antigens taken up into the endosome where they are presented to CD4+ T helper cells (Th) via MHC II molecules (Rink *et al.* 2015). T cells recognise the antigens via their T cell receptor (TCR), start to proliferate (so-called clonal expansion) and migrate into the surrounding tissue. Depending on the cytokines present in the local lymphatic tissue Th cells can differentiate into different subpopulations, *i.e.* Th1, Th2, Th17 and induced regulatory T cells (iTreg). Th1 cells induce a cell-mediated immune response against intracellular pathogens. Th2 cells activate the humoral and Th17 cells the cellular immune response against extracellular pathogens. iTreg suppress the immune response by secreting IL-10 and TGF-β. They are critical for the tolerance of self-antigens and prevent autoimmune diseases. CTL interact with MHC I molecules and recognise aberrant cells, *e.g.* virus-infected cells or tumour cells. They direct the killing response by secreting perforins and granzymes as well as stimulating the Fas receptor (FasR) on the target cell with Fas ligand (FasL), thus activating the extracellular apoptosis pathway (see section 1.3.3) (Rink *et al.* 2015). B lymphocytes are responsible for the humoral immune response by secreting large amounts of antibodies that immobilise pathogens, opsonise them and thus mark them for phagocytosis.

In buffy coat probes, anti-coagulated blood samples that are enriched with leukocytes, peripheral blood lymphocytes (PBL) can be isolated from the peripheral blood mononuclear cell (PBMC) fraction. Due to their differential CD marker expression Th (CD3+CD4+) and CTL (CD3+CD8+) can be distinguished by flow cytometry.

1.2 Reactive oxygen species and oxidative stress

1.2.1 Formation of reactive oxygen and nitrogen species in the cell

Reactive oxygen and nitrogen species (ROS and RNS) are chemically reactive chemical species containing either oxygen or nitrogen and unpaired electrons. They are generated by metabolic processes or by exogenous sources like ionising radiation (so-called radiolysis), UV light, drugs and environmental toxins (Brieger *et al.* 2012). In low amounts, ROS function as signalling molecules in the cell whereas excessive amounts of ROS are deleterious for cell and tissue homeostasis as they damage cellular biomolecules, *i.e.* DNA, proteins and lipids. Consequently, elevated ROS levels are associated with the progression of many inflammatory conditions like atherosclerosis, cancer, diabetes mellitus, neurodegenerative disorders like Alzheimer's and Parkinson's as well as ageing in general (Blesa *et al.* 2015; Ha *et al.* 2008; Manoharan *et al.* 2016; Liou and Storz 2010).

Table 1: A selection of reactive oxygen/nitrogen species and oxidants found in the cell

ROS/RNS/active metabolites	Chemical formula
Superoxide anion	$O_2^{\cdot-}$
Singlet oxygen	$^1O_2$
Peroxyl radical	$ROO^{\cdot}$
Alkoxyl radical	$RO^{\cdot}$
Hydroxyl radical	·OH
Peroxynitrite anion	$ONOO^-$
Nitric oxide	NO·
Hydrogen peroxide	H_2O_2
Hypochlorous acid	HOCl

Endogenous ROS producers are mainly the mitochondria and peroxisomes, and enzymes like NADPH oxidases (NOX), NO synthases (NOS), xanthine oxidase (XO) and myeloperoxidase (MPO). The electron transport chain (ETC) of mitochondria is one the largest contributors of endogenous ROS and it is estimated that ~1 % of all O_2 is converted into $O_2^{\cdot-}$ by this process (Moloney and Cotter 2017). The electrochemical proton gradient that is required for the generation of ATP utilises the transfer of electrons through four electron carriers. *i.e.* complexes I-IV. Complex I (NADH-ubiquinone oxidoreductase) and complex III (ubiquinol cytochrome c reductase) are the sources of $O_2^{\cdot-}$ formation (Mittal *et al.* 2014). As $O_2^{\cdot-}$ is charged it cannot permeate membranes. It is highly reactive and can damage biomolecules in its vicinity. In the presence of nitric oxide (NO·), it forms the highly reactive peroxynitrite ($ONOO^-$) which can damage DNA bases and form 8-nitroguanine. In the presence of Fe^{3+} ions, $O_2^{\cdot-}$ and H_2O_2 can also react to toxic ·OH (Haber-Weiss reaction) (Fig. 3).

The ·OH radical is short-lived and the oxidation process occurs at the site of formation. In the vicinity of DNA, it can lead to oxidised bases, abasic sites, DNA-intrastrand crosslinks,

DNA strand breaks and DNA-protein cross-links (Cadet *et al.* 1999). Ionising radiation (IR) is one of the main sources of ·OH radicals.

Nitric oxide (NO·) is produced from L-arginine in a two-step reaction by NOS. It is an important signalling molecule and a strong vasodilator of the endothelium. Uncoupling of the endothelial NOS (eNOS) can lead to the transfer of electrons onto O_2 rather than arginine, resulting in the formation of $O_2^{\cdot-}$ (Mittal *et al.* 2014). In mice, inducible NOS (iNOS) can be stimulated by inflammatory cytokines (*e.g.* TNF-α, IFN-γ and IL-1) and produce high amounts of NO· as a defence mechanism against pathogens (Bogdan *et al.* 2000) (see section 1.2.2).

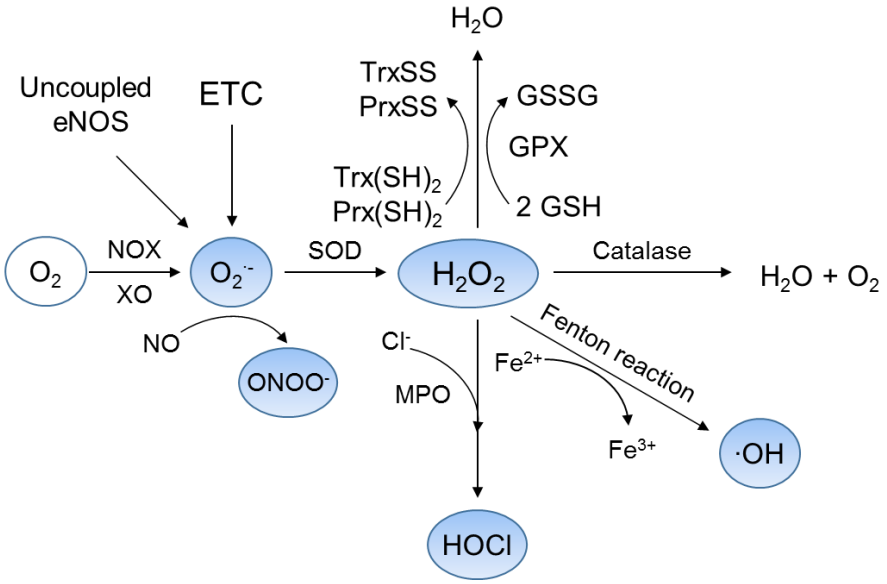

Haber-Weiss reaction

$Fe^{3+} + O_2^{\cdot-} \rightarrow O_2 + Fe^{2+}$

$Fe^{2+} + H_2O_2 \rightarrow Fe^{3+} + OH^- + \cdot OH$ (Fenton reaction)

Detoxification

$2O_2^{\cdot-} + 2H^+ \rightarrow H_2O_2 + O_2$ (SOD)

$2H_2O_2 \rightarrow 2H_2O + O_2$ (Catalase)

$H_2O_2 + 2GSH \rightarrow 2H_2O + GSSG$ (Glutathione peroxidase)

$H_2O_2 + Prx(SH)_2 \rightarrow 2H_2O + PrxSS$ (Peroxiredoxin)

$PrxSS + Trx(SH)_2 \rightarrow Prx(SH)_2 + TrxSS$ (Thioredoxin)

Fig. 3: Intracellular ROS and their detoxification pathways
$O_2^{\cdot-}$ is generated by the leakage of the ETC in the mitochondria, uncoupled endothelial NO synthase (eNOS), NOX or XO. In the presence of $NO^{\cdot}$, it can react to peroxynitrite. The superoxide dismutase (SOD) catalyses $O_2^{\cdot-}$ to less reactive H_2O_2 which is effectively neutralised by catalase, glutathione peroxidase (GPX) and peroxiredoxin (Prx) antioxidant enzymes. Prx uses thioredoxin (Trx) to detoxify H_2O_2. At inflammatory sites, H_2O_2 can be converted to highly reactive hypochlorous acid (HOCl) by MPO. In the presence of ferrous iron (Fe^{2+}) reactive ·OH can be formed via the Fenton reaction.

H_2O_2, although it does not contain unpaired electrons, is still a strong oxidising agent and a precursor for other radicals. It is generated by superoxide dismutase (SOD) in mitochondria when it detoxifies $O_2^{\cdot-}$ (Fig. 3). In the Haber-Weiss reaction, it leads to the formation of ·OH (second step, Fenton reaction). H_2O_2 is not charged and can penetrate cell membranes. It can act as a signalling molecule when it reacts with cytosolic factors such as redox-sensitive transcription factors (*e.g.* hypoxia-inducible factor 1α (HIF-1α) and NFκB) and lead to the formation of pro-inflammatory cytokines (*e.g.* TNF-α, IL-6 and IL-1β) and the assembly of the inflammasome (Wang *et al.* 2010a; Naik and Dixit 2011; Chandel *et al.* 2000). Oxidase-

enriched peroxisomes also produce a lot of H_2O_2. They are small organelles that are involved in many metabolic processes such as the biosynthesis of bile acids, purines and pyrimidines, and polyunsaturated fatty acids, as well as the degradation of long-chained fatty acids via β-oxidation, amino acids, polyamines and prostaglandins. The metabolic activity of peroxisomes requires oxidases that consume O_2 and concomitantly lead to the formation of H_2O_2, $O_2^{\cdot-}$, ·OH and NO· (Schrader and Fahimi 2006). The toxic by-products of oxidases are counteracted by catalase which detoxifies the high amount of H_2O_2 to form water and O_2 (Fig. 3) (Smith and Aitchison 2013).

Other sources of ROS are cyclooxygenases (COX) and lipoxygenases (LOX) which metabolise arachidonic acid to produce prostaglandins and leukotrienes and form $O_2^{\cdot-}$ as a by-product. As $O_2^{\cdot-}$ reacts with unsaturated fatty acids, ROS namely alkyl- (R*), alkoxyl ($RO^{\cdot}$) and peroxyl radicals ($ROO^{\cdot}$) are formed which in turn can damage other macromolecules (Riley 1994). Reactive acrolein, malondialdehyde and crotonaldehyde can bind to DNA and form etheno adducts (ethenoA and ethenoC) or the malondialdehyde-guanosine adduct M1dG (Marnett 1999; Otteneder *et al.* 2006).

Antioxidants protect the cells from ROS-induced damage. ROS scavengers can be enzymatic (*e.g.* SOD, catalase and glutathione peroxidase) or non-enzymatic (*e.g.* ascorbic acid, α-tocopherol, glutathione and vitamin A). Enhanced ROS production or insufficient antioxidant capacity results in damage to lipids (lipid peroxidation), proteins (protein oxidation like nitrotyrosine residues) and DNA (base lesions, strand breaks and crosslinks) which - if not repaired - disturb cell homeostasis. This imbalance is called oxidative stress and plays an important role in the progression of inflammatory disorders (see section 1.2.3).

1.2.2 ROS as an anti-microbial defence mechanism

Whereas ROS generated by mitochondria and peroxisomes are a by-product of their metabolic activity, phagocytes utilise the detrimental effects of ROS to actively damage pathogens. Their explosive release of ROS in the direction of invading microorganisms is called “respiratory burst” or “ROS burst”. Phagocytes like polymorphonuclear neutrophils (PMN), macrophages and monocytes express NADPH oxidase and MPO to produce $O_2^{\cdot-}$ and HOCl respectively.

The NADPH oxidase family consists of seven members (NOX1-5 and Duox 1 and 2) which differ in their structure, their expression level in different tissues and their activation mechanism (Mittal *et al.* 2014). NOX2, expressed in phagocytes, is one of the main ROS producers in the innate immune response of humans. It is a multi-subunit complex that assembles at the plasma membrane to produce $O_2^{\cdot-}$. The core complex or flavocytochrome b558 complex consists of $gp91^{phox}$ and $p22^{phox}$. $gp91^{phox}$ consists of six transmembrane domains and a C-terminal region which contains the flavin-adenine dinucleotide (FAD) and NADPH binding sites. NADPH is the electron donor for the following reaction:

$$NADPH + H^+ + 2O_2 \rightarrow NADP^+ + 2O_2^{\cdot-} + 2H^+$$

Subsequent spontaneous dismutation leads to the formation of H_2O_2:

$$2O_2^{\cdot-} + 2H^+ \rightarrow H_2O_2 + 2O_2$$

The regulatory subunits are the cytosolic factors $p40^{phox}$, $p47^{phox}$ and $p67^{phox}$ and the small GTPase Rac2. Upon stimulation, $p47^{phox}$ becomes phosphorylated and the regulatory factors translocate to the membrane where they associate with the core complex to form

the active oxidase. Upstream of $p47^{phox}$, diacylglycerol (DAG) is an activator of protein kinase C (PKC) which can phosphorylate $p47^{phox}$. Phorbol esters like phorbol 12-myristate 13-acetate (PMA) are pharmacological activators of PKC as they mimic DAG and induce a strong activation of NADPH oxidase. Other kinases that activate $p47^{phox}$ are AKT / protein kinase B (PKB) and p21-activated kinases (PAKs).

Stimulation of the respiratory burst can be induced by different stimuli like pro-inflammatory cytokines (*e.g.* TNF-α, IL-1β and IL-6), LPS, N-formyl-methionyl-leucyl-phenylalanine (fMLP) and opsonised zymosan. Diphenyleneiodonium (DPI) is a strong inhibitor of NADPH oxidase (Ellis *et al.* 1988). In activated leukocytes, approximately 10 nmol of $O_2^{\cdot-}$ are produced per minute per 10^6 cells (Brandes and Kreuzer 2005; Brandes *et al.* 2014; Roy *et al.* 2017). $O_2^{\cdot-}$ cannot cross membranes as it is very reactive and charged; it reacts with molecules in its close vicinity. Its spontaneous reaction with water leads to the formation of reactive, but more stable and uncharged, H_2O_2 that can penetrate membranes and damage intracellular components of pathogens. *In vitro* experiments showed that ROS, namely H_2O_2, generated by neutrophils can cross the membrane and be deposited in the cytosol of adjacent erythrocytes and tumour cells (Cao *et al.* 1993; Fialkow *et al.* 2007; Maher *et al.* 1993).

The importance of NADPH oxidase in the innate host defence is demonstrated in human chronic granulomatous disease (CGD). CGD is a rare hereditary disease (1:250,000 births) in which $O_2^{\cdot-}$ production is disturbed and patients suffer from recurring severe viral, fungal and bacterial infections leading to early mortality. To date, more than 400 mutations have been identified: ~65 % of all mutations occur in the $gp91^{phox}$ gene (X-linked CGD), ~30 % in the $p47^{phox}$ gene and ~5 % in the $p67^{phox}$ and $p22^{phox}$ genes (autosomal recessive types) (Mittal *et al.* 2014; Jackson *et al.* 1995).

Another oxidant utilised by phagocytes to kill pathogens is HOCl, produced by the MPO. The oxidase is highly expressed in PMN (~5 % of total protein) and stored in cytoplasmic granules at very high concentration (~100 mg/ml) (Segal 2005). It halogenates biomolecules like proteins, specifically at tyrosine residues (*i.e.* 3-chlorotyrosine) (Klebanoff *et al.* 2013).

$$H_2O_2 + Cl^- \rightarrow OH^- + HOCl$$

HOCl reacts rapidly with sulphur and nitrogen atoms present in thiols, thiol esters, amines and amides. Glutathione, with its thiol group, is one of the key targets. The oxidation of cysteine residues can disturb protein function and lead to an imbalance in the redox potential of cells. Furthermore, HOCl can halogenate DNA bases forming 5-chlorocytosine, 5-chloro(2'-deoxy) cytidine, 8-chloroadenine or 8-chloro-(2'-deoxy) guanosine (Davies 2011).

NO·, mostly known for its vasodilatory effect on the endothelium, is also known to be released by innate immune cells during infections via inducible NOS (iNOS). However, the importance of NO· in anti-microbial defence varies between organisms. NO· production by granulocytes is substantially higher in rodents than in human (Fialkow *et al.* 2007). In tuberculosis infection models, murine NO· production was essential for killing pathogens whereas in human systems there remains controversy about its importance (Chan *et al.* 2001; Schneemann and Schoedon 2002; Mestas and Hughes 2004).

1.2.3 Oxidative stress and disease

The balance between ROS production and elimination is important for tissue homeostasis. If ROS production exceeds the anti-oxidant system, oxidative stress is inflicted and the resulting damage to cellular components leads to cell and tissue dysfunction. Oxidative stress is an important factor in the progression of chronic inflammatory conditions like rheumatoid arthritis, atherosclerosis, cardiovascular diseases, diabetes mellitus, ischemia/reperfusion, cancer and ageing (Reuter *et al.* 2010).

ROS play an important role in the inflammatory response as they are produced by the innate immune cells to fight off infections. This acute inflammatory reaction is temporary and is usually considered beneficial for the host. However, if the inflammation persists the risk for inflammatory diseases increases. The site of inflammation becomes enriched with ROS, soluble mediators like cytokines, prostaglandins and chemokines attract additional ROS-producing cells. The resulting oxidative stress can damage healthy tissue and lead to endothelial dysfunction as it damages all major macromolecules, *i.e.* lipids, proteins and DNA (Mittal *et al.* 2014). Furthermore, the mediators activate signal transduction cascades that induce NFκB, signal transducer and activator of transcription 3 (STAT3), HIF-1α, activator protein-1 (AP-1), and NF-E2 related factor-2 (NrF2) (Reuter *et al.* 2010) which lead to cellular stress responses. Those include the release of more pro-inflammatory cytokines (*e.g.* TNF-α, IL-1 and IL-6) and chemokines (IL-8 and CXC chemokine receptor 4 (CXCR4)) as well as the expression of COX and iNOS. This sustained oxidative environment ultimately promotes the progression of diseases.

In cancer, ROS-induced oxidative DNA damage can affect the initiation, promotion and progression of the multistage cancer process. Gene mutations, aberrant gene expression, disturbed cell-cell communication, and the modification of second messenger systems result in enhanced cell proliferation with concomitant inhibition of apoptosis (Reuter *et al.* 2010). The induction of HIF-1α, VEGF, fibroblast growth factor (FGF), and PDGF facilitates tumour growth and metastatic spread under hypoxic conditions as angiogenesis is induced (Brieger *et al.* 2012; Liou and Storz 2010; Reuter *et al.* 2010).

The oxidative environment also contributes to the pathophysiological progression of atherosclerosis and subsequently to cardiovascular diseases as it promotes the formation of oxidised low density lipoproteins (oxLDL). oxLDL is considered pro-inflammatory as it inhibits eNOS, promotes vasoconstriction and platelet aggregation, and stimulates cytokines such as IL-1 (Singh and Jialal 2006).

Another feature of persisting inflammatory conditions and elevated ROS levels are the degeneration of tissues and organs followed by an accumulation of connective tissue and extracellular matrix proteins in its place which eventually leads to fibrosis. The release of tissue-remodelling factors like TGF-β, FGF and VEGF are strong inducers of such scarring processes. The ROS-promoted development of fibrosis was observed in many organs, *e.g.* lung (Cheresh *et al.* 2013), kidney (Sedeek *et al.* 2010), heart (Seddon *et al.* 2007), pancreas (Masamune *et al.* 2008) and liver (Minicis and Brenner 2007).

1.2.4 Artesunate – an exogenous source of ROS

Artemisinin is a sesquiterpene produced by *Artemisia annua* L. that has extensively been used in Traditional Chinese Medicine (TMC) to treat chills and fever as well as malaria (Klayman 1985). Its semi-synthetic derivatives artemether and artesunate (ART) are not

only used in anti-malarial therapy but are being considered for cancer therapy as well. The active moiety is the endoperoxide bridge that is cleaved in the presence of ferrous iron and leads to the formation of ROS, namely hydroxyl radicals and superoxide anions. *Plasmodium falciparum* in its asexual stage of its life cycle is found in erythrocytes where heme-iron levels are high and facilitate the cleavage of the endoperoxide bridge of ART (Berman and Adams 1997). The toxic effect is said to be induced by the alkylation of proteins via carbon-centred radical species (Li *et al.* 2008).

For treating severe and complicated malaria the Center for Disease Control and Prevention (CDC) based on a study by the SEAQUAMAT trial (Dondorp *et al.* 2005) recommends ART to be administered intravenously at the dosage of 2.4 mg/kg body weight at 0 h, 12 h, 24 h, and 48 h. Later on, the dose can be modified to a daily administration for an additional three days (Twomey *et al.* 2015). Plasma concentrations in healthy subjects after a single injection of 2.4 mg/kg body weight ART peaked at 306 ± 259 (94-913) nmol/litre within 33 min. ART was rapidly eliminated from plasma with a half-life $t_{½}$ = 1.37 ± 0.59 (1.04-2.06) hours (Ittarat *et al.* 1998). In severe malaria cases, immediate treatment with artesunate led to plasma concentrations of ~3000 ng/ml (median of 1020- 164000 ng/ml) and a half-life $t_{½}$ = 25 min (Byakika-Kibwika *et al.* 2012).

For cancer treatment, the DNA damaging properties of ART are of particular interest. It was shown that ART leads to dose-dependent apoptotic and necrotic cell death in glioblastoma cell lines LN-229, A172 and U87MG (Berdelle *et al.* 2011; Berte *et al.* 2016). ART ameliorates the killing response of the alkylating chemotherapeutic temozolomide (TMZ), the first-line chemotherapeutic in the treatment of glioblastoma multiforme. ART led to oxidative DNA damage, *i.e.* 8-oxoG and ethenoA, and the formation of DNA double-strand breaks (Berdelle *et al.* 2011; Li *et al.* 2008) with subsequent activation of the ATM/Chk2 and ATR/Chk1 DNA damage response signalling pathway. Studies with DNA repair-deficient cell lines showed that impaired base excision repair (Pol $\beta^{-/-}$), homologous recombination (defective in XRCC2 or BRCA2 gene) and non-homologous end-joining (Ku80 gene) sensitised cells to ART. This was not the case for nucleotide excision repair-deficient cells (ERCC3 or ERCC1 gene) (Li *et al.* 2008; Berdelle *et al.* 2011).

1.3 The DNA damage response – DNA damage and DNA repair

The DNA suffers daily damage by endogenous and exogenous factors that lead to base lesions, single- and double-strand breaks (SSBs and DSBs). These DNA lesions play a key role in cellular dysfunction, mutagenesis and carcinogenesis. DNA exists in an aqueous environment and can spontaneously react with water resulting in the loss of DNA bases. Metabolic processes like the oxidative phosphorylation in mitochondria or the catabolic processes in peroxisomes generate ROS and oxidants. Exogenous sources are environmental toxins like exhaust fumes or cigarette smoke containing benzo(a)pyrene, dietary compounds like heterocyclic aromatic amines (HCAs) and N-nitroso compounds (NOC) or physical mutagens like UV light or IR. Many chemotherapeutics directly target the DNA to kill cancer cells (*e.g.* the alkylating agents TMZ, dacarbazine and cyclophosphamide).

If DNA damage remains unrepaired it can result in gene mutation and chromosomal aberrations which could trigger cell death or carcinogenesis (Christmann and Kaina 2013). Genotoxic stress is counteracted by DNA repair mechanisms that maintain genomic integrity. ROS, as mentioned in section 1.2.1, are potent genotoxins. Radicals like ·OH can

directly damage bases and the phosphate backbone, the latter resulting in SSBs. Peroxynitrite can lead to 8-nitroguanine base lesions. ROS-damaged macromolecules like lipids and proteins can become reactive metabolites themselves and form DNA adducts such as etheno adducts or the malondialdehyde-guanosine adduct M1dG. In order to combat these heterogeneous types of DNA lesions, the cell possesses different DNA repair pathways. Except for homologous recombination (HR), all of them are present independent of the cell cycle status. The DNA repair pathways include simple reversion repairs as well as complex, multi-step repair pathways. An example of a single step repair enzyme is the O^6-methylguanine DNA methyltransferase (MGMT) which removes O^6-alkylguanine lesions. DNA SSBs and DSBs are complex DNA lesions that are repaired in multi-step processes.

1.3.1 Base excision repair and DNA single-strand break repair

The base excision repair (BER) pathway is responsible for the removal of small, non-helix-distorting base lesions, the repair of abasic sites and the ligation of SSBs. These alterations are highly mutagenic and require a quick and reliable repair mechanism. It is postulated that up to 10,000 lesions occur in the human genome per day (Kunkel 1999). Most often spontaneous hydrolysis of the base is found (~9,000 per cell) resulting in apurinic/apyrimidinic sites (abasic / AP sites). Oxidative lesions are a product of metabolic processes (*e.g.* oxidative metabolism of mitochondria) or ROS production during the course of the inflammatory response and they include lesions like 8-oxoguanine (8-oxoG), 2,6-diamino-4-hydroxy-5-formamidopyrimidine (Fapy) and thymine glycol. Lipid peroxidation can also directly modify bases and form 3,*N*4-ethenocytosine (ethenoC) and 1,*N*6-ethenoadenine (ethenoA) (el Ghissassi *et al.* 1995). *S*-Adenosyl methionine (SAM), a co-substrate for methyl group transfer, can alkylate bases and form 3-methyladenine and 7-methylguanine (Kim and Wilson 2012; Abbotts and Wilson 2017). Spontaneous deamination of cytosine resulting in uracil or deamination of 5-methylcytosine leading to thymine opposite guanine are also substrates for BER.

Apart from endogenous sources like the oxidative metabolism in the mitochondrial ETC or inflammation-induced ROS production (see section 1.2.1), there are exogenous agents that can lead to base lesions. UV light and IR can cause oxidative damage and carcinogens like nitrosamines as well as anti-cancer drugs (*e.g.* temozolomide and dacarbazine) can alkylate the DNA (Christmann *et al.* 2003; Fahrer and Kaina 2013). SSBs are caused by exogenous agents (*e.g.* IR and ROS), they arise as repair-intermediates in the course of BER as well as during replication and transcription (Caldecott 2003). Left unrepaired, SSBs can be converted into DSBs which increase the risk for chromosomal aberrations, point mutations, translocations and deletions. SSB repair is considered a sub-pathway of BER that utilises BER proteins with PARP-1 and XRCC1 as key proteins in orchestrating the repair machinery (for details see section 1.3.1.1).

First, specific DNA glycosylases recognise and remove the damaged or incorrect base by hydrolysing the N-glycosidic bond between base and deoxyribose. The glycosylases are grouped into mono-functional, type I and bi-functional, type II glycosylases. Type I (*e.g.* N-methylpurine DNA glycosylase (MPG), thymine DNA glycosylase (TDG) and uracil DNA glycosylase (UNG1)) removes the base leaving an AP site, whereas type II (*e.g.* 8-oxoguanine glycosylase (OGG1) and Nei Like DNA Glycosylase 1 (NEIL1)) removes the base and cuts into the AP site resulting in a SSB. For type I glycosylases, the AP

endonuclease 1 (APE1) incises the phosphodiester bond resulting in 5'deoxyribose-5-phosphate (5'dRP) and 3'-OH ends (Christmann *et al.* 2003). Polymerase β (Polβ) then inserts a single nucleotide (Fig. 4). Next, depending on the 5'dRP terminus, the BER will process the damage either by short-patch or long-patch repair. Unaltered AP sites are processed through short patch repair as Polβ removes the 5'dRP residue via its lyase activity (so-called β-elimination) (Christmann *et al.* 2003).

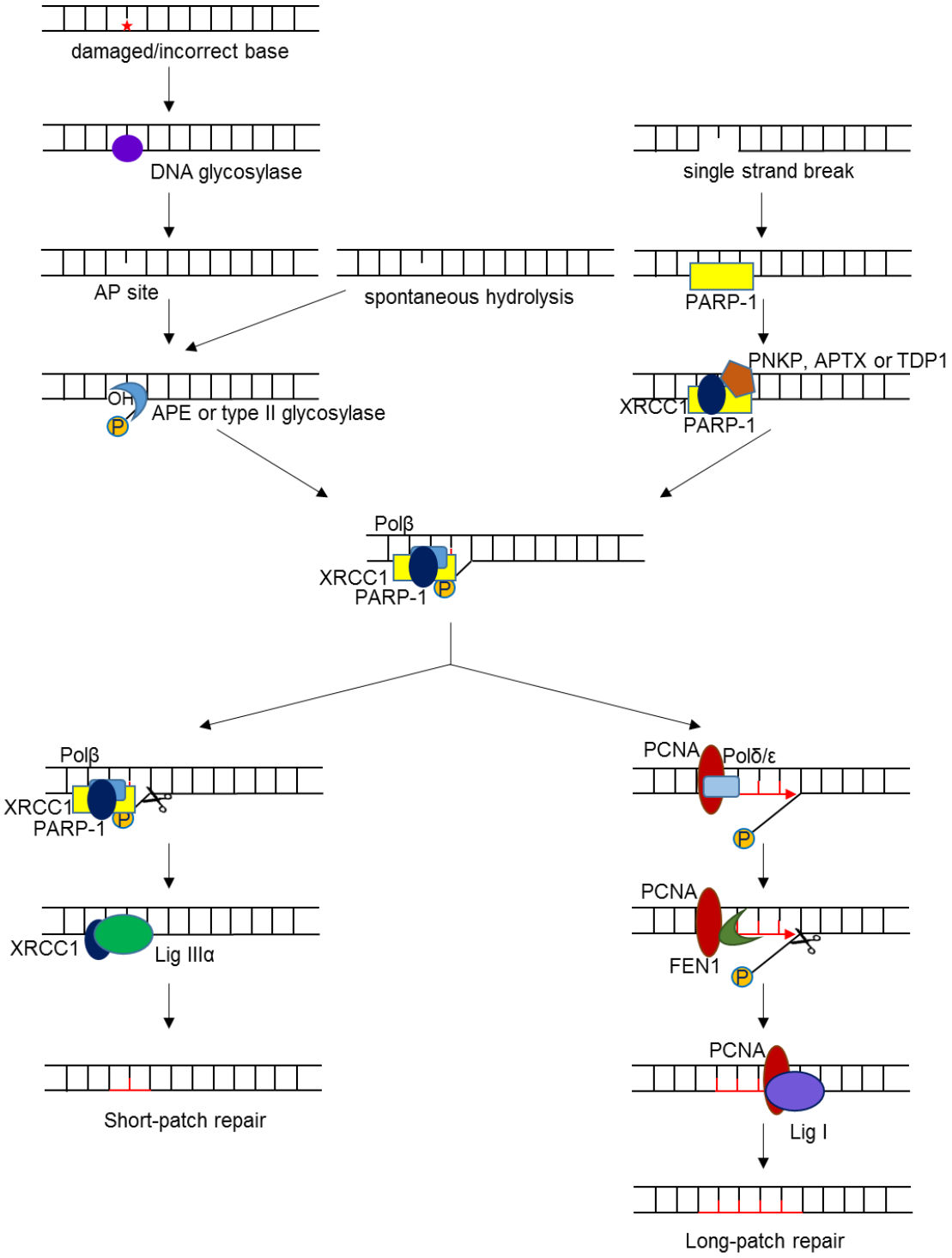

Fig. 4: Base excision repair and single-strand break repair
First, substrate-specific glycosylases excise the incorrect/damaged base creating an AP site. Next, APE1 or type II glycosylases incise the DNA backbone at the AP site creating a SSB that is recognised by PARP-1. Polβ inserts a new nucleotide. Depending on the nature of the DNA ends of the SSB, either short- or long-patch repair is initiated. If the DNA ends consist of 3'-OH and 5'-dRP

short-patch repair occurs and Polβ removes the 5'dRP. PNKP, APTX and TDP1 can process certain DNA termini in order for Polβ to function. A complex of XRCC1 and ligase IIIα then re-ligates the DNA. If the DNA ends are not accessible for β-elimination by Polβ, long-patch repair processes the damage using Polδ or ε together with PCNA and RF-C. Via strand replacement synthesis 2-12 nucleotides are incorporated and the overhanging DNA flap is removed by FEN1. The DNA nick is ligated by ligase I.

For successful re-ligation of the DNA, the 3' end must contain a 3'-OH group. Damaged 3'-α, β unsaturated aldehyde ends are removed by APE1, aprataxin (APTX) removes 3'-phosphoglycolate ends, 5'-polynucleotide kinase 3'-phosphatase (PNKP) removes 3'-phosphate ends and topoisomerase-DNA complexes are processed by tyrosyl-DNA phosphodiesterase (TDP1) (Takahashi *et al.* 2007). If the DNA ends are tidied up the re-ligation can occur. In short-patch repair, a complex of ligase IIIα, poly-(ADP-ribose) polymerase 1 (PARP-1) and X-Ray Repair Complementing Defective Repair In Chinese Hamster Cells 1 (XRCC1) seals the SSB ends. If the AP site is oxidised or reduced the cell undergoes long-patch repair (Leyns and Gonzalez 2012) (Fig. 4). In long-patch repair, Polβ dissociates from the DNA and displacement synthesis via polymerase δ or ε (Polδ or Polε) assisted by proliferating cell nuclear antigen (PCNA) and replication factor C (RF-C) incorporates 2-12 nucleotides. The resulting overhang DNA 'flap' is recognised and cleaved by Flap endonuclease 1 (FEN1) in conjunction with PCNA. Finally, the DNA ends are ligated by ligase I (Abbotts and Wilson 2017).

The decision of which pathway is initiated is not fully understood. Apart from the nature of the 5'-terminus (*i.e.* whether it is a substrate for β-elimination by Polβ), some studies showed that the initiating glycosylase, the intracellular ATP concentration (Petermann *et al.* 2006), the cell cycle phase and the differentiation state (Narciso *et al.* 2007) can influence the BER pathway as well as overall BER capacity. For example, the lesion 8-oxoG excised by OGG1 is mostly repaired by short-patch repair (Fortini and Dogliotti 2007; Dianov *et al.* 1998) whereas tetrahydrofuran lesions, uracil and 5'-dRP-trinucleotide are repaired by long-patch repair (Matsumoto *et al.* 1994; Bennett *et al.* 2001; Prasad *et al.* 2000; Prasad *et al.* 2001).

Narciso *et al.* could show that overall BER capacity in murine myotubes (terminally differentiated myoblasts) declined during the differentiation process as protein levels of XRCC1 and ligases I and IIIα decreased resulting in an accumulation of DNA damage. On the other hand, GM-CSF-induced differentiation of human monocytes into macrophages and GM-CSF + IL-4-induced generation of DCs led to the upregulation of XRCC1, ligase IIIα and PARP-1 (Briegert and Kaina 2007; Bauer *et al.* 2011; Bauer *et al.* 2012). For macrophages and DCs, this led to resistance against oxidative (H_2O_2, *tert*-butyl hydroperoxide (*t*-BOOH) and oxLDL) and alkylating (methyl methanesulfonate, methylnitronitrosoguanidine (MNNG) and TMZ) agents whereas monocytes underwent apoptosis. In short, the BER capacity and the decision to undergo short- or long-patch repair can differ depending on the type of lesion, the level of repair protein expression and the cell types that were analysed.

1.3.1.1 XRCC1 and PARP-1 in SSB repair

SSB repair is part of the BER pathway, as SSB-intermediates are formed by APE1 and type II glycosylases, and utilises BER proteins for the successful re-ligation of nicked DNA. SSBs are recognised by PARP-1 which works in concert with XRCC1 to recruit DNA repair factors to the site of damage (Fig. 4).

PARP-1 catalyses the cleavage of nicotinamide adenine dinucleotide (NAD^+) into nicotinamide and ADP-ribose. The latter forms a highly electronegative macromolecule of poly(ADP-ribose) (PAR) chains of up to 200 units with branching points every 50 units. PAR is attached in a covalent and a non-covalent fashion to proteins and to PARP-1 itself (Bürkle 2005). PARP-1 recognises SSBs and DSBs via two Zinc Fingers, binds to the lesion site and starts its enzymatic activity. PAR is a transient biopolymer that is rapidly degraded by poly(ADP-ribose)glycohydrolase (PARG); PAR levels peak 3 - 5 min after IR or H_2O_2 treatment (Weidele *et al.* 2010). PAR attracts DNA repair proteins like XRCC1, Polβ, ligase IIIα, aprataxin and PNK-like factor (APLF) and APTX via their PAR-motif to the site of damage while simultaneously removing histones from the DNA due to electrostatic repulsion, thus relaxing and opening it for repair (Messner *et al.* 2010).

XRCC1 is a scaffold protein with no known enzymatic function. However, it is essential for the recruitment of Polβ and ligase IIIα. XRCC1 knockout experiments in mice displayed embryonic lethality, emphasising the importance of this protein (Tebbs *et al.* 2003) and the XRCC1-deficient CHO cell line EM9 displayed sensitivity to alkylating agents (*e.g.* methyl and ethyl methanesulfonate (EMS and MMS)), X-ray and UV irradiation, H_2O_2 and topoisomerase inhibitor camptothecin (Abbotts and Wilson 2017). With one of its BRCA1 C Terminus (BRCT) domains, XRCC1 interacts with PARylated PARP-1 and thus is loaded onto sites of SSBs. If PARP-1 is pharmacologically inhibited, XRCC1 recruitment and thereby recruitment of ligase IIIα and Polβ are impaired resulting in slowed SSB repair (Godon *et al.* 2008; Mortusewicz *et al.* 2007) (Fig. 5). XRCC1 is known to stabilise ligase IIIα by forming a heterodimeric complex and ligase IIIα protein levels are reduced if XRCC1 is absent. It was also stated that XRCC1 stimulates phosphatase and kinase activities of recombinant PNKP (Whitehouse *et al.* 2001) which is important for processing of DNA ends for nick ligation.

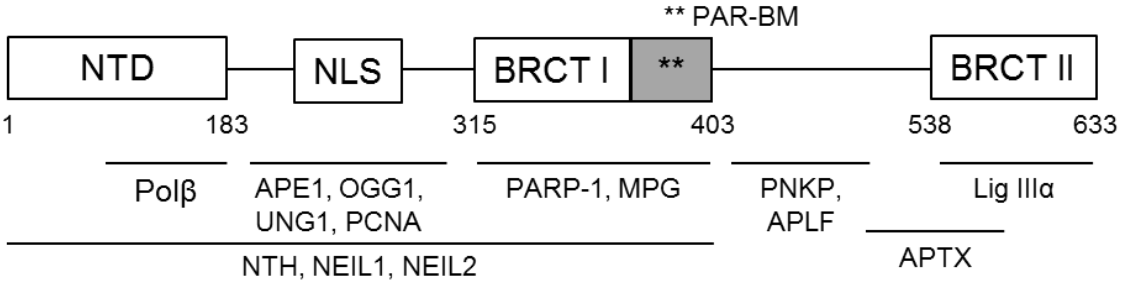

Fig. 5: XRCC1 protein structure
XRCC1 has different interaction sites for other BER and SSB repair proteins. Among them are glycosylases, endonucleases, the DNA ligase IIIα and DNA end-processing enzymes. In its BRCT I domain a PAR-binding motif (PAR-BM) mediates the interaction with PARylated PARP-1. N-terminal domain (NTD), nuclear localisation sequence (NLS), BRCA1 C Terminus (BRCT) domain

With its different domains and linker regions, XRCC1 interacts with several BER proteins required for successful BER (Fig. 5). Among them are DNA glycosylases like MPG, UNG1, OGG1 and the endonuclease VIII-like glycosylases 1 and 2 (NEIL1 and NEIL2); endonucleases APE1 and endonuclease III (NTH); DNA end processing enzymes APTX, PNKP and APLF, and the DNA clamp PCNA (Abbotts and Wilson 2017; Della-Maria *et al.* 2012; Sterpone and Cozzi 2010).

1.3.2 DNA double-strand break repair

DSBs are one of the most severe DNA lesions which if not repaired lead to mutations, deletions, chromosomal aberrations and eventually cell death. The cell can utilise two DNA repair pathways: Non-homologous end-joining (NHEJ) which is cell cycle independent and HR which only occurs in the presence of homologous DNA sequences on sister chromatids. As most of the innate immune cells are non-dividing cells, HR can be neglected and only NHEJ will be described in detail.

1.3.2.1 Non-homologous end-joining (canonical and alternative)

Canonical NHEJ (c-NHEJ) is an error-prone DSB repair pathway that re-ligates two DNA ends. It works in a cell cycle-independent manner. The initial step is the recognition of the DSB by the Ku heterodimer Ku70/Ku80 (also known as X-Ray Repair Complementing Defective Repair In Chinese Hamster Cells 6 and 5 (XRCC6 and XRCC5)) which binds to the DNA ends with high affinity. Ku recruits DNA-Dependent Protein Kinase Catalytic Subunit (DNA-PKcs) to the damage site and stimulates its kinase activity which leads to the recruitment of the nuclease Artemis, and end-processing enzymes like Polymerases μ and λ, and terminal deoxynucleotidyl transferase (TdT). When the DNA ends are compatible for re-ligation, the DNA ends are ligated by the XRCC4 / ligase IV / XRCC4-Like Factor (XLF) complex (Mladenov *et al.* 2016). The DNA end-processing can result in the loss of bases which makes this repair pathway error prone. Gross chromosomal rearrangements (namely translocations) can also occur as NHEJ re-ligates any two DNA ends it binds.

If the c-NHEJ is impaired or blocked an alternative pathway, alternative end-joining (alt-EJ), is used as a backup. It is even more error-prone than c-NHEJ. The central enzyme is PARP-1 which senses the DSB via its zinc fingers and recruits XRCC1 and ligases I and III to the damage site. The translesion DNA polymerase θ fills in missing bases.

NHEJ plays an important role in the development of the adaptive immune system. During the development of lymphocytes, the immunoglobulin and TCR genes undergo somatic rearrangement resulting in a diverse repertoire of immunoglobulins and TCRs to detect foreign material. It is a tightly controlled mechanism in which the resulting DSBs are repaired by c-NHEJ (Schatz and Swanson 2011).

1.3.3 DNA damage signalling and the induction of apoptosis

DNA damage is detected by different sensor proteins that initiate signalling cascades resulting in cell cycle arrest, DNA repair, senescence, autophagy, and – if the damage exceeds repair capacity – apoptotic or necrotic cell death (Roos *et al.* 2016). This DNA damage response (DDR) is strongly activated in the presence of DSBs or polymerase-blocking DNA adducts. DSBs are deleterious lesions that trigger apoptosis if they are not repaired, as shown in cells exposed to IR and methylating agents (*e.g.* TMZ). Overlapping SSBs can also be converted into a DSB (Mladenov *et al.* 2016).

First, the DSB must be detected. The cell has three sensor proteins of the PI3K-related kinase (PIKK) family, *i.e.* ataxia-telangiectasia mutated (ATM), ATM- and Rad3-related (ATR) and DNA-PK. They can phosphorylate more than 700 target proteins, some of which are involved in pro- as well as anti-apoptotic signalling. They activate downstream checkpoint proteins that lead to cell cycle arrest and the recruitment of DNA repair factors to the lesion site. ATM phosphorylates Checkpoint Kinase 2 (CHK2) and ATR

phosphorylates Checkpoint Kinase 1 (CHK1). Both CHK proteins as well as DNA-PK, ATM and ATR can phosphorylate p53 at different positions, *i.e.* Ser15 and Ser20, thereby stabilising it (Lakin and Jackson 1999; Roos *et al.* 2016). Other targets of ATM phosphorylation are histone 2AX (γH2AX) which is a classic marker for DSBs, KRAB-associated protein-1 (KAP1), a transcriptional repressor that mediates gene silencing by increasing the amount of histone 3 methylated lysine 9 (H3K9me), the E3 ubiquitin ligase Siah-1 and p53-Binding Protein 1 (53BP1). Under unstressed conditions Siah-1 complexes with Homeodomain Interacting Protein Kinase 2 (HIPK2). Upon phosphorylation, Siah-1 is degraded and HIPK2 is stabilised (Winter et al. 2008). HIPK2 is an important regulator of pro-apoptotic signalling as it phosphorylates p53 at Ser46 (Puca *et al.* 2010). 53BP1 stimulates NHEJ and represses HR when it localises to DSBs by preventing the resection of the DNA by Meiotic Recombination 11 Homolog 1 (Mre11), CTBP-Interacting Protein (CtIP) and exonuclease 1 (EXO1), important end-resection factors for HR (Roos and Krumm 2016; Chapman *et al.* 2012).

Depending on its phosphorylation status, p53 induces the transcriptional activation of pro-survival or pro-apoptotic proteins. Phosphorylated at Ser46, it leads to the expression of p53 regulated apoptosis-inducing protein 1 (PUMA), Bax and NOXA (Höpker *et al.* 2012). PUMA interacts with the members of the anti-apoptotic B-cell lymphoma 2 (Bcl2) family, thereby freeing Bcl2-bound Bax and Bcl-2 homologous antagonist killer (Bak). Bax and Bak migrate to the mitochondrion, where they stimulate the intrinsic apoptosis pathway. They cause a change in permeability of the outer mitochondrial membrane, so-called mitochondrial outer membrane permeabilisation (MOMP). Cytochrome c is released into the cytoplasm and complexes with pro-caspase-9 and apoptotic protease activating factor 1 (Apaf1) into the so-called apoptosome. Active caspase-9 cleaves effector caspases-3 and -7 which leads to the degradation of proteins and the fragmentation of the DNA (Ichim and Tait 2016).

p53 also induces the expression of FasR (CD95, Apo1) which is responsible for initiating the extrinsic apoptosis pathway. It is a transmembrane death receptor with binding sites for Fas-associated protein with death domains (FADD). The FADD adapter proteins bind pro-caspases-8 and -10 via their death effector domains (DED). Active initiator caspases-8 and -10 cleave pro-caspases-3 and -7. Furthermore, caspase-8 cleaves BH3-interacting death domain agonist (Bid) into truncated Bid (tBid), which activates Bax and Bak, thereby also activating the intrinsic pathway (Ichim and Tait 2016). One of the substrates of caspases is caspase-activated DNase (CAD) which fragments the DNA. Furthermore, many proteins involved in cell cycle, DNA repair signalling, structural proteins and protein kinases are cleaved. PARP-1 and DNA-PK are such proteins (Smith and Jackson 1999). They are cleaved early on as they counteract the apoptotic pathway by stimulating DNA repair. In the case of PARP-1, it is also an energy conserving mechanism. The CAD-induced DNA fragmentation would lead to excessive PARP-1 activation which in turn would deplete the NAD^+ and subsequently the ATP pools. The resulting energy crisis would lead to the abrogation of apoptosis and shift cell death from apoptosis to necrosis. The process of hyper-active PARP-1, for example after genotoxic stress, resulting in necrosis is called parthanatos (Roos *et al.* 2016).

Apoptotic cells are characterised by morphological changes such as cell shrinkage and pyknosis during the early stages. Plasma membrane blebbing occurs, membrane components like the phospholipid phosphatidylserine (PS) are flipped to the outer surface, the target for flow cytometry-based cell death quantification via AnnexinV staining. Later on,

the DNA is fragmented (so-called karyorrhexis) and proteins are degraded. Tightly packed apoptotic bodies are formed during the "budding" process that prevents leakage of intracellular components and activation of the immune system. The apoptotic bodies are phagocytosed and degraded by other cells like macrophages or parenchymal cells (Elmore 2007). If apoptosis cannot occur, *e.g.* when caspases are inhibited, the cell can undergo regulated necrotic cell death, also called necroptosis. The latter depends on the activation of receptor-interacting serine/threonine-protein kinase 3 (RIPK3) by TNF-α receptor signalling via RIPK1. It works caspase-independently and leads to cell swelling with membrane rupture and the release of intracellular components into the surrounding area. Freed DAMPs activate the immune response and cause inflammation (Weinlich *et al.* 2017).

1.3.4 DNA repair in immune cells

The immune system requires DNA repair due to the intentional formation of DSBs in the lymphoid lineage. The diversity of the TCR and immunoglobulin expression is made possible by so-called V(D)J recombination, a site-specific recombination process in developing B and T lymphocytes. It generates a diverse antigen receptor repertoire by rearranging the segments of the antigen receptor gene, *i.e.* the V (variable), D (diversity), and J (joining) segments (Malu *et al.* 2012). The resulting DSBs are repaired by NHEJ. The error-prone repair pathway is even advantageous in this case, as random nucleotide insertions (known as N-additions) or trimming of the DNA ends with the loss of up to 14 bp by DNA processing enzymes increase the required diversity (Lieber 2010). Mutations in NHEJ proteins are associated with immune deficiencies (*e.g.* severe combined immunodeficiency, SCID) and a predisposition to cancers such as leukaemia and lymphoma. In contrast to this intentional DSB formation, immune cells also face exogenous, genotoxic substances. It is well known that one of the limiting factors of chemotherapy and radiation therapy are the severe side effects on the haematopoiesis. However, the subpopulations of immune cells display great differences in their response towards genotoxic stress. For example, myeloid immune cells are generally more resistant towards IR than lymphoid cells and multipotent progenitor cells (Heylmann *et al.* 2014). The DNA crosslinking agent mafosfamide, the metabolically active form of cyclophosphamide, leads to a stronger apoptotic response in Treg than in Th or CTL whereas TMZ (methylating agent), nimustine (chloroethylating agent) and mitomycin C (DNA crosslinker) led to similar responses in all three T cell populations (Heylmann *et al.* 2013).

In myeloid immune cells, the DNA repair capacity differs immensely between monocytes and monocyte-derived macrophages and DCs. Previous studies in our lab showed that monocytes are severely impaired in BER and NHEJ. They do not express XRCC1, PARP-1 and ligase IIIα which are necessary for the re-ligation of DNA single-strand breaks (Bauer *et al.* 2011; Briegert and Kaina 2007). Furthermore, monocytes do not express DNA-PKcs which is responsible for the recruitment of DNA repair factors in c-NHEJ. The backup pathway alt-EJ is also impaired as it requires PARP-1 which recruits XRCC1 and ligase IIIα to re-ligate strand breaks. Therefore, DNA methylating agents like MMS, MNNG and TMZ, oxidants like *t*-BOOH, oxLDL, and H_2O_2, as well as IR lead to an accumulation of SSBs and DSBs in monocytes. Subsequent activation of the ATM/ATR/CHK signalling pathway leads to the stabilisation of p53, followed by cleavage of pro-caspases into active caspases-8, -3 and -7 and finally monocytic cell death (Bauer *et al.* 2011; Bauer *et al.* 2012; Briegert and Kaina 2007). Cytokine-induced differentiation of monocytes into macrophages and DCs abolishes the genotoxic sensitivity. During the maturation process of macrophages and

DCs, the DNA repair proteins are re-expressed after approximately three days, thus promoting effective DNA repair and preventing the initiation of apoptosis after genotoxic stress.

1.4 Epigenetic regulation of genes – DNA methylation

Epigenetic modifications allow for tissue-specific regulation of genes without changing the genetic coding sequence of DNA. The cell has different mechanisms for regulating its gene expression, *e.g.* DNA methylation and post-translational modifications of histones.

5-methylcytosine (5mC) is an epigenetic modification of the DNA with important roles in disease and development. It is conventionally associated with transcriptional repression. The transfer of a methyl moiety onto cytosine is catalysed by DNA-methyltransferases (DNMTs). These enzymes utilise *S*-adenosyl methionine (SAM) as a methyl donor. Methylated cytosines are found in 60-80 % of CpG dinucleotides in the mammalian genome. The overall genome is poor in CpGs (< 1 %) with the exception of clustered CpG dinucleotides in the promoter region of genes. These so-called CpG islands are mostly unmethylated while the genome-wide dispersed CpG dinucleotides are predominantly methylated (Deaton and Bird 2011). Methylation of CpG islands in promoter regions can lead to stable silencing of genes, *e.g.* the MGMT promoter (Switzeny *et al.* 2016).

5mC is a stable covalent modification that can be reversed in a multi-step process initiated by ten-eleven translocation methylcytosine dioxygenases (TETs). TETs are involved in several steps of the demethylation process (so-called iterative oxidation) and catalyse the formation of 5-hydroxymethylcytosine (5hmC), 5-formylcytosine (5fC) and 5-carboxylcytosine (5caC). 5caC is recognised by TDG and a substrate for BER which inserts an unmodified cytosine and re-ligates the nicked DNA. TET enzymes are iron(II)/α-ketoglutarate (Fe(II)/α-KG)-dependent dioxygenases. TETs use molecular oxygen to catalyse the oxidative decarboxylation of α-KG, thereby generating succinate, CO_2 and a reactive enzyme-bound Fe(IV)-oxo intermediate that converts 5mC to 5hmC (Kohli and Zhang 2013). 2-hydroxyglutarate (2-HG) is a competitive inhibitor of TETs as it competes with α-KG for binding TET (Wu and Zhang 2017). In monocytes, undergoing differentiation into DCs, it was shown that TET2 mediates demethylation from 5mC to 5hmC, but does not necessarily correlate to transcriptional changes (Klug *et al.* 2010). Wallner *et al.* could show that monocytes undergoing differentiation into macrophages by M-CSF rapidly demethylated distinct regions in the DNA, likely enhancer regions, and that the process is delayed or abrogated in the presence of 2-HG. Concomitant to the demethylation, repressive histone modifications like histone 3 lysine 27 tri methyl (H3K27me3) were reduced at these sites.

2 Aims of the work

This work focused on the effect of ROS on human immune cells. Myeloid immune cells are specialised in releasing ROS as an anti-microbial defence mechanism. Therefore, the inflammatory site is enriched with oxidants and ROS. It is well known that ROS are capable of damaging biomolecules like DNA.

Previous studies showed that monocytes are severely impaired in BER, SSB and DSB repair as they do not express PARP-1, XRCC1, ligase IIIα and DNA-PKcs (Briegert and Kaina 2007; Bauer *et al.* 2011). This DNA repair defect makes monocytes susceptible to methylating and oxidising genotoxins as DNA strand breaks accumulate in the cell and lead to activation of the DDR with subsequent induction of apoptosis pathways. Cytokine-induced differentiation into macrophages or DCs abolishes the DNA repair defect and leads to genotoxic resistance.

These observations led to the following questions:

- Do neutrophilic granulocytes display a similar DNA repair defect as monocytes?
- Does the DNA repair defect of monocytes lead to DNA damage-mediated cell death after treatment with the anti-malarial drug artesunate?
- Can the oxidative burst of myeloid immune cells be measured *in vitro*?
- Does the oxidative burst lead to auto-intoxication of the producing myeloid cells?
- Does the oxidative burst from adjacent cells damage the DNA and subsequently kill repair defective monocytes?
- Are ROS-damaged monocytes still able to differentiate into macrophages?
- Are lymphoid cells also susceptible to the oxidative burst of myeloid cells?
- Is the DNA repair protein XRCC1 regulated by promoter methylation?
- Which transcription factors bind to the XRCC1 promoter?
- Are other DNA repair proteins differentially expressed in monocytes compared to macrophages?

3 Material and Methods

3.1 Material

3.1.1 Equipment

Equipment	Manufacturer
[137-Cs]-Source Gammacell Irradiator 2000	Molsgaard Medical, Denmark
FACS Canto II	BD Biosciences, Heidelberg
Hemocytometer / Neubauer Chamber	Superior Marienfeld, Landau-Konigshofen
Incubator Hera Cell 150	Heraeus, Munich
Infrared imaging system Odyssey 9120	LI-COR, Bad Homburg
Laser Scanning Microscope LSM 710	Carl Zeiss, Oberkochen
LS and MS columns	Miltenyi Biotec, Bergisch Gladbach
Luminometer Tristar2 Multimode reader LB942	Berthold Technologies GmbH &Co KG, Bad Wildbach
MAC's MIX Tube Rotator	Miltenyi Biotec, Bergisch Gladbach
Microplate Reader Sunrise	Tecan Schweiz AG, Männderdorf, Switzerland
Microscope Axiovert 35	Carl Zeiss, Oberkochen
Photometer, Multiskan EX	Thermo Fisher Scientific Inc., Waltham, MA, USA
SDS-PAGE chamber TransBlot Cell	Bio-Rad, Hercules, CA, USA
SDS-PAGE PowerPac Basic 75W	Bio-Rad, Hercules, CA, USA
Sonifier Cell Disruptor 250	Branson Ultrasonics Corporation, Danbury, CT, USA
T100 Thermal Cycler	Bio-Rad, Hercules, CA, USA
UV-Vis Spectrophotometer NanoDrop 2000	Thermo Fisher Scientific Inc., Waltham, MA, USA
Olympus BX50 equipped with a ColorView camera	Olympus, Münster
Centrifuge Megafuge 1.0R	Heraeus, Munich
Thermomixer comfort	Eppendorf AG, Hamburg
PyroMark Q24 Sequencing instrument	Qiagen, Hilden
PyroMark Q24 Vacuum Workstation	Qiagen, Hilden

3.1.2 Consumables

Consumable	Manufacturer
10 ml plastic pipettes	Greiner Bio-One, Frickenhausen

15/50 ml Greiner tubes	Greiner Bio-One, Frickenhausen
6 well plates	Corning/Costar, Bodenheim
6/12/24/48/96 well plates	Greiner Bio-One, Frickenhausen
Micro-hematocrit glass capillary tube	Marienfeld superior, Lauda Königshofen
Nitrocellulose membrane 0.2 µm	Protran, Amersham, GE Healthcare, Dassel
Nunc EasYFlasks (75 cm^2)	Thermo Fisher Scientific, Waltham
Superfrost slides	Gerhard Menzel GmbH/Thermo Fisher, Braunschweig
Whatman- Filter	GE Healthcare, Freiburg

3.1.3 Software

Software	**Developer**
Adobe Photoshop 7.0	Adobe Systems, Munich
Cell^A Imaging Software for Life Science Microscopy	Olympus Soft Imaging Solutions, Münster
Citavi 5.7	Swiss Academic Software GmbH
Comet IV software	Perceptive Instruments Ltd., Bury St Edmunds, UK
FACSDiva Software 6.0 and 8.0	BD Biosciences, Heidelberg
Flowing Software 2.5.1	www.flowingsoftware.btk.fi
GeneSnap Viewer 3.3.4	Syngene, Cambridge, UK
GraphPad Prism 6.0	GraphPad Software, La Jolla, CA, USA
ICE software	Berthold Technologies, Bad Wildbad
ImageJ	https://imagej.nih.gov/ij/
Odyssey Version 3.0	LI-COR, Lincoln, NE, USA
Patch 1.0	http://gene-regulation.com/index2.html geneXplain GmbH, Am Exer 10B, 38302 Wolfenbüttel
Plasma-DNA-1.4.2	www.plasmadna.net/
PyroMark Q24 Software	Qiagen, Hilden
SnapGene Viewer 3.3.4	GSL Biotech, Chicago, IL, USA
ZEISS ZEN Imaging Software 2.1	Carl Zeiss GmbH, Oberkochen

3.1.4 Chemicals

Name	**Manufacturer**
2',7'-dichlorofluorescin diacetate	Sigma Aldrich, Steinheim
37 % formaldehyde	Carl Roth GmbH & Co. KG, Karlsruhe

Accutase	Sigma-Aldrich, Steinheim PAA, Pasching, Austria
Acetic acid	Carl Roth GmbH & Co. KG, Karlsruhe
Acetone	Carl Roth GmbH & Co. KG, Karlsruhe
Acrylamide-, Bisacrylamide Rotiphorese Gel 40 (37.5:1)	Carl Roth GmbH & Co. KG, Karlsruhe
Agarose	Carl Roth GmbH & Co. KG, Karlsruhe
Ammonium acetate (NH_4Ac)	Carl Roth GmbH & Co. KG, Karlsruhe
Ammonium persulfate	Carl Roth GmbH & Co. KG, Karlsruhe
Annexin V APC	BioLegend/BIOZOL, Munich
Annexin V FITC	Miltenyi Biotec, Bergisch Gladbach
Artesunate	Dafra Pharma International, Turnhout, Belgium
Benzoylbenzoyl-ATP (bzATP)	Sigma-Aldrich, Steinheim Jena Bioscience, Jena
Bicine	Carl Roth GmbH & Co. KG, Karlsruhe
Brilliant blue G	Sigma-Aldrich, Steinheim
Bromphenol blue	Sigma-Aldrich, Steinheim
BSA Albumin Fraction V	Carl Roth GmbH & Co. KG, Karlsruhe
Calcium chloride ($CaCl_2$)	Carl Roth GmbH & Co. KG, Karlsruhe
Carboxyfluorescein succinimidyl ester (CFSE)	Fluka/Sigma-Aldrich, Steinheim
Casein	Carl Roth GmbH & Co. KG, Karlsruhe
CM-H2DCFDA	Life Technologies GmbH, Darmstadt
Dextran sulfate sodium salt	Sigma-Aldrich, Steinheim
Dimethyl sulfoxide (DMSO)	Carl Roth GmbH & Co. KG, Karlsruhe
Dipotassium hydrogenphosphate (K_2HPO_4)	Carl Roth GmbH & Co. KG, Karlsruhe
Disodium hydrogen phosphate (Na_2HPO_4)	Carl Roth GmbH & Co. KG, Karlsruhe
Dithiothreitol (DTT)	Sigma-Aldrich, Steinheim
Ethanol (EtOH)	Carl Roth GmbH & Co. KG, Karlsruhe
Ethylenediaminetetraacetic acid (EDTA)	Carl Roth GmbH & Co. KG, Karlsruhe
Ficoll-Hypaque (Histopaque®-1077)	Sigma-Aldrich, Steinheim
Formamidopyrimidine DNA glycosylase (FPG)	Prof. Bernd Epe, Johannes Gutenberg University Mainz, Germany
Glucose	Carl Roth GmbH & Co. KG, Karlsruhe
Glycerol	Carl Roth GmbH & Co. KG, Karlsruhe
Glycine	Carl Roth GmbH & Co. KG, Karlsruhe
Glycogen (stock 20 mg/ml)	Roche Diagnostics GmbH, Mannheim

HEPES	Carl Roth GmbH & Co. KG, Karlsruhe
Horseradish peroxidase (HRP)	Prof. Jörg Fahrer, Justus Liebig University, Gießen, Germany
Hydrogen chloride (HCl)	Sigma-Aldrich, Steinheim
Hydrogen peroxide (H_2O_2, 30 % w/w in H_2O)	Sigma-Aldrich, Steinheim
Low melting point agarose (UltraPure)	Invitrogen, Life Technologies, Darmstadt
LPS (*E.coli* 0111:B4)	Sigma-Aldrich, Steinheim
LPS (*E.coli* 0127:B8)	Sigma-Aldrich, Steinheim
Luminol	Sigma-Aldrich, Steinheim
Magnesium chloride ($MgCl_2$)	Carl Roth GmbH & Co. KG, Karlsruhe
Methanol	Carl Roth GmbH & Co. KG, Karlsruhe
Milk powder (blotting grade, low fat)	Carl Roth GmbH & Co. KG, Karlsruhe
N,*N'*-dimethylthiourea (DMTU)	Sigma-Aldrich, Steinheim
NAD^+	Sigma-Aldrich, Steinheim
Normal goat serum	Invitrogen, Life Technologies, Carlsbad, USA
NP-40	Fluka Chemie, Buchs, Schweiz
Optiprep (δ 1.32 g/ml)	ProgenBiotechnik GmbH, Heidelberg
Phenazine ethosulphate (PES)	Sigma-Aldrich, Steinheim
Phenylmethane sulfonyl fluoride (PMSF)	Sigma-Aldrich, Steinheim
Phorbol 12-myristate 13-acetate (PMA)	InvivoGen, Toulouse, France
Phosphoric acid (H_3PO_4, 85 % (w/v) in H_2O)	Carl Roth GmbH & Co. KG, Karlsruhe
Polyvinylpyrrolidone	Sigma-Aldrich, Steinheim
Ponceau S	Sigma-Aldrich, Steinheim
Potassium carbonate	Sigma-Aldrich, Steinheim
Potassium chloride (KCl)	Carl Roth GmbH & Co. KG, Karlsruhe
Potassium dihydrogen phosphate (KH_2PO_4)	Carl Roth GmbH & Co. KG, Karlsruhe
Potassium hydroxide (KOH)	Carl Roth GmbH & Co. KG, Karlsruhe
Propidium iodide	Sigma-Aldrich, Steinheim
Protease inhibitor (cOmplete, Mini)	Roche Diagnostics GmbH, Mannheim
Proteinase K	Roche Diagnostics GmbH, Mannheim
RNase A	Sigma-Aldrich, Steinheim
RNase T	Sigma-Aldrich, Steinheim
Roti® Phenol/Chloroform/Isoamylalcohol	Carl Roth GmbH & Co. KG, Karlsruhe
Roti®-Load 1 (4x concentrated)	Carl Roth GmbH & Co. KG, Karlsruhe

RPMI-1640	Gibco Life Technologies, Darmstadt
Silver nitrate	Carl Roth GmbH & Co. KG, Karlsruhe
Sodium chloride (NaCl)	Carl Roth GmbH & Co. KG, Karlsruhe
Sodium dodecyl sulfate (SDS)	Carl Roth GmbH & Co. KG, Karlsruhe
Sodium fluoride (NaF)	Sigma-Aldrich, Steinheim
Sodium hydroxide (NaOH)	Carl Roth GmbH & Co. KG, Karlsruhe
Sodium orthovanadate (Na_3VO_4)	Sigma-Aldrich, Steinheim
Sodium thiosulfate pentahydrate salt	Carl Roth GmbH & Co. KG, Karlsruhe
Streptavidin Sepharose High-Performance beads	GE Healthcare, Darmstadt
tert-Butyl hydroperoxide (*t*-BOOH)	Sigma-Aldrich, Steinheim
Thiazolyl blue formazan (MTT)	Sigma-Aldrich, Steinheim
TO-PRO®-3 (ToPro3)	Invitrogen, Life Technologies, Darmstadt
Tris	Carl Roth GmbH & Co. KG, Karlsruhe
Triton X-100	Carl Roth GmbH & Co. KG, Karlsruhe
Trypan blue	Sigma-Aldrich, Steinheim
Tween20	Carl Roth GmbH & Co. KG, Karlsruhe
Urea	Carl Roth GmbH & Co. KG, Karlsruhe
Vectashield	Vector Labs, Burlingame, CA, USA
X-Vivo 15	Lonza, Basel, Switzerland
β-mercaptoethanol	Sigma-Aldrich, Steinheim

3.1.5 Antibodies

Flow Cytometry

Name/Antigen	**Company**
anti-CD3-PE (BW264/56)	Miltenyi Biotec, Bergisch Gladbach
anti-CD8-APC (BW135/80)	Miltenyi Biotec, Bergisch Gladbach
anti-CD14-Vioblue (TÜK4)	Miltenyi Biotec, Bergisch Gladbach
anti-CD15-APC (VIMC6)	Miltenyi Biotec, Bergisch Gladbach

For flow cytometric analysis of blood cells, antibodies were used 1 µl per ~0.5 to 1 x10^6 cells in 100 µl PBS.

Immunofluorescence

Primary Antibody	**Origin**	**Dilution**	**Company**
anti-53BP1 (A300-272A)	Rabbit polyclonal	1:1000	Bethyl Laboratories, Inc

anti-8-oxoG, 8-OxodG (15A3)	Mouse monoclonal	1:1000	Abcam, Cambridge, UK
anti-CD14 (2D-15C, FMC-32)	Mouse monoclonal	1:200 to 1:400	Abcam, Cambridge, UK
anti-CD15 (H198)	Mouse monoclonal	1:1000	BD Pharmingen
anti-CD3 (KT3)	Rat monoclonal	1:200 to 1:400	AbD Serotec, Bio-Rad Munich
anti-CD68	Mouse monoclonal	1:200 to 1:400	Acris Antibodies GmbH, Herford, Germany
anti-PAR (10H)	Mouse monoclonal	1:300	University of Konstanz, Germany, Prof. A. Bürkle
anti-pATM (phospho S1981) (EP1890Y)	Rabbit monoclonal	1:1000	Abcam, Cambridge, UK
anti-pKAP1 (phospho S824) A300-767A-T	Rabbit polyclonal	1:1000	Bethyl Laboratories
anti-XRCC1 (EPR4389(2))	Rabbit monoclonal	1:400 to 1:1000	Abcam, Cambridge, UK
anti-γH2AX (phospho S139) (EP854(2)Y)	Rabbit monoclonal	1:400 to 1:1000	Abcam, Cambridge, UK
Secondary antibodies	**Origin**	**Dilution**	**Company**
F(ab'2) anti-mouse IgG (H+L), Alexa Fluor 488 conjugated, A11017	Goat polyclonal	1:400	Thermo Fisher Scientific
F(ab'2) anti-rabbit IgG (H+L), Alexa Fluor 488 conjugated, A11070	Goat polyclonal	1:300	Thermo Fisher Scientific
anti-mouse IgG (H+L) Cy3 conjugated, 115 165 146	Goat polyclonal	1:500	Dianova, Hamburg
anti-rat IgG (H+L) Cy3 conjugated, 112 165 143	Goat polyclonal	1:500	Jackson Immuno Research, Suffolk, UK

Western Blot

Primary antibody	**Host**	**Dilution**	**Company**
anti-CHK2 (2662)	Rabbit polyclonal	1:1000	Cell Signaling, USA
anti-ERK2 (C14)	Rabbit polyclonal	1:2000	Santa Cruz Biotechnology, Heidelberg
anti-GAPDH (6C5)	Mouse Monoclonal	1:2000	Santa Cruz Biotechnology, Heidelberg
anti-H2AX	Rabbit	1:1000	Bethyl Laboratories

(A300-082A)	Polyclonal		
anti-HSP90 (F-8)	Mouse monoclonal	1:2000	Santa Cruz Biotechnology, Heidelberg
anti-Ligase III (clone 7)	Mouse Monoclonal	1:1000	BD Transduction Laboratories
anti-p53 (BP 53.12)	Mouse Monoclonal	1:1000	Santa Cruz Biotechnology, Heidelberg
anti-PARP-1 (c-II-10)	Mouse monoclonal	1:300	University of Konstanz, Germany, Prof. A. Bürkle
anti-pCHK2 (phospho Thr68) (2661)	Rabbit polyclonal	1:1000	Cell Signaling, USA
anti-p-p53 (phospho Ser46) (2521)	Rabbit polyclonal	1:1000	Cell Signaling, USA
anti-β-Actin	Mouse monoclonal	1:2000	Santa Cruz Biotechnology, Heidelberg
Secondary antibodies	**Origin**	**Dilution**	**Company**
IgG anti-mouse IRDye 680	Donkey	1:10,000	LI-COR Biosciences, Bad Homburg
IgG anti-rabbit IRDye 680	Donkey	1:10,000	LI-COR Biosciences, Bad Homburg
IgG anti-mouse IRDye 800CW	Donkey	1:10,000	LI-COR Biosciences, Bad Homburg
IgG anti-rabbit IRDye 800CW	Donkey	1:10,000	LI-COR Biosciences, Bad Homburg

3.1.6 Cells

Buffy coats were supplied by the blood bank of the University Medical Center Mainz, Germany. Blood was routinely tested for hepatitis A, B, C and E, syphilis, HIV and CMV.

Blood from the fingertip was supplied by healthy volunteers in the lab.

3.1.7 Cytokines and inhibitors

Cytokine	Stock	Final concentration	Manufacturer
GM-CSF	8x 10^5 U/ml	800 U/ml	Sanofi Aventis, USA
M-CSF	5 µg/ml	50 ng/ml	Miltenyi Biotec, Bergisch Gladbach
IL-4	50.000 U/ml	50 U/ml	Miltenyi Biotec, Bergisch Gladbach
SB203580 p38 MAPK	10 mM	10 µM	Sigma-Aldrich, Steinheim

SP600125 JNK	25 mM	25 µM	Invitrogen, San Diego, USA
2-Hydroxyglutarate	200 mM	1 mM	Sigma-Aldrich, Steinheim
DPI	100 mM	100 µM	Enzo Life Sciences GmbH, Lörrach

3.1.8 Primers

Primers were ordered from Thermo Fisher Scientific, Darmstadt or Eurofins, Mannheim.

Table 2: Primers used for biotinylated XRCC1 promoter PCR products

Name	5' → 3'	Information
BIO_XRCC1_1_for	CCCAAGGAAGCACCCAGTGT	Biotinylated PCR product 1
XRCC1_1_rev	GCCTCGGCCTCTCAAAGTGCT	
BIO_XRCC1_2_for	AGCACTTTGAGAGGCCGAGGC	Biotinylated PCR product 2
XRCC1_2_rev	AATGACGTCCGAACCCTGCTT	
BIO_XRCC1_3_for	AAGCAGGGTTCGGACGTCATT	Biotinylated PCR product 3
XRCC1_3_rev	CCCTCACCGAGTCCTGGC	

Table 3: Primers used for pyrosequencing of the XRCC1 promoter

Name	5' → 3'	Information
R1XRCC1_for	TTTGGTTTTAGGTATAAGGTTGAAAGAGA	
R1XRCC1_seq	GTTGAAAGAGATTTGTTAATTTTT	Seq1
R1XRCC1_rev	CTTCTCTCTATCCCCTTACC	5'-biotinylated
R2XRCC1_for	GTAAGGGGATAGAGAGAAGAG	
R2XRCC1_seqA	TTGAGTTATTTGAAGAGATTTTGT	Seq2A
R2XRCC1_seqB	TTTATAAAAAATATAAAAATTAGT	Seq2B
R2XRCC1_rev	CCAAAAAATCCTCCCACTTCAA	5'-biotinylated
R3XRCC1_for	TTTGTTGTTAGGTTTTTAGAAAGTAGG	
R3XRCC1_seqA	GGTTTTTAGAAAGTAGGG	Seq3A
R3XRCC1_seqB	ATATTTTATTTTATTTTTTTGGTTA	Seq3B
R3XRCC1_rev	CCAACCTCCCCCATACAA	5'-biotinylated

3.1.9 Kits

Name	Company

CD14 MicroBeads	Miltenyi Biotec, Bergisch Gladbach
Verso cDNA Kit	Thermo Fisher Scientific, Darmstadt
EZ DNA Methylation Kit	Zymo Research, Freiburg
PyroMark Q24 Advanced Reagents kit	Qiagen, Hilden
PyroMark PCR Master Mix	Qiagen, Hilden
Q5® High-Fidelity PCR Ki	New England BioLabs, Frankfurt am Main

3.1.10 Buffers and solutions

Cell isolation	
MACS buffer Filtered through 0.22 µm bottle top filter	2 mM EDTA 0.5 % BSA in PBS
CFSE stock solution	5 mM CFSE in ddH_2O
PBS pH 7.4	137 mM NaCl 2.7 mM KCl 6.5 mM Na_2HPO_4 1.5 mM KH_2PO_4 in ddH_2O
Aerated PBS complete	0.5 mM $MgCl_2$ 0.7 mM $CaCl_2$ 0.1 % glucose in PBS
Optiprep dilution buffer	0.85 % NaCl 1 mM EDTA 20 mM HEPES pH 7.4.
Cell death	
1x Annexin V binding buffer	10 mM HEPES 140 mM NaCl 2.5 mM $CaCl_2$ 0.1 % BSA pH 7.4
Propidium iodide stock	1 mg/ml in ddH_2O Stored at 4°C in the dark
Propidium iodide working concentration	50 µg/ml in H_2O Stored at 4°C in the dark
DNA extraction	
TE9 buffer	500 mM Tris 20 mM EDTA 10 mM NaCl pH 9.0
Proteinase K stock solution	25 mg/ml in ddH_2O, store at -20°C
TE9 cell lysis buffer	304 µl TE9 buffer 16 µl 20 %SDS 8 µl Proteinase K
EtOH:NH_4Ac master mix	35 ml 100 % ethanol 5 ml 7.5 M ammonium acetate

Comet Assay	
Alkaline electrophoresis buffer	300 mM NaOH 1 mM EDTA > pH 13
Buffer F	40 mM HEPES 0.1 M KCl, 0.5 mM EDTA 0.2 % BSA pH 8.0
Lysis buffer	2.5 M NaCl 100 mM EDTA 10 mM Tris 10 % DMSO – added fresh 1 % Triton X-100, pH 10 – added fresh
Neutralisation buffer	0.4 M Tris, pH7.5 in ddH_2O
SDS-PAGE and Western Blot	
Whole cell extract lysis buffer	25 mM Tris-HCl pH 8.0 500 mM NaCl 1 mM EDTA 1 mM PMSF 2 mM DTT 1 mM sodium orthovanadate 0.5 % NP-40 1x protease inhibitor (cOmplete, Mini)
Nuclear protein extract – buffer A	10 mM HEPES-KOH, pH 7.9 1.5 mM $MgCl_2$ 10 mM KCl 1 mM DTT 2 mM NaF 5 mM sodium orthovanadate 1x protease inhibitor (cOmplete, Mini)
Nuclear protein extract – buffer B	20 mM HEPES-KOH, pH 7.9 1.5 mM $MgCl_2$ 420 mM NaCl 0.5 mM EDTA 25 % glycerol 1 mM DTT 2 mM NaF 5 mM sodium orthovanadate 1x protease inhibitor (cOmplete, Mini)
Nuclear protein extract – isotonic buffer	10 mM Tris-HCl, pH 7.4 150 mM NaCl
Granulocyte lysis buffer (Kurosawa *et al.* 2003)	6 M urea 2 % SDS 0.5 % glycerol 2 % β-mercaptoethanol 50 mM Tris, pH 6.8 0.1 % bromphenol blue
Bradford reagent	0.01 % Brilliant blue G 8.5 % phosphoric acid 4.75 % ethanol ad 500 ml ddH_2O filtered and stored at 4°C in the dark

10 % APS	1 g ammonium persulfate ad 10 ml ddH_2O
1x SDS-PAGE running buffer	25 mM Tris Base 192 mM glycine 0.1 % (w/v) SDS
1x Western Blot transfer buffer	25 mM Tris Base 192 mM glycine 0.2 % SDS 20 % (v/v) methanol
Ponceau S	0.2 % Ponceau S 5 % acetic acid
TBS	20 mM Tris-HCl 150 mM NaCl pH 7.4
TBS-T	0.1 % (v/v) Tween20 in 1x TBS
PBS-T	0.1 % (v/v) Tween20 In 1x PBS
Silver nitrate detection of proteins	
Basic developer for silver staining	3 % (w/v) potassium carbonate 0.05 % (v/v) 37 % formaldehyde 0.00025 % (w/v) sodium thiosulfate pentahydrate salt
Fixation solution	30 % (v/v) ethanol 10 % (v/v) acetic acid in ddH_2O
Rinse solution	20 % (v/v) ethanol in ddH_2O
Sensitisation solution	0.02 % (w/v) sodium thiosulfate pentahydrate – prepared fresh
Silver nitrate solution	12 mM silver nitrate in ddH_2O, stored in the dark
Stop solution	4 % (w/v) Tris 2 % (v/v) acetic acid prepared fresh
1x NuPAGE lysis buffer (30 µl)	7.5 µl 4x NuPAGE 3 µl 1 M DTT x µl sample + x µl ddH_2O
Immunofluorescence	
Alkaline solution	70 mM NaOH 140 mM NaCl 40 % (v/v) methanol
4 % paraformaldehyde	4 g PFA in 10 ml PBS + 50 ml dH_2O dissolved with NaOH pH 7.4 adjusted with HCl ad 100 ml ddH_2O
RNase A	10 mg/ml RNase A in ddH_2O
RNase T	5000 U/ml RNase T in ddH_2O
Pepsin	60 µg/ml pepsin/HCl pH 6.0
Proteinase K	2 µg/ml Proteinase K 20 mM Tris/HCl

	2 mM $CaCl_2$ pH 7.5
Wash solution (after Proteinase K)	0.2 % (w/v) glycine in PBS
Blocking solution	0.5 % casein in PBS-T
Wash Solution (after 1st antibody)	0.05 % (v/v) Tween 20 in PBS
Tris-NaCl buffer	0.1 M Tris-HCl 2 mM $MgCl_2$ 1 M NaCl 0.05 % Triton X-100 pH 7.5
NAD^+ cycling assay	
1 mg/ml ADH	10 mg ADH in 10 ml 0.1 M Bicine stored as 1 ml aliquots at -20°C
Diluent	0.5 M NaOH 0.25 M H_3PO_4
MTT solution (10 mM)	50 mg MTT 12.07 ml ddH_2O
PES solution (40 mM)	130 mg PES 10 ml ddH_2O
Phosphate buffer pH 7.5	0.33 M K_2HPO_4 0.33 M KH_2PO_4 pH adjusted with KOH
Premix pH 8.0	3.92 g Bicine adjusted pH with NaOH 200 mg BSA 375 mg EDTA 14 % (v/v) ethanol 20 % (v/v) MTT solution ad 50 ml with ddH_20 stored at 4°C in the dark
Reaction mix	5 parts premix (7.2 ml) 1 part PES solution (1.44 ml) 1 part ADH solution (1.44 ml) Prepared fresh
Reverse ChIP for Proteomics	
Buffer DW	10 mM Tris pH 8.0 2 M NaCl 0.5 mM EDTA 0.03 % NP-40
Blocking buffer	20 mM HEPES-NaOH 0.05 mg/ml BSA 0.3 M KCl 0.02 % NP-40 5 mg/ml polyvinylpyrrolidone 0.05 mg/ml glycogen 2.5 mM DTT
Buffer G	20 mM Tris pH 7.4 10 % glycerol 0.1 M KCl 0.2 mM EDTA

	10 mM potassium glutamate 0.04 % NP- 40 2 mM DTT 1x protease inhibitor (cOmplete, Mini)

3.2 Methods

3.2.1 Isolation of leukocytes from buffy coat – monocytes and T cells

For the isolation of human PBMC, buffy coats from healthy donors were obtained from the blood bank of the University Medical Center Mainz, Germany. The PBMC were isolated by Ficoll-Hypaque density centrifugation. 35 ml of blood were underlain with 15 ml Ficoll-Hypaque in a 50 ml Greiner tube and samples were centrifuged at 2500 rpm for 40 min at RT without brake. Afterwards, different layers could be distinguished: erythrocytes were enriched at the bottom of the tube, then the Ficoll fraction, then the PBMC as a whitish-yellow ring and at the top the plasma fraction. Plasma was collected with a 10 ml pipette and then transferred into fresh 50 ml tubes. The plasma was heat-inactivated at 56°C in a water bath for 30 min. It was centrifuged twice at 4000 rpm for 5 min at RT and the supernatant was collected. PBMC were carefully collected with a 10 ml pipette and transferred into fresh 50 ml tubes. The cells were washed four times with MACS buffer: they were centrifuged at 1500 rpm for 10 min at RT, then at 1200 rpm and twice at 900 rpm. After the third washing step, 10 µl of the cell suspension was mixed with 10 µl trypan blue and 80 µl PBS and counted using a hemocytometer. If many cells (~20-30 %) tested positive for trypan blue staining samples were discarded. Samples with excessively high numbers of cells were also avoided (more than 1 x 10^9 cells per 50 ml tube).

Cells were seeded at 1.5 x 10^7 cells / 3 ml / well in six-well plates (Corning/Costar) in RPMI-1640 + 1.5 % heat-inactivated autologous plasma for 30 min at 37°C and 5 % CO_2. Non-adherent T cells were gently removed and transferred into fresh Nunc EasYFlasks (75 cm^2) for a second step of adherence to reduce contamination with adhering monocytes and granulocytes. Cells were harvested and seeded 1 x 10^6 cells/ml in X-Vivo 15.

The adherent cells represented enriched monocytes, which were incubated in RPMI-1640 + 10 % heat-inactivated autologous plasma for at least two hours to detach from the plate again. Monocytes were harvested and cultured at a density of 1 x 10^6 cells/ml in X-Vivo 15.

3.2.2 Generation of macrophages and dendritic cells from monocytes

For the generation of macrophages, freshly isolated monocytes were seeded in X-Vivo 15 + 800 U/ml GM-CSF and incubated for six days. For 24-well plates, cells were seeded at 0.7 x 10^6 cells in 1 ml. For six-well plates, 2.5-3 x 10^6 cells were used. On day six, the old medium was removed, cells were washed with PBS and fresh medium was added. Only non-adherent cells were considered macrophages and used for experiments. Alternatively, macrophages were generated by adding 50 ng/ml M-CSF to the cells and incubating them for six days (Wallner *et al.* 2016).

Immature DCs were generated by adding 800 U/ml GM-CSF and 50 U/ml IL-4 to isolated monocytes. The cells were fed on the third and sixth day with X-Vivo 15, 1600 U/ml GM-CSF and 50 U/ml IL-4. iDCs in suspension were harvested on day eight, adherent cells were discarded.

3.2.3 Isolation of leukocytes from buffy coat – granulocytes

Granulocytes were isolated by the Optiprep density method. Two Optiprep solutions of different densities (1.077 g/ml and 1.095 g/ml) were prepared from Optiprep (density 1.32 g/ml) diluted in 0.85 % NaCl, 1 mM EDTA and 20 mM HEPES pH 7.4. Then, 9 ml blood from buffy coats was mixed with 1 ml 6 % dextran sulphate sodium salt dissolved in 0.85 % NaCl buffer and incubated for 1 h at RT until a clear upper phase became visible. The upper phase was transferred into a fresh 15 ml tube containing an upper layer of 4 ml Optiprep (1.077 g/ml) and a lower layer of 4 ml Optiprep (1.095 g/ml). The tubes were centrifuged at 1900 rpm for 30 min without brake. Two rings of cells became visible and the lower one was collected. The cells were washed in MACS buffer and then seeded in RPMI-1640 + 1.5 % heat-inactivated plasma for 30 min at 37°C. Non-adherent cells were removed and adherent granulocytes were allowed to detach in the presence of RPMI-1640 + 10 % heat-inactivated plasma for 2 h. Afterwards, granulocytes were seeded at 1 x 10^6 cells/ml in X-Vivo 15 medium. For purity testing, neutrophils were stained for the surface marker CD15 and checked via flow cytometry or immunofluorescence microscopy.

3.2.4 Fresh blood from the fingertip for blood smears

Drops of blood were collected from the fingertip using a lancing aid. The blood was collected in sodium-heparinised micro-haematocrit glass capillary tubes. The glass tubes were stored in 15 ml Greiner tubes for transport and irradiation. Afterwards, the blood was spread onto glass slides by tapping the glass tube onto the slide or adding a drop of PBS into the glass tube. The sample was spread onto the whole area of the glass slide and air-dried. Samples were then prepared for immunofluorescence staining (see section 3.2.12).

3.2.5 Detection of extracellular and intracellular ROS

For the detection of intracellular ROS production, a flow cytometry-based assay was used. Cells were loaded with either CM-H2DCFA (Life Technologies) or 2',7'-dichlorofluorescin diacetate (Sigma-Aldrich). CM-H2DCFA is a chloromethyl-derivative of 2',7'dichlorofluorescin diacetate with a higher retention time in living cells. Both dyes diffuse into the cell where they react with ROS and become fluorescent. Both ROS dyes were solubilised in DMSO and stored at -20°C. For experiments, 1 x 10^6 cells/ml X-Vivo 15 were loaded with either 10 µM CM-H2DCFDA or 100 µM 2',7'-dichlorofluorescin diacetate. Cells were incubated at 37°C and 5 % CO_2 for 30 min. After loading, cells were immediately treated with LPS, PMA or *t*-BOOH. Adherent macrophages were detached from the plate by adding 500 µl accutase for 20 min at 37°C. Cells were washed with PBS, pelleted by centrifugation and resuspended in 200-300 µl PBS before they were analysed by flow cytometry. At least 10,000 cells were counted and the mean fluorescence intensity at 530/30 nm was determined using the FACS Canto II Diva software.

The detection of extracellular ROS has been described elsewhere (Chou *et al.* 2004). Briefly, 0.5 x 10^6 cells were suspended in 500 µl PBS supplemented with 0.5 mM $MgCl_2$, 0.7 mM $CaCl_2$ and 0.1 % glucose (aerated PBS complete). 10 µg/ml horseradish peroxidase (HRP) and 10 µM luminol were added to the cells before the ROS burst was induced with 100 ng/ml PMA. If the ROS burst was induced with LPS/bzATP, cells were

primed with 1 µg/ml LPS for 16 h (Pfeiffer *et al.* 2007). Then, cells were incubated in PBS complete with luminol and HRP and 250 µM bzATP was added for the ROS burst induction. The chemiluminescence was measured in a Berthold TriStar^2 LB 942 luminometer at RT for the indicated time points. The area under the curve (AUC) was determined for the quantification of ROS.

3.2.6 Co-culture of monocytes or T cells with activated phagocytes

Monocyte-derived macrophages were generated in 24-well plates. On day six, non-adherent cells were washed away and adherent macrophages were incubated in the presence of CFSE (5 µM for 8 min in the dark at RT) for labelling. Thereafter, the cells were washed twice in PBS + 0.5 % BSA and once in PBS before 500 µl X-Vivo 15 was added to each well. Cells were equilibrated for at least one hour at 37°C before they were used for co-culture experiments. Granulocytes were isolated on the same day as monocytes. They were labelled with CFSE similar to the macrophages, seeded at 1 x 10^6 cells/ml in X-Vivo 15 and equilibrated for at least one hour at 37°C before the experiment.

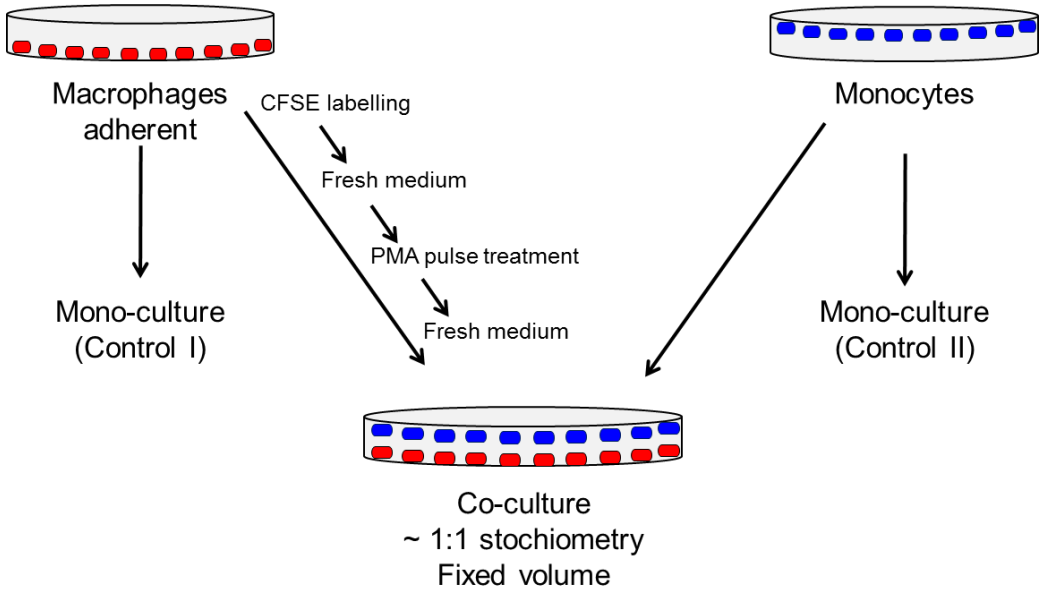

Fig. 6: Scheme for co-culture experiments
First, macrophages were labelled with CFSE. Then they were supplied with fresh medium and equilibrated for > 1 h. They were pulse-activated with PMA for 15 min, washed with PBS and supplied with fresh medium before 0.5 x 106 monocytes in 500 µl medium were added to the activated macrophages. In parallel, macrophages and monocytes in mono-culture were treated the same way.

Monocytes were freshly isolated on day six and resuspended at 1 x 10^6 cells/ml in X-Vivo 15. For co-culture experiments, 0.5 x 10^6 monocytes were added to macrophages (approximately 1:1 ratio in a 1 ml assay) before treatment. For PMA-pulse treatment, macrophages were treated with 100 ng/ml PMA for 15 min at 37°C; then the medium was removed, cells were washed with PBS and monocytes were added immediately. Granulocytes were treated with 100 ng/ml PMA for 10 min in a 15 ml Greiner tube, then they were washed with PBS, centrifuged at 1400 rpm for 5 min and resuspended at 1 x 10^6 cells/ml with X-Vivo 15 before they were added to monocytes in a 24-well plate. Continuous PMA treatment for 24 h or 48 h means that both cell types were exposed to PMA for the period of the assay (Fig. 6). DMSO was used as solvent control. After treatment, monocytes and macrophages or monocytes and granulocytes were carefully removed from

the plates by accutase (15 min, 37°C). Monocytes were stained for CD14 marker before they were subjected to flow cytometry. Macrophages and granulocytes were distinguished from monocytes by their CFSE signal. For Annexin V staining see section 3.2.7. For co-culture experiments with LPS/bzATP, monocytes and macrophages were primed with 1 µg/ml LPS (0127:B8) for 16 h before macrophages were pulse-treated with 250 µM bzATP for 15 min. The medium was removed, macrophages were washed with PBS and monocytes were added. Monocytes were stained for CD14 and gated by exclusion of CFSE-positive macrophages and concomitant CD14 positivity. Cell death was measured 24 h or 48 h after treatment.

For co-culture experiments using T cells, macrophages were not stained with CFSE. Freshly isolated PBLs were suspended at 1 x 10^6 cells/ml in X-Vivo 15 and 0.5 x 10^6 cells were added to PMA-activated macrophages. For cell death quantification using flow cytometry, T cells were harvested and gated for CD3+ CD8+ cytotoxic T cells specifically.

In parallel to the co-culture experiments, cells were also treated with PMA or solvent in mono-culture settings.

3.2.7 Quantification of cell death using Annexin V / PI

After genotoxic treatment, cells were incubated for the indicated time points (*e.g.* 24 h or 48 h). The medium was collected, the cells were washed with PBS, which was also collected, and adherent cells were incubated with accutase for 15 – 20 min at 37°C to detach from the plate. Cells were carefully removed by pipetting up and down. Samples were centrifuged at 1400 rpm for 5 min at 4°C. For CD marker detection, cells were resuspended in 100 µl PBS + 1 µl of CD antibody and incubated for 30 min on ice in the dark. Cells were washed with 2 ml PBS and centrifuged at 1400 rpm for 5 min at 4°C. Cells were resuspended in 25 – 50 µl 1x Annexin V binding buffer containing 1.25 – 2.0 µl Annexin V-FITC or Annexin V-APC for 20 min on ice in the dark. Then, samples were topped up with 220 – 440 µl 1x Annexin V binding buffer containing 5 – 10 µl PI (stock: 50 µg/ml). Cell death was measured using a FACS Canto II and data was analysed using the FACS Canto II Diva software.

If the emission of the CD antibody fluorophore overlapped with the emission pattern of PI, PI was not added to the cells and only Annexin V was used to measure cell death. Viable cells have intact plasma membranes. Therefore, phosphatidylserine (PS) residues on the intracellular side of the cell are not accessible for Annexin V. Viable cells stain Annexin V and PI negative. Cells undergoing apoptosis flip PS to the outside and can be stained with Annexin V but remain negative for PI which binds to DNA. Necrosis and late-stage apoptosis are associated with rupture of the plasma membrane. This allows Annexin V and PI to enter the cell.

3.2.8 Quantification of cell death using trypan blue

Freshly isolated PBMC were counted in a hemocytometer using trypan blue exclusion. PBMC were diluted 1:10 in PBS and 10 µl of the cell suspension were mixed with 80 µl PBS and 10 µl trypan blue. If more than 20 % were positive for trypan blue, samples were discarded.

3.2.9 CFSE staining of cells

Carboxyfluorescein succinimidyl ester (CFSE) is a fluorescent cell staining dye that covalently binds to amine groups of amino acids/proteins. The fluorescent signal is stable for a long time and is not transferred to other cells once it has been incorporated. It has an excitation and emission maximum at 490 nm and 520 nm, respectively. For CFSE staining, the medium was removed and cells were washed with PBS. Cells were stained with 5 µM CFSE for 8 min at RT in the dark. Then, cells were quickly washed with MACS buffer and washed twice with PBS before fresh X-Vivo 15 medium was added. Cells equilibrated 1-2 h at 37°C before experiments were started. In co-culture experiments, the CFSE-labelled cells were easily distinguishable from the other cell populations. CFSE staining was detected at 530/30 nm using the FACS Canto II.

3.2.10 Treatment with genotoxic agents

For genotoxic treatment of cells with H_2O_2, H_2O_2 working solutions were prepared shortly before the start of the treatment. The medium was removed and cells were exposed to 100 µM or 1 mM H_2O_2 in PBS for 5 – 10 min at 37°C. Then, H_2O_2 was removed and cells were washed with PBS. Fresh medium was added to the cells, or cells were fixed for immunofluorescence staining.

For *t*-BOOH, stock solutions of 10 mM were prepared in ddH_2O and stored at 4°C for up to one week. *t*-BOOH was added to the cells in medium. Pulse treatment ranged from 20 min to 1 h. Then, the medium was removed, cells were washed with PBS and fresh medium was added for further incubation.

The [137-Cs]-Source Gammacell Irradiator was used for treating cells with ionising irradiation. Cells were irradiated in 15 ml Greiner tubes or in 6 cm dishes. Positive controls were exposed to 2 Gy irradiation.

3.2.11 Comet assay for the detection of SSBs and oxidative DNA lesions

The single cell gel electrophoresis method, also known as the Comet assay, allows for the detection of DNA damage on a single cell level. Cells are embedded in agarose and denatured until only genomic DNA remains. In an electrical field, fragmented DNA moves to the anode forming a comet or tail which can be stained with PI and quantified. Intact genomic DNA is too big for migration and remains stationary. Depending on the buffer conditions, different types of DNA lesions can be detected: under pH neutral conditions DSBs can be measured. Under alkaline pH conditions, the hydrogen bonds between the two DNA strands separate and SSBs and DSBs, as well as alkali-labile lesions, can be analysed (Olive and Banáth 2006). The FPG-modified alkaline Comet assay allows for the detection of oxidative DNA lesions. The DNA is treated with formamidopyrimidine DNA glycosylase (FPG) which recognises several oxidative DNA lesions, *e.g.* 8-oxoG, 2,6-diamino-4-hydroxy-5-formamidopyrimidine (FapyG) and 4,6-diamino-5-formamidopyrimidine (FapyA) (Perlow-Poehnelt *et al.* 2004) and converts them into SSBs. The resulting comets are then compared to samples which were not treated with FPG, in order to assess the oxidative DNA damage burden.

For Comet assays, glass slides were washed with 100 % methanol and then flamed off over a Bunsen burner. Slides were coated with 1 % agarose on one side and allowed to dry. For

the alkaline Comet assay 1 - 2 x 10^5 cells were harvested after treatment and centrifuged at 1400 rpm for 5 min at 4°C. The cell pellet was resuspended in 120 µl 37°C low melting point agarose and the suspension was spread onto agarose-coated glass slides. The cell suspension solidified on ice before the samples were incubated in lysis buffer for 1 h at 4°C. Slides were transferred into an electrophoresis chamber and DNA unwound in alkaline electrophoresis buffer for 22 min at 4°C before electrophoresis was performed for 20 min at 0.74 V/cm and 300 mA. Slides were washed three times in neutralisation buffer. The samples were fixed in 100 % methanol for at least 10 min at -20°C, air-dried and stained with 50 µl PI (50 µg/ml) for detection.

For the FPG-modified alkaline Comet assay, two slides per sample were prepared. After incubation in lysis buffer, the slides were removed and equilibrated 2 x 5 min in buffer F at RT (Smith *et al.* 2006). FPG was diluted in buffer F and 50 µl was added to one slide of each sample. The other slide was incubated in buffer F only. Samples were incubated in a humid chamber at 37°C for 45 min. Similar to the normal alkaline Comet assay, samples were transferred into the alkaline electrophoresis buffer and unwound for 22 min at 4°C before electrophoresis was performed for 20 min at 0.74 V/cm and 300 mA. The slides were washed three times in neutralisation buffer and fixed in 100 % methanol for 10 min at -20°C. Comets were analysed by fluorescence microscopy using an Olympus BX50 equipped with a ColorView camera. At least 100 cells were scored in each experiment by means of Comet IV software. DNA damage was measured as tail intensity in percent which is the sum of all pixel intensity values in the comet tail:

Tail intensity (%) = (total intensity of tail DNA / total intensity of cell DNA) x 100

Alternatively the damage was measured as Olive Tail Moment (OTM). The OTM is computed as the summation of each tail intensity multiplied by its relative distance from the centre of the head to the centre of the tail length (also called tail moment length):

OTM = tail intensity (%) x tail moment length

3.2.12 Immunofluorescence staining of cells with CD markers and DDR factors

The isolation of blood cells from buffy coats is time-consuming and provides limited numbers of cells that can be used for assays (*e.g.* Western Blotting). Immunofluorescence staining was used as an alternative method for the detection of DNA repair factors as it required less cells. In addition, cells were also stained for CD marker expression to identify cell types in mixed populations or insufficiently isolated samples.

Immunostaining of CD markers and DNA repair factors: suspension cells (*e.g.* T cells) were harvested and centrifuged at 1400 rpm for 5 min. The cell pellet was resuspended in 5 – 10 µl PBS and 2 – 3 µl cell suspension was spread onto a cover slip and air-dried. Adherent cells were seeded on cover slips. Cells were fixed in ice-cold methanol:acetone (7:3 ratio) for 6 min at -20°C. The samples were rinsed with PBS and fixed with 2.5 % paraformaldehyde for 10 min at RT. Samples were washed in PBS and then blocked in 10 % normal goat serum in PBS for 1 h at RT. Primary antibodies were diluted in 1 % BSA in PBS-T and incubated overnight at 4°C in a humid chamber. For γH2AX detection, the antibody was diluted in 1 % BSA in PBS without Tween20. Samples were washed 3 x 5 min in PBS and incubated with secondary antibody for at least 1 h at RT. Afterwards, cover slips were washed 3 x 5 min in PBS and the DNA was stained with 100 µM ToPro3 for 15 min.

Samples were rinsed with PBS, mounted with one drop of Vectashield onto glass slides and sealed with nail polish.

Immunostaining for poly(ADP-ribose) (PAR): Cells were treated with 1 mM H_2O_2 in PBS for 5 min at 37°C before they were fixed in ice-cold methanol for 7 min at -20°C (Mangerich *et al.* 2016). Cover slips were washed 3 x 5 min in PBS and samples were blocked in 5 % dry milk in PBS-T for 1 h at RT. Primary PAR antibody was diluted 1:300 in blocking solution and incubated overnight at 4°C. Samples were washed 3 x 10 min and incubated with secondary antibody in blocking solution for 1 h at RT. Cover slips were washed 3 x 10 min in PBS and DNA was stained using ToPro3 as described above. Cover slips were mounted onto glass slides and sealed with nail polish.

Immunostaining of 8-oxoguanine (8-oxoG): Adherent cells were seeded on cover slips. Suspension cells were centrifuged at 1400 rpm for 5 min, resuspended in 5 – 10 µl PBS and 2 – 3 µl cell suspension was spread on Superfrost slides and dried for approximately 5 min before fixation with ice-cold 100 % methanol for 15 min. Cells were washed 2 x 5 min in PBS and slides were transferred into a humidified chamber. RNA was digested with RNase A (200 µg/ml) and RNase T (50 U/ml) in PBS for 1 h at 37°C. Cells were washed for 5 min in PBS before the DNA was denatured in alkaline solution on ice for 5 min. Slides were washed 3 x 5 min in PBS. Proteins were digested with 60 µg/ml pepsin for 10 min at 37°C. Slides were washed with PBS before the samples were digested with proteinase K for 10 min at 37°C. Slides were washed with 0.2 % glycine in PBS for 10 min. Samples were blocked in 0.5 % casein in PBS-T for 1 h at RT. Primary mouse 8-oxoG antibody was diluted 1:1000 in blocking solution and incubated overnight at 4°C. Samples were washed 5 x 5 min in PBS-T. Secondary goat α-mouse antibody was diluted 1:600 in blocking solution and samples incubated for 1 h at RT. Afterwards, slides were washed 5 x 5 min in PBS-T and 2 x 15 min in Tris-NaCl buffer. DNA was stained with 100 µM ToPro3 for 15 min at RT. Samples were rinsed with PBS, mounted with one drop of Vectashield and cover slips sealed with nail polish.

Images were acquired using a laser scanning microscope (LSM 710) and analysed using ZEN Software from Carl Zeiss and ImageJ. For the quantification of signal intensity 60 – 90 cells per sample were scored and the mean fluorescence was measured using ImageJ software.

3.2.13 NAD^+ cycling assay

The intracellular NAD^+ content of equal numbers of cells was determined with an enzymatic NAD^+ cycling assay (Bernofsky and Swan 1973). For the assay, an overplus of alcohol dehydrogenase (ADH), methyl thiazolyl blue (MTT), ethanol and phenazine ethosulphate (PES) was provided which made NAD^+ from cell lysates the reaction limiting factor of the cycling reaction. ADH utilises NAD^+ to oxidise ethanol to acetaldehyde and thereby produces reduced $NADH/H^+$. This reduces MTT via PES and generates NAD^+ again. At 570 nm the colour change of MTT was measured in a photometer which allowed for the subsequent calculation of the NAD^+ concentration. The intracellular NAD^+ concentration was determined by means of a NAD^+ standard curve.

For the NAD cycling assay, at least $3x\ 10^6$ cells were used per treatment. Cells were treated with 30 µg/ml ART for 24 h. As a positive control cells were treated with 100 µM H_2O_2 for 5 min. The cells were harvested and counted in a hemocytometer. The cell pellet was

resuspended in 250 µl cold PBS. The cells were lysed adding 12 µl 11.63 M perchloric acid and incubating the samples on ice for 15 min. The lysate was centrifuged for 10 min at 1500x g and 4°C. The supernatant was transferred to new test tubes. 175 µl phosphate buffer was added and the samples were kept on ice for 15 min. The samples were centrifuged for 10 min at 1500x g and 4°C and the supernatant was snap frozen in liquid nitrogen. Samples were stored at -80°C. The samples were thawed on ice and centrifuged at 1500x g for 10 min at 4°C. The supernatant was transferred to a new test tube and kept on ice. For the assay, NAD^+ standards were prepared:

Final concentration of NAD^+ (µM)	Diluent (µl)	1 µM NAD^+stock (µl)
0.00	700	0
0.01	693	7
0.02	686	14
0.04	672	28
0.08	644	56
0.12	616	84
0.24	532	168
0.48	364	336

In technical triplicates, 200 µl of each standard was pipetted into a 96-well plate. 10-100 µl of the samples were complemented with diluent to a final volume of 200 µl. The reaction mix was prepared in the dark and 100 µl was added to each well. The plate incubated for 30 min at RT in the dark. The absorption was determined at 570 nm using a microplate reader.

3.2.14 SDS-PAGE and Western Blotting

Cell lysis and protein quantification: Cells were harvested, and lysed on ice in an appropriate amount of whole cell extract lysis buffer. Samples were sonified for 2 x 10 pulses (Duty Cycle 30-40 %, output 3-4) on ice and then centrifuged at 13,000 g at 4°C for 15 min. The supernatants were recovered and the protein content was determined via the Bradford method. Briefly, the Bradford assay is a colourimetric assay in which Coomassie Brilliant Blue G-250 binds to protein sidechains under acidic conditions and thereby shifts its absorbance from 470 nm to 595 nm (Bradford 1976). A calibration curve of 1 – 5 µg BSA per well was pipetted into a 96-well plate in technical triplicates. 1 µl protein samples were loaded onto the plate and 200 µl Bradford reagent was added to samples and calibration values. The absorbance at 595 nm was measured after 5 min incubation time in the dark. 50 – 100 µg protein were boiled in Roti®-Load loading buffer for 5 min at 95°C.

For protein expression analysis in neutrophilic granulocytes, an additional cell lysis protocol was used (Kurosawa *et al.* 2003). Briefly, freshly isolated granulocytes were lysed in granulocyte lysis buffer and then boiled at 95°C for 2 min. Then samples were sonified with 2 x 10 pulses (Duty Cycle 30-40 %, output 3-4) and separated in an SDS-PAGE gel.

Sodium dodecyl sulphate polyacrylamide gel electrophoresis (SDS-PAGE) and Western Blotting: Depending on the size of the protein of interest different compositions for the separation gels were used. For very small proteins (< 30 kDa) 12 % gels were used:

Components	Stagging gel (4 %)	Separation gel (10 %)	Separation gel (12 %)
ddH_2O	8.8 ml	11.4 ml	10.2 ml
1.5 M Tris (pH 8.8)	-/-	6 ml	6 ml
0.5 M Tris (pH 6.8)	1.5 ml	-/-	-/-
acrylamide	1.5 ml	6 ml	7.2 ml
10 % SDS	120 µl	240 µl	240 µl
10 % APS	12 µl	120 µl	120 µl
TEMED	12 µl	12 µl	12 µl

During the concentration of the sample in the stacking gel phase 70 V was applied. During the separation phase, the voltage was increased to 110 V. Proteins were blotted onto nitrocellulose membranes for 2 h using 300 mA at RT or overnight using 100 mA at 4°C. Proteins were stained with Ponceau S for 2 min to determine successful transfer and equal loading. The membrane was de-stained using TBS-T. Unspecific binding of antibodies to the membrane was prevented by incubating the membrane with 2 – 5 % BSA-PBS or 5 % dry milk in TBS-T for 1 h at RT. Membranes were incubated with primary antibody overnight at 4°C. Membranes were washed 3 x 10 min with TBS-T. Secondary antibody coupled to an infrared dye was diluted 1:10,000 in TBS-T and membranes were incubated for at least 2 h at RT in the dark. Membranes were washed 3 x 10 min with TBS-T before detection with the LI-COR® Odyssey system.

3.2.15 Nuclear protein extract preparation

The cell pellet was carefully resuspended in 125 µl nuclear protein extraction buffer A and incubated on ice for 15 min. Then, 10 % (v/v) NP-40 was added (= 12.5 µl per 125 µl sample) and the sample was vortexed for 30 s. Samples were centrifuged at 3000 g for 5 min at 4°C and the supernatant (= cytoplasmic fraction) was transferred to a fresh 1.5 ml tube. The pellet was resuspended in 500 µl isotonic buffer and centrifuged. The supernatant was removed, the pellet resuspended in 45 µl nuclear protein extraction buffer B and incubated on ice for 15 min. Samples were centrifuged at 20,000 g for 10 min at 4°C and the supernatant (= nuclear protein extract) was collected.

3.2.16 DNA extraction using chloroform/phenol

Cell pellets were suspended in freshly prepared 300 µl TE9 cell lysis buffer containing SDS and proteinase K. Samples were incubated at 48°C on a thermomixer at 1100 rpm overnight. Next, 700 µl phenol/chloroform was added and samples were vortexed for 15 s. Samples were centrifuged at 14,000 rpm for 5 min at RT. The aqueous upper layer was carefully removed with a 200 µl pipette tip and transferred to a fresh 1.5 ml test tube. 700 µl phenol/chloroform was added once more and the sample was vortexed and centrifuged. The aqueous solution was transferred to a new 1.5 ml test tube and 750 µl EtOH:NH_4Ac master mix was added. Samples were inverted four times and incubated for 30 min at RT until DNA precipitated. If the DNA concentration was low (*e.g.* ChIP or PCR experiments) 2 µl glycogen (stock: 20 mg/ml) was added to the sample. Next, samples were centrifuged at 14,000 rpm for 45 min at 4°C. The supernatant was carefully removed and the pelleted DNA was washed with 1 ml 70 % ethanol and centrifuged at 14,000 rpm for 15 min. The supernatant was discarded and samples were centrifuged for 1 min to remove residual

ethanol. Samples were resuspended in 50 µl diethyl pyrocarbonate (DEPC) treated ddH_2O. The DNA concentration was measured using a NanoDrop and stored at -20°C.

3.2.17 Amplification of the XRCC1 promoter as three PCR products

The DNA sequence of the human XRCC1 promoter was obtained from the National Center for Biotechnology Information (NCBI) database. It contained the E2F1 binding site as described previously (Chen *et al.* 2008). Chen *et al.* set the promoter region at -881 bp and +158 bp relative to the transcription start site. For the PCR products, the promoter sequence was extended and covered -1236 bp and +163 bp relative to the transcription start (see chapter 7.8).

The XRCC1 promoter template of 1399 bp was provided by ..... (Miriam Pons 2016). The promoter was split into three parts of 634 bp (product 1, distal from the transcription start), 444 bp (product 2) and 363 bp (product 3, proximal to the transcription start). Each PCR product was amplified by regular endpoint PCR using 5'-biotinylated reverse PCR primers. The 5'-biotin bait allowed for streptavidin agarose binding without influencing the binding efficiency of transcription factors in reverse ChIP experiments later on.

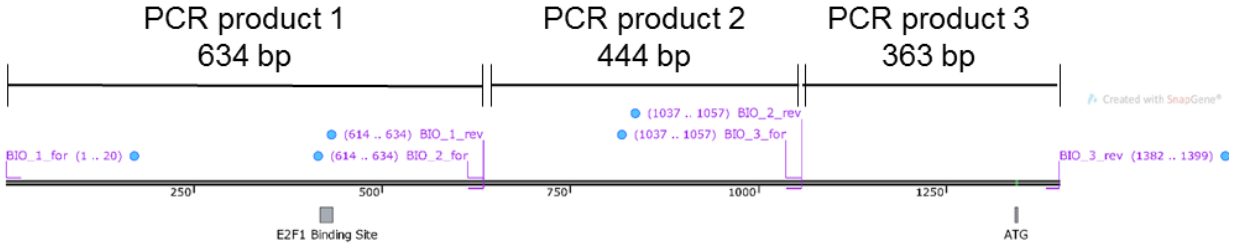

Fig. 7: XRCC1 promoter split into three parts and amplified using 5'-biotinylated primers
Each PCR product was amplified by regular endpoint PCR using 5'-biotinylated primers to provide a bait for streptavidin agarose beads.

The PCR mix for 5'-biotinylated PCR products was as follows:

Table 4: PCR reaction mix for 5'-biotinylation of the XRCC1 promoter split into three PCR products

Composition	µl
5x buffer	10
10 mM dNTPs	1
10 µM Primer for (1:10)	2.5
10 µM Primer rev (1:10)	2.5
Template DNA	1-2
Q5 enzyme	0.5
ddH_2O	10
Σ	25

As template DNA the amplified full length (1399 bp) XRCC1 promoter construct was used and diluted in ddH_2O to ~40 pg per PCR. The PCR protocol was as follows:

Table 5: PCR protocol for 5'-biotinylation of XRCC1 promoter in three parts

Step	Temp (°C)	Time (min)	
Initial denaturation	98	0:30	
Denaturation	98	0:20	44x
Annealing	60	0:40	
Extension	72	1:00	
Final extension	72	2:00	
Hold	8	∞	

After the PCR, the three amplified 5'-biotinylated PCR products were precipitated by adding 2 µl glycogen and then 750 µl EtOH:NH_4Ac master mix (see section 3.2.16) and subsequent centrifugation and washing of the DNA. The PCR products were resuspended in ddH_2O, the concentration was measured using a NanoDrop and then stored at-20°C.

3.2.18 Reverse ChIP for the detection of transcription factors for XRCC1

Reverse chromatin immunoprecipitation (ChIP) with subsequent mass spectrometry analysis was used to find transcription factors binding to the XRCC1 promoter. The protocol was adapted from a previous publication (Unnikrishnan *et al.* 2016). The XRCC1 promoter sequence was split into three parts of 643 bp (product 1), 444 bp (product 2) and 363 bp (product 3) and amplified by endpoint PCR (see section 3.2.17). The precipitation efficiency of DNA was tenfold higher in the presence of glycogen (> 170 ng/µl).

The 5'-biotin bait was used to bind the PCR products to streptavidin agarose beads. 300 µl streptavidin agarose was washed twice with 1 ml PBS and centrifuged at 3000 rpm for 5 min at 4°C. The beads were resuspended in 300 µl PBS and 1.5 µg of each 5'-biotinylated PCR product was added. The DNA baits were immobilised onto streptavidin-coated beads for 3 h at RT with constant rotation. The samples were centrifuged at 3000 rpm for 5 min at 4°C and the supernatant was discarded. The DNA was washed with 1 ml Buffer DW and then centrifuged again at 3000 rpm for 5 min at 4°C. The DNA-conjugated streptavidin beads were blocked in 1 ml blocking buffer for 1 h at RT and constant rotation.

Monocytes (Day 0) and monocyte-derived macrophages at day 4 of differentiation (Day 4) were pooled from 4-5 different donors and nuclear extracts were prepared and quantified via Bradford method (see section 3.2.14). 450 µg nuclear extract was mixed with one volume of buffer G and potassium glutamate (final concentration 10 mM):

Sample	Protein concentration	450 µg protein	Buffer G	Potassium glutamate (stock 100 mM)
Day 0	4.259 µg/µl	106 µl	106 µl	21.2
Day 4	3.226 µg/µl	140 µl	140 µl	28

2 x 100 µl streptavidin agarose beads (not bound to DNA) were washed twice with 1 ml PBS. The beads were incubated with the nuclear extracts for 1 h at 4°C to remove any non-specific binding of proteins to the beads. The samples were centrifuged 3000 rpm for 5 min at 4°C and the supernatant (pre-cleared nuclear extract) was incubated with the blocked DNA-streptavidin beads for 3 h at 4°C. Afterwards, the samples were washed twice with 1 ml buffer G and centrifuged at 3000 rpm for 5 min at 4°C. Proteins bound to the DNA-streptavidin agarose were eluted by boiling in 60 µl 1x NuPAGE lysis buffer at 70°C for 10 min. 15 µl samples were separated with SDS-PAGE and stained with silver nitrate. The

remaining protein lysate was analysed by mass spectrometry approach at the Proteomics Core Facility at the Institute for Molecular Biology (IMB), Mainz, Germany.

3.2.19 Silver staining of proteins in polyacrylamide gels

Silver staining of polyacrylamide gels allows for the detection of proteins in the low nanomolar range with relatively cheap chemicals. The protocol was taken from Nature Protocols (Chevallet *et al.* 2006) and slightly adapted. Briefly, nuclear protein samples were boiled in 30 – 60 µl 1x NuPAGE lysis buffer for 10 min at 70°C. Nuclear extracts were separated in a 10 % SDS polyacrylamide gel. The gel was removed from the glass plates and rinsed once with ddH_2O. All the following steps were done with gentle agitation at ~40 shakes/min. The gel was fixed in 30 % (v/v) ethanol and 10 % (v/v) acetic acid for 30-40 min. The gel was rinsed 2 x 10 min in 20 % (v/v) ethanol and then 2 x 10 min in ddH_2O. The samples were sensitised by soaking in 0.02 % (w/v) sodium thiosulfate pentahydrate for 1 min and then rinsed 2 x 1 min in ddH_2O. It was impregnated with 12 mM silver nitrate for 40 min. The gel was rinsed with ddH_2O for 10 s and then transferred to the basic developer for 2 – 5 min. The reaction was stopped by removing the developer and adding the stop solution for 30 min. The gel was washed 2 x 30 min in ddH_2O and was detected using a scanner afterwards.

3.2.20 Mass spectrometry analysis of proteins

The detection of potential transcriptions factors for the XRCC1 promoter was analysed using a proteomics approach. The XRCC1 promoter was amplified (see section 3.2.17) before it was incubated with nuclear protein extracts (see section 3.2.18). The samples were analysed by the IMB Proteomics Core Facility in Mainz by Anja Freiwald and Mario Dejung, in particular, are gratefully acknowledged. The samples were analysed using uHPLC, EASY-nLC 1000 coupled to a Q Exactive Plus mass spectrometer (Thermo Scientific). Sample preparation was performed as described elsewhere (Bluhm *et al.* 2016). Samples were dimethyl-labelled as describes elsewhere (Hsu *et al.* 2003). Samples were measured in reverse, meaning that a label switch was performed and samples were measured in duplicates:

Sample 1	**Label**	**Ratio**
Macrophage	Heavy	Heavy / Light
Monocyte	Light	
Sample 2	**Label**	**Ratio**
Monocyte	Heavy	Heavy / Light
Macrophage	Light	

3.2.21 Pyrosequencing

Pyrosequencing is a method that detects methylated cytosines in DNA sequences. In order to analyse the methylation status of the XRCC1 promoter in monocytes and macrophages, monocytes were isolated from buffy coats first by adherence followed by CD14 positive selection via bead isolation according to the manufacturer's instructions. Samples were cultured in 6 well plates in the presence of GM-CSF to generate macrophages. The DNA of monocytes and macrophages was isolated by phenol/chloroform extraction and 1 µg DNA

was bisulphite converted using the EZ DNA methylation kit according to the manufacturer's protocol. All unmethylated cytosines were converted to uracil while 5mC remained unaltered. The converted DNA was eluted in 25 µl DNase-free water. DNA methylation of the XRCC1 promoter was analysed by pyrosequencing in collaboration with Olivier Switzeny. The promoter was analysed in five pieces (Fig. S32) using the PyroMark Q24 Advanced Reagents kit for long-read pyrosequencing reactions. Sequencing occurred in the Pyromark Q24 Instrument. First, the bisulphite converted DNA was amplified by regular endpoint PCR using the PyroMark PCR Master Mix according to the manufacturer's instructions to amplify the region of interest. The reverse primer for this PCR was biotinylated at the 5' end. According to the manufacturer's instructions, the PCR products were incubated with Streptavidin Sepharose High-Performance beads, before sequencing primers were added and the pyrosequencing reaction plate was placed into a Vacuum Workstation. The liquid was aspirated while the bead-bound PCR products remained stationary. The samples were washed with 70 % ethanol, then they were treated with denaturation buffer and wash buffer before the now single-stranded bead-bound DNA was placed into the Pyrosequencer.

4 Results

4.1 DNA repair deficits in myeloid immune cells

As previously reported, monocytes are severely impaired in BER and DSB repair by NHEJ (Briegert and Kaina 2007; Bauer *et al.* 2011; Bauer *et al.* 2012). It was shown that monocytes do not or only weakly express XRCC1, ligase IIIα and PARP-1 which are essential proteins for the re-ligation step of BER and SSB repair. This phenotype renders monocytes susceptible to DNA oxidising and alkylating agents. GM-CSF-induced maturation into macrophages led to an upregulation of the proteins in question and resulted in resistance to DNA-damaging substances. As the isolation of monocytes is a time-consuming process and Western Blot analysis requires a lot of material (~10 x 10^6 cells for 50 µg of protein), an alternative method of detecting XRCC1 was established. XRCC1 protein expression was determined via immunofluorescence staining measuring the mean fluorescence signal intensity in arbitrary units (AU) (Fig. 8). Monocytes (Day 0) with their characteristic bean-shaped nucleus displayed no or only weak XRCC1 signals. GM-CSF-triggered differentiation into macrophages led to an upregulation of XRCC1 expression (Fig. 8, Day 6).

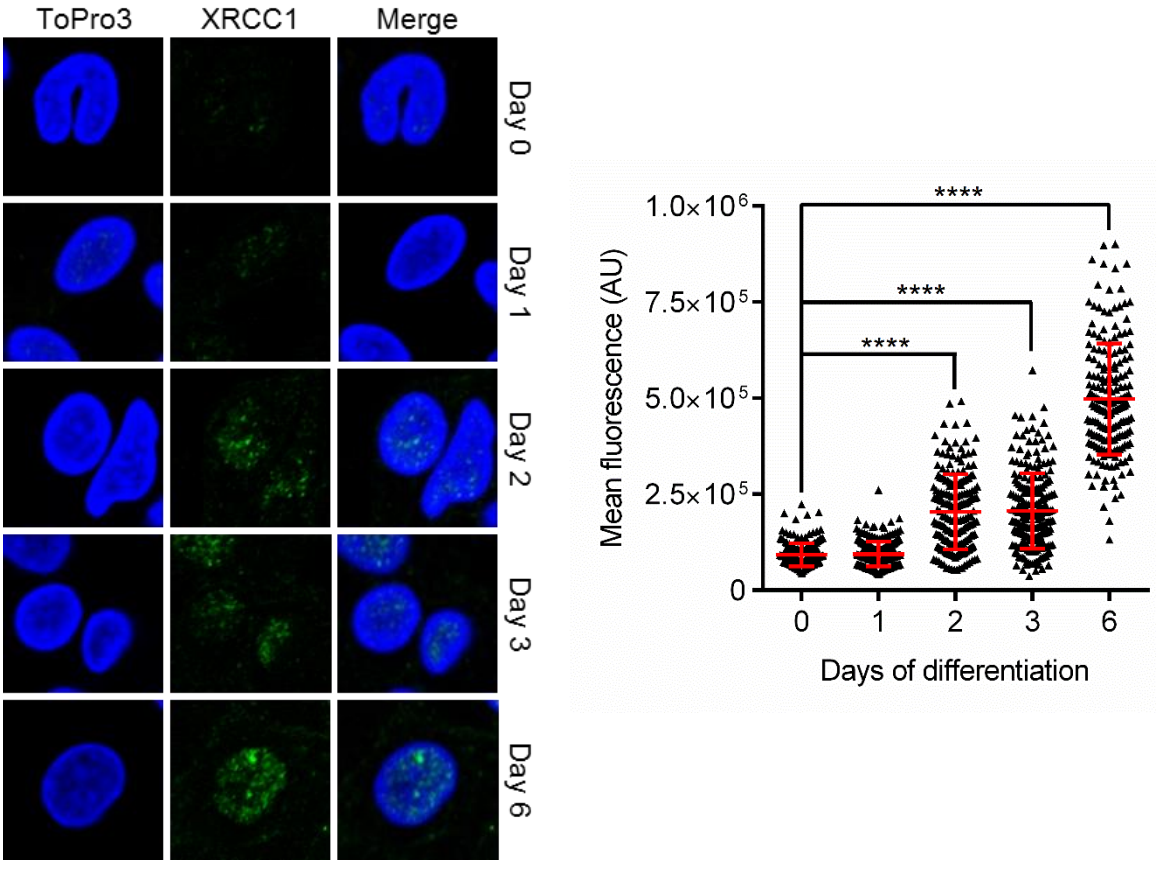

Fig. 8: XRCC1 expression during macrophage maturation
*The left panel shows representative images of the immunofluorescence staining of XRCC1 in monocytes (Day 0) differentiating into macrophages through GM-CSF treatment over a period of six days. The right panel shows the quantification of the mean fluorescence signal of XRCC1 in arbitrary units (AU). Each dot represents the fluorescence intensity of a single cell. Data are from two independent experiments with at least 90 cells counted for each sample per experiment ± SD, 1-way ANOVA, Tukey's Multiple Comparison Test, ****p < 0.0001*

Over the course of six days, the signal for XRCC1 increased and already became clearly visible after two to three days. At day six, when adherent and spindle-shaped macrophages were at the bottom of the plate, XRCC1 expression was the strongest. Quantification of the XRCC1 signal in single cells confirmed the microscopic observations (Fig. 8, right panel).

Ligase IIIα is stabilised by XRCC1 (Whitehouse *et al.* 2001). Western Blot analysis showed that ligase IIIα protein levels increased during macrophage maturation (Fig. 9). Concomitant to XRCC1 expression, ligase IIIα was first detectable after three days of GM-CSF treatment and peaked after six days.

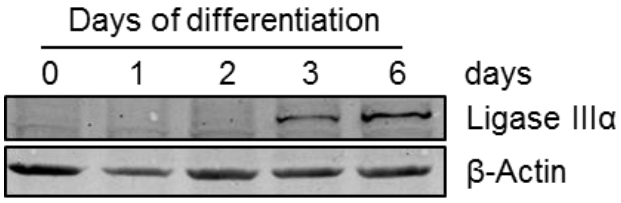

Fig. 9: Ligase IIIα expression in maturing macrophages
Cell differentiation was induced by adding GM-CSF. Ligase IIIα protein expression was detected via Western Blot. β-Actin was used as loading control.

Instead of detecting PARP-1 directly, its enzymatic product PAR was analysed by immunofluorescence staining. PARP-1 catalyses the formation of PAR chains when it detects DNA strand breaks. Therefore, monocytes and monocyte-derived macrophages at day three of differentiation were treated with the DNA-damaging agent H_2O_2 (1 mM for 5 min) as previously reported (Mangerich *et al.* 2016). Cells were immediately fixed, as PAR is a transient biopolymer, and stained for PAR (Fig. 10).

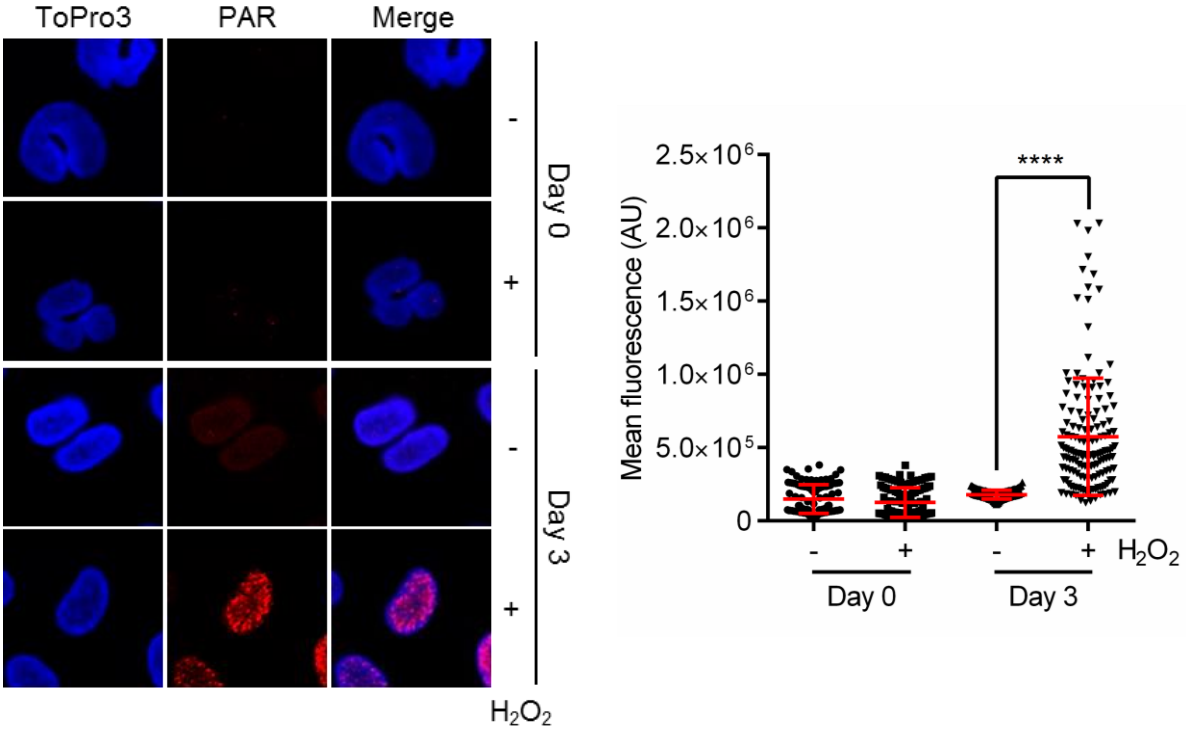

Fig. 10: PAR formation in monocytes and monocyte-derived macrophages after H_2O_2 treatment
*PAR formation was induced by treating monocytes or differentiating macrophages at day three with H_2O_2 (1 mM for 5 min). H_2O_2 induced SSBs which led to the catalytic activation of PARP-1 and thus PAR production. Data are from two independent experiments with at least 50 cells counted for each sample per experiment ± SD, 1-way ANOVA, Tukey's Multiple Comparison Test, ****p < 0.0001*

In monocytes (Day 0) genotoxic treatment did not result in PAR formation in the nucleus (Fig. 10). Developing macrophages at day three displayed massive PAR formation after genotoxic insult but not in the control (Fig. 10, lower panel). Quantification of the signal intensity (Fig. 10, right panel) confirmed the microscopic observation.

As monocytes and granulocytes originate from the same progenitor cell (*i.e.* the CMP), it was then determined whether granulocytes were also impaired in DNA repair protein expression. The granulocyte fraction, which mostly consists of neutrophils (95 % neutrophils compared to 1 % basophils and 1-4 % eosinophils), was isolated from buffy coats and PARP-1, XRCC1, and ligase IIIα protein expression was determined by Western Blot analysis (Fig. 11A). Granulocytes from four different donors (G1 – G4) showed no BER protein expression compared to the PBL control. Previous work on the DSB protein expression in granulocytes showed a lack of ATM expression. One of the main targets of active ATM is the DSB marker H2AX. Its phosphorylated form, γH2AX, was not detectable (Tobias Haak 2015). Therefore, unphosphorylated H2AX was detected as a control. H2AX protein was found in the granulocytes from four donors (Fig. 11).

In addition to Western Blot analysis, XRCC1 was also detected via immunofluorescence staining (Fig. 11B). Granulocytes were stained for CD15 marker (red ring) and XRCC1 protein (green) expression. PBL were used as positive control and showed strong XRCC1 signals compared to granulocytes. Ionising radiation (2 Gy, 1 h incubation) led to a condensed XRCC1 signal at the site of DNA damage in PBL (Fig. 11B, lower panel).

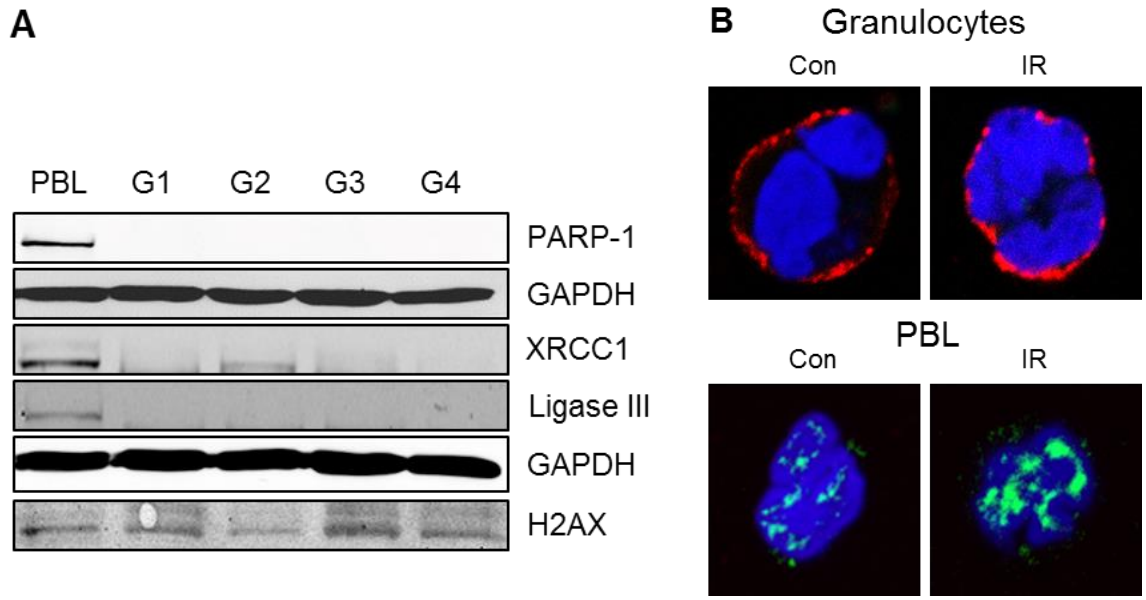

Fig. 11: BER protein expression in granulocytes
A) Standard whole cell extract lysis buffer was used for cell lysis. Granulocytes from four donors (G1 – G4) were analysed for BER protein expression and compared to the PBL control. Western Blot analysis was kindly performed by ..... under supervision. B) Immunofluorescence staining of XRCC1 (green) in granulocytes and PBL after 2 Gy irradiation. Granulocytes were additionally stained for CD15 marker (red).

As granulocytes are full of lytic enzymes (Korkmaz et al. 2010; Pham 2006), it was proposed that our standard cell lysis and protein isolation method using whole cell lysis buffer may not be effective enough in neutralising all proteases. It was suggested that the proteases degraded our proteins of interest before we could detect them. Therefore, a published protocol by Kurosawa *et al.* was used for detecting DNA repair proteins by Western Blot analysis. As an additional control, PBL and granulocytes were counted and mixed in a 2:1

ratio before lysis. If lytic enzymes degraded our proteins of interest, it was postulated that the signal would also be lost in the mixed cell lysate. Cell material from two different donors was used for Western Blot analysis. Both showed that granulocytes do not express PARP-1 nor XRCC1. The mixed fraction (2L : 1G) showed weaker bands than the PBL control fraction (Fig. 12). PBL alone displayed the strongest protein expression.

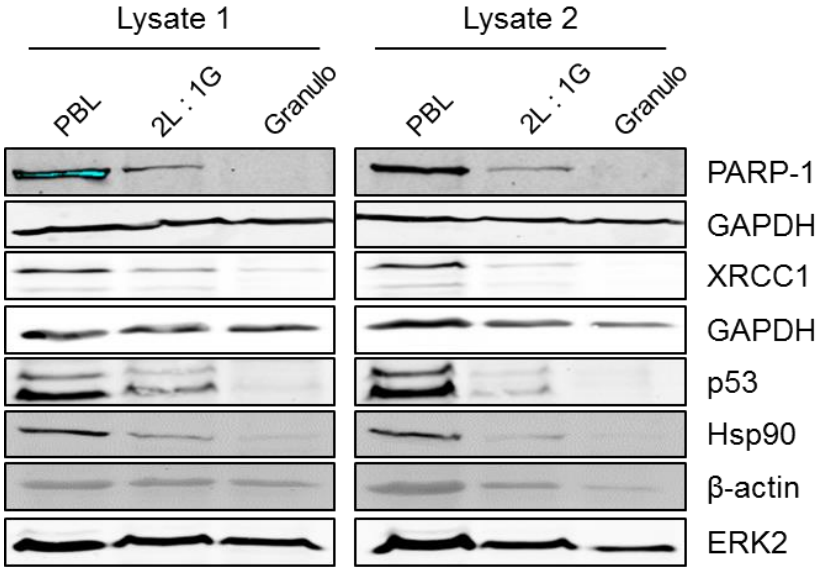

Fig. 12: DNA repair protein expression in two granulocyte lysates from different donors
PBL and granulocytes were counted and mixed in a 2:1 ratio (2L : 1G). Cells were lysed using an alternative lysis protocol (Kurosawa et al. 2003). The BER protein expression of PBL, granulocytes and the mixed lysate was determined using Western Blot analysis. GAPDH and ERK2 were used as loading controls.

Furthermore, the transcription factor p53, the heat-shock protein 90 (Hsp90) and the cytoskeletal factor β-actin were undetectable in granulocytes. GAPDH and ERK2 were used as loading controls.

As an additional control experiment, fresh blood samples were also analysed for DNA damage response factors. Blood was taken from the fingertip of a healthy volunteer and collected in heparinised glass capillaries (Heylmann and Kaina 2016). The cells were irradiated with 2 Gy and incubated for 1 h at 37°C before the cells were fixed as blood smears on glass slides. The DNA damage response factor pATM and its phosphorylation targets KAP1 and H2AX were detected via immunofluorescence staining (Fig. 13).

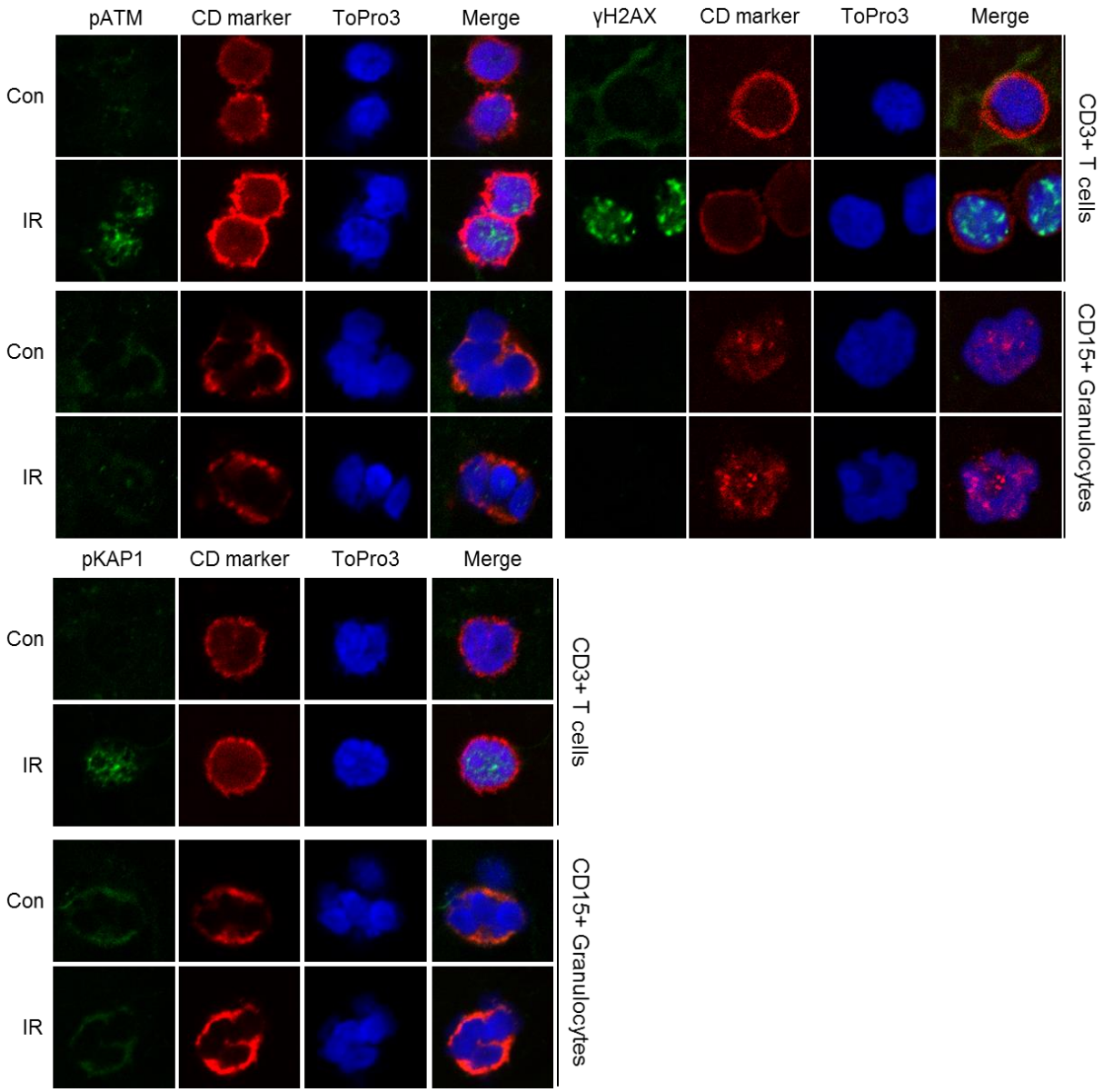

Fig. 13: DDR is impaired in granulocytes after IR – measured in fresh blood from the fingertip
Blood was collected in heparinised glass capillaries and irradiated with 2 Gy. Cells were fixed as blood smears after 1 h incubation at 37°C. CD15+ neutrophils and CD3+ T cells were distinguished by their characteristic marker expression (red). DDR factor pATM and its phosphorylation targets γH2AX and pKAP1 were detected (green).

Granulocytes and T cells were stained in parallel for their respective markers, *i.e.* CD15 and CD3. Only CD marker-positive cells (red) were analysed for pATM, pKAP1 and γH2AX signals (green). Control samples did not show a signal for phosphorylated ATM, KAP1 nor H2AX. After 2 Gy irradiation, a strong signal was observed in the CD3+ T cells for pATM and its downstream targets pKAP1 and γH2AX. Granulocytes did not or only weakly showed any signal (CD15+ cells).

In summary, it was shown that monocytes and granulocytes both display severe impairment in their expression of DNA repair factors, *i.e.* XRCC1, ligase IIIα and PARP-1, and DNA damage response factors, *i.e.* pATM and γH2AX. The lymphoid control cells, on the other hand, expressed all indicated DNA repair proteins.

4.2 ART leads to DNA damage and cell death in immune cells

The anti-malarial drug ART is being considered for cancer therapy as it induces DNA damage (Berdelle *et al.* 2011; Li *et al.* 2008) and enhances the therapeutic response of cancer cells to the alkylating agent temozolomide (Berte *et al.* 2016). As ART is applied intravenously, we addressed the question of whether immune cells also displayed cytotoxic effects. It was of particular interest whether the DNA repair defective monocytes showed an altered sensitivity towards ART compared to DNA repair-competent macrophages, DCs and PBL.

First, monocytes, macrophages, DCs and PBL were treated with low concentrations of 2.5 – 20 µg/ml ART for 24 h before oxidative DNA damage was assessed using the FPG-modified alkaline Comet assay. In the absence of FPG, only SSBs were detected. The induced amount of SSBs was similar in monocytes, macrophages, DCs and PBL (Fig. 14). There was a trend towards more strand breaks in macrophages when treated with 20 µg/ml ART. In the presence of FPG, oxidative lesions were detected and excised resulting in additional SSBs. In all cell populations, oxidative DNA damage was observed in a concentration-dependent manner. Macrophages showed slightly more oxidative damage after treatment with 5 and 10 µg/ml ART compared to monocytes and DCs. PBL displayed less oxidative damage compared to the myeloid cells and did not reach saturation levels. Overall oxidative DNA damage burden reached a plateau at 15 µg/ml ART when the tail intensity reached ~60 %.

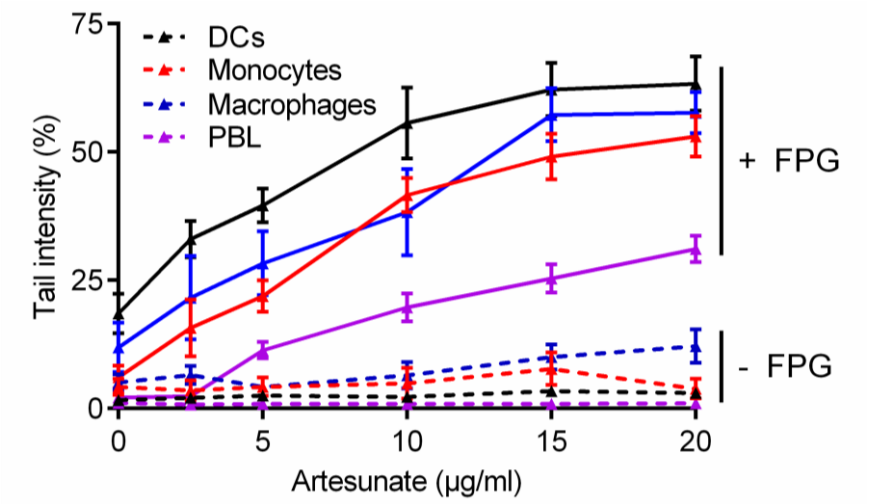

Fig. 14: FPG-modified alkaline Comet assay of ART-treated immune cells
Cells were treated with low concentrations of ART (2.5 – 20 µg/ml) for 24 h before oxidative DNA damage was assessed. In the absence of FPG, SSBs were detected (chequered lines). In the presence of FPG oxidative DNA lesions were converted into SSBs. Data are the mean of three to five independent experiment ± SEM. For each experiment at 50 - 100 cells per samples were analysed.

Next, ART-induced cell death of immune cells was analysed using Annexin V / PI staining. Annexin V positive, PI negative cells were considered apoptotic. Annexin V positive, PI positive cells were considered necrotic. After treatment with low concentrations of ART for 24 h macrophages showed a slight increase in cell death. This was not observed in monocytes or PBL (see supplement Fig. S3). After 48 h, a concentration-dependent increase in necrotic cell death was observed in macrophages (~10-20 %) (Fig. 15C). Monocytes and PBL showed only a slight increase in cell death (~10 %). Monocytes

displayed mainly apoptotic cell death whereas PBL showed necrotic and apoptotic cell death (Fig. 15, A and B).

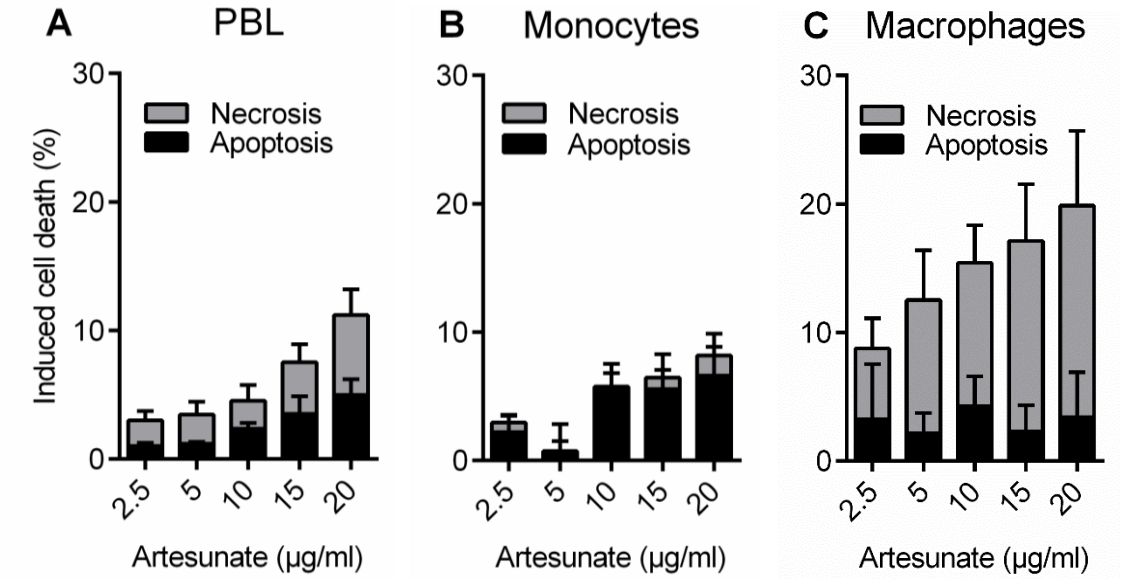

Fig. 15: Cell death of immune cells after ART treatment
Immune cells were treated with 2.5 – 20 µg/ml ART and cell death was measured 48 h later using Annexin V / PI. Analysed were A) PBL, B) monocytes and C) macrophages. Data are the mean of five to twelve independent experiments ± SEM. Some experiments were kindly performed by ..... under supervision.

Next, it was determined whether higher concentrations of ART ranging from 10 - 100 µg/ml induced a similar DNA damaging and subsequent killing response as previously reported for the glioma cell line LN-229 (Berdelle *et al.* 2011). As the detection of oxidative DNA damage was already saturated at 15 µg/ml ART, SSB damage was assessed instead using the alkaline Comet assay (Fig. 16). There was a concentration-dependent increase in SSB formation in all cell types. Macrophages showed the strongest SSB formation with a tail intensity of ~60 % after the highest concentration of ART. DCs and PBL showed a similar SSB formation pattern whereas monocytes showed a relatively low SSB accumulation.

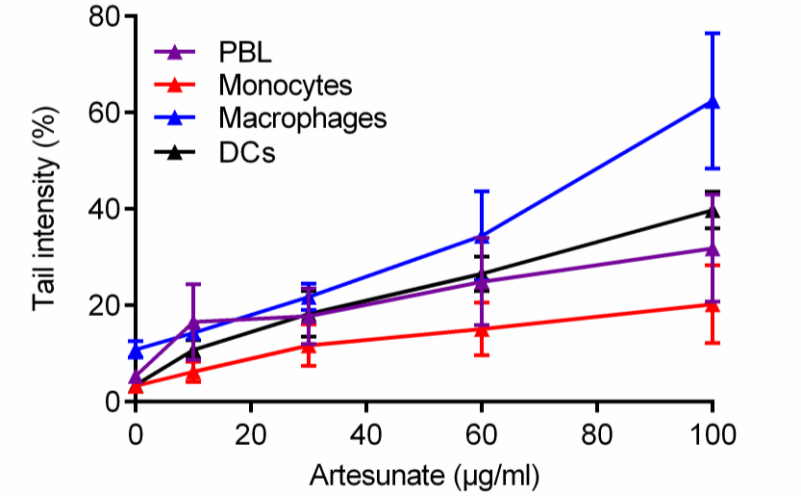

Fig. 16: SSB formation after treatment with high concentrations of ART
Cells were treated with 10-100 µg/ml ART for 24 h. DNA damage was assessed using the alkaline Comet assay. Data are the mean of three to five independent experiment ± SEM. Some experiments were kindly performed by ..... under supervision.

Following SSB formation, cell death was measured after ART treatment for 48 h. All cell types displayed a concentration-dependent increase in cell death (Fig. 17). PBL showed the highest sensitivity towards ART with ~40 % apoptosis and ~15 % necrosis at 100 µg/ml ART. In monocytes and macrophages overall cell death was ~40 % at the highest ART concentration. However, monocytes predominately died by apoptosis (Fig. 17B) whereas macrophages mostly by necrosis (Fig. 17C). DCs could not be analysed by flow cytometry as cell debris accumulated during DC differentiation and artificially increased the percentage of dying cells (data not shown).

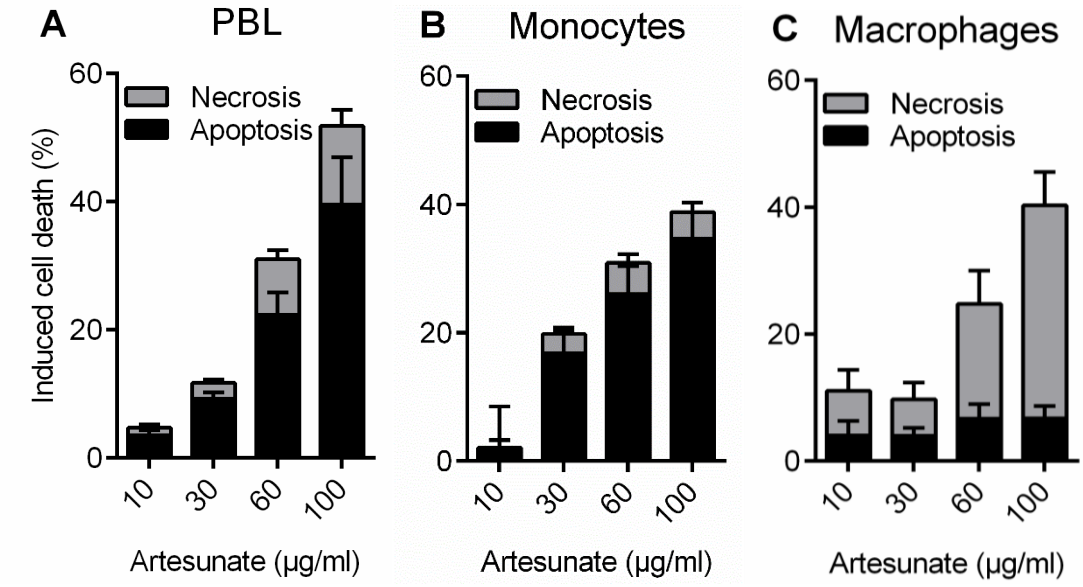

Fig. 17: Cell death of immune cells treated with high concentrations of ART
Immune cells were treated with 10 – 100 µg/ml ART and cell death was measured 48 h later using Annexin V / PI. Analysed were A) PBL, B) monocytes and C) macrophages. Data are the mean of four to eleven independent experiments ± SEM. Some experiments were kindly performed by ..... under supervision.

Upon DNA damage, PARP-1 is activated and consumes NAD^+ to generate PAR. Over-activation of PARP-1 can lead to NAD^+ and subsequent ATP depletion. It is often associated with necrotic cell death. Therefore, the NAD^+ content of ART-treated cells was analysed. Equal numbers of PBL, monocytes and macrophages were subjected to an NAD^+ cycling assay. Normalised to the control, ART-treated PBL and monocytes showed little to no NAD^+ loss after treatment with 30 µg/ml ART (Fig. 18, A and B). Macrophages showed a significant reduction in NAD^+ of approximately 20 %. 1 mM H_2O_2 was used as positive control and showed a massive depletion of NAD^+ in macrophages (~60 %) and PBL (50 %). In monocytes, NAD^+ levels dropped to 60 %. The raw data for the NAD^+ contents in equal numbers of cells showed that PBL had very little NAD^+ in general. Macrophages, on the other hand, had very high amounts of NAD^+ (see supplement Fig. S6).

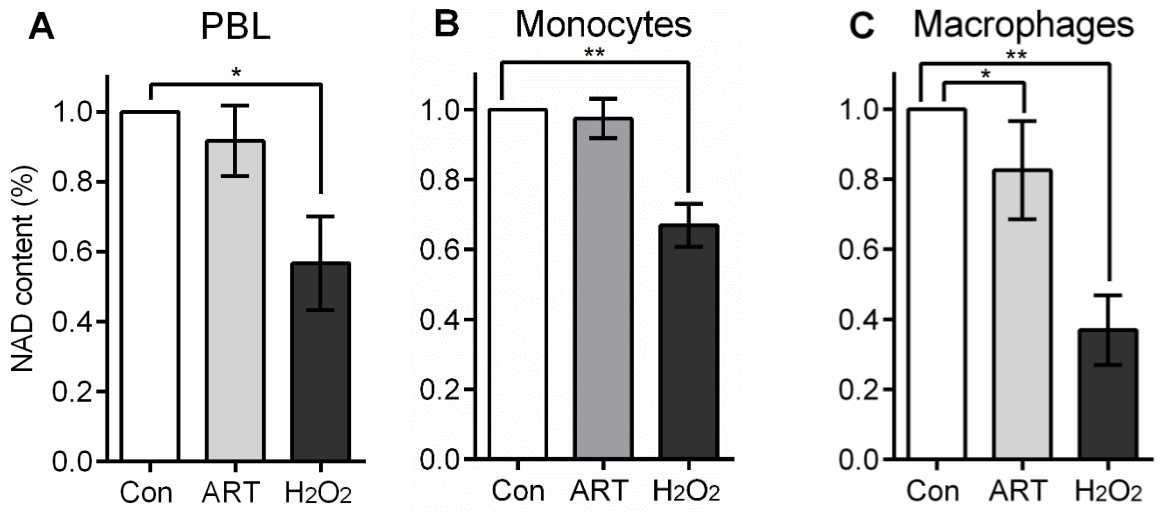

Fig. 18: NAD⁺ levels in immune cells after treatment with ART
*The NAD⁺ content was measured using the NAD⁺ cycling assay. A) PBL, B) monocytes and C) macrophages were treated with 30 µg/ml ART for 24 h before the cells were harvested. 1 mM H_2O_2 was used as a positive control. Data are the mean of four to five independent experiments ± SEM, 1-way ANOVA, Tukey's Multiple Comparison Test, *p < 0.05, **p < 0.01. The experiments were kindly performed by .....*

In summary, it was shown that exposure to ROS-producing ART led to similar amounts of oxidative lesions in myeloid immune cells. SSB formation, on the other hand, was more pronounced in macrophages than in monocytes. The ensuing cell death response was different between monocytes and monocyte-derived macrophages. Whereas monocytes underwent apoptotic cell death, macrophages pre-dominantly died necrotic cell death, possibly due to NAD⁺ depletion by PARP-1.

4.3 Stimulating myeloid immune cells to produce ROS

Phagocytes like monocytes, macrophages and neutrophils are known to kill pathogens by their respiratory burst, the explosive release of $O_2^{\cdot-}$ and other ROS like NO, H_2O_2 and OH·. *In vitro*, isolated monocytes and monocyte-derived macrophages were stimulated with different agents to elicit the ROS burst. It was then analysed whether the production of ROS also led to DNA damage in the ROS producing cells (auto-intoxication).

First, intracellular ROS was detected using a flow cytometry-based assay. The ROS dyes CM-H2DCFDA and 2′,7′-Dichlorofluorescin diacetate react with ROS resulting in a fluorescent molecule that can be detected by flow cytometry. Monocytes and macrophages were treated with 1 µg/ml PMA or 50 ng/ml LPS for 30 min and 24 h. In comparison to the untreated control, LPS alone did not lead to higher amounts of ROS inside monocytes and macrophages (Fig. 19). PMA treatment for 30 min led to a robust 3x fold increase in ROS levels in both cell types. 24 h PMA treatment did not show any ROS. *t*-BOOH is a strong oxidising agent and was used as a positive control (Fig. 19).

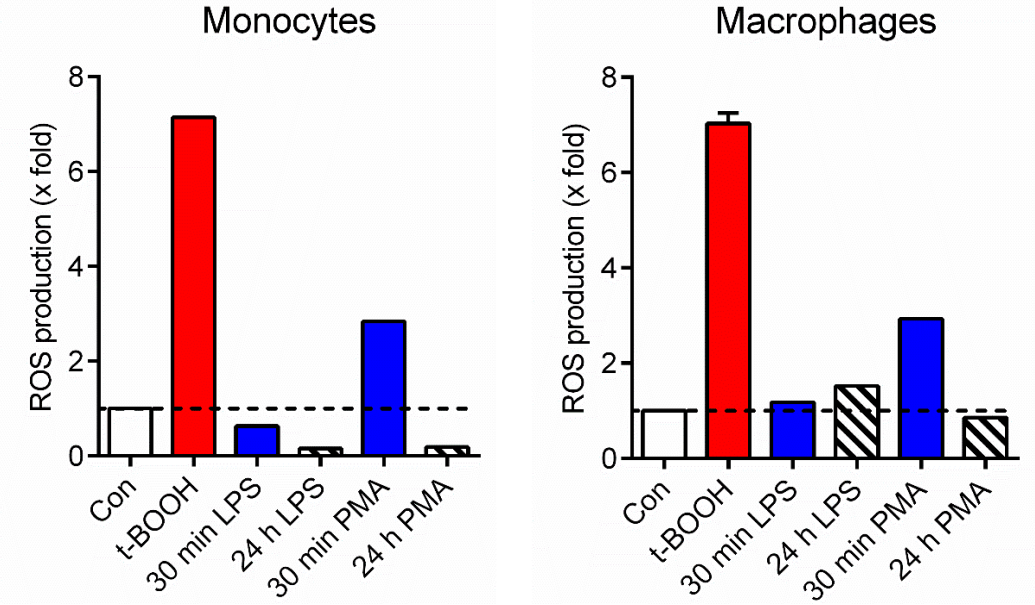

Fig. 19: Intracellular ROS in monocytes and macrophages after stimulation with LPS or PMA
Cells were treated with 50 ng/ml LPS (E.coli 0127:B8) or 1 µg/ml PMA for 24 h or 30 min. Cells were stained with the ROS dye CM-H2DCFDA for 30 min. ROS was detected by flow cytometry. As a positive control, cells were treated with 100 µM t-BOOH for 30 min.

In the preliminary experiments, PMA led to a robust increase in intracellular ROS. Next, the optimal PMA concentration was determined using concentrations ranging from 1 - 1000 ng/ml as described in the literature (O'Donnell *et al.* 1993; Ashkenazi *et al.* 2009; Raad *et al.* 2009; Wind *et al.* 2010; Kuwabara *et al.* 2015). Monocytes were treated with PMA for 30 min before intracellular ROS was detected. ROS levels were highest after treatment with 10 - 1000 ng/ml PMA (Fig. 20). 1 ng/ml did not lead to a significant increase in intracellular ROS. In addition, cells were pre-treated with the ROS scavenger N-acetyl cysteine (NAC) for 1 h before PMA was added. In the presence of NAC intracellular ROS levels were strongly reduced.

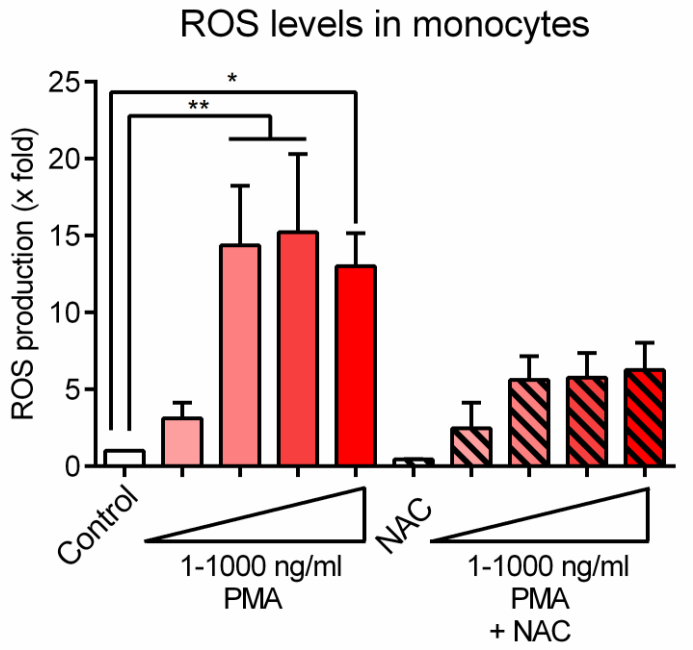

Fig. 20: Intracellular ROS formation after PMA treatment was reduced by the ROS scavenger NAC

*Monocytes were treated with 5 mM NAC for 1 h prior to treatment. Then, cells were stained with 10 µM CM-H2DCFDA or 100 µM 2',7'-dichlorofluorescin diacetate and treated with 1, 10, 100 or 1000 ng/ml PMA for 30 min. Mean fluorescence was measured via flow cytometry. Data were normalised to the untreated dye control. Data are the mean of three independent experiments ± SEM, 1-way ANOVA, Dunnett's Multiple Comparison Test, *p < 0.05, **p < 0.01*

As PMA is a strong and reliable activator of PKC, which in turn activates NADPH oxidase, ROS production of monocytes and macrophages was then detected in parallel. Cells were pre-treated with 5 mM NAC for 1 h before they were stimulated with PMA. *t*-BOOH was used as a positive control. Both cell types displayed an increase in intracellular ROS compared to the untreated control (Fig. 21). The response was stronger in monocytes (~6x fold higher) than in macrophages (3.5x fold higher). NAC pre-treatment reduced intracellular ROS to control levels. The same was observed when pre-treated cells were exposed to *t*-BOOH.

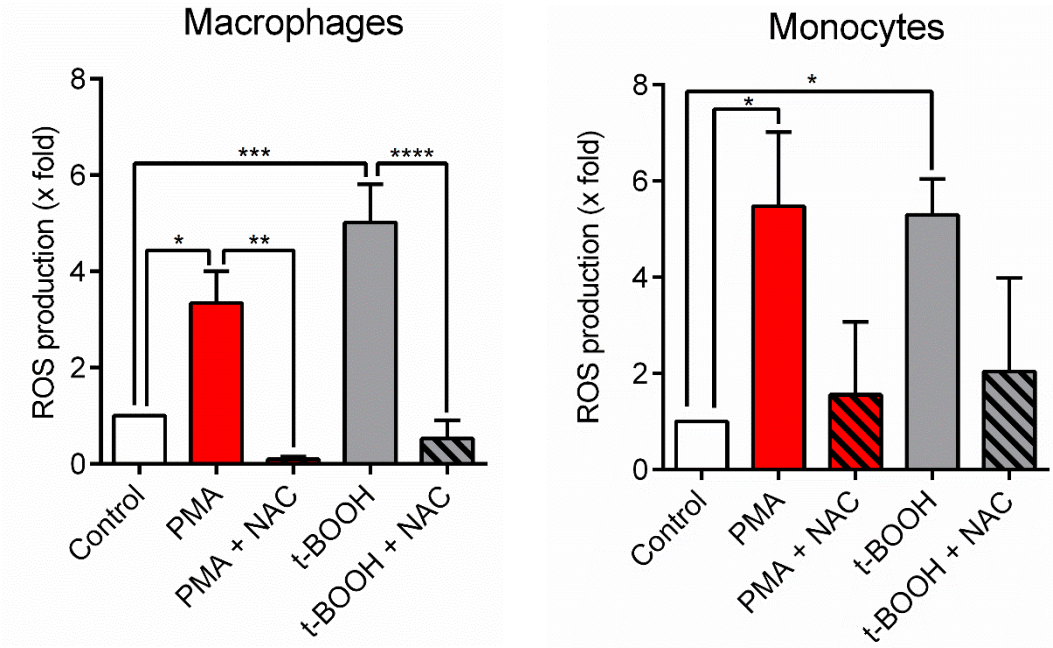

Fig. 21: Intracellular ROS formation in macrophages and monocytes
*Cells were pre-treated with 5 mM NAC for 1 h. ROS levels were measured after treatment with 1000 ng/ml PMA or 100 µM t-BOOH for 30 min. t-BOOH was used as a positive control. For macrophages, the data are the mean of four to five independent experiments ± SEM. For monocytes data are the mean of two (NAC samples) to five independent experiments ± SEM. NAC samples were excluded from the analysis of monocytes. Statistical analysis: 1-way ANOVA, Tukey's Multiple Comparison Test, *p < 0.05, **p < 0.01, ***p < 0.001, ****p < 0.0001*

Next, it had to be determined whether PMA treatment led to extracellular ROS production. Therefore, cells were activated by PMA and the ensuing ROS production was measured in a chemiluminescence-based assay using luminol and horseradish peroxidase (HRP). Monocytes and macrophages were pre-treated with the NADPH oxidase inhibitor diphenyleneiodonium chloride (DPI, 100 µM for 10 min) before ROS production was induced with 100 ng/ml PMA. The release of ROS into the extracellular space was detected over 80 min. Monocytes caused a fast and strong ROS burst that peaked at ~30 min after the addition of PMA (Fig. 22A, upper left panel, red line). In the presence of DPI, the ROS burst was almost completely abolished (purple line). Treatment with DPI alone reduced ROS below control level (blue line). Macrophages displayed a slower induction of ROS that persisted over time (Fig. 22A, lower left panel, red line). Inhibition of the NADPH oxidase with DPI reduced extracellular ROS to almost control level (purple line). Similar to monocytes, DPI alone reduced the ROS level below control level. Quantification of ROS

production (measured as area under the curve) displayed similar amounts of ROS in monocytes and macrophages despite different kinetics (Fig. 22B, right panels).

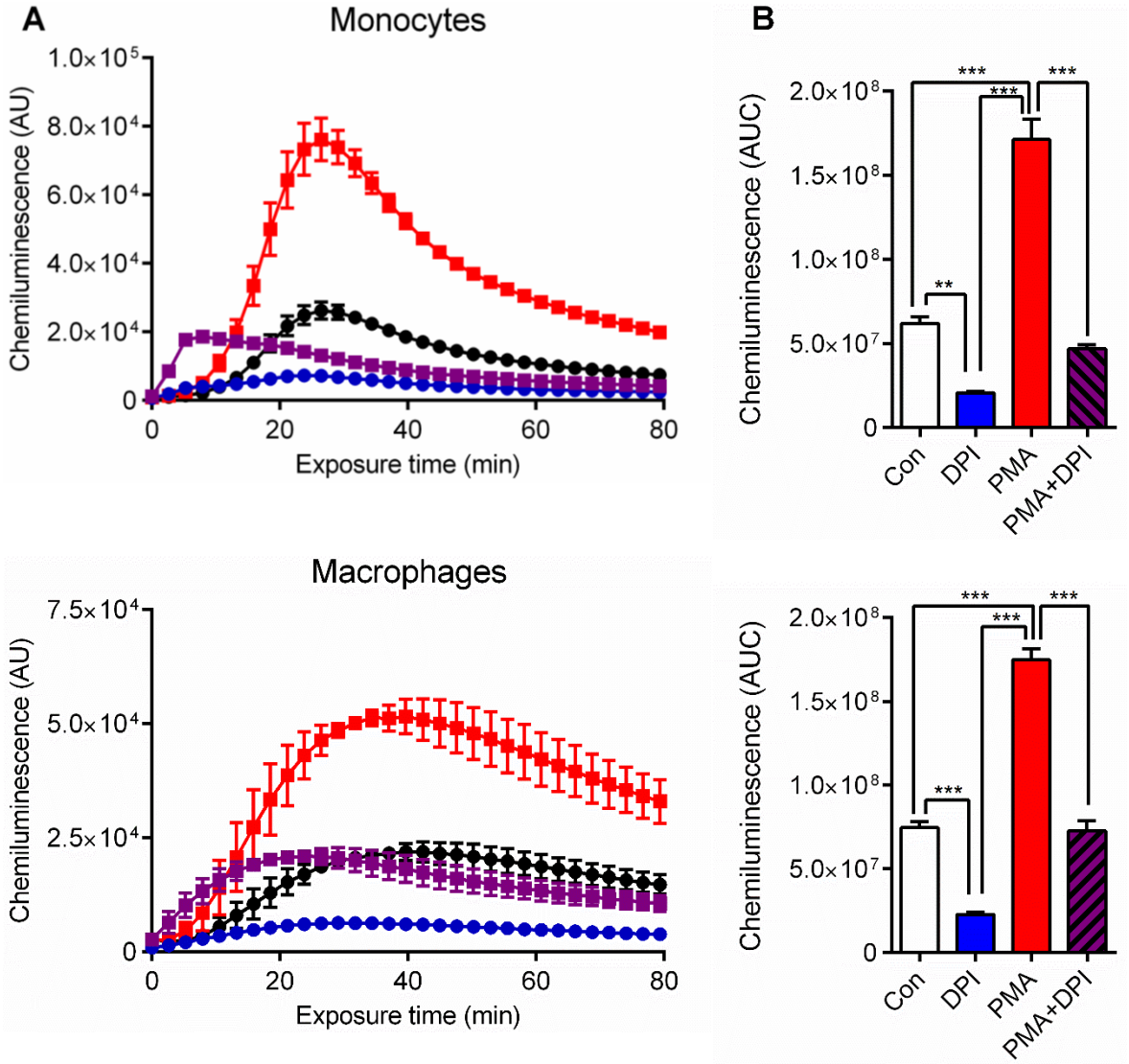

Fig. 22: ROS production in monocytes and macrophages ± inhibitor
*A) The extracellular ROS production of monocytes and macrophages was measured over time (left panel). Cells were treated with 100 ng/ml PMA (red line) to induce ROS production. Controls cells are shown in black. Cells treated with the NADPH oxidase inhibitor DPI (100 µM) are depicted in blue. Cells pre-treated with DPI followed by PMA are shown in purple. DPI was added 10 min before the stimulation with PMA. B) For the quantification of extracellular ROS generated by macrophages and monocytes the area under the curve (AUC) was determined. Data are the mean of three to four independent experiments ± SEM, 1-way ANOVA, Tukey's Multiple Comparison Test, **p < 0.01, ***p < 0.001*

PMA-stimulated T cells were also analysed for extracellular ROS production. In comparison to monocytes, T cells showed only slightly elevated ROS levels (Fig. 23A). Quantification of the ROS production displayed no significant increase in PMA-stimulated T cells compared to the control (Fig. 23B). Monocytes showed a strong and fast ROS burst after stimulation.

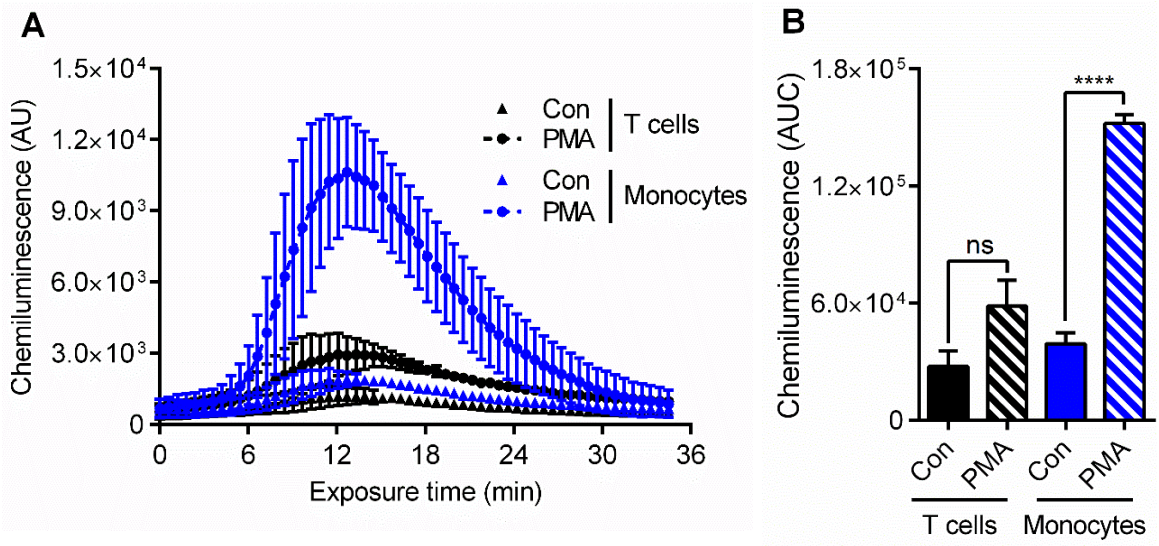

Fig. 23: Extracellular ROS burst in monocytes and T cells
*A) Monocytes and T cells were stimulated with 100 ng/ml PMA. ROS production was detected over time. B) Quantification of ROS. Data are the mean of three independent experiments ± SEM, 1-way ANOVA, Tukey's Multiple Comparison Test, ****p < 0.0001*

In summary, PMA-induced activation of the NADPH oxidase with subsequent release of ROS is a predominant feature of myeloid phagocytes (*i.e.* monocytes and macrophages) and not of lymphoid T cells. It leads to an extracellular ROS burst and elevated ROS levels within the cell. The NADPH oxidase inhibitor DPI successfully inhibited the production of ROS to control level.

4.4 Oxidative DNA damage and apoptosis in phagocytes

Oxidative DNA damage like 8-oxoG lesions form continuously in the human genome of every cell every day due to metabolic processes. They are detected and repaired by BER. As shown in section 4.3, phagocytes, *i.e.* monocytes and macrophages, can be stimulated with PMA to produce high amounts of ROS in a short period of time. The ROS burst led to elevated ROS levels outside as well as inside the cells. Therefore, it was of interest whether the ROS burst led to DNA damage in the phagocytes (auto-intoxication). It was also of interest, whether DNA-repair deficient monocytes reacted differently compared to DNA-repair competent macrophages.

First, a reliable detection method for 8-oxoG had to be established. Therefore, immunofluorescence staining of 8-oxoG was tested in macrophages treated with 1 mM H_2O_2 for 10 min. In comparison to the medium control, H_2O_2 led to massive DNA damage in macrophages with a strong immunofluorescence signal inside the nucleus (Fig. 24).

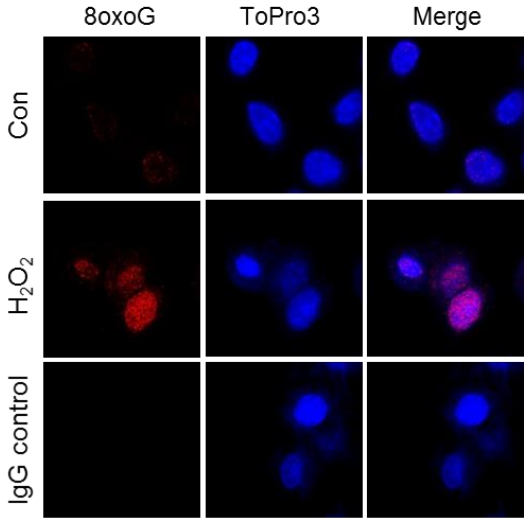

Fig. 24: Immunofluorescence staining of 8-oxoG in macrophages
Cells were treated with 1 mM H_2O_2 for 10 min and then fixed for immunofluorescence staining of 8-oxoG. Basal 8-oxoG levels were determined (Con) and compared to the oxidising agent H_2O_2. The secondary antibody control (IgG control) showed no unspecific signals.

In vivo, LPS is considered a regular activator of phagocytes. *Ex vivo*, intracellular ROS levels were not increased after LPS treatment for 30 min and 24 h (Fig. 19). 8-oxoG formation after LPS was analysed in macrophages at various time points. Cells were treated with 50 ng/ml LPS over a period of 24 h. Cells were fixed and stained for 8-oxoG lesions. H_2O_2 was used as a positive control. In comparison to the medium controls taken at different time points (10 min, 6 h and 24 h after the start of treatment), LPS-treated cells showed increased 8-oxoG signals after 10 and 20 min as well as 1 and 3 h after the start of treatment (Fig. 25).

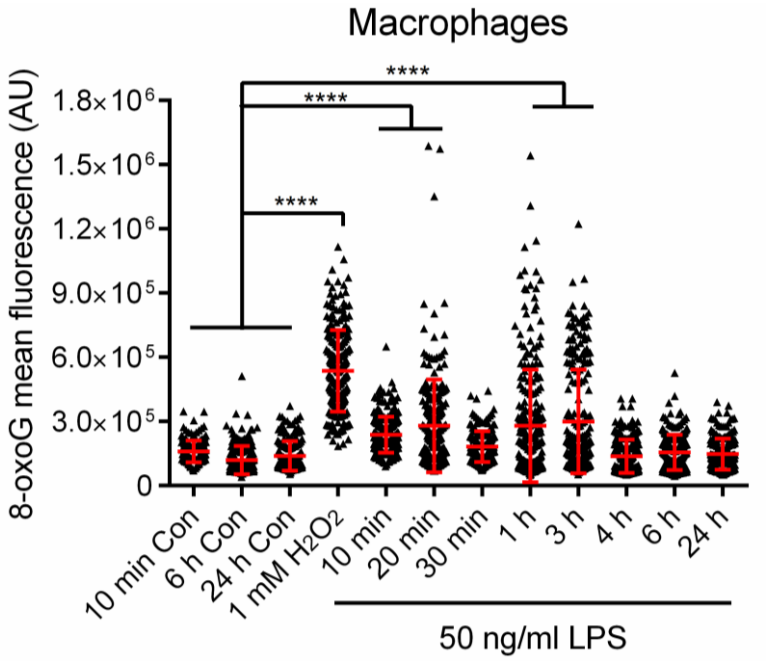

Fig. 25: Quantification of the 8oxoG fluorescence intensity after LPS treatment
*Macrophages were treated with 50 ng/ml LPS (E.coli 0127:B8) for the indicated time points. In addition, three medium controls at 10 min, 6 h and 24 h were collected. As a positive control, macrophages were treated with 1 mM H_2O_2 for 10 min. Data display two to three independent experiments ± SD. For each experiment 40 - 80 cells were analysed per sample. Statistical analysis: 1-way ANOVA, Tukey's Multiple Comparison Test, ****p < 0.0001*

Later time points (4 – 24 h) showed 8-oxoG signals similar to control level. There was a high variance of LPS-associated 8-oxoG formation within the experiments compared to the oxidising agent H_2O_2. LPS was considered unsuitable for further experiments as neither the ROS production nor the subsequent DNA lesions could be detected in a reliable manner. PMA was considered a better alternative for robust induction of ROS bursts.

Next, 8-oxoG formation was measured in monocytes and macrophages after they were activated by PMA. The cells were pulse-activated for 15 min to initiate ROS production. Then, the medium was removed, cells were washed with PBS and supplied with fresh, PMA-free medium. After an additional 45 min, the cells were fixed and stained for 8-oxoG to determine the initial DNA damage burden. Pulse-activation of monocytes and macrophages with 100 ng/ml PMA led to an increase in 8-oxoG formation (Fig. 26). The solvent control displayed low levels of 8-oxoG in both cell types. As a positive control, macrophages were treated with 1 mM H_2O_2 for 10 min.

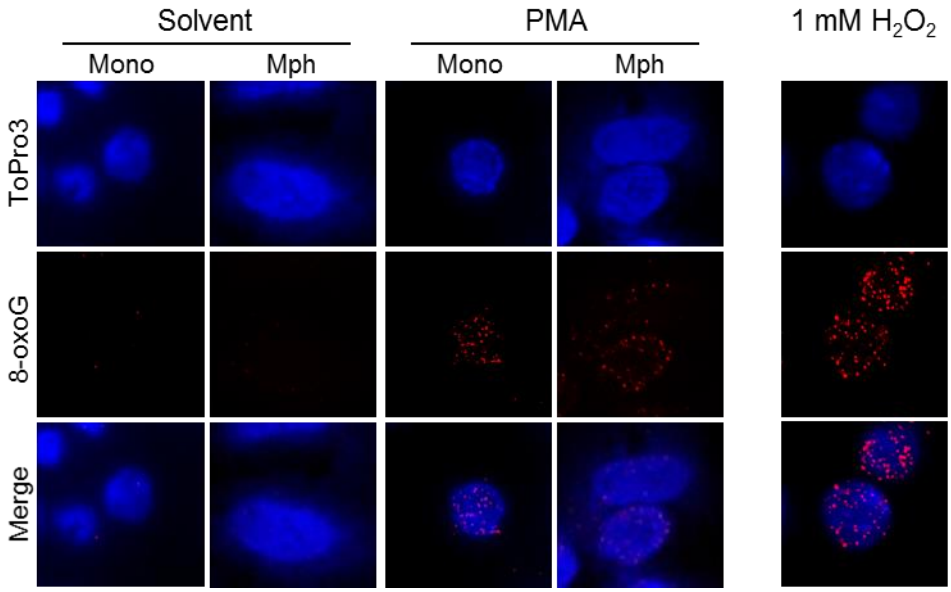

Fig. 26: 8-oxoG formation in monocytes and macrophages after stimulation with PMA
Monocytes (Mono) and macrophages (Mph) were treated with 100 ng/ml PMA for 15 min and then incubated for additional 45 min in PMA-free medium. Afterwards, cells were fixed and stained for 8-oxoG lesions. 1 mM H_2O_2 for 10 min was used as a positive control.

In addition to 8-oxoG immunofluorescence staining, DNA damage was also assessed using the FPG-modified alkaline Comet assay. FPG recognises and excises the oxidative DNA lesion resulting in a SSB. In comparison to cells subjected to alkaline Comet assay without FPG, the oxidative DNA damage burden can be visualised and quantified. Monocytes and macrophages were pulse-activated with PMA and then incubated for another 45 min in fresh medium to assess the initial oxidative damage burden. PMA-induced ROS production led to DNA damage in monocytes and macrophages (Fig. 27). The solvent control showed no or little DNA damage in both cell types. Both cell types displayed similar amounts of SSBs in the absence of FPG (tail intensity ~25 %). In the presence of FPG, the amount of SSBs was slightly higher than without FPG (tail intensity ~30 %) but did not reach significance. Both monocytes and macrophages showed the same amount of initial damage within 1 h and both converted most of the oxidative damage to SSBs within that time.

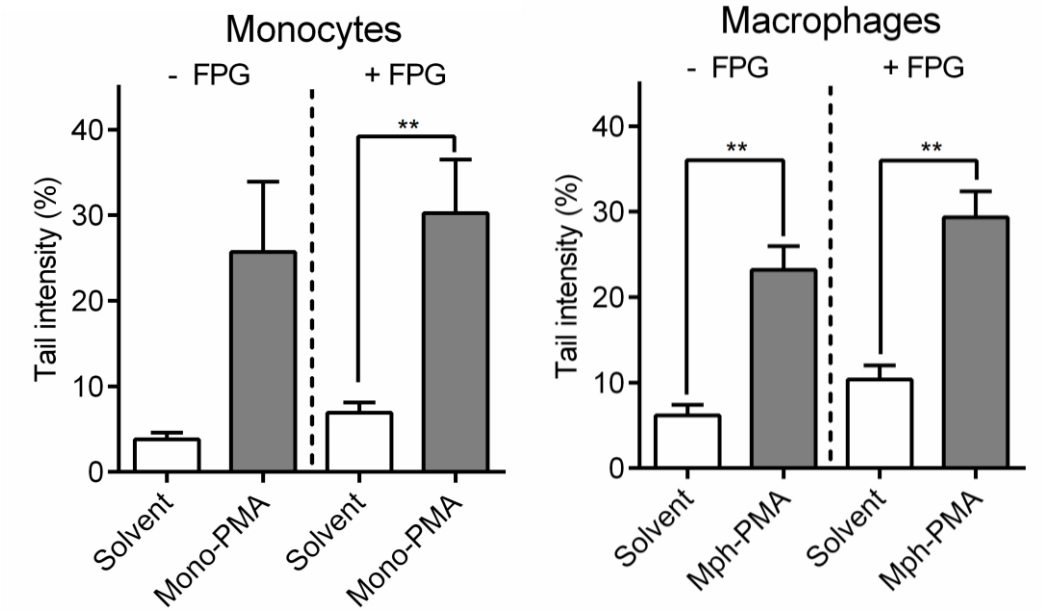

Fig. 27: Oxidative DNA damage and SSB formation in monocytes and macrophages
*Cells were treated with PMA for 15 min (Mono-PMA and Mph-PMA) and were then incubated in PMA-free medium for 45 min. Initial DNA damage was assessed using the FPG-modified Comet assay. Without FPG, SSBs were measured. In the presence of FPG oxidative DNA lesions were converted to SSBs. Data are the mean of four-five independent experiments ± SEM, Test for statistical significance was performed by Student's unpaired t-test (two-tailed), **p < 0.01*

Next, the amount of DNA fragmentation was assessed over time using the alkaline Comet assay. Monocytes and macrophages were pulse-activated with PMA and SSB formation was measured immediately after treatment (0 h) as well as 1 h and 4 h later. Monocytes displayed a strong formation of SSBs within 1 h (Fig. 28).

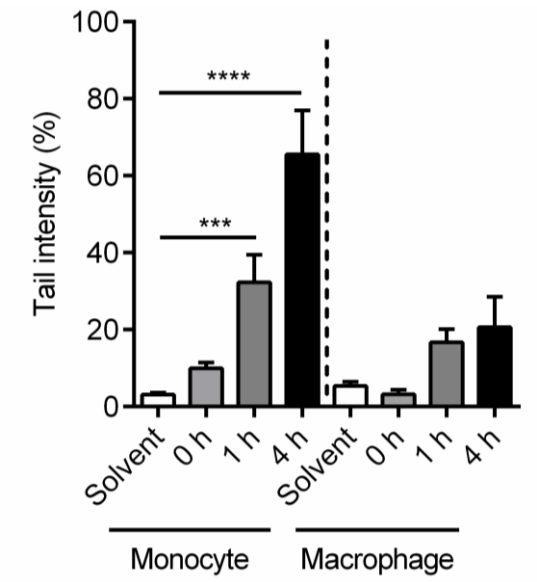

Fig. 28: SSB formation in monocytes and macrophages after the ROS burst provoked by PMA
*Cells were pulse-treated with PMA for 15 min to stimulate ROS production and then incubated for up to 4 h in fresh medium. SSB formation was measured in monocytes and macrophages over a period of 4 h. Data are the mean of at least three independent experiments ± SEM, 1-way ANOVA, Tukey's Multiple Comparison Test, ***p < 0.001*

As the monocytes displayed increasing amounts of oxidative DNA damage and SSBs when activated, cell death was measured after 24 h and 48 h using Annexin V staining. Cell death data for 24 h can be found in the supplements (Fig. S9). Monocytes and macrophages were

either pulse-activated for 15 min (Mono-PMA and Mph-PMA respectively) or stimulated continuously for 48 h (48 h PMA) to produce ROS. Monocytes showed an increase in apoptosis of ~25 % after pulse-activation (Fig. 29A) and ~40 % when stimulated for 48 h with PMA (Fig. 29A, 48 h PMA). Macrophages showed no increase in apoptosis after pulse-activation (Mph-PMA) and a moderate increase in apoptosis of ~20 % after 48 h PMA treatment (Fig. 29B, 48 h PMA).

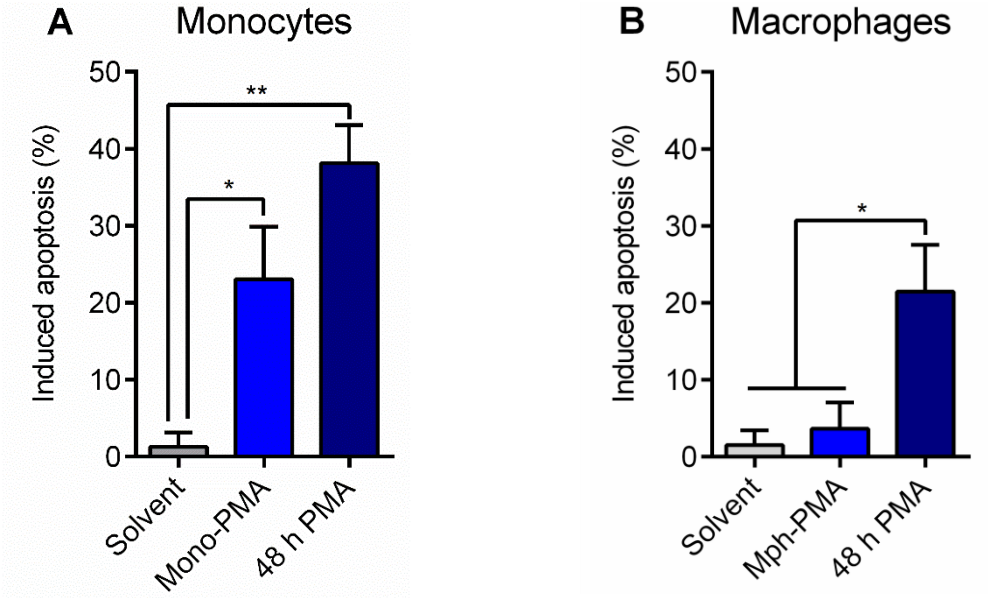

Fig. 29: Cell death of monocytes and macrophages after the ROS burst was induced by PMA treatment

*Cells were either pulse-activated with 100 ng/ml PMA for 15 min (Mono-PMA and Mph-PMA) or continuously exposed to PMA for 48 h (48 h PMA). Cell death was measured in A) monocytes and B) macrophages using Annexin V. Data are the mean of four independent experiments ± SEM, 1-way ANOVA, Tukey's Multiple Comparison Test, *p < 0.05, **p < 0.01*

In summary, a PMA-induced ROS burst in monocytes and macrophages led to intracellular ROS formation which damaged the DNA (auto-intoxication). Oxidative DNA lesions were detected in monocytes and macrophages. The DNA repair-deficient monocytes showed an accumulation of SSBs over time and underwent apoptosis after 48 h. DNA repair competent macrophages showed similar initial DNA damage levels but not an accumulation of SSBs. Their pulse-activation did not lead to apoptosis. Continuous stimulation with PMA for 48 h led to a strong induction of apoptosis in monocytes and a moderate response in macrophages.

4.5 Co-culture of ROS-producing macrophages and unstimulated monocytes

As was shown in section 4.4, monocytes are more sensitive to their own ROS than macrophages. ROS-induced oxidative DNA damage led to SSB formation followed by apoptosis. During an inflammatory response, monocytes are recruited to the site of damage to engage in the host's defence. In inflammatory tissues, ROS levels are elevated (Mittal *et al.* 2014) and may not only damage pathogens but also the surrounding tissue and recruited immune cells. Therefore, we addressed the questions of whether ROS from adjacent cells were strong enough to damage DNA repair-deficient monocytes in their vicinity. Freshly isolated monocytes were co-cultured in a ~1:1 ratio with PMA-activated, ROS-producing phagocytes, namely macrophages.

First, oxidative DNA damage was detected via immunofluorescence staining of 8-oxoG in monocytes that were co-cultured with pulse-activated macrophages or solvent-treated macrophages for 1 h. Macrophages were pulse-activated with PMA for 15 min. Then, the medium was removed, the cells were washed with PBS and fresh PMA-free medium was added before equal numbers of monocytes were added to the macrophages (Fig. 6). Monocytes displayed 8-oxoG lesions when co-cultured with activated macrophages (Fig. 30, Mph-PMA). In the presence of solvent-treated macrophages, monocytes showed fewer 8-oxoG lesions (Solvent). Concomitant PMA treatment of both cell types led to high 8-oxoG damage in monocytes (Fig. 30, PMA).

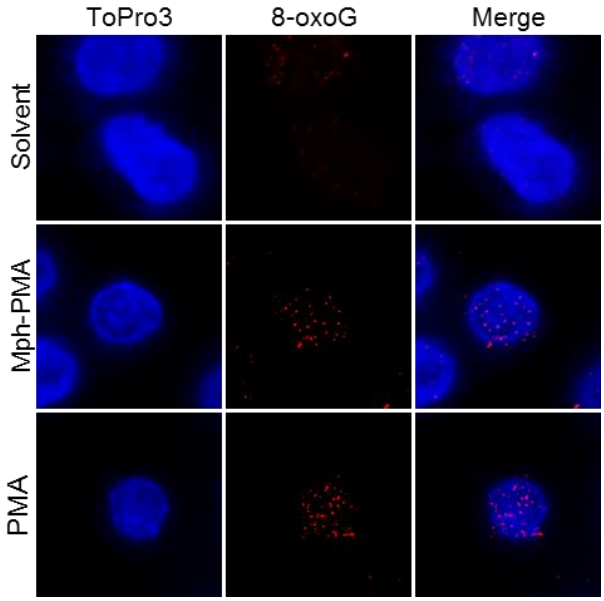

Fig. 30: Oxidative DNA damage in monocytes co-cultured with activated macrophages
Monocytes were exposed to PMA-activated macrophages (Mph-PMA) for 1 h or they were co-cultured with non-activated macrophages (Solvent). Monocytes, were harvested and stained for 8-oxoG. In addition, co-cultured cells were concomitantly treated with PMA for 1 h and monocytes were stained for 8-oxoG (PMA).

Next, the oxidative DNA damage and SSB formation were assessed in monocytes co-cultured with activated macrophages using the FPG-modified alkaline Comet assay. Macrophages were pulse-activated for 15 min to initiate their ROS burst. Then, the PMA-medium was removed, the cells were washed with PBS and fresh, PMA-free medium was added before monocytes were added to the culture. After 1 h of co-culture, monocytes in suspension were removed from the plate and subjected to the Comet assay. Non-activated macrophages did not cause DNA damage in monocytes as their DNA did not migrate (Fig. 31A, Solvent). Pulse-activated macrophages led to oxidative DNA damage in monocytes. In the presence of FPG, the oxidative damage in monocytes was converted to SSBs and led to DNA migration (Fig. 31A, Mph-PMA). Concomitant exposure of both cell types to PMA led to oxidative DNA damage and SSBs in monocytes (Fig. 31A, PMA). The migration of the DNA was quantified and showed an accumulation of oxidative lesions in monocytes that were not yet converted into SSBs by BER (Fig. 31B, Mph-PMA). Concomitant exposure of monocytes and macrophages to PMA for 1 h led to SSB formation and massive oxidative lesions in monocytes (Fig. 31B, PMA).

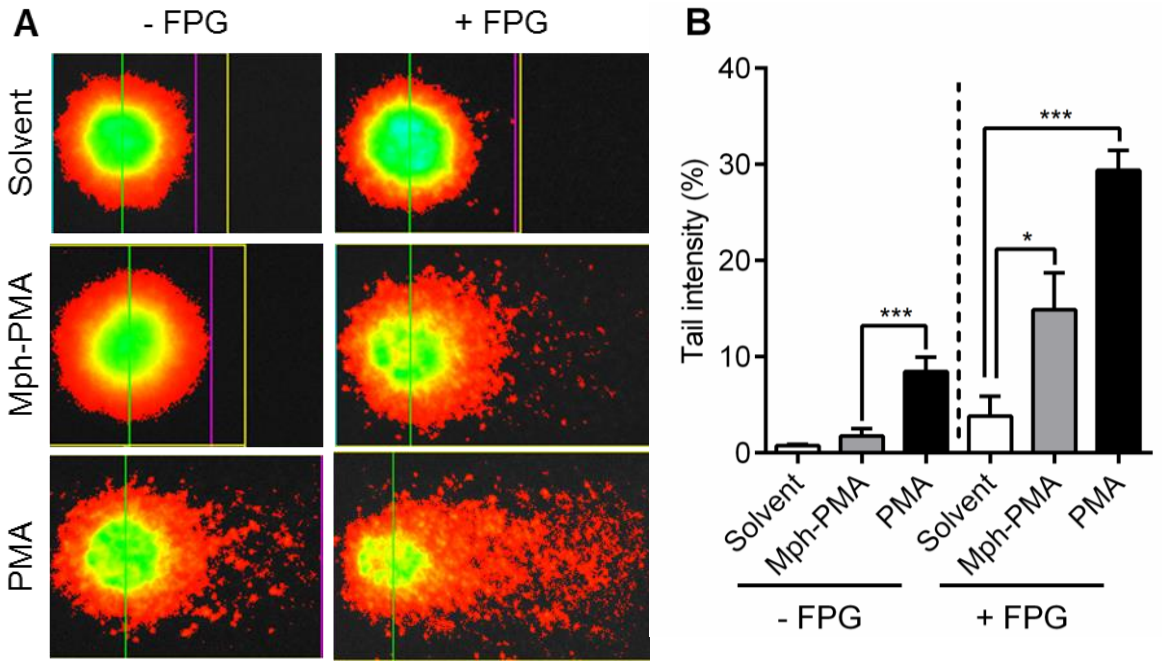

Fig. 31: Oxidative DNA damage and SSB formation in co-cultured monocytes
*A) Representative images of DNA fragmentation in monocytes after exposure to PMA-activated macrophages (Mph-PMA) or concomitant exposure of both monocytes and macrophages (PMA) for 1 h. B) Monocytes were co-cultured with PMA-activated macrophages for 45 min. Monocytes were harvested and subjected to the FPG-modified alkaline Comet assay to assess the SSB (-FPG) and oxidative DNA damage (+FPG). Data are the mean of four independent experiments ± SEM, 1-way ANOVA, Dunnett's Multiple Comparison Test, *p < 0.05, ***p < 0.001*

As monocytes were very susceptible to ROS-producing macrophages and showed oxidative DNA damage, the DNA damage response in co-cultured monocytes was analysed. After 24 h of co-culture with solvent-treated macrophages (Solvent) or pulse-activated macrophages (Mph-PMA), monocytes were harvested and DNA damage recognition and repair factors were assessed using immunofluorescence staining and Western Blot analysis. Increased amounts of phosphorylated ATM were detected in monocytes co-cultured with ROS-producing macrophages but not in monocytes exposed to solvent-treated macrophages (Fig. 32A). Monocytic basal ATM expression was the same in both co-culture conditions (Fig. 32B). The DSB marker 53BP1 also accumulated in monocytes that were co-cultured with activated macrophages (Fig. 32C). Furthermore, phosphorylation of CHK2 was observed in stressed monocytes. p53 stabilised in the cells and was phosphorylated at position 46, a marker for pro-apoptotic signalling (Fig. 32D). KAP1, another target of pATM was not phosphorylated (Fig. S11). These results indicate that the ROS-induced DNA damage was sufficient in activating the DNA damage response of monocytes and that apoptosis may be initiated.

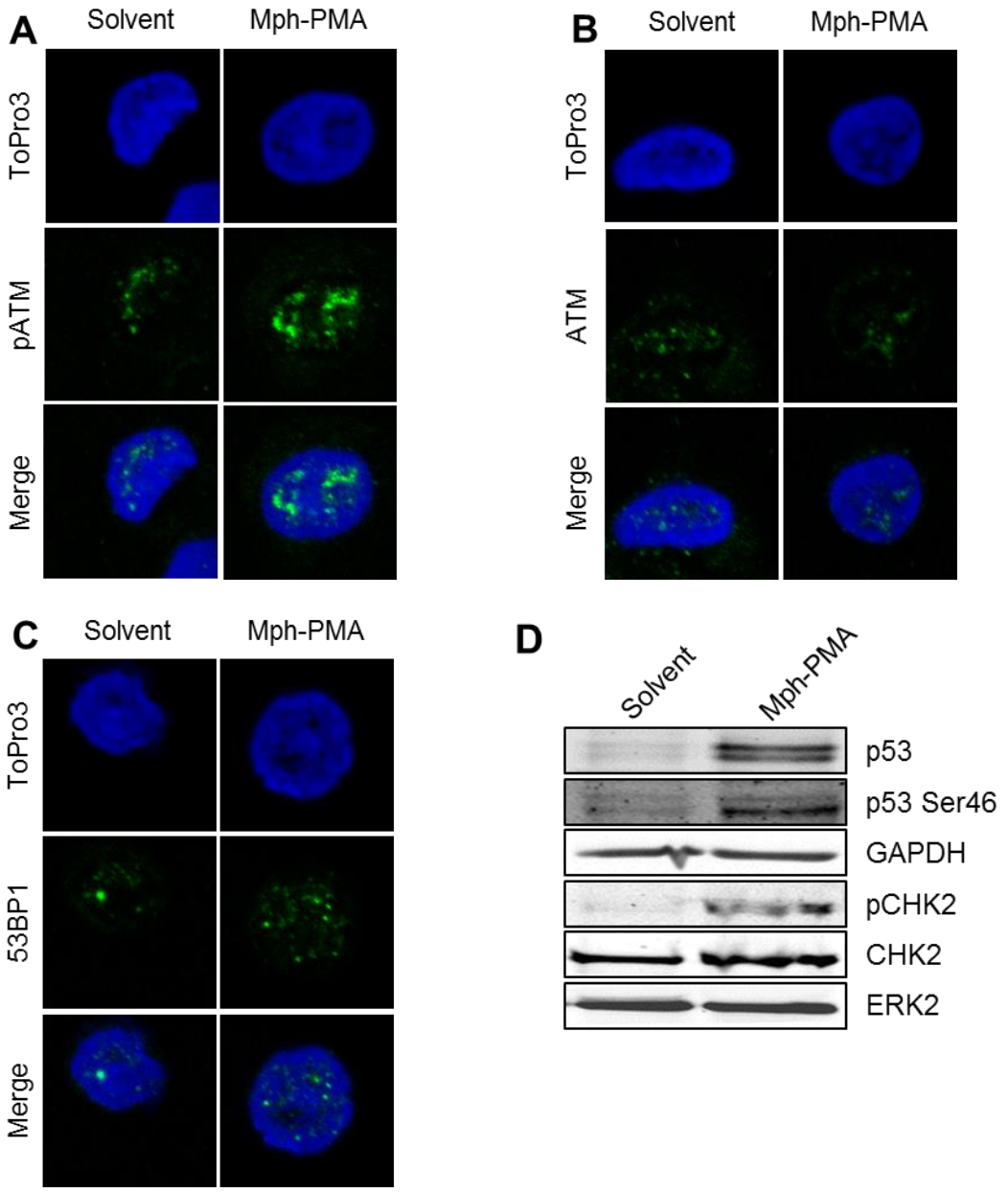

Fig. 32: Activation of the DDR in co-cultured monocytes
Monocytes were co-cultured with PMA-activated (Mph-PMA) or solvent-treated macrophages (Mph-Solvent) for 24 h. Monocytes were harvested and DDR factors were detected via immunofluorescence staining and Western Blot analysis. A) Phosphorylated ATM, B) unphosphorylated ATM and C) 53BP1 were detected via immunofluorescence staining. D) The DDR factors pCHK2 and p53 phosphorylated at position Ser46 were analysed using Western Blot technique. ERK2 and GAPDH were used as loading controls.

As the DDR was activated in co-cultured monocytes and p53 was phosphorylated at Ser46, apoptosis was measured in co-cultured monocytes and macrophages after 24 h (see supplements Fig. S13) and 48 h. For the gating strategy see supplements Fig. S12. Macrophages displayed no increase in apoptosis when treated with solvent (Solvent) or when they were pulse-activated with PMA for 15 min (Mph-PMA) (Fig. 33A). Chronic exposure of the co-cultured cells to PMA for 48 h led to ~30 % apoptosis in macrophages and 40 % in monocytes (Fig. 33B, 48 h PMA). Monocytes co-cultured with pulse-activated macrophages displayed an increase in apoptosis by ~20 % (Fig. 33B, PMA-Mph).

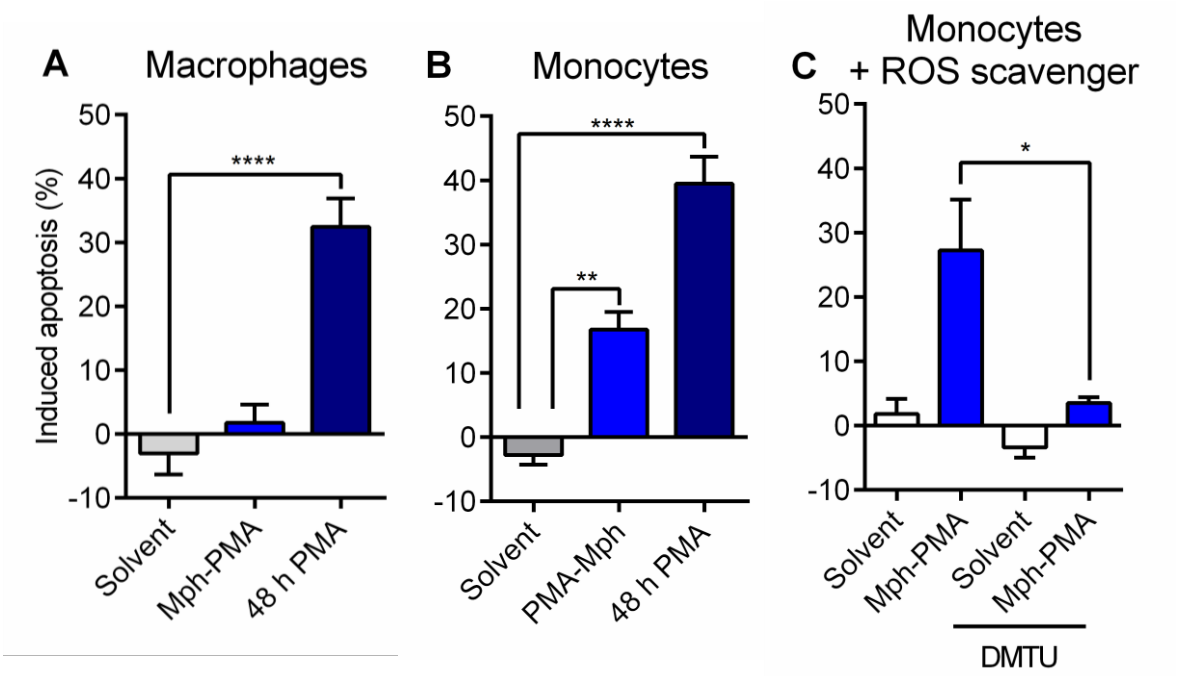

Fig. 33: Cell death of monocytes in co-culture with activated macrophages
*Macrophages were pulse-activated with PMA for 15 min (Mph-PMA), washed with PBS and supplemented with fresh medium before monocytes were added. Alternatively, co-cultured cells were concomitantly exposed to PMA for 48 h (48 h PMA). Cell death of macrophages (A) and monocytes (B) was measured 48 h later using Annexin V. C) Monocytes were co-cultured with solvent-treated or PMA pulse-activated macrophages (Mph-PMA) ± ROS scavenger DMTU (10 mM) and cell death was measured 48 h later. Data are the mean of five independent experiments ± SEM, 1-way ANOVA, Tukey's Multiple Comparison Test, *p < 0.05, **p < 0.01, ****p < 0.0001*

Monocytes were also co-cultured in the presence of ROS scavenger DMTU (10 mM) (Fig. 33C). Without the ROS scavenger monocytes displayed ~25-30 % apoptosis when exposed to activated macrophages. Apoptosis dropped to ~5 % when DMTU was present in the medium.

In short, it was shown that DNA repair-deficient monocytes are susceptible to ROS generated from adjacent macrophages. PMA pulse-activated macrophages generated enough ROS to damage the DNA of monocytes in their vicinity. Monocytes activated their DDR and underwent apoptosis within 48 h of co-culture. In the presence of the ROS scavenger DMTU, a significant reduction in apoptosis was observed in monocytes. DNA repair-competent macrophages displayed similar initial DNA damage levels but did not convert it to persisting SSBs. Macrophages showed no increase in apoptosis after their pulse activation. Continuous stimulation with PMA led to an increase in cell death in macrophages but it was slightly lower than in monocytes.

4.6 Co-culture of ROS-sensitive monocytes with other stimulated phagocytes

As was shown in the previous section, monocytes are susceptible to the ROS burst of macrophages as they suffered DNA damage, activated the DDR, and finally underwent apoptosis. Next, it was tested whether neutrophilic granulocytes were also able to kill monocytes with their respiratory burst. Neutrophils are the most common leukocytes in the blood and they are the first to be recruited to sites of inflammation. In contrast to macrophages, they are very short-lived and die after their host defence action.

Similar to monocytes and macrophages (see section 4.3) the extracellular ROS burst of freshly isolated granulocytes was measured. Granulocytes displayed a very rapid response to PMA-activation. Their respiratory burst peaked within 12 to 14 min and dropped to basal levels within 25 min (Fig. 34). Hence, for cell death studies of co-cultured monocytes and granulocytes, the pulse-activation treatment of granulocytes had to be adjusted. Instead of pulse-treating the cells for 15 min, cells were triggered for 8 min, washed in PBS and centrifuged before they were re-suspended in PMA-free medium. Then, they were added to monocytes.

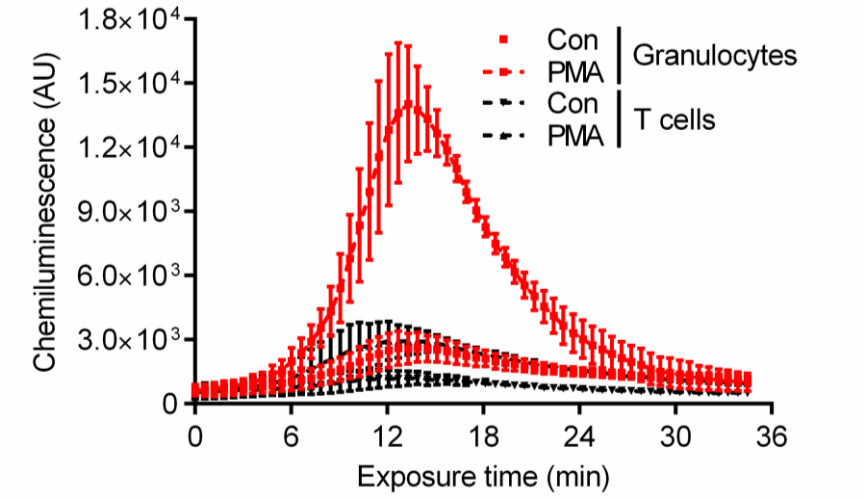

Fig. 34: Extracellular ROS burst in granulocytes and T cells
ROS production of granulocytes and T cells was measured over time. Cells were stimulated with 100 ng/ml PMA to induce ROS production. Data are the mean of three independent experiments ± SEM.

Oxidative damage in co-cultured monocytes was assessed using the FPG-modified alkaline Comet assay (see supplements Fig. S16). Granulocytes and monocytes are both suspension cells and thus they could not be co-cultured in normal plates as they could not be separated afterwards. Instead, trans-well plates had to be used which separated both cell types by a membrane and increased the distance between them. Monocytes displayed oxidative damage in the presence of activated granulocytes. The response was not as pronounced as in the co-culture set-up with monocytes and macrophages.

For cell death studies, granulocytes and monocytes could be distinguished by their staining properties; granulocytes were labelled with CFSE and monocytes were labelled for CD14 marker expression. Monocytes were considered CFSE negative and CD14+. Co-cultured monocytes displayed massive apoptosis (~80 %) when co-cultured with pulse-activated granulocytes (Fig. 35A).

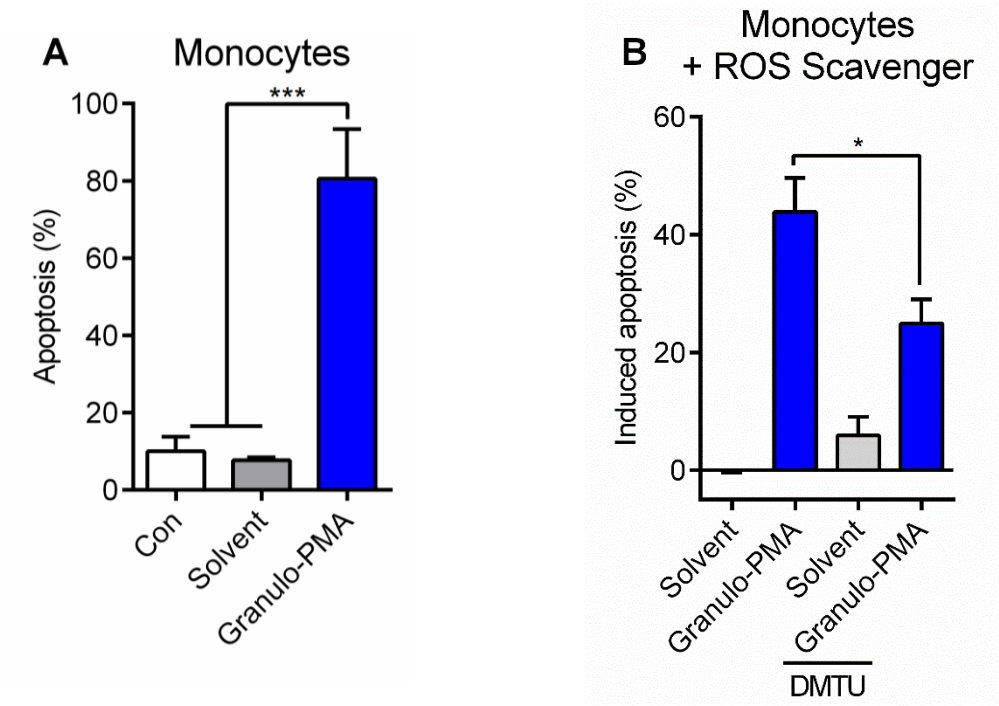

Fig. 35: Cell death of monocytes in co-culture with activated granulocytes
*Granulocytes were pulse-activated with PMA for 10 min (Granulo-PMA), washed with PBS and supplemented with fresh medium before monocytes were added. A) Cell death of co-cultured monocytes was measured after 48 h using Annexin V. Corresponding data of granulocytes can be found in the supplements (Fig. S17). B) Monocytic cell death after co-culture with activated granulocytes (Granulo-PMA) in the presence of ROS scavenger DMTU (10 mM) was measured after 48 h. Data are the mean of four to six independent experiments ± SEM, 1-way ANOVA, Tukey's Multiple Comparison Test, * p < 0.05, ***p < 0.001*

Solvent-treated granulocytes did not induce apoptosis in co-cultured monocytes. By adding the ROS scavenger DMTU to the medium, monocytic apoptosis dropped significantly (Fig. 35B) from ~40 % to ~20 %. Short-lived granulocytes were all dead after 48 h, independent of treatment (Fig. S17).

As PMA is a pharmacological activator of the PKC and subsequently the NADPH oxidase, an alternative activation mechanism was used to confirm the data. As previously described (Aga *et al.* 2004), LPS in combination with 2′(3′)-O-(4-Benzoylbenzoyl) ATP (bzATP) can also elicit a respiratory burst in murine macrophages. Similar to the published treatment, human macrophages were activated with LPS/bzATP to stimulate ROS production. A release of ROS was detectable in macrophages (Fig. 36A). It was weaker compared to PMA (Fig. 22). Monocytes co-cultured with LPS-primed and bzATP-activated macrophages for 24 h led to an increase in apoptosis compared to the untreated control (Fig. 36B).

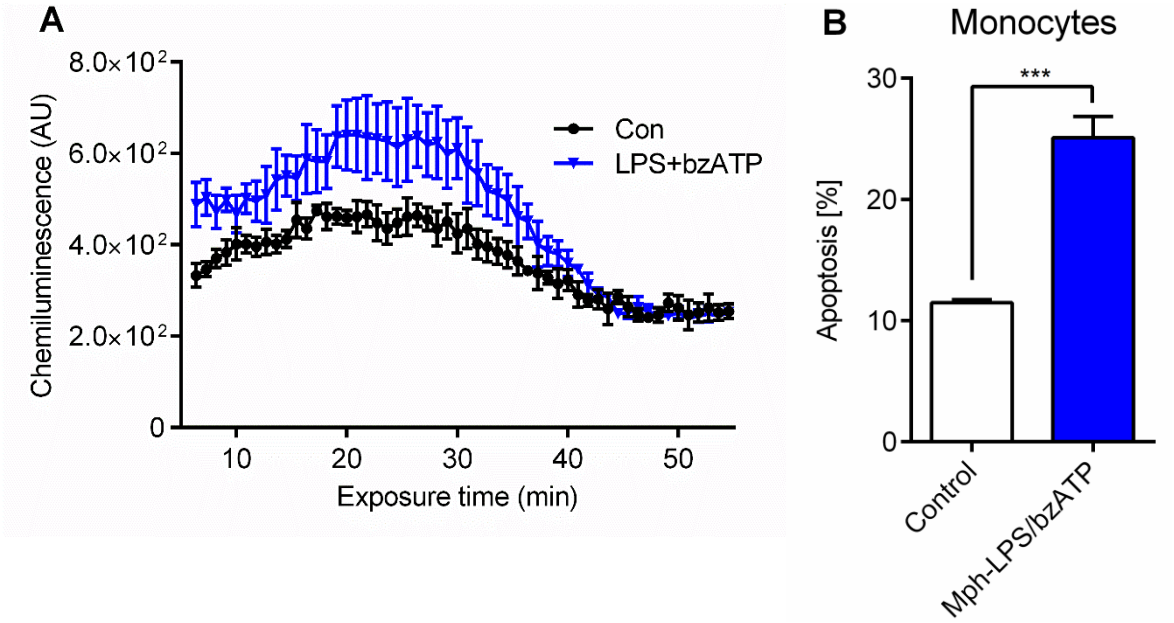

Fig. 36: LPS/bzATP-activated macrophages produce extracellular ROS and kill monocytes
*A) Macrophages were primed with 1 µg/ml LPS for 16 h. The ROS burst was initiated by adding 250 µM bzATP. Data are the mean of three independent experiments ± SEM. B) Macrophages were primed with 1 µg/ml LPS for 16 h before they were pulse-activated with 250 µM bzATP for 15 min. Monocytes were co-cultured with macrophages for 24 h and cell death was measured using Annexin V. Corresponding data of macrophages can be found in the supplements (Fig. S18). Data are the mean of three independent experiments ± SEM, Student's unpaired t-test (two-tailed), p*** < 0.001*

4.7 Co-culture of peripheral blood lymphocytes with activated phagocytes

Unstimulated PBL are known for their hypersensitivity towards DNA damaging agents such as ionising radiation (Heylmann *et al.* 2014) and alkylating chemotherapeutics (Heylmann *et al.* 2013). Here, PBL were analysed for ROS-induced cytotoxicity. They were exposed to ROS-producing macrophages and apoptosis was measured 48 h later. Macrophages displayed a stronger apoptotic response (~30 %) to PMA than the lymphoid cells (~10 %) (Fig. 37A and B). CD3+CD8+ CTL gated from the PBL population showed ~15 % apoptosis (Fig. 37C).

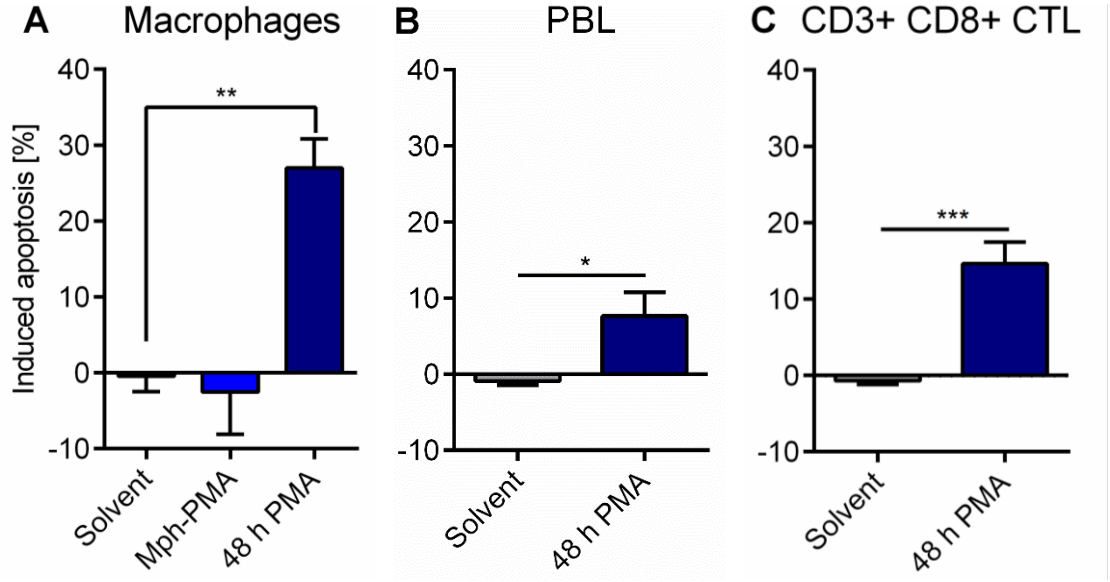

Fig. 37: Cell death of mono-cultured macrophages, PBL and CD3+ CD8+ CTL
*A) Macrophages were pulse-activated with 100 ng/ml PMA for 15 min (Mph-PMA) or continuously exposed to PMA (48 h PMA) and apoptosis was measured 48 h later using Annexin V. B) PBL were treated with PMA for 48 h before cell death was measured. C) Using CD3+ CD8+ markers, CTL were gated from the PBL population and analysed for increases in apoptosis after treatment with PMA. Data are the mean of five to six independent experiments ± SEM, 1-way ANOVA, Tukey's Multiple Comparison Test, *p < 0.05, **p < 0.01, ***p < 0.001*

Next, PBL were co-cultured with activated macrophages and apoptosis was measured 48 h later. Macrophages displayed a 15 % increase in cell death after continuous exposure to PMA for 48 h and no response to their own pulse activation (Mph-PMA) (Fig. 38A). PBL and their CTL fraction displayed 15-20 % cell death when exposed to activated macrophages (Fig. 38B and C). PMA exposure for 48 h led to an increase of ~35 % in the PBL and ~50 % in the CTL fraction.

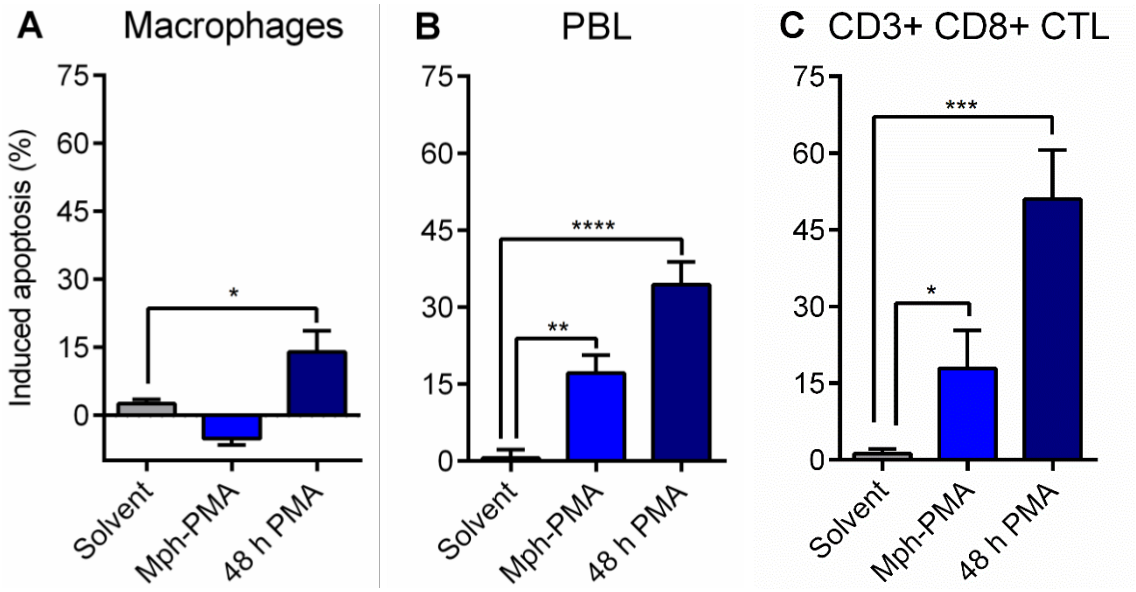

Fig. 38: Cell death of co-cultured PBL and CTL with PMA-activated macrophages
*Macrophages were activated with PMA for 15 min (Mph-PMA), washed with PBS, supplemented with fresh medium and then incubated with PBL. Apoptosis was measured in A) macrophages, B) PBL and C) CD3+CD8 CTL gated from the PBL population after 48 h using Annexin V. Data are the mean of five to six independent experiments ± SEM, 1-way ANOVA, Tukey's Multiple Comparison Test, *p < 0.05, **p < 0.01, ***p < 0.001, ****p < 0.0001*

In mono-cultured PBL, continuous PMA exposure led to a moderate induction of apoptosis (~10 %) whereas the co-cultured PBL showed ~40 % apoptosis. Similar effects were observed in the CTL fraction of PBL. In mono-culture, CTL responded with 15 % apoptosis to PMA and in co-culture, the apoptotic fraction increased to 50 %. PBL and CTL were both susceptible to activated macrophages and underwent apoptosis (~20 %). In summary, similar to monocytes, PBL underwent apoptosis when exposed to ROS-producing macrophages.

4.8 Impaired differentiation potential of monocytes after ROS-induced damage

As was shown in section 4.4 (Fig. 29), monocytes are susceptible to their own ROS (auto-intoxication) and undergo apoptosis. However, not all cells died at the indicated time point. The same was observed in monocytes exposed to ROS from adjacent phagocytes, *i.e.* macrophages and granulocytes (section 4.5, Fig. 33 & Fig. 35). Therefore, it was addressed whether surviving monocytes were still capable of differentiating into macrophages.

First, monocytes were treated with solvent or PMA for 24 h. Then, the cells were washed with PBS and re-seeded in fresh medium containing GM-CSF. The cells matured into macrophages over six days. On the last day, non-adherent cells were washed away with PBS and adherent macrophages were analysed. Control and solvent-treated former monocytes developed into many, adherent macrophages (Fig. 39A, upper panel) with their characteristic elongated shape. Monocytes previously exposed to PMA were not able to mature into healthy macrophages afterwards (Fig. 39A, lower panel). There were fewer cells and the morphology was different compared to the controls. Then, all adherent cells were subjected to Annexin V staining. Control and solvent-treated cells showed 20-25 % apoptosis whereas PMA-treated cells were 70 % Annexin V positive, implying that the few differentiated cells were most likely not functional.

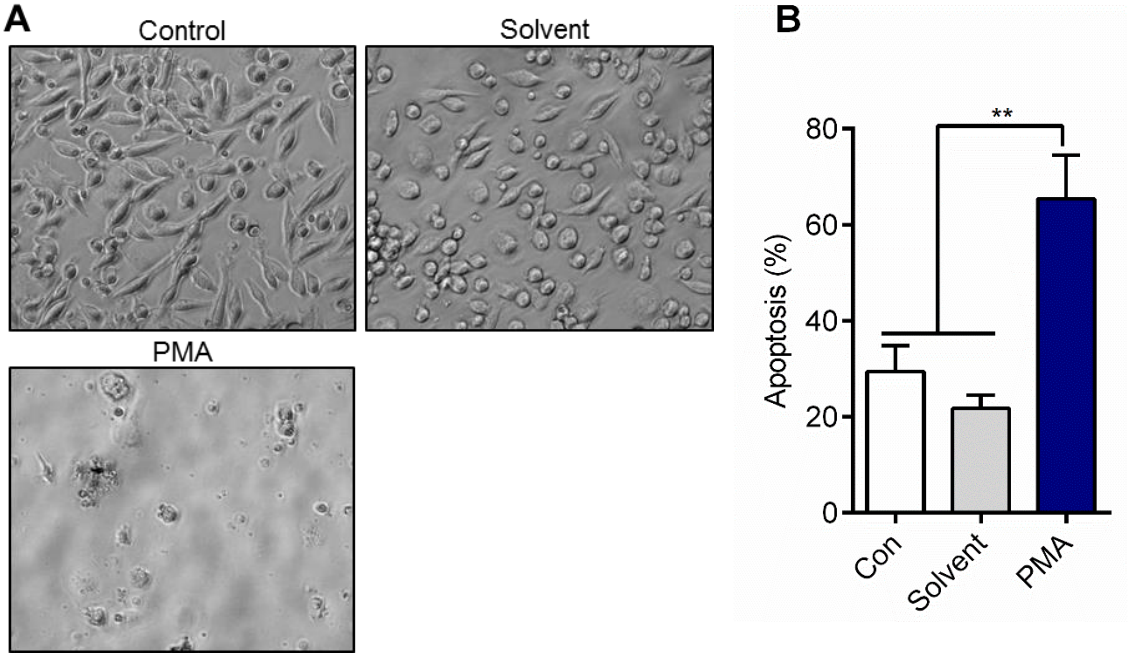

Fig. 39: Maturation of monocytes into macrophages when previously activated with PMA
*A) Representative images of monocyte-derived macrophages. Before differentiation was induced with GM-CSF, monocytes were treated with solvent (Solvent) or PMA for 24 h (PMA). After six days of differentiation, non-adherent cells were washed away and images were taken of the remaining cells. B) Cells were harvested and apoptosis was measured using Annexin V. Data are the mean of four independent experiments ± SEM, 1-way ANOVA, Tukey's Multiple Comparison Test, **p < 0.01*

Monocytes exposed to PMA-activated macrophages in co-culture for 24 h were also subjected to re-seeding and subsequent differentiation into macrophages. Similar to mono-cultured monocytes, maturation into new macrophages was severely impaired. Co-cultured with control or solvent-treated macrophages, monocytes were able to differentiate into functional and healthy looking macrophages (Fig. 40A, upper panel). However, monocytes exposed to PMA pulse-activated macrophages (Fig. 40A, lower panel, Mph-PMA) did not differentiate into new macrophages. Concomitant exposure of monocytes and macrophages to PMA for 24 h and subsequent re-seeding of monocytes in the presence of GM-CSF did not lead to maturation into macrophages (Fig. 40A, lower panel, PMA). The adherent cells were then subjected to Annexin V staining. Previous exposure to control or solvent-treated macrophages did not impair monocyte maturation into new macrophages. They showed 30 % Annexin V positive cells whereas cells previously exposed to activated macrophages or concomitant exposure to PMA resulted in 70 % apoptosis (Fig. 40B).

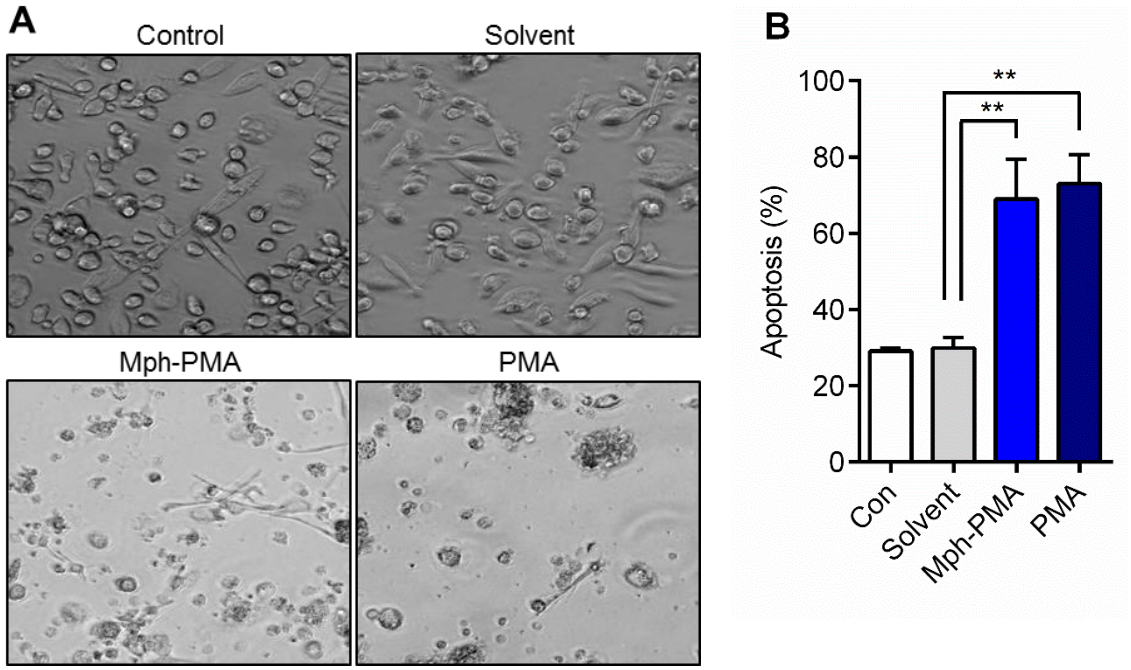

Fig. 40: GM-CSF-induced differentiation of monocytes after co-culture with PMA-activated macrophages

A) *Representative images of monocytes previously co-cultured with PMA-activated macrophages (Mph-PMA) and subsequent re-seeding in the presence of GM-CSF. Monocytes were co-cultured with untreated (Control), solvent-treated (Solvent) or PMA-stimulated macrophages (Mph-PMA). In addition, cells were concomitantly exposed to PMA. After 24 h, monocytes were separated from macrophages, re-seeded and differentiated into macrophages by adding GM-CSF. On day 6, the new macrophages were analysed. B) Apoptosis was measured using Annexin V. Data are the mean of at least three independent experiments ± SEM, 1-way ANOVA, Bonferroni's Multiple Comparison Test, **p < 0.01, ***p < 0.001.*

In summary, these data showed that monocytes, even if they survived their own respiratory burst or the ROS burst from adjacent cells, were unable to differentiate into new macrophages. The few remaining cells were apoptotic and, therefore, most likely non-functional.

4.9 XRCC1 expression in M-CSF- and GM-CSF-generated macrophages

In the preceding experiments monocytes were always differentiated into macrophages by adding GM-CSF. GM-CSF-generated macrophages display a pro-inflammatory cytokine profile with some features of M1 cells whereas M-CSF-generated macrophages have an anti-inflammatory cytokine profile and express some features of M2 cells. (Lacey *et al.* 2012). If M-CSF-generated macrophages were exposed to IFNγ or LPS their polarisation would shift to the classically activated M1 type. In the presence of IL-4, they would be considered alternatively activated M2 macrophages. These macrophages mostly differ in their cytokine profiles and immune response repertoire. The GM-CSF-generated macrophages show overlapping gene expression profiles with DCs. We addressed the question, whether M-CSF-generated macrophages were able to produce ROS to a similar degree as GM-CSF-generated macrophages. Furthermore, it was of interest whether XRCC1 expression was altered in M-CSF-matured macrophages compared to GM-CSF-macrophages.

Freshly isolated monocytes were differentiated into macrophages by adding either GM-CSF or M-CSF and incubating the cells for six days. Both types of macrophages were adherent.

GM-CSF-macrophages were mostly elongated whereas M-CSF-macrophages had a round shape (Fig. 41).

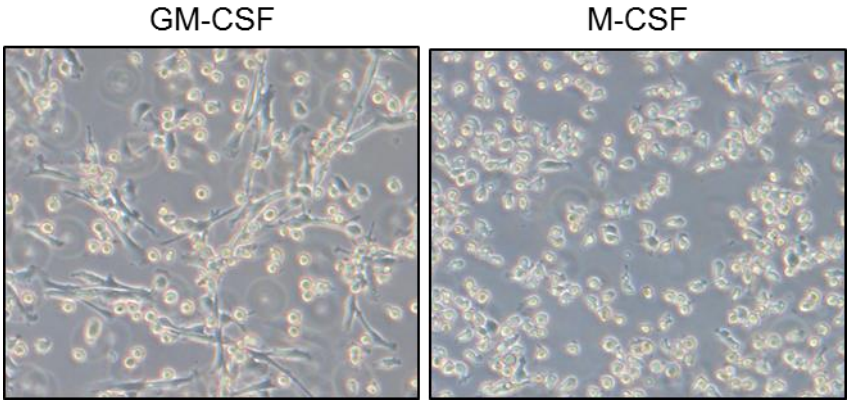

Fig. 41: Morphology of GM-CSF- and M-CSF-generated macrophages
GM-CSF-matured macrophages had mostly an elongated shape. M-CSF-macrophages had a round shape.

Next, both sets of macrophages were stimulated with PMA to produce ROS. The respiratory burst was measured over two hours. Both sets of macrophages showed a respiratory burst that reached its maximum at ~30-40 min after PMA addition. It declined slowly over time but did not drop to control levels after two hours (Fig. 42A). The quantification of the ROS burst showed no differences between GM-CSF- and M-CSF-generated macrophages (Fig. 42B).

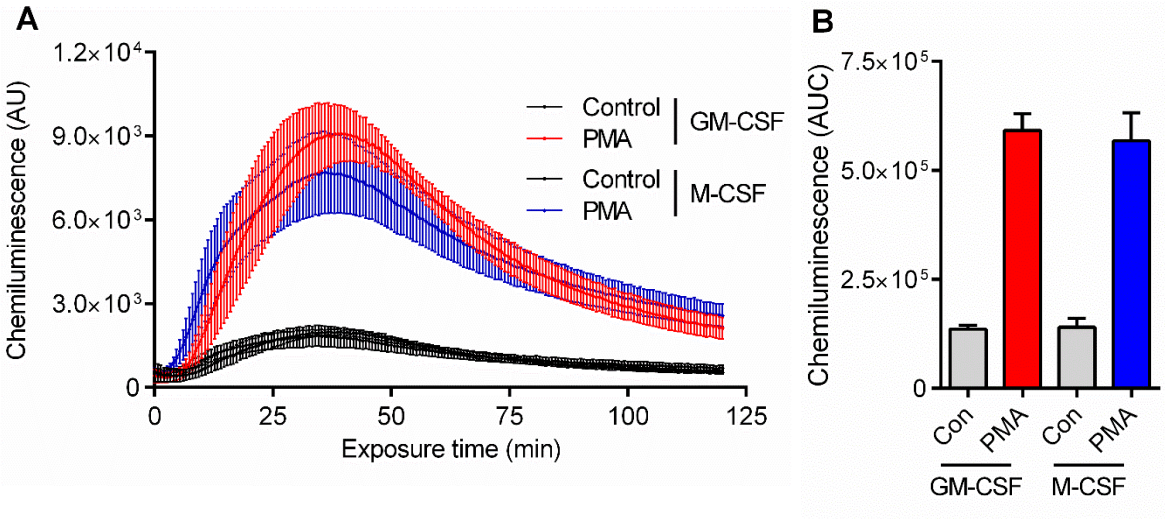

Fig. 42: Respiratory burst of macrophages generated with either GM-CSF or M-CSF
Monocytes matured into macrophages by adding either M-CSF or GM-CSF. A) The extracellular ROS burst was induced by PMA and measured over time. B) The amount of ROS was quantified by calculating the area under the curve (AUC). Data are the mean of six independent experiments ± SEM. Extracellular ROS detection was kindly performed by ..... under supervision.

XRCC1 expression was analysed in M-CSF- and GM-CSF-maturing macrophages. Monocytes were seeded onto cover slips and matured into macrophages by adding either M-CSF or GM-CSF. XRCC1 protein expression was detected via immunofluorescence staining. Samples were taken at days 0, 2, 4 and 6 of differentiation. Microscopic images showed no differences in overall XRCC1 protein expression between GM-CSF- and M-CSF- generated macrophages. Both showed similar kinetics in their XRCC1 expression; there was little XRCC1 protein detected at day 2 of differentiation. The amount of XRCC1 peaked at day 4 in both samples (Fig. 43).

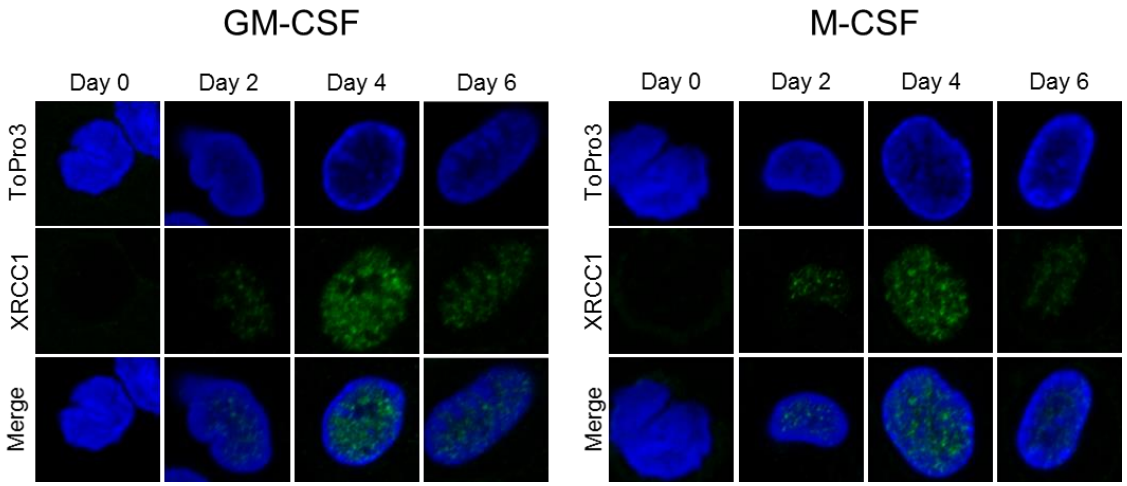

Fig. 43: Representative images of XRCC1 immunofluorescence staining in GM-CSF- and M-CSF-generated macrophages
Monocytes underwent differentiation into macrophages in the presence of either GM-CSF or M-CSF. Samples were collected at day 0 (monocyte), 2, 4 and 6 and were stained for XRCC1.

The quantification of the signal intensity verified the microscopic observation. XRCC1 expression increased over the course of maturation and reached its maximum at day 4 (Fig. 44). The levels were similar in M-CSF and GM-CSF generated macrophages.

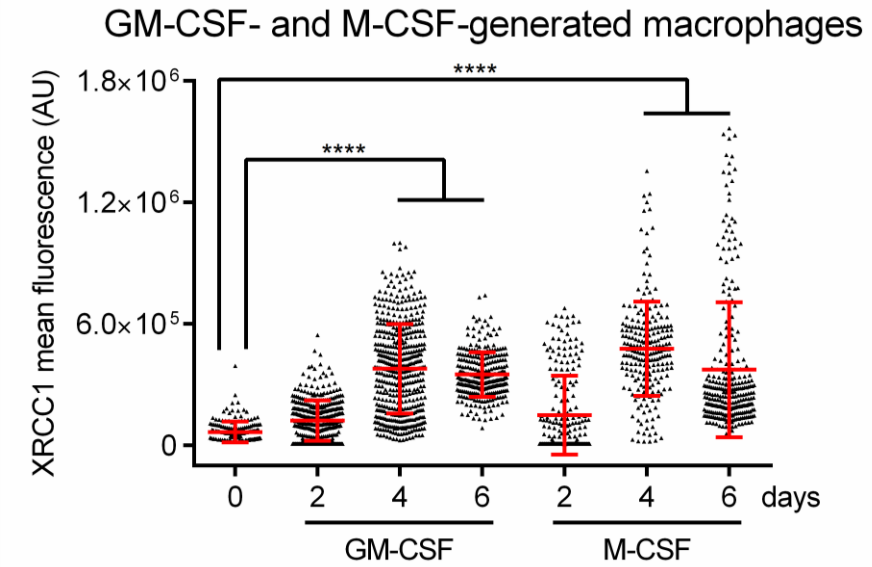

Fig. 44: Quantification of the XRCC1 signal intensity of GM-CSF- and M-CSF-generated macrophages
The XRCC1 expression in M-CSF- and GM-CSF-generated macrophages was quantified by measuring the mean fluorescence signal of XRCC1 in arbitrary units (AU). Each dot represents the fluorescence intensity of a single cell. Samples were collected at days 0, 2, 4 and 6. The data consist of three to four independent experiments ± SD*. For each condition, 60 - 100 cells were counted, 1-Way ANOVA, Tukey's Multiple Comparison Test, ****p < 0.0001. Quantification of XRCC1 signal intensity was kindly performed by ..... under supervision.*

In summary, M-CSF- and GM-CSF-generated macrophages are both ROS-producing and XRCC1-expressing phagocytes. It is reasonable to posit that in an inflammatory environment, M-CSF-matured macrophages could kill DNA repair-deficient monocytes with their respiratory burst without killing themselves, similar to GM-CSF-matured macrophages (see section 4.7).

4.10 Attenuated XRCC1 expression in maturing macrophages in the presence of the demethylation inhibitor 2-HG

The hypersensitivity of monocytes towards DNA-damaging ROS produced by themselves (auto-intoxication) or by adjacent phagocytes (killing *in trans*) is due to their DNA repair deficiency, caused by the lack of BER protein expression. During the course of differentiation into macrophages or DCs, they upregulate the BER protein expression of XRCC1, PARP-1 and ligase IIIα. The genome of monocytes is described as differentially methylated (Hachiya *et al.* 2017; Wallner *et al.* 2016; Klug *et al.* 2010). It is said that during the course of maturation into macrophages or DCs, genome-wide demethylation occurs. It was hypothesised that the XRCC1 gene may be methylated in monocytes and thus not expressed. Over the course of cytokine-induced differentiation into macrophages demethylation of the promoter would then lead to its expression.

In order to test this hypothesis, XRCC1 expression was measured in maturing macrophages in the presence of the demethylation inhibitor 2-HG. 2-HG inhibits TETs which are required for the demethylation of 5mC (Xu *et al.* 2011). Monocytes were treated with M-CSF or GM-CSF to induce differentiation before 2-HG was added to the cells. XRCC1 expression was monitored after four and six days of differentiation. With GM-CSF, XRCC1 expression increased from day 0 to day 4. 2-HG led to a reduction in XRCC1 signal (Fig. 45A). Fully matured macrophages at day 6 showed no attenuated XRCC1 signal in the presence of 2-HG. The quantification of the XRCC1 signal intensity verified the microscopic observations (Fig. 45B).

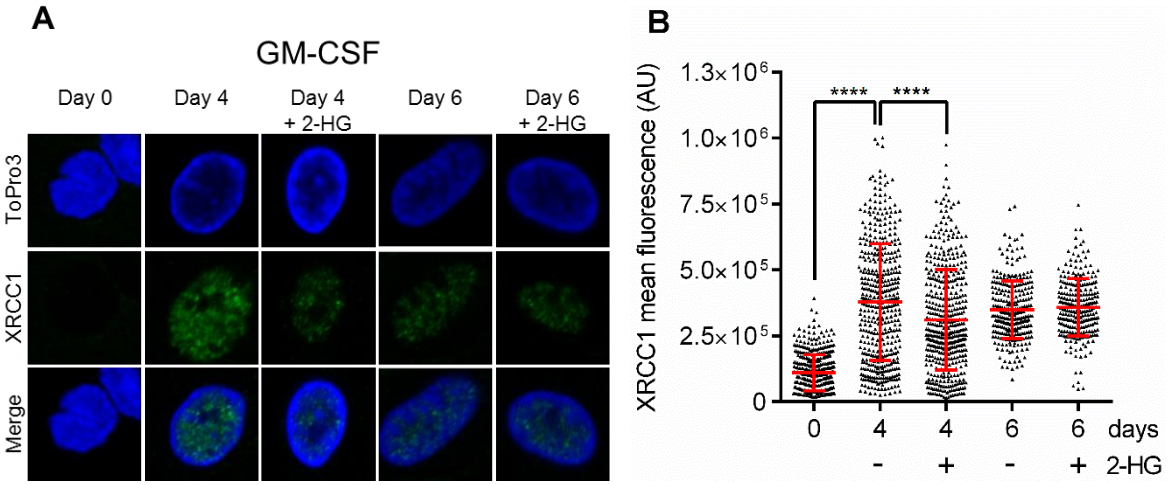

Fig. 45: XRCC1 immunofluorescence staining of GM-CSF-matured macrophages ± 2-HG
*Monocytes (Day 0) were differentiated into macrophages with GM-CSF ± 1 mM 2-HG. A) Representative images of XRCC1 protein expression in maturing macrophages. B) Quantification of the XRCC1 signal intensity. Each dot represents the fluorescence intensity of a single cell. The data consists of three to four independent experiments ± SD. For each condition, 60 - 100 cells were counted, 1-Way ANOVA, Tukey's Multiple Comparison Test, ****p < 0.0001. Quantification of XRCC1 signal intensity was kindly performed by ..... under supervision.*

The immunofluorescence data was confirmed by Western Blot analysis. XRCC1 protein expression was reduced in the presence of 2-HG at day 4. The amount of PARP-1 was lower in the presence of 2-HG at days 4 and 6. Ligase IIIα showed no differential protein expression (Fig. 46).

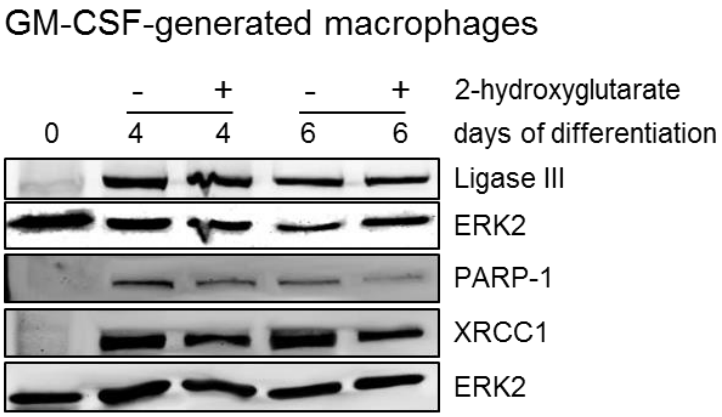

Fig. 46: BER protein expression in differentiating monocytes ± 2-HG
The BER protein expression in differentiating monocytes ± 2-HG was analysed by Western Blot. ERK2 was used as loading control. Western Blot analysis was kindly performed by ..... under supervision.

In parallel to GM-CSF-generated macrophages, M-CSF-generated macrophages were treated with 2-HG at the beginning of their maturation. Similar to GM-CSF, M-CSF generated macrophages showed an attenuated XRCC1 signal in immunofluorescence staining (Fig. 47).

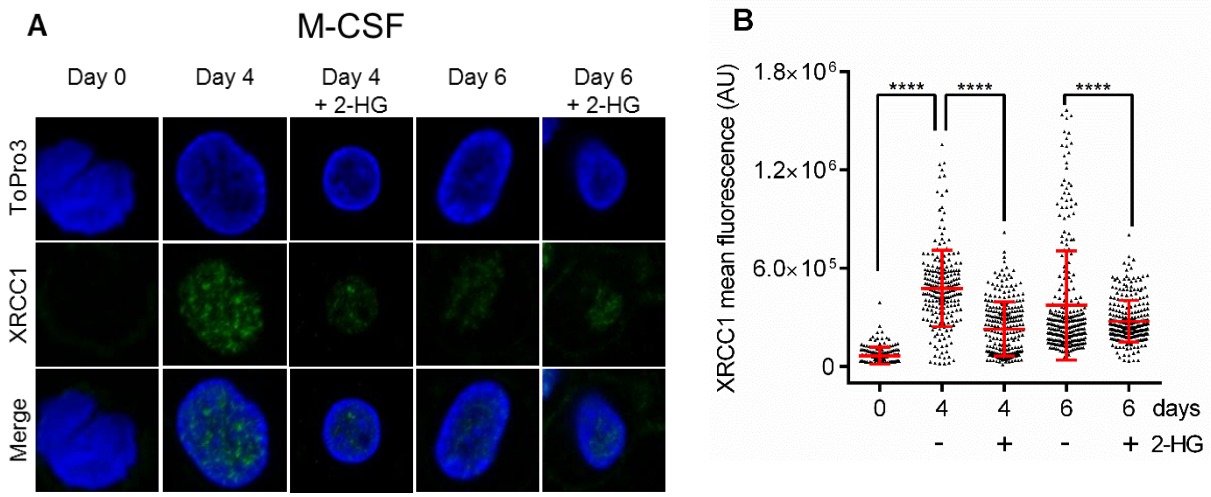

Fig. 47: XRCC1 immunofluorescence staining of M-CSF-matured macrophages ± 2-HG
*A) Representative image of XRCC1 expression in maturing macrophages. B) Quantification of the XRCC1 signal intensity. Each dot represents the fluorescence intensity of a single cell. The data consists of three independent experiments ± SD. For each condition, 60 - 100 cells were counted, 1-Way ANOVA, Tukey's Multiple Comparison Test, ****p < 0.0001. Quantification of XRCC1 signal intensity was kindly performed by ..... under supervision.*

Preliminary experiments with the demethylation inhibitor 2-HG showed that XRCC1 expression was attenuated in monocytes undergoing differentiation. It was not clear whether the XRCC1 gene itself was methylated or regulatory elements like binding sites for transcription factors or enhancers were methylated. Furthermore, it may be possible that genes encoding for transcriptions factors required for the expression of XRCC1 are methylated. Therefore, the XRCC1 promoter was analysed for differential methylation patterns in monocytes and monocyte-derived macrophages.

4.11 Methylation pattern of the XRCC1 promoter

As shown in the previous section, XRCC1 expression was attenuated in maturing macrophages when the demethylation inhibitor 2-HG was present. It was hypothesised that promoter methylation may lead to the downregulation of XRCC1 in monocytes. During their maturation into macrophages, the promoter then becomes demethylated. Using the pyrosequencing technique, the XRCC1 promoter region was analysed for changes in methylation patterns. It covered -947 bp to +75 bp from the ATG start codon. Sequencing of the region was split into five parts: Seq1, 2a, 2b, 3a and 3b (Fig. S25) with Seq1 distal and Seq3b proximal to the transcription site. Two to four different sets of monocytes and monocyte-derived macrophages were analysed. Monocytes (day 0) and macrophages (day 6) showed no differences in their degree of methylation (Fig. 48). Both showed a heavily methylated distal region (> 85 %). Methylation decreased steadily nearing the transcription start site (~1 %) independent of the differentiation stage.

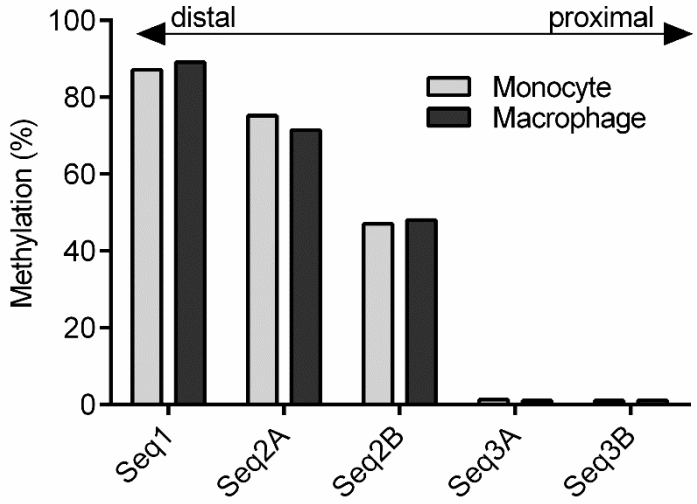

Fig. 48: Pyrosequencing data of the XRCC1 promoter
The degree of methylation in percent. The XRCC1 promoter was split into five parts covering ~800 bp. The transcription start site is covered in Seq3B. Data are the mean of two to four different samples.

4.12 Regulation of XRCC1 protein expression

The regulation of XRCC1 still remains unclear. Although 2-HG treatment led to reduced XRCC1 levels, no direct effect on the methylation status of the XRCC1 promoter was observed (see section 4.11). It was hypothesised that GM-CSF signalling via the CSF2R may lead to the (trans-) activation of a transcription factor which then induces the expression of XRCC1. Therefore, signal transduction proteins in the MAPK pathway were targeted with pharmacological inhibitors, *i.e.* p38 and JNK inhibitors. After seeding and addition of GM-CSF, 10 µM p38 and 25 µM JNK inhibitor respectively were added to the cells. XRCC1 expression was analysed after 3 and 6 days of differentiation using immunofluorescence staining. In the presence of the inhibitors, XRCC1 mean fluorescence was attenuated at days 3 and 6 compared to their respective controls (Fig. 49).

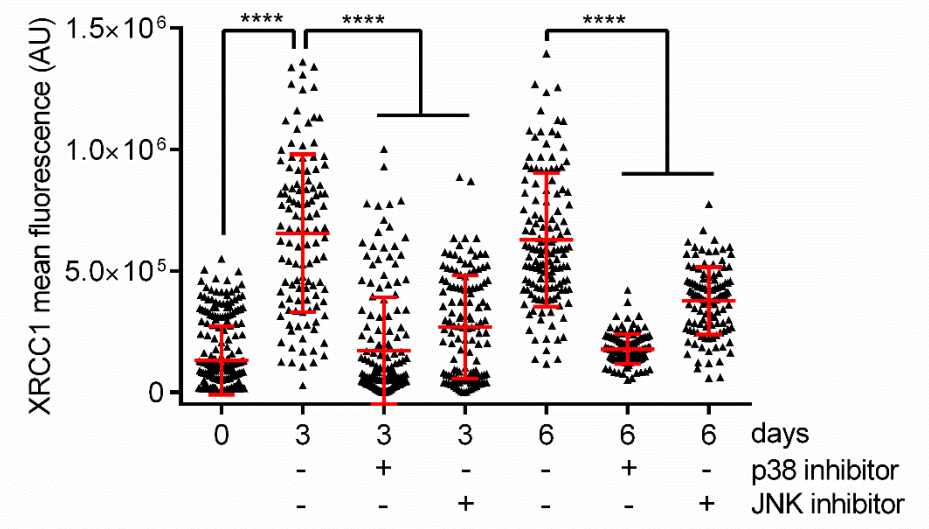

Fig. 49: Attenuated XRCC1 expression after inhibiting JNK or p38
*Monocytes were treated with 10 µM p38 and 25 µM JNK inhibitors before adding GM-CSF. At days three and six of differentiation cells were harvested and XRCC1 was detected via immunofluorescence staining. The data consists of two to three independent experiments ± SD. For each condition, 30 - 80 cells were counted, 1-Way ANOVA, Tukey's Multiple Comparison Test, ****p < 0.0001. Some of the experiments were kindly performed by ..... (Miriam Pons 2016).*

In order to find potential transcription factors in the p38-MAPK and JNK-MAPK pathways responsible for the expression of XRCC1, nuclear protein extracts of monocytes and macrophages from four to five donors were collected and pooled. Then, the XRCC1 promoter sequence, amplified by PCR and tagged with biotin at the 5'-position, was incubated with the nuclear protein extracts. DNA-bound proteins were pulled down and sent for mass spectrometry analysis. Differential expression of transcription factors in monocytes and macrophages were the primary target during data analysis. As a control experiment, part of the DNA-bound protein lysates was subjected to SDS-PAGE followed by silver nitrate staining (Fig. 50) to confirm successful binding of proteins to the DNA.

Fig. 50: Silver nitrate staining of nuclear protein extracts incubated with the XRCC1 promoter

Nuclear extracts of monocytes (day 0) and macrophages (day 4) from several, different donors were pooled and then incubated with the XRCC1 promoter. Samples were subjected to SDS-PAGE and proteins were stained using silver nitrate. M = marker

The silver nitrate-mediated staining of the samples occurred very fast (< 2 min) and showed different patterns between monocytes (day 0) and macrophages (day 4) implying different protein compositions and a potentially different set of transcription factors.

Proteomics identified > 1100 proteins (see supplement section 7.9). The data were sorted by upregulated protein expression in macrophages (log2 of ratio Mph/Mono) with coinciding downregulation of proteins in the monocytes (log2 of ration Mono/Mph). The data were searched for (strongly) upregulated transcription factors in the macrophage sample as they seemed the most likely candidate to be responsible for the regulation of XRCC1 and other DNA repair proteins. The candidates are listed in Table 6. Other differentially expressed transcription factors can be found in chapter 7.9, Table 9.

Table 6: Upregulated transcription factors in the macrophage sample

Protein	Gene	log2 of Ratio Heavy to Light Mph/Mono	log2 of Ratio Heavy to Light Mono/Mph
ETS-related transcription factor Elf-1	ELF1	3.7262	-2.9168
Transcription factor PU.1	SPI1	3.3518	-2.6539
CCAAT/enhancer-binding protein alpha	CEBPA	3.2286	-2.5823
Transcription initiation factor TFIID subunit 6	TAF6	2.4592	-2.0316
Transcriptional repressor CTCF	CTCF	2.1439	-1.9844
General transcription factor II-I	GTF2I	2.0685	-2.2325
Transcription intermediary factor 1-beta	TRIM28	1.9701	-2.0436
Transcription factor jun-B	JUNB	1.0902	-1.2293

Furthermore, the dataset was screened for DNA repair factors found upregulated in the macrophage sample and downregulated in the monocyte sample. They were also pulled down with the XRCC1 promoter construct and detected by mass spectromtery (Table 7). The data confirmed that XRCC1, ligase IIIα and DNA-PK were strongly expressed in macrophages but not in monocytes. Apart from XRCC1 and ligase IIIα other BER factors like PNKP, MPG, POLβ and APEX1 were also upregulated in macrophages. The DSB repair proteins XRCC5 (Ku80), XRCC6 (Ku70) and Rad21, the NER proteins RPC1, XPC and RAD23 and the general DNA repair factors RECQL1, RPA2, RPA1, TOP2A and RFC1 were strongly expressed in macrophages and not or only weakly expressed in monocytes.

Table 7: DNA repair protein expression in macrophages vs monocytes - pull down assay using the XRCC1 promoter

Protein	Gene	log2 of Ratio Heavy to Light Mph/Mono	log2 of Ratio Heavy to Light Mono/Mph
DNA topoisomerase 2-alpha	TOP2A	4.2227	-2.1528
Replication factor C subunit 1	RFC1	3.1976	-2.5608
DNA repair protein XRCC1	XRCC1	3.0330	-3.0132
DNA ligase 3;DNA ligase	LIG3	2.9184	-2.2490
UV excision repair protein RAD23 homolog B; UV excision repair protein RAD23 homolog A	RAD23B; RAD23A	2.7783	-1.5844
DNA-dependent protein kinase catalytic subunit	PRKDC	1.8614	-1.6031
Replication protein A 32 kDa subunit	RPA2	1.7592	-1.3727
Replication protein A 70 kDa DNA-binding subunit	RPA1	1.6972	-1.2798
DNA repair protein complementing XP-C cells	XPC	1.6656	-1.4547
Bifunctional polynucleotide phosphatase/kinase	PNKP	1.6607	-1.0834
Replication protein A 14 kDa subunit	RPA3	1.6258	-1.1424
X-ray repair cross-complementing protein 5	XRCC5	1.5928	-1.0987
X-ray repair cross-complementing protein 6	XRCC6	1.5432	-1.0137
ATP-dependent DNA helicase Q1	RECQL	1.3177	-1.0130
Double-strand-break repair protein rad21 homolog	RAD21	0.9993	-1.0943
DNA topoisomerase 2-beta;DNA topoisomerase 2	TOP2B	0.9707	-0.6328
DNA-3-methyladenine glycosylase	MPG	0.5673	-0.1845
DNA polymerase beta	POLB	0.4730	-0.0023
DNA-(apurinic or apyrimidinic site)lyase	APEX1	0.3922	-0.0090
Poly [ADP-ribose] polymerase 1	PARP1	0.1948	0.1208
DNA mismatch repair protein Msh2	MSH2	0.1908	0.1082

DNA damage-binding protein 2	DDB2	0.1661	0.3629
DNA damage-binding protein 1	DDB1	0.1140	0.2629
DNA mismatch repair protein Msh3	MSH3	0.0433	0.0938
Three-prime repair exonuclease 1	TREX1	-0.9250	0.8091
Flap endonuclease 1	FEN1	-0.9815	1.2295

In summary, the reverse ChIP experiment coupled with mass spectrometry detected several transcription factors that may be involved in the regulation of XRCC1. It needs to be addressed whether the XRCC1 promoter sequence contains the corresponding binding sites and whether these binding sites are also found in other differentially expressed DNA repair proteins. This point is discussed in chapter 5.12.

DNA repair factors and many other proteins were also pulled down with the XRCC1 promoter sequence. Not all proteins were necessarily interacting specifically with the DNA probe. It is likely due to unspecific interactions with the biotin tag or the agarose beads. Further experiments are required to verify these findings.

5 Discussion

The myeloid immune system is the first line of defence against invading pathogens during an infection. In contrast to the highly specialised T and B lymphocytes, myeloid immune cells recognise general patterns of pathogens, *i.e.* PAMPs and DAMPs, which activate the acute inflammatory response. Myeloid immune cells counteract pathogens by releasing ROS and lytic enzymes, secreting cytokines for recruitment of other immune cells, and by phagocytosis of foreign material. The main players are the neutrophilic granulocytes, monocytes, macrophages and DCs. The half-life of these cells varies greatly; neutrophils are constantly replenished as they die within 24 h after they are released into the bloodstream (Pillay *et al.* 2010). Monocytes, without pro-survival stimuli (*e.g.* GM-CSF), undergo apoptosis within days (Parihar *et al.* 2010). Macrophages and DCs, on the other hand, can last for weeks to months. Especially, tissue-resident macrophages are known to last for a very long time.

During the course of their anti-microbial response, myeloid immune cells release genotoxic ROS which damage pathogenic biomolecules. Here, it was addressed whether the release of ROS also damages the producer cells themselves (auto-intoxication). The capacity for DNA repair after genotoxic insult varies greatly between the different myeloid cells and was the focus of this work.

5.1 DNA repair deficits in myeloid immune cells

As was previously shown in our lab, monocytes are severely impaired in base excision and DNA double-strand break repair. Monocytes isolated from buffy coats were stressed with genotoxins like *t*-BOOH or oxLDL. In comparison to monocyte-derived macrophages or DCs, monocytes were highly susceptible towards oxidants as well as alkylating agents (*i.e.* MNNG, TMZ and MMS) and underwent apoptosis (Bauer *et al.* 2011; Bauer *et al.* 2012; Briegert and Kaina 2007). This effect was due to impaired BER and NHEJ. Monocytes do not express XRCC1, PARP-1, ligase IIIα nor DNA-PKcs resulting in an accumulation of SSBs and DSBs after genotoxic treatment. Base lesions were still recognised by BER-glycosylases and processed by APE1. However, the ensuing SSB-intermediates could not be re-ligated and SSBs accumulated in the cells. Eventually, the high burden of strand breaks induced pro-apoptotic signalling by the ATM/ATR/CHK pathways resulting in the cleavage of pro-caspases-8, -3 and -7 and the subsequent induction of apoptosis (Bauer *et al.* 2012). Cytokine-induced differentiation into macrophages or DCs abolished this repair-deficiency as the cells re-expressed the DNA repair factors. They became resistant towards the mentioned genotoxins. The re-expression of XRCC1 and ligase IIIα was observed two to three days after cytokines were added to the monocytes and differentiation was initiated. PARP-1 was detectable after three days. All proteins were strongly expressed in differentiated macrophages at day 6 or DCs at day 8 (Bauer *et al.* 2012).

The isolation of monocytes is a time-consuming and cost-intensive procedure which is limited by the number of cells that can be isolated from a buffy coat. Furthermore, the isolation of monocytes by adherence method does not render pure monocyte samples. For very high purity samples (> 95 %), bead-assisted isolation kits are required which are very expensive. For Western Blot analysis, contamination with other cell types can lead to false-positive results in protein expression analyses. Therefore, an alternative immunofluorescence-based staining method for the detection of XRCC1 and PARP-1 was

established. Freshly isolated monocytes were stained for XRCC1 protein and compared to GM-CSF-matured macrophages. It was confirmed that monocytes do not, or only weakly, express XRCC1. The XRCC1 signal intensity was much lower in monocytes than in maturing (2 – 3 days) and mature (day 6) macrophages (Fig. 8). PARP-1 was measured indirectly via its enzymatic product PAR. PARP-1 is the main producer of genotoxic stress-mediated PAR formation (~90 %) (Beneke and Bürkle 2007). Monocytes and maturing macrophages were treated with H_2O_2 for 5 min and then stained for PAR. Monocytes did not display any PAR signals whereas maturing macrophages at day 3 stained positive for PAR (Fig. 10). Ligase IIIα was detected via Western Blot analysis and showed similar expression kinetics as XRCC1. It was not expressed in monocytes but protein levels increased after three days of GM-CSF-induced maturation and peaked after six days (Fig. 9). These findings confirmed previous observations (Bauer *et al.* 2011; Bauer *et al.* 2012; Briegert and Kaina 2007) of DNA-repair defects in monocytes which were abolished when monocytes undergo differentiation into macrophages or DCs. XRCC1 detection via immunofluorescence staining requires less material than Western Blot analysis and was therefore used as the main method for screening. Freshly isolated monocytes are often contaminated with PBL. In this case, monocytes can be distinguished from other cell types by their characteristic bean-shaped nucleus. Alternatively, monocytes can be co-stained for CD14 marker expression and XRCC1.

Next, it was addressed whether neutrophilic granulocytes showed similar DNA repair defects as monocytes. Granulocytes and monocytes stem from the same progenitor cell, *i.e.* the myeloblast. Unlike monocytes, neutrophils are terminally differentiated cells with a very high turnover rate and a very short half-life of less than 24 h (Simon and Kim 2010; Summers *et al.* 2010; Pillay *et al.* 2010). Previous data from our lab indicated that granulocytes did not express DNA repair factors required for DSB repair, *i.e.* ATM, ATR, γH2AX and DNA-PK. Similar results were described by Kurosawa *et al.* who showed a lack of DNA-PK in neutrophils. Granulocytes isolated from buffy coats showed DNA damage-independent cell death over time which did not increase after 2 Gy irradiation (Tobias Haak 2015). These findings were extended towards BER protein expression. Granulocytes of four different donors were isolated from buffy coats and the BER factors XRCC1, PARP-1 and ligase IIIα were detected via Western Blot analysis and immunofluorescence staining. None of the granulocyte samples showed any BER protein expression unlike the PBL positive control (Fig. 11). According to the master thesis by [redacted], granulocytes did not show any γH2AX as the upstream kinases were not expressed. Here, it was confirmed that unmodified H2AX is present in granulocytes and that it is indeed not phosphorylated as the upstream kinases are missing.

As granulocytes are full of lytic enzymes, the question arose whether the isolation and subsequent lysis of the cells to generate protein extracts may lead to the degradation of DNA repair proteins resulting in false-negative results. Therefore, a published protocol for the detection of DNA repair proteins in granulocytes was used (Kurosawa *et al.* 2003) and control experiments were performed. It was postulated that activation of lytic enzymes would not only degrade granulocytic proteins but also PBL proteins when the two cell types were mixed together during protein lysis. Therefore, granulocytes and PBL of two independent donors were isolated from buffy coats and mixed in a 2:1 ratio of PBL to granulocytes. The Western Blot analysis for PARP-1, XRCC1 and the tumour suppressor p53 showed that PBL, and the mixed cell population, expressed these proteins. Granulocytes on the other did not (Fig. 12). Finally, fresh blood samples from the fingertip were used to stain for the DSB-activated factor pATM. ATM is strongly activated, *i.e.*

phosphorylated, upon DSB formation after IR treatment. It phosphorylates many downstream targets like the DSB markers γH2AX and pKAP1 (White *et al.* 2012). In CD3+ T cells, there were strong signals for pATM, γH2AX and pKAP1 when cells were treated with 2 Gy. CD15+ granulocytes on the other did not show any signals independent of genotoxic treatment (Fig. 13).

In summary, it was shown via two different Western Blot lysing protocols as well as by immunofluorescence staining that granulocytes do not express key proteins required for base excision/SSB repair and DSB repair. The lack of DNA repair protein expression in neutrophils seems logical as DNA repair is a time and energy consuming process that is required for the survival and homeostasis of cells. Neutrophils, however, are short-lived cells and they are constantly replenished in very high numbers (Rink *et al.* 2015; Parihar *et al.* 2010). Their function in the innate immune response is likely another reason for the lack of DNA repair factors. Neutrophils produce high amounts of ROS and oxidants like $O_2^{\cdot-}$, H_2O_2 and HOCl to damage and kill pathogens. However, potential leakage of these toxic oxidants inside the host cell may damage intracellular biomolecules. Furthermore, the granules of neutrophils are enriched with lytic enzymes like elastase, cathepsin G, proteinase 3 and MPO, which can also damage intracellular components. During the course of the acute inflammatory reaction of neutrophils, it is likely that all of these toxic molecules and peptides not only damage pathogens but also intracellular biomolecules. The repair of these lesions are energy expensive and may restrict neutrophils in their function. Finally, neutrophils undergo “suicidal” death when they lay down their neutrophil extracellular traps in order to engulf pathogens. The ejection of their genomic DNA into the ECS does not require intact DNA. Wasting energy on DNA repair seems rather pointless in this case.

Monocytes are different from granulocytes. First of all, they are not as abundantly produced as granulocytes. They persist longer in the bloodstream and they are able to differentiate into long-living macrophages and DCs. Without pro-survival stimuli like M-CSF or GM-CSF, they undergo apoptosis (Parihar *et al.* 2010). Monocytic DNA repair defects are not as severe as those found in granulocytes. They express ATM, ATR and p53 (Fig. 32)(Bauer *et al.* 2011; Bauer *et al.* 2012). They do not express the essential repair proteins PARP-1, XRCC1 and ligase IIIα which are required for BER and alt-EJ. DNA-PKcs is required for c-NHEJ and is also not expressed in monocytes (Bauer *et al.* 2011). Unlike granulocytes, they displayed a genotoxin-dependent increase in apoptosis (Bauer *et al.* 2011).

During the course of this work, it was addressed whether the repair defect in monocytes is detrimental to the cell’s survival during an acute immune response as an acute immune response is accompanied by a massive production of ROS. Most of the ROS-induced DNA lesions are targets for BER. Therefore, the cellular responses of monocytes were analysed when the cells were exposed to an exogenous source of ROS, *i.e.* ART, as well as the endogenously generated ROS by the NADPH oxidase.

5.2 ART leads to DNA damage and cell death in immune cells

ART is a semi-synthetic drug which is regularly administered during infections with *Plasmodium falciparum.* Untreated patients suffer from severe cases of malaria which can lead to death. In the presence of ferrous iron, the endoperoxide bridge of ART generates ROS which kill the pathogens by oxidative stress (Gopalakrishnan and Kumar 2015). ART is administered intravenously and can lead to plasma concentrations ranging from the upper nanogram to the microgram range within 30 min of injection (Byakika-Kibwika *et al.* 2012;

Ittarat *et al.* 1998). It is reasonable to assume that not only infected erythrocytes are targeted but immune cells as well. Therefore, myeloid and lymphoid immune cells were treated with different concentrations of ART in order to determine whether haematotoxicity occurred. As ART is considered for chemotherapy which is often accompanied by immunosuppression it is important to known of potential cytotoxic side effects of ART on the immune system.

First, low concentrations of ART were added to lymphoid PBL and myeloid DCs, macrophages and monocytes. 2.5 – 20 µg/ml ART led to massive oxidative DNA damage in the myeloid cells (Fig. 14) which reached saturation levels in the FPG-modified Comet assay. PBL, on the other hand, showed a concentration-dependent increase in oxidative lesions but did not reach saturation levels. Using the same concentrations of ART, the induction of cell death was analysed using Annexin V / PI staining. In this concentration range, PBL displayed a slight increase in cell death by apoptosis and necrosis. The myeloid cells reacted differently. Monocytes showed a low amount of dead cells similar to PBL but predominately died by apoptosis whereas macrophages showed up to 20 % cell death but were mostly necrotic (Fig. 15).

Next, the effects of high concentration ART (10 – 100 µg/ml) were analysed. The alkaline Comet assay showed that macrophages displayed the strongest SSB formation (tail intensity up to ~60 %) whereas monocytes were relatively resistant with a tail intensity of ~20 % (Fig. 16). DCs and PBL showed moderate SSB formation of ~35 %. The overall killing response was increased in all cell types. PBL were the most sensitive population and showed a concentration-dependent increase in mostly apoptotic cell death of up to 60 % after 100 µg/ml ART. Monocytes also displayed concentration-dependent cell death but predominately died by apoptosis whereas macrophages died by necrosis (Fig. 17). The differences in the mode of death are attributed to PARP-1. This enzyme catalyses the formation of the biopolymer PAR and requires NAD^+. Excessive PARP-1 activity, *e.g.* after severe genotoxic insult, leads to the depletion of NAD^+. *De novo* synthesis of NAD^+ requires ATP and the depletion of NAD^+ by PARP-1 can lead to a critical loss of energy. As apoptosis requires ATP (Leist et al. 1997; Eguchi et al. 1997), over-activation of PARP-1 can lead to the abrogation of apoptosis and shift the cell towards necrosis. In order to test this hypothesis, the intracellular NAD^+ content was measured. The reduction of NAD^+ after ART treatment was significant in macrophages (~20 %) but not in monocytes or PBL (Fig. 18). ART-induced NAD^+ consumption was low compared to the positive control treated with H_2O_2 where NAD^+ levels dropped 40 – 60 %. This discrepancy may be explained by the different modes of action of the two substances. H_2O_2 is a very fast and transient molecule. It leads to massive DNA damage in a very short period of time (5 min) and results in immediate (hyper-)activation of PARP-1 (Weidele *et al.* 2010; Mangerich *et al.* 2016). It is rapidly inactivated in medium. Therefore, the loss of NAD^+ is immediate and severe. ART, however, is relatively stable and leads to a sustained accumulation of DNA damage over time (Berdelle *et al.* 2011) which likely leads to a sustained activation of PARP-1 and constant consumption of NAD^+ that can last for hours to days. In order to determine the role of PARP-1-mediated loss of NAD^+ leading to necrotic cell death future experiments should be conducted using PARP-1 inhibitors, *e.g.* ABT-888 or olaparib. In the presence of these inhibitors, ART-mediated necrosis should decrease in macrophages and shift the cells towards apoptosis. Furthermore, one could supplement cells with the NAD^+ precursor nicotinic acid which was shown to successfully increase intracellular NAD^+ levels, improve DNA repair and reduce necrotic cell death after genotoxic insult in PBMC (Weidele *et al.* 2010; Weidele *et al.* 2017).

ART is on the World Health Organisation's list of essential medicines as its efficacy in malaria treatment make it indispensable. It is generally well-tolerated with few adverse side effects that only include fever and skin rash. In some cases, reversible reticulocytopenia can occur (Clark 2012). Due to its cytotoxic properties, it is also being evaluated for cancer therapy. ART is not exported by multidrug resistance transporters, making it an attractive drug in the treatment of chemotherapy-resistant tumours (Efferth *et al.* 2007b). *In vitro* studies showed that concentrations ranging from 0.5 to 6 µg/ml ART led to the generation of ROS followed by the activation of the intrinsic apoptosis pathway in the human cancer cell lines Jurkat, Hut-78, CEM and Molt-4 (Efferth *et al.* 2007a). In glioblastoma cell lines, LN-229, A172 and U87MG, 15 and 30 µg/ml ART boosted the TMZ-mediated killing response (Berte *et al.* 2016). It was shown that ART causes oxidative DNA damage and DNA strand breaks resulting in the activation of the DDR. The genotoxic effects are exacerbated when DNA repair pathways are impaired (Li *et al.* 2008; Berdelle *et al.* 2011). In a phase I study with breast cancer patients doses of 100 - 200 mg ART were administered daily for 4 ± 1 weeks. Adverse side effects like reversible reticulocytopenia, leukopenia, neutropenia and general anaemia were observed at high doses in some of the patients (Hagens *et al.* 2017). Therefore, as ART emerges as an effective adjuvant in chemotherapy a thorough analysis of ART-induced haematotoxicity needs to be conducted. It has to be addressed whether immunosuppression of bone-marrow and peripheral immune cells occurs and whether this is reversible.

5.3 Stimulating myeloid immune cells to produce ROS

The phagocytic oxidative burst is an effective and essential defence mechanism in the immediate response against pathogens. Without it, the organism suffers from severe recurring infections leading to early death (Jackson *et al.* 1995). In humans, phagocytic NADPH oxidase is the main contributor of ROS in the oxidative burst. It is activated by PKC, which in turn is activated by DAG. Apart from the classic PAMPs fMLP, LPS and opsonised zymosan, DAG can also be released by endogenous triggers like Angiotensin II via the Angiotensin II receptor type 1 (AT1 receptor) -mediated activation of phospholipase C (PLC) or oxLDL. Furthermore, hyperglycemia and mechanical strain/hypertension also activate NADPH oxidase isoforms in a PKC-dependent manner (Brandes and Kreuzer 2005).

In order to address the question of whether endogenous ROS can lead to auto-intoxication of the producer cell, ROS was first detected intra- and extracellularly using a flow cytometry-based and a chemiluminescence-based assay. *In vitro*, monocytes and monocyte-derived macrophages were stimulated with LPS or PMA to induce the ROS burst. The first experiments showed that LPS did not lead to ROS production in the cells at the indicated time points (Fig. 19). *In vivo*, LPS is a strong activator of the acute inflammatory response. It is captured by LBP and binds the CD14/TLR4 receptor complex triggering a signal transduction cascade which activates the NADPH oxidase via the MAPK pathway (Yan 2006). *In vitro*, LBP is probably missing or present in very low quantity as it is washed out during the isolation procedure of the cells resulting in insufficient signalling of CD14/TLR4. PMA mimics the structure of DAG and is a common pharmacological activator of PKC (O'Donnell *et al.* 1993; Ashkenazi *et al.* 2009; Raad *et al.* 2009; Wind *et al.* 2010; Kuwabara *et al.* 2015). It led to elevated ROS levels after 30 min of treatment (Fig. 19). Concentrations ranging from 10 - 1000 ng/ml led to robust intracellular ROS production which was attenuated when cells were pre-incubated with the antioxidant NAC (Fig. 20 and Fig. 21).

The extracellular ROS production was measured using luminol and HRP. The assay is a sensitive indicator for ROS and oxidants in general, *e.g.* $O_2^{\cdot-}$ and H_2O_2. Stimulated with 100 ng/ml PMA monocytes produced a rapid oxidative burst that peaked within 30 min and declined afterwards. Macrophages on the other hand showed slower kinetics (Fig. 22). ROS production also peaked after ~30 min but ROS levels were sustained over time. In the presence of the NADPH inhibitor DPI, ROS production dropped to, and even below, control levels. This confirmed that NADPH oxidase is the main contributor of ROS in the oxidative burst and that depending on the cell type, and the applied stimulus, ROS production can vary in strength and duration (Cathcart 2004). Neutrophils, in particular, are very fast ROS producers as was shown in figure Fig. 34, whereas lymphoid cells are not equipped to produce ROS (Fig. 23). It is a characteristic feature of myeloid immune cells. The concentrated release of ROS in a short period of time is an effective tool in inducing maximal damage to a pathogen. Pathogens engulfed in a phagosome are particularly affected as ROS and an acidic milieu with lytic enzymes, attack the microbe from all sides contributing to bacterial killing (Hampton *et al.* 1998). Furthermore, the generation of ROS is a prerequisite for NETosis – another bactericidal defence mechanism of myeloid cells (Paiva and Bozza 2014). However, excessive ROS levels can also be detrimental to the host. Oxidative stress is a common feature of chronic inflammatory diseases. The prolonged ROS production of macrophages (Fig. 22) may contribute to the progression of such conditions. Here, it was addressed whether sustained ROS levels disturb cellular homeostasis and lead to auto-intoxication of the producer cells. Therefore, the detrimental effects of endogenous ROS on the DNA of myeloid immune cells was analysed.

5.4 Oxidative DNA damage and apoptosis in phagocytes

Oxidative DNA damage is predominantly repaired by BER and SSB repair. One of the most common oxidative DNA lesions are 8-oxoG modifications. Using an immunofluorescence-based assay, as well as the FPG-modified Comet assay, the amount of oxidative lesions after the respiratory bursts were induced in monocytes and macrophages was analysed. Independent of their DNA repair capacity, both cell types showed the same initial damage (Fig. 26 and Fig. 27). However, the ensuing repair of the lesions emphasised the DNA repair defect of monocytes. Unlike macrophages, monocytes showed a strong accumulation of SSBs over time (Fig. 28). Although they could still recognise damaged bases, excise them and insert new nucleotides, monocytes were unable to repair the SSB-intermediates as they lack XRCC1, PARP-1 and ligase IIIα. In macrophages, the amount of SSBs are much lower. The slight increase after 4 h may be due to the sustained ROS production as seen in figure Fig. 22 leading to a prolonged oxidative damage formation. These findings confirmed previous data by Bauer *et al.* who found persisting DNA strand breaks in monocytes when they were treated with exogenous ROS sources like *t*-BOOH. The accumulation of DNA damage eventually led to monocytic cell death (Fig. 29) whereas macrophages were resistant. Chronic stimulation of the NADPH oxidase (48 h PMA) exacerbated the killing effect in monocytes and also led to moderate cell death in macrophages (Fig. 29). These results demonstrated that although monocytes, as part of the innate immune response, are prototypical ROS producer they are harmed by their own ROS. The ROS-induced DNA damage remains unrepaired likely activating the DDR with subsequent induction of apoptosis by the ATM/CHK2/p53 signalling pathway that cleaves pro-caspases. Similar observations were made when monocytes were treated with an exogenous ROS source and oxidants, *i.e. t*-BOOH, IR and oxLDL (Bauer *et al.* 2011).

The experiments support the hypothesis that the DNA repair defect of monocytes has biological consequences in terms of selective monocyte killing in a ROS-enriched environment such as in the inflamed tissue. Their vulnerability to ROS restricts their role during the acute inflammatory response to hours or days at most. Their death prevents them from differentiating into inflammatory, DNA repair-competent macrophages. The lack of PARP-1 likely averts necrotic cell death which would stimulate further pro-inflammatory reactions. This supports the notion that the DNA repair defect is not necessarily detrimental to the host. It rather limits toxic ROS production to a confined timeframe and thus may prevent unwanted cytotoxic side effects. Furthermore, cytokine-mediated recruitment of other immune cells may be down-regulated when monocytes are depleted at the site of inflammation. *In vivo*, this hypothesis may be tested by labelling monocytes *ex vivo* before they are reintroduced into a model organism like the mouse. After introducing (local) inflammation, the recruitment of the labelled monocytes may be monitored. It needs to be assessed whether these monocytes suffer damage in the inflamed tissue, undergo cell death or phagocytosis and whether they still have the potential to differentiate into macrophages or DCs.

5.5 Co-culture of ROS-producing macrophages and unstimulated monocytes

In the previous section, it was shown that the PMA-induced stimulation of monocytes led to auto-intoxication with ROS manifesting in DNA damage and subsequent cell death. During the acute inflammatory response, monocytes are surrounded by other immune cells, namely recruited neutrophils and local macrophages who are also professional ROS-producing cells. Therefore, it was addressed, whether monocytes are killed by adjacent ROS-generating cells (so-called killing *in trans*). Monocytes were co-cultured with PMA-pulse activated macrophages. It was shown that ROS from other cells were strong enough to damage monocytic DNA (Fig. 30 and Fig. 31). The damage led to the activation of the DDR as ATM was phosphorylated and 53BP1 was recruited to the site of DNA damage. CHK2 was phosphorylated and p53 stabilised (Fig. 32). pATM and pCHK2 marked the presence of DSBs, the recruitment of 53BP1 and the fact that monocytes are resting G0 cells indicated that NHEJ was the favoured DNA repair pathway. However, as monocytes do not express the essential DSB repair protein DNA-PKcs (Bauer *et al.* 2011) the attempt at repair was likely futile. DNA-PKcs is a kinase that phosphorylates DSB repair factors, *e.g.* XRCC4, ligase IV, XLF and Artemis (Davis and Chen 2013). Furthermore, alt-EJ as a last resort for DNA repair was also not possible as it requires XRCC1, PARP-1 and ligase IIIα. Thus, the phosphorylation of p53 at position Ser46 marked the initiation of apoptosis. It leads to the transcriptional activation of pro-apoptotic PUMA, Bax and NOXA that are involved in the intrinsic apoptosis pathway (Roos *et al.* 2016). These observations matched previous findings, where genotoxic insults by *t*-BOOH (Bauer *et al.* 2011) and the methylating agent TMZ (Bauer *et al.* 2012) led to the activation of the DDR with subsequent apoptotic signalling and cleavage of pro-caspases. Monocytes in co-culture with ROS-producing macrophages underwent apoptosis (Fig. 33B, PMA-Mph) whereas DNA repair competent macrophages remained viable (Fig. 33A). Chronic, co-stimulation of both monocytes and macrophages exacerbated the killing and auto-intoxication effect in monocytes (Fig. 33B, 48 h PMA) and was also highly toxic for macrophages. Monocyte killing was averted when the ROS scavenger DMTU was present (Fig. 33C) in the medium confirming that ROS were responsible for the cell death. Direct inhibition of the NADPH

oxidase with DPI was not feasible as the inhibitor was cytotoxic over prolonged periods of time (data not shown).

These findings further support the hypothesis that the DNA repair defect in monocytes is of biological relevance. Monocytes are regularly recruited to site of inflammation that contain a lot of ROS (Mittal *et al.* 2014). In the *in vitro* assays, monocytes suffered fatal DNA damage and underwent apoptosis in a ROS-enriched environment. *In vivo*, this may be beneficial in so far as the cells do not further contribute to the pro-inflammatory signalling by secreting cytokines or dying a necrotic death. Furthermore, they cannot differentiate into long-living, ROS-resistant inflammatory macrophages that may aggravate or prolong the immune response. The timely death of monocytes contributes to the restricted nature of the acute inflammatory response and may help prevent the transition of the acute into a chronic inflammatory condition. The activation of the NADPH oxidase is a contributing factor in the progression of inflammatory joint disease rheumatoid arthritis. NOX is activated by crystal depositions and leads to the degradation of hyaluronic acid and other proteoglycans. ROS may also inactivate protease inhibitors while activating neutrophil collagenase (Knight 2000). In hypertensive patients, immune cells exhibit increased oxidative stress and pro-inflammatory signalling which contributes and aggravates the hypertension-related vascular damage (La Fuente et al. 2005). These syndromes demonstrate how ROS released by immune cells ameliorate certain pathological conditions. Therefore, the ROS-mediated monocyte killing should be assessed in *in vivo* models.

5.6 Co-culture of ROS-sensitive monocytes with other stimulated phagocytes

It was shown that the ROS burst of macrophages was strong enough to kill monocytes in their vicinity. In the case of macrophages, ROS production was sustained over time (Fig. 22), leading to a prolonged exposure to toxic ROS. During the inflammatory response, neutrophils are the first responders and infiltrate the infected tissue in great numbers. Their ROS burst is very strong but temporary (Fig. 34). However, their oxidative burst was also able to kill monocytes *in trans* with very high efficiency (Fig. 35). The killing response was attenuated when the ROS scavenger DMTU was present, further demonstrating the toxic potential of ROS for DNA repair-deficient monocytes. In the case of neutrophil-mediated monocyte killing, additional defence mechanisms may have contributed to the high induction of apoptosis. NETosis can be induced by PMA within hours (Kaplan and Radic 2012; Konig and Andrade 2016). The DNA-bound lytic enzymes may further damage monocytic biomolecules which can only partially be rescued by ROS scavengers. In order to verify this hypothesis, neutrophils need to be stained by immunofluorescence staining of histones, elastase or MPO bound to DNA in the ECS as was described elsewhere (Donis-Maturano *et al.* 2015; Li *et al.* 2015). Neutrophils with their very short half-life died independent of the PMA stimulus (Fig. S17). Other ROS-inducing stimuli like LPS/bzATP-mediated activation of macrophages also led to a killing response in monocytes (Fig. 36). The ensuing ROS burst was not as pronounced as with PMA which may be due to the lack of LBP in the medium. Future experiments should include “physiological” stimuli like opsonised zymosan or fMLP.

In summary, it was shown that the DNA-repair defect renders monocytes vulnerable to an oxidative environment independent of the source and the kinetics of ROS production. At a site of inflammation, they are in close contact with neutrophilic granulocytes that are recruited in high numbers to the damage site. They are also exposed to local macrophages.

Therefore, monocytes are prime targets for ROS-producing cell. Unlike terminally differentiated granulocytes which die by PICD or NETosis, monocytes are still able to differentiate into DCs and macrophages. If they are prematurely removed from the inflammation site by ROS-induced apoptosis they cannot give rise to other myeloid cells which may pose a regulatory mechanism of the innate immune system to control the balance of monocytes / macrophages / DCs. As mentioned above this hypothesis needs to be addressed in an *in vivo* model.

5.7 Co-culture of peripheral blood lymphocytes with activated phagocytes

Severe haematotoxicity is one of the limiting factors in chemotherapy. PBL, although they are DNA repair competent, are very susceptible to genotoxic stress; IR treatment or alkylating chemotherapeutics lead to the induction of massive amounts of cell death (Heylmann *et al.* 2014; Heylmann *et al.* 2013). On the other hand, low dose IR is also used in the treatment of chronic inflammatory diseases such as arthritis as it modulates the inflammatory response towards anti-inflammatory signalling by reducing leukocyte adhesion, inducing apoptosis and promoting the release of TGF-β (Rödel *et al.* 2012). Here, it was addressed whether ROS-producing macrophages also elicited a killing response in PBL and CD3+CD8+ CTL in particular. As was shown in figureFig. 23, PBL do not produce ROS when stimulated with PMA. Continuous exposure to PMA for 48 h induced apoptosis very strongly in monocytes and macrophages (Fig. 29). In PBL, the killing effect was low with only a ~10 % increase in apoptosis (Fig. 37). CTL were slightly more susceptible to PMA. However, co-cultured with activated macrophages PBL/CTL displayed an increase in cell death, *i.e.* killing *in trans*. Continuous PMA stimulation of both cell populations in co-culture exacerbated this effect – likely due to constant ROS production from macrophages. The underlying mechanisms for this killing effect remain elusive as PBL are *de facto* capable of repairing DNA damage but undergo cell death anyway. Therefore, the expression of DNA repair proteins cannot be the only determining factor for genotoxic resistance. DNA damage signalling may also influence cell fate as was shown elsewhere (Daniel Heylmann 2017). Heylmann could show that unstimulated PBL are very susceptible towards IR whereas stimulated PBL are resistant. Both are DNA repair competent cells. In the presence of ATM and CHK inhibitors, the unstimulated PBL also became IR-resistant. Furthermore, he could show that the expression levels of ATM were reduced in the stimulated population indicating an ATM-mediated cell death mechanism. If ATM-mediated signalling is responsible for ROS-mediated cell death, adding ATM and CHK inhibitors should attenuate or abolish the macrophage-mediated killing response.

Another factor which may influence cell fate is GSH. GSH synthesis requires cysteine which is limited in the circulation and T cells do not express the necessary cystine (oxidised cysteine) transporter. They are dependent on DCs to supply them with cysteine. Detoxification of ROS can deplete GSH levels and thus alter the redox state of the cell leading to impaired T cell function and proliferative potential. Furthermore, low levels of ROS alter the gene expression profile by upregulating the transcription of the subunits of NFκB, IL-2 and IL-2 receptor (Alcaraz *et al.* 2013). It is also known that prolonged exposure to high concentration of ROS inhibit T cell proliferation, induce apoptosis and impair their TCR signalling. Therefore, an in-depth analysis of the role of phagocytic ROS production on the adaptive immune cells is required.

5.8 Impaired differentiation potential of monocytes after ROS-induced damage

It was shown that DNA repair-deficient monocytes undergo apoptosis when their ROS burst was stimulated (Fig. 29) or when they were co-cultured with ROS-producing macrophages or granulocytes (Fig. 33 and Fig. 35). However, not all cells were Annexin V positive after 48 h. Therefore, the differentiation potential of "surviving" monocytes was analysed. After mono- or co-culture for 24 h, cell death in monocytes was low to moderate (Fig. S9 and Fig. S13). The cells were re-seeded and differentiation was induced by adding GM-CSF. Monocytes that were previously exposed to the solvent or to solvent-treated macrophages matured into new macrophages (Fig. 39, Solvent and Fig. 40, Solvent). If they had been exposed to PMA or to PMA-stimulated macrophages they were unable to differentiate into "healthy" macrophages (Fig. 39, PMA and Fig. 40, Mph-PMA). There were fewer cells with a grainy morphology and they mostly stained positive for Annexin V. Similar observations concerning impaired differentiation after genotoxic treatment were made when monocytes were treated with polyaromatic hydrocarbons like benzo[a]pyrene (BP). BP treatment inhibited cell adhesion during GM-CSF triggered differentiation. The characteristic CD marker expression profile, as well as the cytokine expression, were altered (van Grevenynghe *et al.* 2003). Similar experiments should be considered after exposure to ROS-producing cells. Monocyte/macrophage functions may be altered in their cytokine production, CD marker expression, phagocytosis potential and the ability to present antigens to T lymphocytes. *In vivo*, it should be addressed whether the ROS-mediated depletion of monocytes in addition to their diminished differentiation potential a) occurs and b) influences the number of innate immune cells in the inflammatory tissue. If monocytes are depleted in the inflamed tissue and do not give rise to new macrophages (and potentially DCs) this may have an impact on the intensity and length of the acute inflammatory response.

5.9 XRCC1 expression in M-CSF- and GM-CSF-generated macrophages

The DNA repair defect played a pivotal role in ROS-mediated monocytic cell death. The regulation of the repair factors remains elusive. In GM-CSF-generated macrophages and GM-CSF + IL-4-generated DCs a clear increase in protein levels was detectable (Bauer *et al.* 2011; Bauer *et al.* 2012). It is unknown whether this was a cytokine-specific phenomenon or a general feature of monocyte differentiation. Therefore, M-CSF-mediated differentiation was also analysed on the account of XRCC1 expression.

M-CSF is a constitutively expressed cytokine that induces the differentiation of monocytes into macrophages under homeostatic conditions. *In vivo*, M-CSF promotes macrophage proliferation via a negative feedback loop. High CSF1R expression (= high number of mononuclear phagocytes) leads to efficient scavenging of circulating M-CSF, thus contributing to its clearance. Decreased M-CSF levels then lead to a reduced cell proliferation whereby maintaining a steady cell number (Italiani and Boraschi 2014). In the clinic, it is used to stimulate myeloid haematopoiesis; it promotes monocyte development, osteoclast and monocyte differentiation. Upon binding to the CSF1R, multiple intracellular amino acids become phosphorylated and function as binding platforms for adapter proteins like growth factor receptor-bound protein 2 (Grb2) and Son of Sevenless, Drosophila, homolog 1 (SOS) which interact with Ras and Raf proteins. These activate the multiple MEK kinases, *e.g.* MEK1/2 (also known as MAP2K1/2), which in turn phosphorylate ERK1/2 that leads to the activation of Ets2, a transcription factor. ERK also phosphorylates Elk1 which

then activates c-fos (Fig. 52). MEK kinases also stimulate the p38 isoforms α, β, γ, and δ as well as JNK 1, 2 and 3, involved in cell differentiation, inflammation and apoptosis. Similar signalling cascades are found in the GM-CSF-mediated signal transduction pathway (Perugini *et al.* 2010; Corey and Anderson 1999; Wagner and Matsuo 2003). GM-CSF is mainly involved in haematopoiesis under inflammatory conditions. The M-CSF- and GM-CSF-induced differentiations are accompanied by different macrophage phenotypes: M-CSF leads to a more anti-inflammatory, M2-like phenotype whereas GM-CSF leads to M1-like inflammatory cells. Both cytokines activate overlapping signalling pathways. *In vitro*, GM-CSF-generated macrophages were elongated and spindle-shaped whereas M-CSF-generated cells were round (Fig. 41). Both sets of macrophages were capable of producing ROS in similar amounts and with similar kinetics (Fig. 42). Furthermore, the expression of the DNA repair protein XRCC1 was upregulated to a similar degree in both types of macrophages. The kinetics of XRCC1 expression were similar: there was little XRCC1 protein after two days of differentiation. After four days XRCC1 protein was strongly expressed. Both sets displayed variance in XRCC1 signal intensity after six days of differentiation (Fig. 44).

These results indicate that the upregulation of DNA repair factors is a general feature during monocyte differentiation. It occurs in DCs, M-CSF- and GM-CSF-macrophages. It is likely that XRCC1 expression is regulated by one of the overlapping signalling pathways of M-CSF and GM-CSF that is stimulated in all three phagocytes. As described above, the PI3K and MAPK pathways are of particular interest here and should be considered for further analysis to elucidate the XRCC1-relevant signalling cascade and the corresponding transcription factor(s) (van de Laar *et al.* 2012; Jack *et al.* 2009; Corey and Anderson 1999; Reuter *et al.* 2000).

5.10 Attenuated XRCC1 expression in maturing macrophages in the presence of the demethylation inhibitor 2-HG

Over the course of cytokine-induced differentiation, demethylation processes are observed in DCs and macrophages (Wallner *et al.* 2016; Klug *et al.* 2010). The differential methylation status of monocytes and macrophages led to the hypothesis that the XRCC1 promoter may be methylated in monocytes. As an initial experiment, differentiating monocytes were treated with the demethylation inhibitor 2-HG. It inhibits TET2 which is required for monocytic demethylation events (Klug *et al.* 2010). 2-HG-treated cells displayed attenuated XRCC1 signals during differentiation (Fig. 45 and Fig. 46). The effect was observed in both M-CSF- and GM-CSF-generated macrophages (Fig. 45 and Fig. 47). After differentiation was completed on day 6 no discernible differences in XRCC1 signals could be observed (Fig. 45). This may be due to the stability of 2-HG in the medium. The inhibitor was applied once at day 0 of differentiation. Repetitive applications may be required.

5.11 Methylation pattern of the XRCC1 promoter

Changes in the methylation status of haematopoietic cells occur at different stages of haematopoiesis. Klug *et al.* showed that monocytes undergo active demethylation when their differentiation into DCs is induced by GM-CSF + IL-4. The demethylation process, measured by the appearance of 5hmC, was mediated by TET2 (a protein often mutated in myeloid malignancies) (Klug *et al.* 2010). The demethylation also coincided with the

appearance of activating histone marks such as mono- and demethylation of H3K4 or acetylation of histones H3 and H4. Wallner *et al.* analysed the methylation status of monocytes undergoing differentiation into macrophages in the presence of M-CSF. They found differentially expressed genes, mRNAs and miRNAs. At methylation hot spots (so-called differentially methylated regions, DMR), a rapid demethylation process was observed within 24 h of cytokine addition. The demethylation process was inhibited by adding 2-HG to the cells (Wallner *et al.* 2016). However, the authors also found that gene expression changes did not correlate with DNA methylation changes at transcription start sites.

In the case of XRCC1, it was hypothesised that the XRCC1 promoter may be methylated and thus silenced. Over the course of GM-CSF-induced differentiation, demethylation of the XRCC1 promoter may lead to re-expression of XRCC1. The analysis of the XRCC1 promoter region spanning up to ~800 bp before the transcription start site (TSS) was analysed. It was shown that distal to the promoter the DNA was heavily methylated. The degree of methylation dropped rapidly proximal to the TSS. However, this demethylation occurred in both monocytes and macrophages (Fig. 48). Direct methylation of the XRCC1 promoter was not responsible for the downregulation of XRCC1.

5.12 Regulation of XRCC1 protein expression

As the degree of methylation of the XRCC1 promoter did not seem to be influenced by cytokine-induced differentiation, the idea of methylation-specific gene silencing as a regulatory mechanism for DNA repair factors in human immune cells became doubtful. The question remains how the XRCC1 gene is regulated. It was postulated that a specific transcription factor may be responsible, which is not expressed in monocytes, but becomes upregulated during cytokine-induced differentiation. Preliminary data by ..... showed an attenuated XRCC1 signal when monocytes were treated with JNK or p38 inhibitors. At days 3 and 6 of GM-CSF-induced differentiation the XRCC1 signal was significantly reduced compared to the controls (Fig. 49). The effect was strongest in p38 inhibitor-treated cells at day 6. Inhibitor-treated macrophages also displayed morphological differences with fewer spindle-shaped and more round-shaped cells (Miriam Pons 2016). JNK and p38 are both regulated by the upstream MAPK pathways which are stimulated by GM-CSF-mediated activation of the CSFR2 as well as the M-CSF-mediated activation of the CSFR1 (van de Laar *et al.* 2012; Corey and Anderson 1999).

In order to find the elusive transcription factor(s), nuclear protein extracts of monocytes and macrophages (day 4 of differentiation) were incubated with the XRCC1 promoter sequence. The DNA-bound proteins were subjected to mass spectrometry analysis and the data was evaluated by upregulated protein expression in macrophages with concomitant downregulation of the proteins in monocytes. As a first observation, several hundred proteins were detected using this approach. It seems unlikely that all of these proteins were bound to the DNA. Future experiments may require modifications of the protocol with added washing steps to remove unspecific protein-DNA interactions. The data were scored for strongly regulated transcriptions factors. Promising candidates were ETS-related transcription factor Elf-1 (ELF1), PU.1 (SPI1), CCAAT/enhancer-binding protein alpha (CEBPA), transcriptional repressor CTCF, transcription initiation factor TFIID subunit 6 (TAF6), general transcription factor II-I (GTF2I), transcription intermediary factor 1-beta (TRIM28) and JunB (JUNB).

Trim28, also known as KAP1, mediates transcriptional control via the Krüppel-associated box repression domain found in many transcription factors. It enhances transcriptional repression by coordinating the increase in H3K9me3. It has E3 SUMO-protein ligase activity and ubiquitinates p53 leading to its proteasomal degradation (Wang *et al.* 2005). It seems an unlikely candidate for the upregulation of XRCC1.

Similar to Trim28, CTCF is a questionable candidate for the upregulation of XRCC1. Its functions are manifold as it acts as both a transcriptional repressor and an activator. It works as a protein insulator by blocking the interaction of enhancers and promoters (Kim *et al.* 2015). CTCF knockout mice display a mild phenotype. Isolated macrophages demonstrate normal phagocytosis and upon TLR stimulation normal levels of pro-inflammatory cytokines, *e.g.* IL-12 and IL-6 are released. (Nikolic *et al.* 2014). However, the cells are impaired in TNF and IL-10 productions. The authors postulate a CTCF-mediated fine-tuning of the macrophage function. As CTCF knockout mice exist, isolation of monocytes and macrophages from the bone marrow (monocytes) and the peritoneum (macrophages) with subsequent XRCC1 detection may shed some light on the role of this transcription factor and its putative role in DNA repair protein regulation.

TAF6, also known as TATA-Box Binding Protein Associated Factor 6, is part of the transcription factor IID (TFIID) complex which coordinates RNA polymerase II-mediated transcription. TFIID participates in basal transcription and serves as a co-activator. Surprisingly only TAF6 and TAF15 were differently expressed in monocytes/macrophages (see supplement 7.9). Other TAF proteins, *i.e.* TAF1-15, were not detected. Its importance for the upregulated expression of DNA repair factors remains elusive.

Another upregulated transcription factor in the macrophage sample was the general transcription factor II-I (GTF2I). Ras-mediated activation of GTF2I leads to transcriptional activation of c-fos – which was not detected in the proteomics data. c-fos is part of the Fos family (c-Fos, FosB, Fra-1 and Fra-2) which interacts with members of the jun family (c-Jun, JunB and JunD) to form the activator protein 1 (AP-1) transcription complex. JunB, which was also present in macrophages, binds to the DNA sequence 5'-TGA[CG]TCA-3'. The AP-1 complex regulates many cellular processes, including proliferation, differentiation, apoptosis and responses to stress (Piechaczyk and Farràs 2008). Despite the lack of Fos proteins, a closer look at Jun/Fos-mediated gene expression may be required as they are activated by MAPK-mediated activation of JNK and p38.

The transcription factor CEBPA (C/EBPα) is crucial for haematopoiesis and its functions are manifold. Studies with $Cebpa^{-/-}$ mice showed a complete lack of neutrophil development as the differentiation of multipotent common myeloid progenitor to granulocyte progenitor cells (GMP) is blocked (Manz and Boettcher 2014). One of its target genes is the Granulocyte-CSF receptor (CSF3R, CD114). CEBPA can lead to transdifferentiation of B and T cells into macrophages. Together with PU.1, it can also lead to transdifferentiation of fibroblasts (murine NIH3T3 cells) into macrophages by upregulating myeloid gene expression (Cirovic *et al.* 2017; van Oevelen *et al.* 2015; Friedman 2007). As a homo- or heterodimer CEBPA binds to the consensus DNA sequence 5'-T[TG]NNGNAA[TG]-3', but tolerates considerable variations. It can also interact with the CCAAT motif (Ramji and Foka 2002). One of its targets is the PU.1 promoter. Furthermore, it binds and inhibits the E2F1 transcription factor. E2F1 prevents terminal differentiation of myeloid immune cells. Therefore, CEBPA is important for the differentiation of myeloid immune cells (Friedman 2007).

PU.1 binds to the DNA consensus sequence 5'-AAAG(A/C/G)GGAAG-3' via its C-terminal ETS domain. It activates transcription via its N-terminal domains. PU.1 is expressed at

many stages of haematopoiesis. PU.1$^{-/-}$ mice lack B cells and monocytes and have diminished amounts of neutrophils. Exogenous PU.1 leads to transdifferentiation of B and T cells to monocyte/macrophages (Friedman 2007).

ELF1 is part of the ETS family. The ETS family of transcription factors comprises more than 20 members. Each of them shares a conserved 'E26 transformation-specific' (ETS) domain that recognises DNA sequences containing a GGAA/T core element. Other members of the ETS family are PU.1, Spi-B, Ets-1 and Myeloid Elf-1-Like Factor (MEF). These transcription factors play important roles in the development and maintenance of haematopoietic lineages. In the case of Ets-1 and MEF it has been shown that they are critical in the development of NK and NKT cells. ELF1 is highly expressed in both embryonic and adult lymphoid tissues as well as endothelial cells (Choi *et al.* 2011).

Interestingly, the transcription factor E2F1 was not detected by mass spectrometry. Published data showed that E2F1 upregulated the XRCC1 promoter cloned into a luciferase reporter assay expressed in Saos2 cells and mouse embryonic fibroblasts (Chen et al. 2008). However, monocytes and macrophages are (mostly) non-replicative cells which do not require a replication and cell cycle regulating transcription factor. E2F1 leads to the re-entry into the cell cycle by upregulating cyclins (Li et al. 2003).

In addition, promoter sequences of the other differentially regulated DNA repair factors, *i.e.* PARP-1, ligase III and PRKDC were analysed *in silico* (Table 8). Starting from the ATG start codon, the upstream DNA sequences of *XRCC1, PARP-1, PRKDC (DNA-PKcs)* and *ligase III* were copied from the NCBI database. DNA sequences ranged from ~1000 to 2300 bp (see supplements 7.8). They were screened for potential transcription factor binding sites using Patch 1.0 software and compared to the proteins identified by mass spectrometry (Table 8).

Table 8: Potential transcription factors regulating DNA repair proteins

Transcription Factors	XRCC1	PARP-1	PRKDC	Ligase III	Mass Spec.
CTCF	+	+	+	+	+
CEBPA	+	+		+	+
ELF1					+
PU.1					+
JUNB				(+)	+
other AP-1 factors	+	+	+	+	+
c-Ets-2	+	+	+	+	
c-Ets-1		+	+	+	

In silico, all sequences were positive for the transcription factor CTCF (Table 8 and Fig. 51). With the exception of PRKDC, they were also positive for CEBPA. The CCAAT box was found in all four sequences. The four DNA regions upstream of *XRCC1, PARP-1, PRKDC* and *ligase III* (Fig. 51) depict multiple binding sites for the transcription factors CTCF, AP-1 and c-Ets. They also show several CCAAT motifs. CEBPA and other factors are known to interact with this sequence, however in *PRKDC*, CCAAT transcription factor/nuclear factor-1 (CTF/NF-1) was listed as a potential binding factor and not CEBPA. Many binding sites are found in close vicinity to the ATG codon.

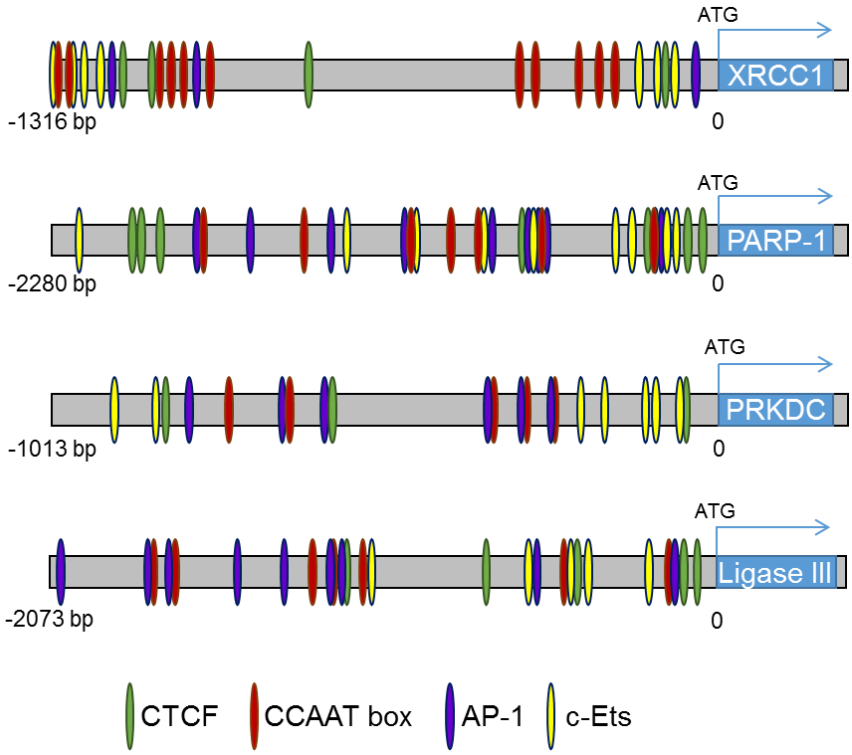

Fig. 51: Schematic representation of potential transcription factor binding sites regulating DNA repair genes

DNA sequences ranging from ~1000 to ~2300 bp upstream of the ATG start codon of the indicated DNA repair factors are depicted. Potential transcription factor binding sites for CTCF, AP-1 and c-Ets are displayed. The CCAAT box is recognised by several transcription factors, *e.g.* CEBPA and CCAAT transcription factor/nuclear factor-1 (CTF/NF-1).

The ETS transcription factor family encompasses 27 members which share the conserved ETS domain responsible for DNA binding. c-Ets-1 and c-Ets-2 are closely related and share 96 % of the amino acid identity in the ETS domain (John et al. 2014). Computational analysis of the sequences were mostly positive for c-Ets-1 and 2. In the proteomics data, they were not found. Instead, the ETS members ELF1 and PU.1 were detected. They share the ETS DNA binding domain and the activation domain also found in c-Ets-1 and 2 (Gutierrez-Hartmann et al. 2007). Therefore, a closer look at this family of proteins is required. Furthermore, proteomics detected JunB, one of the subunits of the heterodimeric AP-1 transcription factor. As mentioned above, AP-1 consists of jun members associating with fos members.

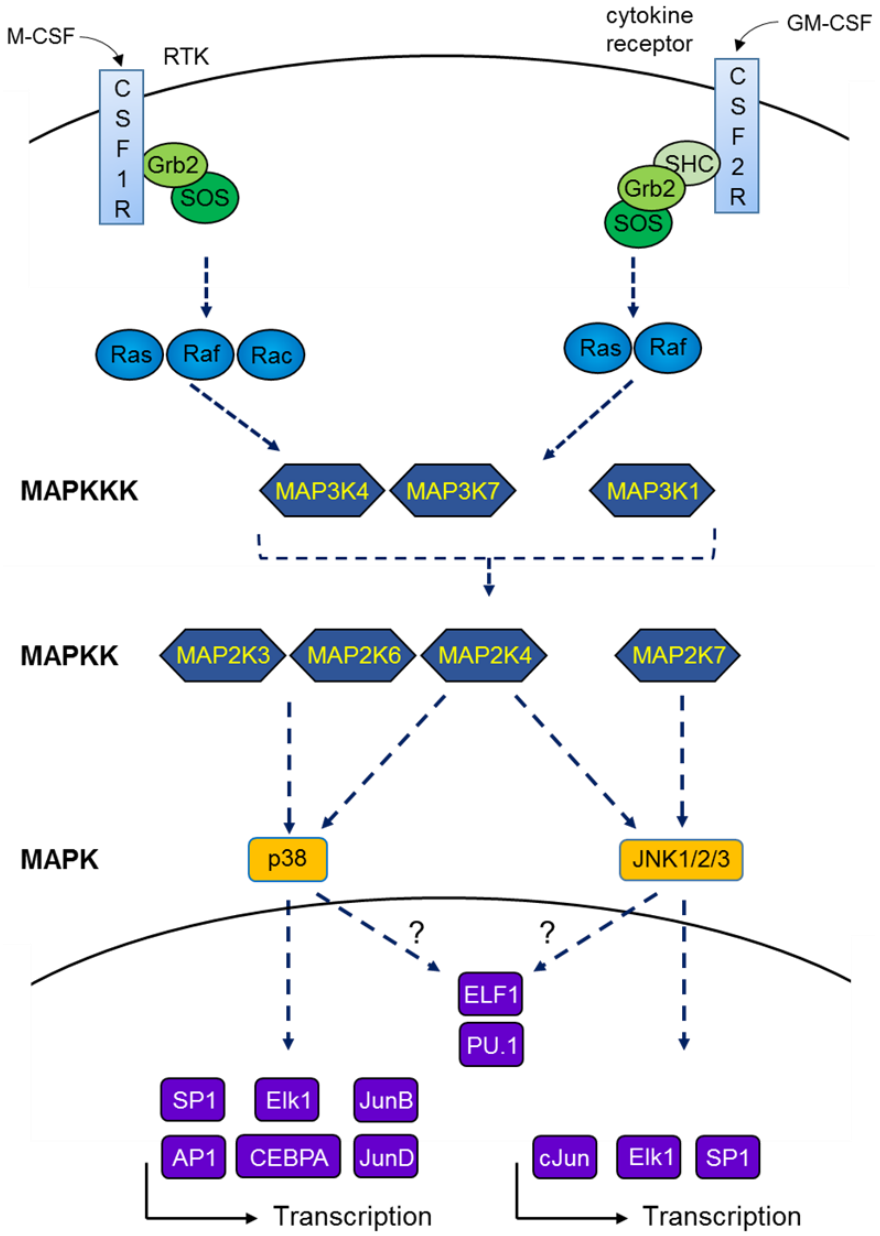

Fig. 52: Cytokine-mediated signal transduction in monocytes (simplified scheme)
Cytokine-induced differentiation of monocytes into macrophages can be achieved by either M-CSF or GM-CSF. In both cases, differentiation is associated with an upregulation of XRCC1 protein expression. Both cytokines have overlapping signalling pathways such as the MAPK signalling cascade. Downstream targets are the JNK 1/2/3 (MAPK8/9/10) and the p38α (MAPK14), β (MAPK11), γ (MAPK12/ERK6), and δ (MAPK13/SAPK4) proteins. Potential regulators of XRCC1 expression – mediated by p38 and/or JNK – are listed in lilac. MAPKKK - Mitogen-Activated Protein Three Kinase, MAPKK - MAP Two Kinase, MAPK - MAP Kinase.

It was postulated that upregulation of XRCC1 is due to a signalling cascade found in both M-CSF- and GM-CSF-mediated differentiation pathways. The MAPK pathway is activated by both cytokines and their respective receptors. Via Ras, Raf and Rac proteins, both the CSF1R (for M-CSF) and CSF2R (for GM-CSF), activate the upstream MAP Three Kinases (MAPKKK) (Fig. 52). Those phosphorylate MAP Two Kinases (MAPKK) who in turn activate MAP Kinases (MAPK) like the JNK proteins 1, 2 and 3 (JNK1/2/3) and the p38 MAPK (p38α/β/γ/δ) (Fig. 52). These kinases signal into the nucleus and modulate the activity of transcription factors. Some of these transcriptions factors were also found by mass

spectrometry, *i.e.* JUNB and CEBPA. ELF1, a member of the ETS family, was also detected by mass spectrometry.

In order to elucidate the XRCC1-relevant transcription factor, experiments have to be conducted in which the consensus sequences are mutated or deleted. This can be achieved by a site-directed mutagenesis method. The required XRCC1 promoter plasmid was constructed by ..... (Miriam Pons 2016).

Last but not least, the proteomics data was screened for differentially expressed DNA repair factors that were pulled down with the XRCC1 promoter PCR products. As it was not a full nuclear proteome analysis it only provides limited information on the overall (differential) expression of DNA repair proteins in monocytes vs macrophages. The data confirmed previous findings of BER protein expression defects in monocytes, *i.e.* there was no detectable XRCC1 nor ligase IIIα. (Table 7). The increase of PARP-1 protein level in macrophages was not as pronounced as with the other BER proteins. Interestingly, other DNA repair proteins were also differentially expressed in monocytes compared to macrophages, *e.g.* PNKP. In BER, PNKP is a DNA end processing enzyme which removes 3'-phosphate ends at SSBs to make them accessible for re-ligation. The DNA glycosylase MPG, the endonuclease APEX1 and Polβ were slightly stronger expressed in macrophages than in monocytes. MPG removes 3-methyladenine and 7-methylguanine leaving an AP site. APEX1 (also known as APE1) incises the phosphodiester bond at the AP site resulting in a SSB with 5'dRP and 3'-OH ends (Christmann *et al.* 2003). Surprisingly, the long-patch BER-associated endonuclease Fen1 was upregulated in monocytes but not in macrophages. A similar trend was observed by Bauer *et al.* using Western Blot analysis.

DSB repair related factors were also differentially expressed between the two samples. The strong expression of DNA-PKcs (gene name PRKDC) in macrophages confirmed previous data showing a lack of DNA-PKcs protein in monocytes that is overcome during cytokine-induced differentiation into DCs and macrophages (Bauer *et al.* 2011). In contrast to Bauer *et al.* a clear upregulation of XRCC5 (Ku80) and XRCC6 (Ku70) was observed in macrophages. The Ku proteins are required for NHEJ. They act as a regulatory subunit of DNA-PKcs, increasing the affinity of the DNA-PK catalytic subunit to the DNA by 100-fold. DNA-PKcs, XRCC4, ligase IV and XLF are recruited to the DSB to re-ligate the two DNA ends (Davis and Chen 2013). DNA-PKcs is a member of the PI3K family and can phosphorylate many DNA repair-relevant proteins such as Ku70/80, XRCC4, ligase IV, XLF, Werner Syndrome RecQ Like Helicase (WRN), Artemis, H2AX and p53 (Mahaney *et al.* 2009). Without DNA-PKcs, monocytes are unable to perform c-NHEJ and DSBs can only be repaired by either alt-EJ or HR. As monocytes are non-replicative cells HR cannot occur. Alt-EJ requires XRCC1, PARP-1 and ligase IIIα which are not expressed in monocytes rendering monocytes susceptible to DNA strand break-inducing genotoxins.

The interpretation of the differentially expressed proteins in this experiment must be undertaken with care. The DNA repair factors mentioned so far are recruited to DNA damage sites. The XRCC1 promoter PCR products are a scaffold for such protein/DNA interactions. The DNA molecules mimic DSBs as they are in linear conformation. Therefore, the recruitment of DNA-PKcs, Ku70 and Ku80 seems likely. The PCR products may contain some BER-relevant DNA lesions, *e.g.* hydrolytic cleavage of bases due to the aqueous environment resulting in the recruitment of APEX1 to the DNA. The ensuing SSB may lead to the recruitment of Polβ, XRCC1 and ligase III.

Other DNA repair relevant factors were also found. For example, RAD23, DDB1, DDB2 and XPC. They are part of the nucleotide excision repair (NER) pathway. NER is responsible for the repair of helix-distorting lesions and bulky DNA-adducts. UV light induces 6-4 photoproducts and thymine dimers which disturb the helix conformation (Christmann et al. 2003). Polyaromatic hydrocarbons (*e.g.* benzo[a]pyrene-7,8-dihydrodiol-9,10-epoxide, BPDE) can form prototypical bulky DNA adducts. The heterotrimeric replication protein A complex consists of RPA1, 2 and 3. RPA binds and stabilises ssDNA intermediates formed during replication and DNA repair. In NER, it is recruited to the damage site by XPA and XPG. It binds the DNA and prevents annealing of the two ssDNA molecules during repair.

The experimental conditions did not lead to NER-specific DNA damage. The samples were incubated under visible light and they were incubated at physiological pH and temperature. The presence of helix-distorting lesions or ssDNA seems unlikely. The detection of RAD23, DDB1/2, XPC and RPA (Table 7) may be attributed to unspecific binding to the DNA and to insufficient washing steps leading to “contamination” with the nuclear protein lysate. Still, the strong upregulation of RPA and XPC in macrophages may indicate a differential NER protein expression in monocytes versus macrophages. Interestingly, NER proteins XPF, ERCC1 and XPG are known to be regulated by the transcription factor AP-1 (Christmann and Kaina 2013). Future experiments using mass spectrometry analysis of whole nuclear extracts may shed light on the NER capacity of monocytes compared to macrophages.

TOP2A and TOP2B were also detected. They are topoisomerases which alter the topological state of the DNA during transcription and replication. They reduce torsional stress by catalysing a transient break in the DNA thus allowing strand relaxation. They are a common target in anticancer treatment. Both proteins were detected in the macrophage sample.

5.13 Concluding remarks

In summary, it was shown that human myeloid immune cells differentially express DNA repair proteins. In the case of neutrophilic granulocytes, the DNA repair defect seems to have no discernible effect as they die independent of DNA damage. Monocytes, on the other hand, are sensitive towards exogenous and endogenous ROS. Activation of NADPH Oxidase followed by the production of superoxide leads to elevated ROS levels inside and outside the cell. In monocytes, an accumulation of DNA damage due to ROS occurs and activates the DDR that eventually results in monocytic cell death. Cytokine-induced differentiation into macrophages (or DCs) leads to the re-expression of DNA repair proteins. Macrophages are resistant towards their own ROS.

The regulation of DNA repair proteins, namely XRCC1, PARP-1, ligase IIIα and DNA-PKcs, in immune cells remains elusive. Promoter methylation is not the mechanism of regulation. However, the mass spectrometry data hint at potential transcription factors that are required for the expression of DNA repair factors.

6 References

Abbotts, R., Wilson, D. M., 2017. Coordination of DNA single strand break repair. Free radical biology & medicine 107: 228‐244. 10.1016/j.freeradbiomed.2016.11.039.

Aga, M., Watters, J. J., Pfeiffer, Z. A., Wiepz, G. J., Sommer, J. A., Bertics, P. J., 2004. Evidence for nucleotide receptor modulation of cross talk between MAP kinase and NF-kappa B signaling pathways in murine RAW 264.7 macrophages. American journal of physiology. Cell physiology 286 (4): C923-30. 10.1152/ajpcell.00417.2003.

Alcaraz, M. J., Gualillo, O., Sánchez-Pernaute, O., 2013. Studies on Arthritis and Joint Disorders. New York, NY: Springer.

Ashkenazi, A., Abu-Rabeah, K., Marks, R. S., 2009. Electrochemistry and chemiluminescence techniques compared in the detection of NADPH oxidase activity in phagocyte cells. Talanta 77 (4): 1460‐1465. 10.1016/j.talanta.2008.09.035.

Banchereau, J., Steinman, R. M., 1998. Dendritic cells and the control of immunity. Nature 392 (6673): 245‐252. 10.1038/32588.

Bauer, M., Goldstein, M., Christmann, M., Becker, H., Heylmann, D., Kaina, B., 2011. Human monocytes are severely impaired in base and DNA double-strand break repair that renders them vulnerable to oxidative stress. Proceedings of the National Academy of Sciences of the United States of America 108 (52): 21105‐21110. 10.1073/pnas.1111919109.

Bauer, M., Goldstein, M., Heylmann, D., Kaina, B., 2012. Human monocytes undergo excessive apoptosis following temozolomide activating the ATM/ATR pathway while dendritic cells and macrophages are resistant. PloS one 7 (6): e39956. 10.1371/journal.pone.0039956.

Beneke, S., Bürkle, A., 2007. Poly(ADP-ribosyl)ation in mammalian ageing. Nucleic acids research 35 (22): 7456‐7465. 10.1093/nar/gkm735.

Bennett, S. E., Sung, J. S., Mosbaugh, D. W., 2001. Fidelity of uracil-initiated base excision DNA repair in DNA polymerase beta-proficient and -deficient mouse embryonic fibroblast cell extracts. The Journal of biological chemistry 276 (45): 42588‐42600. 10.1074/jbc.M106212200.

Berdelle, N., Nikolova, T., Quiros, S., Efferth, T., Kaina, B., 2011. Artesunate induces oxidative DNA damage, sustained DNA double-strand breaks, and the ATM/ATR damage response in cancer cells. Molecular cancer therapeutics 10 (12): 2224‐2233. 10.1158/1535-7163.MCT-11-0534.

Berman, P. A., Adams, P. A., 1997. Artemisinin enhances heme-catalysed oxidation of lipid membranes. Free radical biology & medicine 22 (7): 1283‐1288.

Bernofsky, C., Swan, M., 1973. An improved cycling assay for nicotinamide adenine dinucleotide. Analytical biochemistry 53 (2): 452‐458.

Berte, N., Lokan, S., Eich, M., Kim, E., Kaina, B., 2016. Artesunate enhances the therapeutic response of glioma cells to temozolomide by inhibition of homologous recombination and senescence. Oncotarget 7 (41): 67235‐67250. 10.18632/oncotarget.11972.

Blesa, J., Trigo-Damas, I., Quiroga-Varela, A., Jackson-Lewis, V. R., 2015. Oxidative stress and Parkinson's disease. Frontiers in neuroanatomy 9: 91. 10.3389/fnana.2015.00091.

Bluhm, A., Casas-Vila, N., Scheibe, M., Butter, F., 2016. Reader interactome of epigenetic histone marks in birds. Proteomics 16 (3): 427‐436. 10.1002/pmic.201500217.

Bogdan, C., Röllinghoff, M., Diefenbach, A., 2000. The role of nitric oxide in innate immunity. Immunological reviews 173: 17‐26.

Bradford, M. M., 1976. A rapid and sensitive method for the quantitation of microgram quantities of protein utilizing the principle of protein-dye binding. Analytical biochemistry 72: 248‐254.

Brandes, R. P., Kreuzer, J., 2005. Vascular NADPH oxidases: Molecular mechanisms of activation. Cardiovascular research 65 (1): 16‐27. 10.1016/j.cardiores.2004.08.007.

Brandes, R. P., Weissmann, N., Schröder, K., 2014. Nox family NADPH oxidases: Molecular mechanisms of activation. Free radical biology & medicine 76: 208‐226. 10.1016/j.freeradbiomed.2014.07.046.

Brieger, K., Schiavone, S., Miller, F. J., Krause, K.-H., 2012. Reactive oxygen species: From health to disease. Swiss medical weekly 142: w13659. 10.4414/smw.2012.13659.

Briegert, M., Kaina, B., 2007. Human monocytes, but not dendritic cells derived from them, are defective in base excision repair and hypersensitive to methylating agents. Cancer research 67 (1): 26–31. 10.1158/0008-5472.CAN-06-3712.

Broeke, T. ten, Wubbolts, R., Stoorvogel, W., 2013. MHC class II antigen presentation by dendritic cells regulated through endosomal sorting. Cold Spring Harbor perspectives in biology 5 (12): a016873. 10.1101/cshperspect.a016873.

Bürkle, A., 2005. Poly(ADP-ribose). The most elaborate metabolite of NAD+. The FEBS journal 272 (18): 4576–4589. 10.1111/j.1742-4658.2005.04864.x.

Byakika-Kibwika, P., Lamorde, M., Mayito, J., Nabukeera, L., Mayanja-Kizza, H., Katabira, E., Hanpithakpong, W., Obua, C., Pakker, N., Lindegardh, N., Tarning, J., Vries, P. J. de, Merry, C., 2012. Pharmacokinetics and pharmacodynamics of intravenous artesunate during severe malaria treatment in Ugandan adults. Malaria journal 11: 132. 10.1186/1475-2875-11-132.

Cadet, J., Delatour, T., Douki, T., Gasparutto, D., Pouget, J. P., Ravanat, J. L., Sauvaigo, S., 1999. Hydroxyl radicals and DNA base damage. Mutation research 424 (1-2): 9–21.

Caldecott, K. W., 2003. Protein-protein interactions during mammalian DNA single-strand break repair. Biochemical Society transactions 31 (Pt 1): 247–251.

Cao, D., Boxer, L. A., Petty, H. R., 1993. Deposition of reactive oxygen metabolites onto and within living tumor cells during neutrophil-mediated antibody-dependent cellular cytotoxicity. Journal of cellular physiology 156 (2): 428–436. 10.1002/jcp.1041560227.

Castiello, L., Sabatino, M., Jin, P., Clayberger, C., Marincola, F. M., Krensky, A. M., Stroncek, D. F., 2011. Monocyte-derived DC maturation strategies and related pathways: A transcriptional view. Cancer immunology, immunotherapy CII 60 (4): 457–466. 10.1007/s00262-010-0954-6.

Cathcart, M. K., 2004. Regulation of superoxide anion production by NADPH oxidase in monocytes/macrophages: Contributions to atherosclerosis. Arteriosclerosis, thrombosis, and vascular biology 24 (1): 23–28. 10.1161/01.ATV.0000097769.47306.12.

Chan, E. D., Chan, J., Schluger, N. W., 2001. What is the role of nitric oxide in murine and human host defense against tuberculosis?Current knowledge. American journal of respiratory cell and molecular biology 25 (5): 606–612. 10.1165/ajrcmb.25.5.4487.

Chandel, N. S., Trzyna, W. C., McClintock, D. S., Schumacker, P. T., 2000. Role of oxidants in NF-kappa B activation and TNF-alpha gene transcription induced by hypoxia and endotoxin. Journal of immunology (Baltimore, Md. 1950) 165 (2): 1013–1021.

Chapman, J. R., Taylor, M. R. G., Boulton, S. J., 2012. Playing the end game: DNA double-strand break repair pathway choice. Molecular cell 47 (4): 497–510. 10.1016/j.molcel.2012.07.029.

Chen, D., Yu, Z., Zhu, Z., Lopez, C. D., 2008. E2F1 regulates the base excision repair gene XRCC1 and promotes DNA repair. The Journal of biological chemistry 283 (22): 15381–15389. 10.1074/jbc.M710296200.

Cheresh, P., Kim, S.-J., Tulasiram, S., Kamp, D. W., 2013. Oxidative stress and pulmonary fibrosis. Biochimica et biophysica acta 1832 (7): 1028–1040. 10.1016/j.bbadis.2012.11.021.

Chevallet, M., Luche, S., Rabilloud, T., 2006. Silver staining of proteins in polyacrylamide gels. Nature protocols 1 (4): 1852–1858. 10.1038/nprot.2006.288.

Choi, H.-J., Geng, Y., Cho, H., Li, S., Giri, P. K., Felio, K., Wang, C.-R., 2011. Differential requirements for the Ets transcription factor Elf-1 in the development of NKT cells and NK cells. Blood 117 (6): 1880–1887. 10.1182/blood-2010-09-309468.

Chou, W.-C., Jie, C., Kenedy, A. A., Jones, R. J., Trush, M. A., Dang, C. V., 2004. Role of NADPH oxidase in arsenic-induced reactive oxygen species formation and cytotoxicity in myeloid leukemia cells. Proceedings of the National Academy of Sciences of the United States of America 101 (13): 4578–4583. 10.1073/pnas.0306687101.

Christmann, M., Kaina, B., 2013. Transcriptional regulation of human DNA repair genes following genotoxic stress: Trigger mechanisms, inducible responses and genotoxic adaptation. Nucleic acids research 41 (18): 8403–8420. 10.1093/nar/gkt635.

Christmann, M., Tomicic, M. T., Roos, W. P., Kaina, B., 2003. Mechanisms of human DNA repair: An update. Toxicology 193 (1-2): 3‐34.

Chung, E. Y., Liu, J., Homma, Y., Zhang, Y., Brendolan, A., Saggese, M., Han, J., Silverstein, R., Selleri, L., Ma, X., 2007. Interleukin-10 expression in macrophages during phagocytosis of apoptotic cells is mediated by homeodomain proteins Pbx1 and Prep-1. Immunity 27 (6): 952‐964. 10.1016/j.immuni.2007.11.014.

Cirovic, B., Schönheit, J., Kowenz-Leutz, E., Ivanovska, J., Klement, C., Pronina, N., Bégay, V., Leutz, A., 2017. C/EBP-Induced Transdifferentiation Reveals Granulocyte-Macrophage Precursor-like Plasticity of B Cells. Stem cell reports 8 (2): 346‐359. 10.1016/j.stemcr.2016.12.015.

Clark, R. L., 2012. Effects of artemisinins on reticulocyte count and relationship to possible embryotoxicity in confirmed and unconfirmed malarial patients. Birth defects research. Part A, Clinical and molecular teratology 94 (2): 61‐75. 10.1002/bdra.22868.

Corey, S. J., Anderson, S. M., 1999. Src-related protein tyrosine kinases in hematopoiesis. Blood 93 (1): 1‐14.

Daniel Heylmann, 2017. Sensitivität humaner Immunzellen gegenüber ionisierender Strahlung und anderen genotoxischen Noxen. Dissertation. Mainz.

Daniels, M. A., Devine, L., Miller, J. D., Moser, J. M., Lukacher, A. E., Altman, J. D., Kavathas, P., Hogquist, K. A., Jameson, S. C., 2001. CD8 binding to MHC class I molecules is influenced by T cell maturation and glycosylation. Immunity 15 (6): 1051‐1061.

Davies, M. J., 2011. Myeloperoxidase-derived oxidation: Mechanisms of biological damage and its prevention. Journal of clinical biochemistry and nutrition 48 (1): 8‐19. 10.3164/jcbn.11-006FR.

Davis, A. J., Chen, D. J., 2013. DNA double strand break repair via non-homologous end-joining. Translational cancer research 2 (3): 130‐143. 10.3978/j.issn.2218-676X.2013.04.02.

Deaton, A. M., Bird, A., 2011. CpG islands and the regulation of transcription. Genes & development 25 (10): 1010‐1022. 10.1101/gad.2037511.

Della-Maria, J., Hegde, M. L., McNeill, D. R., Matsumoto, Y., Tsai, M.-S., Ellenberger, T., Wilson, D. M., Mitra, S., Tomkinson, A. E., 2012. The interaction between polynucleotide kinase phosphatase and the DNA repair protein XRCC1 is critical for repair of DNA alkylation damage and stable association at DNA damage sites. The Journal of biological chemistry 287 (46): 39233‐39244. 10.1074/jbc.M112.369975.

Dianov, G., Bischoff, C., Piotrowski, J., Bohr, V. A., 1998. Repair pathways for processing of 8-oxoguanine in DNA by mammalian cell extracts. The Journal of biological chemistry 273 (50): 33811‐33816.

Dondorp, A., Nosten, F., Stepniewska, K., Day, N., White, N., 2005. Artesunate versus quinine for treatment of severe falciparum malaria: A randomised trial. Lancet (London, England) 366 (9487): 717‐725. 10.1016/S0140-6736(05)67176-0.

Donis-Maturano, L., Sánchez-Torres, L. E., Cerbulo-Vázquez, A., Chacón-Salinas, R., García-Romo, G. S., Orozco-Uribe, M. C., Yam-Puc, J. C., González-Jiménez, M. A., Paredes-Vivas, Y. L., Calderón-Amador, J., Estrada-Parra, S., Estrada-García, I., Flores-Romo, L., 2015. Prolonged exposure to neutrophil extracellular traps can induce mitochondrial damage in macrophages and dendritic cells. SpringerPlus 4: 161. 10.1186/s40064-015-0932-8.

Efferth, T., Giaisi, M., Merling, A., Krammer, P. H., Li-Weber, M., 2007a. Artesunate induces ROS-mediated apoptosis in doxorubicin-resistant T leukemia cells. PloS one 2 (8): e693. 10.1371/journal.pone.0000693.

Efferth, T., Li, P. C. H., Konkimalla, V. S. B., Kaina, B., 2007b. From traditional Chinese medicine to rational cancer therapy. Trends in molecular medicine 13 (8): 353‐361. 10.1016/j.molmed.2007.07.001.

Eguchi, Y., Shimizu, S., Tsujimoto, Y., 1997. Intracellular ATP levels determine cell death fate by apoptosis or necrosis. Cancer research 57 (10): 1835‐1840.

el Ghissassi, F., Barbin, A., Nair, J., Bartsch, H., 1995. Formation of 1,N6-ethenoadenine and 3,N4-ethenocytosine by lipid peroxidation products and nucleic acid bases. Chemical research in toxicology 8 (2): 278–283.

Ellis, J. A., Mayer, S. J., Jones, O. T., 1988. The effect of the NADPH oxidase inhibitor diphenyleneiodonium on aerobic and anaerobic microbicidal activities of human neutrophils. The Biochemical journal 251 (3): 887–891.

Elmore, S., 2007. Apoptosis: A review of programmed cell death. Toxicologic pathology 35 (4): 495–516. 10.1080/01926230701320337.

Fahrer, J., Kaina, B., 2013. O6-methylguanine-DNA methyltransferase in the defense against N-nitroso compounds and colorectal cancer. Carcinogenesis 34 (11): 2435–2442. 10.1093/carcin/bgt275.

Fialkow, L., Wang, Y., Downey, G. P., 2007. Reactive oxygen and nitrogen species as signaling molecules regulating neutrophil function. Free radical biology & medicine 42 (2): 153–164. 10.1016/j.freeradbiomed.2006.09.030.

Flajnik, M. F., Kasahara, M., 2010. Origin and evolution of the adaptive immune system: Genetic events and selective pressures. Nature reviews. Genetics 11 (1): 47–59. 10.1038/nrg2703.

Fortini, P., Dogliotti, E., 2007. Base damage and single-strand break repair: Mechanisms and functional significance of short- and long-patch repair subpathways. DNA repair 6 (4): 398–409. 10.1016/j.dnarep.2006.10.008.

Friedman, A. D., 2007. Transcriptional control of granulocyte and monocyte development. Oncogene 26 (47): 6816–6828. 10.1038/sj.onc.1210764.

Godon, C., Cordelières, F. P., Biard, D., Giocanti, N., Mégnin-Chanet, F., Hall, J., Favaudon, V., 2008. PARP inhibition versus PARP-1 silencing: Different outcomes in terms of single-strand break repair and radiation susceptibility. Nucleic acids research 36 (13): 4454–4464. 10.1093/nar/gkn403.

Gopalakrishnan, A. M., Kumar, N., 2015. Antimalarial action of artesunate involves DNA damage mediated by reactive oxygen species. Antimicrobial agents and chemotherapy 59 (1): 317–325. 10.1128/AAC.03663-14.

Gordon, S., Plűddemann, A., 2013. Tissue macrophage heterogeneity: Issues and prospects. Seminars in immunopathology 35 (5): 533–540. 10.1007/s00281-013-0386-4.

Gordon, S., Taylor, P. R., 2005. Monocyte and macrophage heterogeneity. Nature reviews. Immunology 5 (12): 953–964. 10.1038/nri1733.

Gray, S. G., Baird, A.-M., O'Kelly, F., Nikolaidis, G., Almgren, M., Meunier, A., Dockry, E., Hollywood, D., Ekström, T. J., Perry, A. S., O'Byrne, K. J., 2012. Gemcitabine reactivates epigenetically silenced genes and functions as a DNA methyltransferase inhibitor. International journal of molecular medicine 30 (6): 1505–1511. 10.3892/ijmm.2012.1138.

Groen, R. A. de, Boltjes, A., Hou, J., Liu, B.-S., McPhee, F., Friborg, J., Janssen, H. L. A., Boonstra, A., 2015. IFN-λ-mediated IL-12 production in macrophages induces IFN-γ production in human NK cells. European journal of immunology 45 (1): 250–259. 10.1002/eji.201444903.

Gutierrez-Hartmann, A., Duval, D. L., Bradford, A. P., 2007. ETS transcription factors in endocrine systems. Trends in endocrinology and metabolism: TEM 18 (4): 150–158. 10.1016/j.tem.2007.03.002.

Ha, H., Hwang, I.-A., Park, J. H., Lee, H. B., 2008. Role of reactive oxygen species in the pathogenesis of diabetic nephropathy. Diabetes research and clinical practice 82 Suppl 1: S42-5. 10.1016/j.diabres.2008.09.017.

Hachiya, T., Furukawa, R., Shiwa, Y., Ohmomo, H., Ono, K., Katsuoka, F., Nagasaki, M., Yasuda, J., Fuse, N., Kinoshita, K., Yamamoto, M., Tanno, K., Satoh, M., Endo, R., Sasaki, M., Sakata, K., Kobayashi, S., Ogasawara, K., Hitomi, J., Sobue, K., Shimizu, A., 2017. Genome-wide identification of inter-individually variable DNA methylation sites improves the efficacy of epigenetic association studies. npj Genomic Medicine 2 (1): 529. 10.1038/s41525-017-0016-5.

Hagens, C. von, Walter-Sack, I., Goeckenjan, M., Osburg, J., Storch-Hagenlocher, B., Sertel, S., Elsässer, M., Remppis, B. A., Edler, L., Munzinger, J., Efferth, T., Schneeweiss, A., Strowitzki,

T., 2017. Prospective open uncontrolled phase I study to define a well-tolerated dose of oral artesunate as add-on therapy in patients with metastatic breast cancer (ARTIC M33/2). Breast cancer research and treatment 164 (2): 359‐369. 10.1007/s10549-017-4261-1.

Hampton, M. B., Kettle, A. J., Winterbourn, C. C., 1998. Inside the neutrophil phagosome: Oxidants, myeloperoxidase, and bacterial killing. Blood 92 (9): 3007‐3017.

Hercus, T. R., Thomas, D., Guthridge, M. A., Ekert, P. G., King-Scott, J., Parker, M. W., Lopez, A. F., 2009. The granulocyte-macrophage colony-stimulating factor receptor: Linking its structure to cell signaling and its role in disease. Blood 114 (7): 1289‐1298. 10.1182/blood-2008-12-164004.

Heylmann, D., Bauer, M., Becker, H., Gool, S., Bacher, N., Steinbrink, K., Kaina, B., 2013. Human CD4+CD25+ regulatory T cells are sensitive to low dose cyclophosphamide: Implications for the immune response. PloS one 8 (12): e83384. 10.1371/journal.pone.0083384.

Heylmann, D., Kaina, B., 2016. The γH2AX DNA damage assay from a drop of blood. Scientific Reports 6: 22682. 10.1038/srep22682.

Heylmann, D., Rödel, F., Kindler, T., Kaina, B., 2014. Radiation sensitivity of human and murine peripheral blood lymphocytes, stem and progenitor cells. Biochimica et biophysica acta 1846 (1): 121‐129. 10.1016/j.bbcan.2014.04.009.

Höpker, K., Hagmann, H., Khurshid, S., Chen, S., Schermer, B., Benzing, T., Reinhardt, H. C., 2012. Putting the brakes on p53-driven apoptosis. Cell cycle (Georgetown, Tex.) 11 (22): 4122‐4128. 10.4161/cc.21997.

Hoving, J. C., Wilson, G. J., Brown, G. D., 2014. Signalling C-type lectin receptors, microbial recognition and immunity. Cellular microbiology 16 (2): 185‐194. 10.1111/cmi.12249.

Hsu, J.-L., Huang, S.-Y., Chow, N.-H., Chen, S.-H., 2003. Stable-isotope dimethyl labeling for quantitative proteomics. Analytical chemistry 75 (24): 6843‐6852. 10.1021/ac0348625.

Ichim, G., Tait, S. W. G., 2016. A fate worse than death: Apoptosis as an oncogenic process. Nature reviews. Cancer 16 (8): 539‐548. 10.1038/nrc.2016.58.

Italiani, P., Boraschi, D., 2014. From Monocytes to M1/M2 Macrophages: Phenotypical vs. Functional Differentiation. Frontiers in immunology 5: 514. 10.3389/fimmu.2014.00514.

Ittarat, W., Looareesuwan, S., Pootrakul, P., Sumpunsirikul, P., Vattanavibool, P., Meshnick, S. R., 1998. Effects of alpha-thalassemia on pharmacokinetics of the antimalarial agent artesunate. Antimicrobial agents and chemotherapy 42 (9): 2332‐2335.

Jack, G. D., Zhang, L., Friedman, A. D., 2009. M-CSF elevates c-Fos and phospho-C/EBPalpha(S21) via ERK whereas G-CSF stimulates SHP2 phosphorylation in marrow progenitors to contribute to myeloid lineage specification. Blood 114 (10): 2172‐2180. 10.1182/blood-2008-11-191536.

Jackson, S. H., Gallin, J. I., Holland, S. M., 1995. The p47phox mouse knock-out model of chronic granulomatous disease. The Journal of experimental medicine 182 (3): 751‐758.

Jaguin, M., Houlbert, N., Fardel, O., Lecureur, V., 2013. Polarization profiles of human M-CSF-generated macrophages and comparison of M1-markers in classically activated macrophages from GM-CSF and M-CSF origin. Cellular immunology 281 (1): 51‐61. 10.1016/j.cellimm.2013.01.010.

Jakubzick, C. V., Randolph, G. J., Henson, P. M., 2017. Monocyte differentiation and antigen-presenting functions. Nature reviews. Immunology 17 (6): 349‐362. 10.1038/nri.2017.28.

Janeway, C. A., 2001. Immunobiology 5: The immune system in health and disease / Charles A. Janeway ⋯ [et al.]. New York: Garland; Edinburgh Churchill Livingstone.

John, S., Russell, L., Chin, S. S., Luo, W., Oshima, R., Garrett-Sinha, L. A., 2014. Transcription factor Ets1, but not the closely related factor Ets2, inhibits antibody-secreting cell differentiation. Molecular and cellular biology 34 (3): 522‐532. 10.1128/MCB.00612-13.

Jounai, N., Kobiyama, K., Takeshita, F., Ishii, K. J., 2012. Recognition of damage-associated molecular patterns related to nucleic acids during inflammation and vaccination. Frontiers in cellular and infection microbiology 2: 168. 10.3389/fcimb.2012.00168.

Kaplan, M. J., Radic, M., 2012. Neutrophil extracellular traps: Double-edged swords of innate immunity. Journal of immunology (Baltimore, Md. 1950) 189 (6): 2689–2695. 10.4049/jimmunol.1201719.

Kawai, T., Akira, S., 2007. Signaling to NF-kappaB by Toll-like receptors. Trends in molecular medicine 13 (11): 460–469. 10.1016/j.molmed.2007.09.002.

Kevin Woods, 2016. Expression von BER-Proteinen in Granulozyten. Bachelor Thesis. Mainz.

Kim, S., Yu, N.-K., Kaang, B.-K., 2015. CTCF as a multifunctional protein in genome regulation and gene expression. Experimental & molecular medicine 47: e166. 10.1038/emm.2015.33.

Kim, Y.-J., Wilson, D. M., 2012. Overview of base excision repair biochemistry. Current molecular pharmacology 5 (1): 3–13.

Klayman, D. L., 1985. Qinghaosu (artemisinin): An antimalarial drug from China. Science (New York, N.Y.) 228 (4703): 1049–1055.

Klebanoff, S. J., Kettle, A. J., Rosen, H., Winterbourn, C. C., Nauseef, W. M., 2013. Myeloperoxidase: A front-line defender against phagocytosed microorganisms. Journal of leukocyte biology 93 (2): 185–198. 10.1189/jlb.0712349.

Klug, M., Heinz, S., Gebhard, C., Schwarzfischer, L., Krause, S. W., Andreesen, R., Rehli, M., 2010. Active DNA demethylation in human postmitotic cells correlates with activating histone modifications, but not transcription levels. Genome biology 11 (6): R63. 10.1186/gb-2010-11-6-r63.

Knight, J. A., 2000. Review: Free radicals, antioxidants, and the immune system. Annals of clinical and laboratory science 30 (2): 145–158.

Koh, T. J., DiPietro, L. A., 2011. Inflammation and wound healing: The role of the macrophage. Expert reviews in molecular medicine 13: e23. 10.1017/S1462399411001943.

Kohli, R. M., Zhang, Y., 2013. TET enzymes, TDG and the dynamics of DNA demethylation. Nature 502 (7472): 472–479. 10.1038/nature12750.

Kolaczkowska, E., Kubes, P., 2013. Neutrophil recruitment and function in health and inflammation. Nature reviews. Immunology 13 (3): 159–175. 10.1038/nri3399.

Konig, M. F., Andrade, F., 2016. A Critical Reappraisal of Neutrophil Extracellular Traps and NETosis Mimics Based on Differential Requirements for Protein Citrullination. Frontiers in immunology 7: 461. 10.3389/fimmu.2016.00461.

Korkmaz, B., Horwitz, M. S., Jenne, D. E., Gauthier, F., 2010. Neutrophil elastase, proteinase 3, and cathepsin G as therapeutic targets in human diseases. Pharmacological reviews 62 (4): 726–759. 10.1124/pr.110.002733.

Kumar, V., Abbas, A. K., Aster, J. C., Robbins, S. L., 2013. Robbins basic pathology. Philadelphia PA: Elsevier/Saunders.

Kunkel, T. A., 1999. The high cost of living. American Association for Cancer Research Special Conference: Endogenous sources of mutations, Fort Myers, Florida, USA, 11-15 November 1998. Trends in genetics TIG 15 (3): 93–94.

Kurosawa, A., Shinohara, K.-i., Watanabe, F., Shimizu-Saito, K., Koiwai, O., Yamamoto, K., Teraoka, H., 2003. Human neutrophils isolated from peripheral blood contain Ku protein but not DNA-dependent protein kinase. The international journal of biochemistry & cell biology 35 (1): 86–94.

Kuwabara, W. M. T., Zhang, L., Schuiki, I., Curi, R., Volchuk, A., Alba-Loureiro, T. C., 2015. NADPH oxidase-dependent production of reactive oxygen species induces endoplasmatic reticulum stress in neutrophil-like HL60 cells. PloS one 10 (2): e0116410. 10.1371/journal.pone.0116410.

La Fuente, M. de, Hernanz, A., Vallejo, M. C., 2005. The immune system in the oxidative stress conditions of aging and hypertension: Favorable effects of antioxidants and physical exercise. Antioxidants & redox signaling 7 (9-10): 1356–1366. 10.1089/ars.2005.7.1356.

Lacey, D. C., Achuthan, A., Fleetwood, A. J., Dinh, H., Roiniotis, J., Scholz, G. M., Chang, M. W., Beckman, S. K., Cook, A. D., Hamilton, J. A., 2012. Defining GM-CSF- and macrophage-CSF-dependent macrophage responses by in vitro models. Journal of immunology (Baltimore, Md. 1950) 188 (11): 5752–5765. 10.4049/jimmunol.1103426.

Lakin, N. D., Jackson, S. P., 1999. Regulation of p53 in response to DNA damage. Oncogene 18 (53): 7644‐7655. 10.1038/sj.onc.1203015.

Leist, M., Single, B., Castoldi, A. F., Kühnle, S., Nicotera, P., 1997. Intracellular adenosine triphosphate (ATP) concentration: A switch in the decision between apoptosis and necrosis. The Journal of experimental medicine 185 (8): 1481‐1486.

Lena Schröder, 2017. Artesunate and Curcumin in the hematopoietic system. Master Thesis. Mainz.

Leyns, L., Gonzalez, L., 2012. Genomic Integrity of Mouse Embryonic Stem Cells.

Li, F. X., Zhu, J. W., Hogan, C. J., DeGregori, J., 2003. Defective gene expression, S phase progression, and maturation during hematopoiesis in E2F1/E2F2 mutant mice. Molecular and cellular biology 23 (10): 3607‐3622.

Li, H., Itagaki, K., Sandler, N., Gallo, D., Galenkamp, A., Kaczmarek, E., Livingston, D. H., Zeng, Y., Lee, Y. T., Tang, I. T., Isal, B., Otterbein, L., Hauser, C. J., 2015. Mitochondrial damage-associated molecular patterns from fractures suppress pulmonary immune responses via formyl peptide receptors 1 and 2. The journal of trauma and acute care surgery 78 (2): 272-9; discussion 279-81. 10.1097/TA.0000000000000509.

Li, P. C. H., Lam, E., Roos, W. P., Zdzienicka, M. Z., Kaina, B., Efferth, T., 2008. Artesunate derived from traditional Chinese medicine induces DNA damage and repair. Cancer research 68 (11): 4347‐4351. 10.1158/0008-5472.CAN-07-2970.

Lieber, M. R., 2010. The mechanism of double-strand DNA break repair by the nonhomologous DNA end-joining pathway. Annual review of biochemistry 79: 181‐211. 10.1146/annurev.biochem.052308.093131.

Lina Hallack, 2017. Untersuchung der Wirkung von 2-Hydroxyglutarat und Gemcitabin auf die durch GM-CSF stimulierte Expression von DNA-Reparaturproteinen in Monozyten versus Makrophagen. Bachelor Thesis. Mainz.

Liou, G.-Y., Storz, P., 2010. Reactive oxygen species in cancer. Free radical research 44 (5): 479‐496. 10.3109/10715761003667554.

Lu, Y.-C., Yeh, W.-C., Ohashi, P. S., 2008. LPS/TLR4 signal transduction pathway. Cytokine 42 (2): 145‐151. 10.1016/j.cyto.2008.01.006.

Mahaney, B. L., Meek, K., Lees-Miller, S. P., 2009. Repair of ionizing radiation-induced DNA double-strand breaks by non-homologous end-joining. The Biochemical journal 417 (3): 639‐650. 10.1042/BJ20080413.

Maher, R. J., Cao, D., Boxer, L. A., Petty, H. R., 1993. Simultaneous calcium-dependent delivery of neutrophil lactoferrin and reactive oxygen metabolites to erythrocyte targets: Evidence supporting granule-dependent triggering of superoxide deposition. Journal of cellular physiology 156 (2): 226‐234. 10.1002/jcp.1041560203.

Malu, S., Malshetty, V., Francis, D., Cortes, P., 2012. Role of non-homologous end joining in V(D)J recombination. Immunologic research 54 (1-3): 233‐246. 10.1007/s12026-012-8329-z.

Mangerich, A., Debiak, M., Birtel, M., Ponath, V., Balszuweit, F., Lex, K., Martello, R., Burckhardt-Boer, W., Strobelt, R., Siegert, M., Thiermann, H., Steinritz, D., Schmidt, A., Bürkle, A., 2016. Sulfur and nitrogen mustards induce characteristic poly(ADP-ribosyl)ation responses in HaCaT keratinocytes with distinctive cellular consequences. Toxicology letters 244: 56‐71. 10.1016/j.toxlet.2015.09.010.

Manoharan, S., Guillemin, G. J., Abiramasundari, R. S., Essa, M. M., Akbar, M., Akbar, M. D., 2016. The Role of Reactive Oxygen Species in the Pathogenesis of Alzheimer's Disease, Parkinson's Disease, and Huntington's Disease: A Mini Review. Oxidative medicine and cellular longevity 2016: 8590578. 10.1155/2016/8590578.

Mantegazza, A. R., Magalhaes, J. G., Amigorena, S., Marks, M. S., 2013. Presentation of phagocytosed antigens by MHC class I and II. Traffic (Copenhagen, Denmark) 14 (2): 135‐152. 10.1111/tra.12026.

Manz, M. G., Boettcher, S., 2014. Emergency granulopoiesis. Nature reviews. Immunology 14 (5): 302‐314. 10.1038/nri3660.

Marnett, L. J., 1999. Lipid peroxidation-DNA damage by malondialdehyde. Mutation research 424 (1-2): 83–95.

Masamune, A., Watanabe, T., Kikuta, K., Satoh, K., Shimosegawa, T., 2008. NADPH oxidase plays a crucial role in the activation of pancreatic stellate cells. American journal of physiology. Gastrointestinal and liver physiology 294 (1): G99-G108. 10.1152/ajpgi.00272.2007.

Matsumoto, Y., Kim, K., Bogenhagen, D. F., 1994. Proliferating cell nuclear antigen-dependent abasic site repair in Xenopus laevis oocytes: An alternative pathway of base excision DNA repair. Molecular and cellular biology 14 (9): 6187–6197.

McCracken, J. M., Allen, L.-A. H., 2014. Regulation of human neutrophil apoptosis and lifespan in health and disease. Journal of cell death 7: 15–23. 10.4137/JCD.S11038.

Messner, S., Altmeyer, M., Zhao, H., Pozivil, A., Roschitzki, B., Gehrig, P., Rutishauser, D., Huang, D., Caflisch, A., Hottiger, M. O., 2010. PARP1 ADP-ribosylates lysine residues of the core histone tails. Nucleic acids research 38 (19): 6350–6362. 10.1093/nar/gkq463.

Mestas, J., Hughes, C. C. W., 2004. Of mice and not men: Differences between mouse and human immunology. Journal of immunology (Baltimore, Md. 1950) 172 (5): 2731–2738.

Minicis, S. de, Brenner, D. A., 2007. NOX in liver fibrosis. Archives of biochemistry and biophysics 462 (2): 266–272. 10.1016/j.abb.2007.04.016.

Miriam Pons, 2016. Promoteranalyse und Regulation des DNA-Reparaturproteins XRCC1 in primären Blutzellen und myeloiden Zelllinien. Master Thesis. Mainz.

Mittal, M., Siddiqui, M. R., Tran, K., Reddy, S. P., Malik, A. B., 2014. Reactive oxygen species in inflammation and tissue injury. Antioxidants & redox signaling 20 (7): 1126–1167. 10.1089/ars.2012.5149.

Mladenov, E., Magin, S., Soni, A., Iliakis, G., 2016. DNA double-strand-break repair in higher eukaryotes and its role in genomic instability and cancer: Cell cycle and proliferation-dependent regulation. Seminars in cancer biology 37-38: 51–64. 10.1016/j.semcancer.2016.03.003.

Moloney, J. N., Cotter, T. G., 2017. ROS signalling in the biology of cancer. Seminars in cell & developmental biology. 10.1016/j.semcdb.2017.05.023.

Mortusewicz, O., Amé, J.-C., Schreiber, V., Leonhardt, H., 2007. Feedback-regulated poly(ADP-ribosyl)ation by PARP-1 is required for rapid response to DNA damage in living cells. Nucleic acids research 35 (22): 7665–7675. 10.1093/nar/gkm933.

Naik, E., Dixit, V. M., 2011. Mitochondrial reactive oxygen species drive proinflammatory cytokine production. The Journal of experimental medicine 208 (3): 417–420. 10.1084/jem.20110367.

Narciso, L., Fortini, P., Pajalunga, D., Franchitto, A., Liu, P., Degan, P., Frechet, M., Demple, B., Crescenzi, M., Dogliotti, E., 2007. Terminally differentiated muscle cells are defective in base excision DNA repair and hypersensitive to oxygen injury. Proceedings of the National Academy of Sciences of the United States of America 104 (43): 17010–17015. 10.1073/pnas.0701743104.

Nikolic, T., Movita, D., Lambers, M. E. H., Ribeiro de Almeida, C., Biesta, P., Kreefft, K., Bruijn, M. J. W. de, Bergen, I., Galjart, N., Boonstra, A., Hendriks, R., 2014. The DNA-binding factor Ctcf critically controls gene expression in macrophages. Cellular & molecular immunology 11 (1): 58–70. 10.1038/cmi.2013.41.

O'Donnell, B. V., Tew, D. G., Jones, O. T., England, P. J., 1993. Studies on the inhibitory mechanism of iodonium compounds with special reference to neutrophil NADPH oxidase. The Biochemical journal 290 (Pt 1): 41–49.

Olive, P. L., Banáth, J. P., 2006. The comet assay: A method to measure DNA damage in individual cells. Nature protocols 1 (1): 23–29. 10.1038/nprot.2006.5.

Otteneder, M. B., Knutson, C. G., Daniels, J. S., Hashim, M., Crews, B. C., Remmel, R. P., Wang, H., Rizzo, C., Marnett, L. J., 2006. In vivo oxidative metabolism of a major peroxidation-derived DNA adduct, M1dG. Proceedings of the National Academy of Sciences of the United States of America 103 (17): 6665–6669. 10.1073/pnas.0602017103.

Paiva, C. N., Bozza, M. T., 2014. Are reactive oxygen species always detrimental to pathogens? Antioxidants & redox signaling 20 (6): 1000–1037. 10.1089/ars.2013.5447.

Palucka, K., Banchereau, J., 2012. Cancer immunotherapy via dendritic cells. Nature reviews. Cancer 12 (4): 265‑277. 10.1038/nrc3258.

Papayannopoulos, V., Zychlinsky, A., 2009. NETs: A new strategy for using old weapons. Trends in immunology 30 (11): 513‑521. 10.1016/j.it.2009.07.011.

Parihar, A., Eubank, T. D., Doseff, A. I., 2010. Monocytes and macrophages regulate immunity through dynamic networks of survival and cell death. Journal of innate immunity 2 (3): 204‑215. 10.1159/000296507.

Perlow-Poehnelt, R. A., Zharkov, D. O., Grollman, A. P., Broyde, S., 2004. Substrate discrimination by formamidopyrimidine-DNA glycosylase: Distinguishing interactions within the active site. Biochemistry 43 (51): 16092‑16105. 10.1021/bi048747f.

Perugini, M., Brown, A. L., Salerno, D. G., Booker, G. W., Stojkoski, C., Hercus, T. R., Lopez, A. F., Hibbs, M. L., Gonda, T. J., D'Andrea, R. J., 2010. Alternative modes of GM-CSF receptor activation revealed using activated mutants of the common beta-subunit. Blood 115 (16): 3346‑3353. 10.1182/blood-2009-08-235846.

Petermann, E., Keil, C., Oei, S. L., 2006. Roles of DNA ligase III and XRCC1 in regulating the switch between short patch and long patch BER. DNA repair 5 (5): 544‑555. 10.1016/j.dnarep.2005.12.008.

Pfeiffer, Z. A., Guerra, A. N., Hill, L. M., Gavala, M. L., Prabhu, U., Aga, M., Hall, D. J., Bertics, P. J., 2007. Nucleotide receptor signaling in murine macrophages is linked to reactive oxygen species generation. Free radical biology & medicine 42 (10): 1506‑1516. 10.1016/j.freeradbiomed.2007.02.010.

Pham, C. T. N., 2006. Neutrophil serine proteases: Specific regulators of inflammation. Nature reviews. Immunology 6 (7): 541‑550. 10.1038/nri1841.

Piechaczyk, M., Farràs, R., 2008. Regulation and function of JunB in cell proliferation. Biochemical Society transactions 36 (Pt 5): 864‑867. 10.1042/BST0360864.

Pillay, J., den Braber, I., Vrisekoop, N., Kwast, L. M., Boer, R. J. de, Borghans, J. A. M., Tesselaar, K., Koenderman, L., 2010. In vivo labeling with 2H2O reveals a human neutrophil lifespan of 5.4 days. Blood 116 (4): 625‑627. 10.1182/blood-2010-01-259028.

Prasad, R., Dianov, G. L., Bohr, V. A., Wilson, S. H., 2000. FEN1 stimulation of DNA polymerase beta mediates an excision step in mammalian long patch base excision repair. The Journal of biological chemistry 275 (6): 4460‑4466.

Prasad, R., Lavrik, O. I., Kim, S. J., Kedar, P., Yang, X. P., Vande Berg, B. J., Wilson, S. H., 2001. DNA polymerase beta -mediated long patch base excision repair. Poly(ADP-ribose)polymerase-1 stimulates strand displacement DNA synthesis. The Journal of biological chemistry 276 (35): 32411‑32414. 10.1074/jbc.C100292200.

Puca, R., Nardinocchi, L., Givol, D., D'Orazi, G., 2010. Regulation of p53 activity by HIPK2: Molecular mechanisms and therapeutical implications in human cancer cells. Oncogene 29 (31): 4378‑4387. 10.1038/onc.2010.183.

Raad, H., Paclet, M.-H., Boussetta, T., Kroviarski, Y., Morel, F., Quinn, M. T., Gougerot-Pocidalo, M.-A., Dang, P. M.-C., El-Benna, J., 2009. Regulation of the phagocyte NADPH oxidase activity: Phosphorylation of gp91phox/NOX2 by protein kinase C enhances its diaphorase activity and binding to Rac2, p67phox, and p47phox. FASEB journal official publication of the Federation of American Societies for Experimental Biology 23 (4): 1011‑1022. 10.1096/fj.08-114553.

Ramji, D. P., Foka, P., 2002. CCAAT/enhancer-binding proteins: Structure, function and regulation. The Biochemical journal 365 (Pt 3): 561‑575. 10.1042/bj20020508.

Reuter, C. W., Morgan, M. A., Bergmann, L., 2000. Targeting the Ras signaling pathway: A rational, mechanism-based treatment for hematologic malignancies? Blood 96 (5): 1655‑1669.

Reuter, S., Gupta, S. C., Chaturvedi, M. M., Aggarwal, B. B., 2010. Oxidative stress, inflammation, and cancer: How are they linked? Free radical biology & medicine 49 (11): 1603‑1616. 10.1016/j.freeradbiomed.2010.09.006.

Riley, P. A., 1994. Free radicals in biology: Oxidative stress and the effects of ionizing radiation. International journal of radiation biology 65 (1): 27‐33.

Rink, L., Kruse, A., Haase, H., 2015. Immunologie für Einsteiger. Berlin: Springer Berlin.

Robb, L., 2007. Cytokine receptors and hematopoietic differentiation. Oncogene 26 (47): 6715‐6723. 10.1038/sj.onc.1210756.

Rödel, F., Frey, B., Gaipl, U., Keilholz, L., Fournier, C., Manda, K., Schöllnberger, H., Hildebrandt, G., Rödel, C., 2012. Modulation of inflammatory immune reactions by low-dose ionizing radiation: Molecular mechanisms and clinical application. Current medicinal chemistry 19 (12): 1741‐1750.

Roos, W. P., Krumm, A., 2016. The multifaceted influence of histone deacetylases on DNA damage signalling and DNA repair. Nucleic acids research 44 (21): 10017‐10030. 10.1093/nar/gkw922.

Roos, W. P., Thomas, A. D., Kaina, B., 2016. DNA damage and the balance between survival and death in cancer biology. Nature reviews. Cancer 16 (1): 20‐33. 10.1038/nrc.2015.2.

Roy, J., Galano, J.-M., Durand, T., Le Guennec, J.-Y., Lee, J. C.-Y., 2017. Physiological role of reactive oxygen species as promoters of natural defenses. FASEB journal official publication of the Federation of American Societies for Experimental Biology. 10.1096/fj.201700170R.

Schäfer, A., Schomacher, L., Barreto, G., Döderlein, G., Niehrs, C., 2010. Gemcitabine functions epigenetically by inhibiting repair mediated DNA demethylation. PloS one 5 (11): e14060. 10.1371/journal.pone.0014060.

Schatz, D. G., Swanson, P. C., 2011. V(D)J recombination: Mechanisms of initiation. Annual review of genetics 45: 167‐202. 10.1146/annurev-genet-110410-132552.

Schneemann, M., Schoedon, G., 2002. Species differences in macrophage NO production are important. Nature immunology 3 (2): 102. 10.1038/ni0202-102a.

Schrader, M., Fahimi, H. D., 2006. Peroxisomes and oxidative stress. Biochimica et biophysica acta 1763 (12): 1755‐1766. 10.1016/j.bbamcr.2006.09.006.

Seddon, M., Looi, Y. H., Shah, A. M., 2007. Oxidative stress and redox signalling in cardiac hypertrophy and heart failure. Heart (British Cardiac Society) 93 (8): 903‐907. 10.1136/hrt.2005.068270.

Sedeek, M., Callera, G., Montezano, A., Gutsol, A., Heitz, F., Szyndralewiez, C., Page, P., Kennedy, C. R. J., Burns, K. D., Touyz, R. M., Hébert, R. L., 2010. Critical role of Nox4-based NADPH oxidase in glucose-induced oxidative stress in the kidney: Implications in type 2 diabetic nephropathy. American journal of physiology. Renal physiology 299 (6): F1348-58. 10.1152/ajprenal.00028.2010.

Segal, A. W., 2005. How neutrophils kill microbes. Annual review of immunology 23: 197‐223. 10.1146/annurev.immunol.23.021704.115653.

Shi, C., Pamer, E. G., 2011. Monocyte recruitment during infection and inflammation. Nature reviews. Immunology 11 (11): 762‐774. 10.1038/nri3070.

Simon, S. I., Kim, M.-H., 2010. A day (or 5) in a neutrophil's life. Blood 116 (4): 511‐512. 10.1182/blood-2010-05-283184.

Singh, U., Jialal, I., 2006. Oxidative stress and atherosclerosis. Pathophysiology the official journal of the International Society for Pathophysiology 13 (3): 129‐142. 10.1016/j.pathophys.2006.05.002.

Smith, C. C., O'Donovan, M. R., Martin, E. A., 2006. hOGG1 recognizes oxidative damage using the comet assay with greater specificity than FPG or ENDOIII. Mutagenesis 21 (3): 185‐190. 10.1093/mutage/gel019.

Smith, G. C., Jackson, S. P., 1999. The DNA-dependent protein kinase. Genes & development 13 (8): 916‐934.

Smith, J. J., Aitchison, J. D., 2013. Peroxisomes take shape. Nature reviews. Molecular cell biology 14 (12): 803‐817. 10.1038/nrm3700.

Sterpone, S., Cozzi, R., 2010. Influence of XRCC1 Genetic Polymorphisms on Ionizing Radiation-Induced DNA Damage and Repair. Journal of nucleic acids 2010. 10.4061/2010/780369.

Summers, C., Rankin, S. M., Condliffe, A. M., Singh, N., Peters, A. M., Chilvers, E. R., 2010. Neutrophil kinetics in health and disease. Trends in immunology 31 (8): 318‐324. 10.1016/j.it.2010.05.006.

Switzeny, O. J., Christmann, M., Renovanz, M., Giese, A., Sommer, C., Kaina, B., 2016. MGMT promoter methylation determined by HRM in comparison to MSP and pyrosequencing for predicting high-grade glioma response. Clinical epigenetics 8: 49. 10.1186/s13148-016-0204-7.

Takahashi, T., Tada, M., Igarashi, S., Koyama, A., Date, H., Yokoseki, A., Shiga, A., Yoshida, Y., Tsuji, S., Nishizawa, M., Onodera, O., 2007. Aprataxin, causative gene product for EAOH/AOA1, repairs DNA single-strand breaks with damaged 3'-phosphate and 3'-phosphoglycolate ends. Nucleic acids research 35 (11): 3797‐3809. 10.1093/nar/gkm158.

Tebbs, R. S., Thompson, L. H., Cleaver, J. E., 2003. Rescue of Xrcc1 knockout mouse embryo lethality by transgene-complementation. DNA repair 2 (12): 1405‐1417.

Tobias Haak, 2015. Untersuchung der Induktion von DNA-Schäden durch ionisierende Strahlung in menschlichen Blutzellen, insbesondere in Granulozyten. Master Thesis. Mainz.

Twomey, P. S., Smith, B. L., McDermott, C., Novitt-Moreno, A., McCarthy, W., Kachur, S. P., Arguin, P. M., 2015. Intravenous Artesunate for the Treatment of Severe and Complicated Malaria in the United States: Clinical Use Under an Investigational New Drug Protocol. Annals of internal medicine 163 (7): 498‐506. 10.7326/M15-0910.

Unnikrishnan, A., Guan, Y. F., Huang, Y., Beck, D., Thoms, J. A. I., Peirs, S., Knezevic, K., Ma, S., Walle, I. V. de, Jong, I. de, Ali, Z., Zhong, L., Raftery, M. J., Taghon, T., Larsson, J., MacKenzie, K. L., Vlierberghe, P., Wong, J. W. H., van Pimanda, J. E., 2016. A quantitative proteomics approach identifies ETV6 and IKZF1 as new regulators of an ERG-driven transcriptional network. Nucleic acids research 44 (22): 10644‐10661. 10.1093/nar/gkw804.

Ushach, I., Zlotnik, A., 2016. Biological role of granulocyte macrophage colony-stimulating factor (GM-CSF) and macrophage colony-stimulating factor (M-CSF) on cells of the myeloid lineage. Journal of leukocyte biology 100 (3): 481‐489. 10.1189/jlb.3RU0316-144R.

van de Laar, L., Coffer, P. J., Woltman, A. M., 2012. Regulation of dendritic cell development by GM-CSF: Molecular control and implications for immune homeostasis and therapy. Blood 119 (15): 3383‐3393. 10.1182/blood-2011-11-370130.

van Grevenynghe, J., Rion, S., Le Ferrec, E., Le Vee, M., Amiot, L., Fauchet, R., Fardel, O., 2003. Polycyclic aromatic hydrocarbons inhibit differentiation of human monocytes into macrophages. Journal of immunology (Baltimore, Md. 1950) 170 (5): 2374‐2381.

van Oevelen, C., Collombet, S., Vicent, G., Hoogenkamp, M., Lepoivre, C., Badeaux, A., Bussmann, L., Sardina, J. L., Thieffry, D., Beato, M., Shi, Y., Bonifer, C., Graf, T., 2015. C/EBP α Activates Pre-existing and De Novo Macrophage Enhancers during Induced Pre-B Cell Transdifferentiation and Myelopoiesis. Stem cell reports 5 (2): 232‐247. 10.1016/j.stemcr.2015.06.007.

Vignali, D. A., Doyle, C., Kinch, M. S., Shin, J., Strominger, J. L., 1993. Interactions of CD4 with MHC class II molecules, T cell receptors and p56lck. Philosophical transactions of the Royal Society of London. Series B, Biological sciences 342 (1299): 13‐24. 10.1098/rstb.1993.0130.

Wagner, E. F., Matsuo, K., 2003. Signalling in osteoclasts and the role of Fos/AP1 proteins. Annals of the rheumatic diseases 62 Suppl 2: ii83-5.

Wallner, S., Schröder, C., Leitão, E., Berulava, T., Haak, C., Beißer, D., Rahmann, S., Richter, A. S., Manke, T., Bönisch, U., Arrigoni, L., Fröhler, S., Klironomos, F., Chen, W., Rajewsky, N., Müller, F., Ebert, P., Lengauer, T., Barann, M., Rosenstiel, P., Gasparoni, G., Nordström, K., Walter, J., Brors, B., Zipprich, G., Felder, B., Klein-Hitpass, L., Attenberger, C., Schmitz, G., Horsthemke, B., 2016. Epigenetic dynamics of monocyte-to-macrophage differentiation. Epigenetics & chromatin 9: 33. 10.1186/s13072-016-0079-z.

Wang, C., Ivanov, A., Chen, L., Fredericks, W. J., Seto, E., Rauscher, F. J., Chen, J., 2005. MDM2 interaction with nuclear corepressor KAP1 contributes to p53 inactivation. The EMBO journal 24 (18): 3279‐3290. 10.1038/sj.emboj.7600791.

Wang, D., Malo, D., Hekimi, S., 2010a. Elevated mitochondrial reactive oxygen species generation affects the immune response via hypoxia-inducible factor-1alpha in long-lived Mclk1+/- mouse

mutants. Journal of immunology (Baltimore, Md. 1950) 184 (2): 582–590. 10.4049/jimmunol.0902352.

Wang, P., Tang, J. T., Peng, Y. S., Chen, X. Y., Zhang, Y. J., Fang, J. Y., 2010b. XRCC1 downregulated through promoter hypermethylation is involved in human gastric carcinogenesis. Journal of digestive diseases 11 (6): 343–351. 10.1111/j.1751-2980.2010.00459.x.

Weidele, K., Beneke, S., Bürkle, A., 2017. The NAD(+) precursor nicotinic acid improves genomic integrity in human peripheral blood mononuclear cells after X-irradiation. DNA repair 52: 12–23. 10.1016/j.dnarep.2017.02.001.

Weidele, K., Kunzmann, A., Schmitz, M., Beneke, S., Bürkle, A., 2010. Ex vivo supplementation with nicotinic acid enhances cellular poly(ADP-ribosyl)ation and improves cell viability in human peripheral blood mononuclear cells. Biochemical pharmacology 80 (7): 1103–1112. 10.1016/j.bcp.2010.06.010.

Weinlich, R., Oberst, A., Beere, H. M., Green, D. R., 2017. Necroptosis in development, inflammation and disease. Nature reviews. Molecular cell biology 18 (2): 127–136. 10.1038/nrm.2016.149.

White, D., Rafalska-Metcalf, I. U., Ivanov, A. V., Corsinotti, A., Peng, H., Lee, S.-C., Trono, D., Janicki, S. M., Rauscher, F. J., 2012. The ATM substrate KAP1 controls DNA repair in heterochromatin: Regulation by HP1 proteins and serine 473/824 phosphorylation. Molecular cancer research MCR 10 (3): 401–414. 10.1158/1541-7786.MCR-11-0134.

Whitehouse, C. J., Taylor, R. M., Thistlethwaite, A., Zhang, H., Karimi-Busheri, F., Lasko, D. D., Weinfeld, M., Caldecott, K. W., 2001. XRCC1 stimulates human polynucleotide kinase activity at damaged DNA termini and accelerates DNA single-strand break repair. Cell 104 (1): 107–117.

Wind, S., Beuerlein, K., Eucker, T., Müller, H., Scheurer, P., Armitage, M. E., Ho, H., Schmidt, H. H. H. W., Wingler, K., 2010. Comparative pharmacology of chemically distinct NADPH oxidase inhibitors. British journal of pharmacology 161 (4): 885–898. 10.1111/j.1476-5381.2010.00920.x.

Winter, M., Sombroek, D., Dauth, I., Moehlenbrink, J., Scheuermann, K., Crone, J., Hofmann, T. G., 2008. Control of HIPK2 stability by ubiquitin ligase Siah-1 and checkpoint kinases ATM and ATR. Nature cell biology 10 (7): 812–824. 10.1038/ncb1743.

Wu, X., Zhang, Y., 2017. TET-mediated active DNA demethylation: Mechanism, function and beyond. Nature reviews. Genetics 18 (9): 517–534. 10.1038/nrg.2017.33.

Xu, W., Yang, H., Liu, Y., Yang, Y., Wang, P., Kim, S.-H., Ito, S., Yang, C., Wang, P., Xiao, M.-T., Liu, L.-x., Jiang, W.-q., Liu, J., Zhang, J.-y., Wang, B., Frye, S., Zhang, Y., Xu, Y.-h., Lei, Q.-y., Guan, K.-L., Zhao, S.-m., Xiong, Y., 2011. Oncometabolite 2-hydroxyglutarate is a competitive inhibitor of α-ketoglutarate-dependent dioxygenases. Cancer cell 19 (1): 17–30. 10.1016/j.ccr.2010.12.014.

Xue, J., Schmidt, S. V., Sander, J., Draffehn, A., Krebs, W., Quester, I., Nardo, D. de, Gohel, T. D., Emde, M., Schmidleithner, L., Ganesan, H., Nino-Castro, A., Mallmann, M. R., Labzin, L., Theis, H., Kraut, M., Beyer, M., Latz, E., Freeman, T. C., Ulas, T., Schultze, J. L., 2014. Transcriptome-based network analysis reveals a spectrum model of human macrophage activation. Immunity 40 (2): 274–288. 10.1016/j.immuni.2014.01.006.

Yan, Z.-q., 2006. Regulation of TLR4 expression is a tale about tail. Arteriosclerosis, thrombosis, and vascular biology 26 (12): 2582–2584. 10.1161/01.ATV.0000250933.92917.dd.

Zola, H., Swart, B., Banham, A., Barry, S., Beare, A., Bensussan, A., Boumsell, L., D Buckley, C., Bühring, H.-J., Clark, G., Engel, P., Fox, D., Jin, B.-Q., Macardle, P. J., Malavasi, F., Mason, D., Stockinger, H., Yang, X., 2007. CD molecules 2006--human cell differentiation molecules. Journal of immunological methods 319 (1-2): 1–5. 10.1016/j.jim.2006.11.001.

Cited scientific theses generated at the Institute of Toxicology at the University Medical Center Mainz:

Kevin Woods, 2016, Expression von BER-Proteinen in Granulozyten, Bachelor Thesis

Lina Hallack, 2017, Untersuchung der Wirkung von 2-Hydroxyglutarat und Gemcitabin auf die durch GM-CSF stimulierte Expression von DNA-Reparaturproteinen in Monozyten vs Makrophagen, Bachelor Thesis

Tobias Haak, 2015, Untersuchung der Induktion von DNA-Schäden durch ionisierende Strahlung in menschlichen Blutzellen, insbesondere in Granulozyten, Master Thesis

Miriam Pons, 2016, Promoteranalyse und Regulation des DNA-Reparaturproteins XRCC1 in primären Blutzellen und myeloiden Zelllinien, Master Thesis

Lena Schröder, 2017, Die genotoxische Wirkung von Artesunat und Kurkumin auf Zellen des hämato-poetischen Systems (running title), Master Thesis

Daniel Heylmann, 2017, Sensitivität humaner Immunzellen gegenüber ionisierender Strahlung und anderen genotoxischen Noxen, Dissertation

7 Supplements

7.1 Isolation of granulocytes from buffy coats

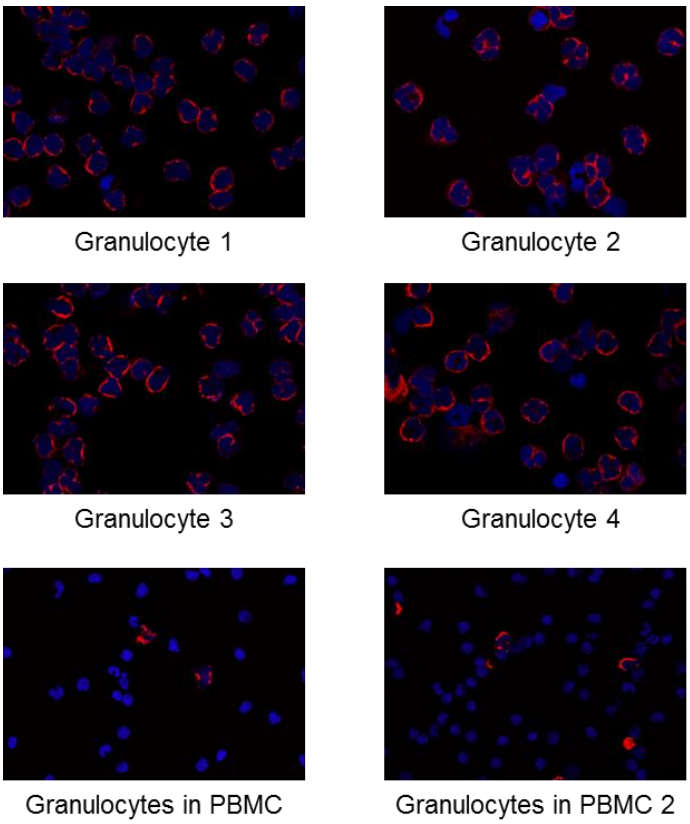

Fig. S1: Immunofluorescence staining of CD15+ granulocytes after isolation from buffy coats *Granulocytes were isolated from four different buffy coats (Granulocyte fractions 1 to 4) using the Optiprep density method and were stained for CD15+ marker expression (red ring). CD15+ cells were enriched compared to the amount of granulocytes in the PBMC fraction isolated by Ficoll gradient centrifugation. Immunofluorescence staining was kindly performed by ..... under supervision.*

7.2 Artesunate-induced DNA damage and cell death in immune cells after 24 h

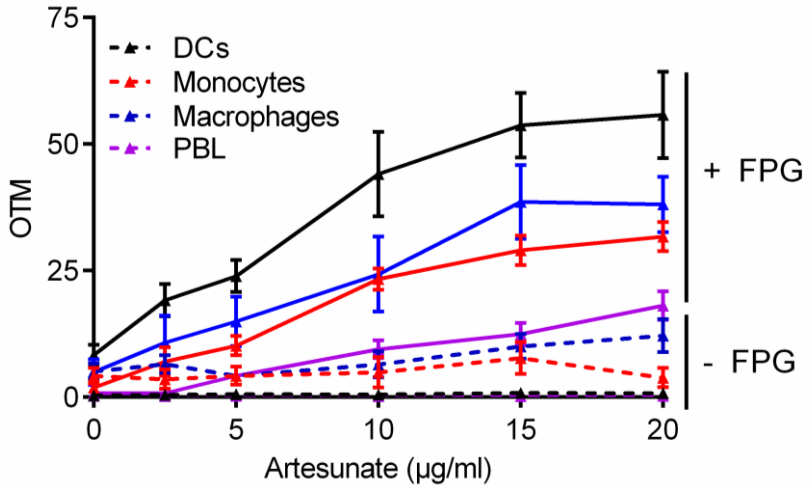

Fig. S2: FPG-modified alkaline Comet assay of ART-treated immune cells (low concentrations)

Supplemented OTM data for figureFig. 14. Cells were treated with low concentrations of ART (2.5 – 20 µg/ml) for 24 h before oxidative DNA damage was assessed. In the absence of FPG, SSBs were detected (chequered lines). In the presence of FPG oxidative DNA lesions were converted into SSBs. Data are the mean of three to five independent experiment ± SEM. For each experiment at 50 - 100 cells per samples were analysed.

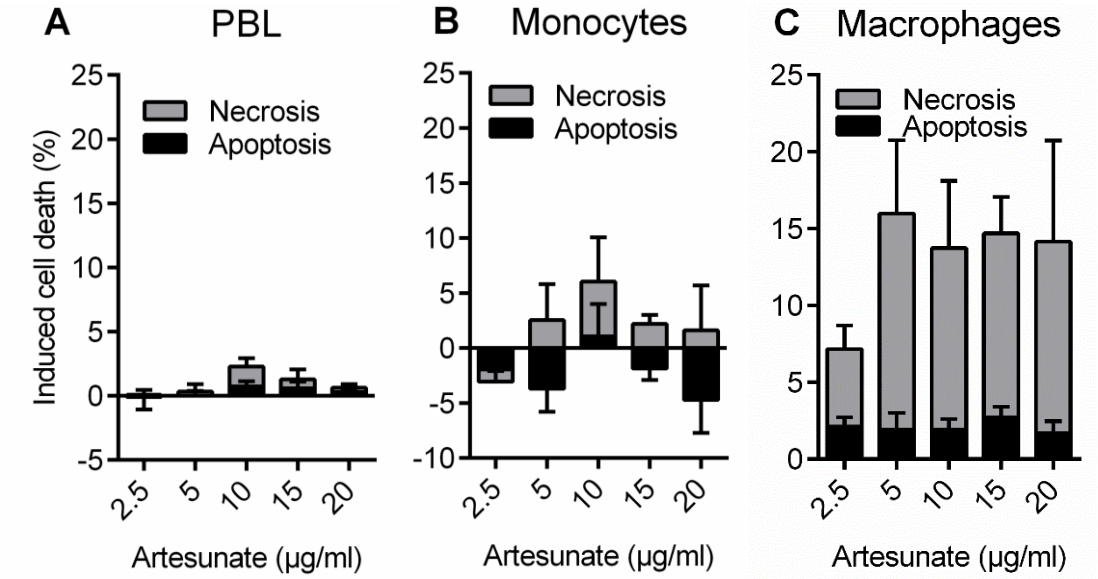

Fig. S3: Cell death of immune cells after 24 h ART treatment (low concentrations)
Induced cell death was measured with Annexin V / PI. PBL and monocytes showed no induction of cell death. Macrophages displayed ~15 % necrotic cell death at 5-20 µg/ml ART. Data are the mean of two to six independent experiments ± SEM. Some experiments were kindly performed by ..... under supervision.

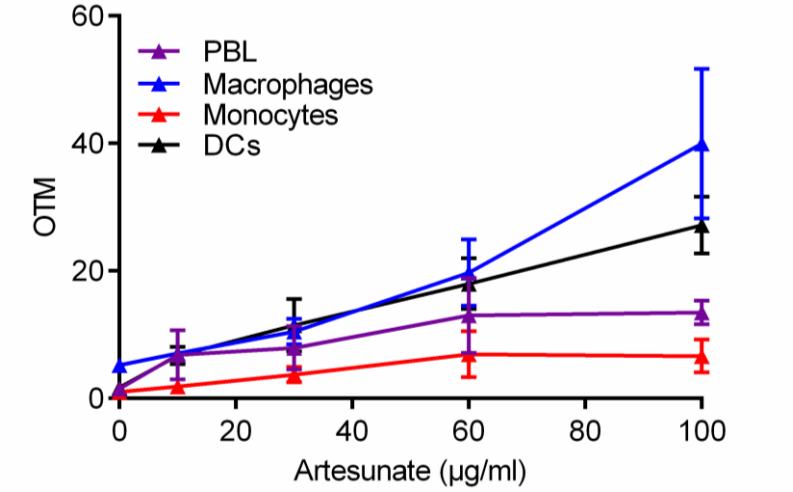

Fig. S4: Alkaline Comet assay of ART-treated immune cells (high concentrations)
Supplemented OTM data for Fig. 16. Cells were treated with 10-100 µg/ml ART for 24 h. DNA damage was assessed using the alkaline Comet assay. Data are the mean of three to five independent experiment ± SEM. Some experiments were kindly performed by ..... under supervision.

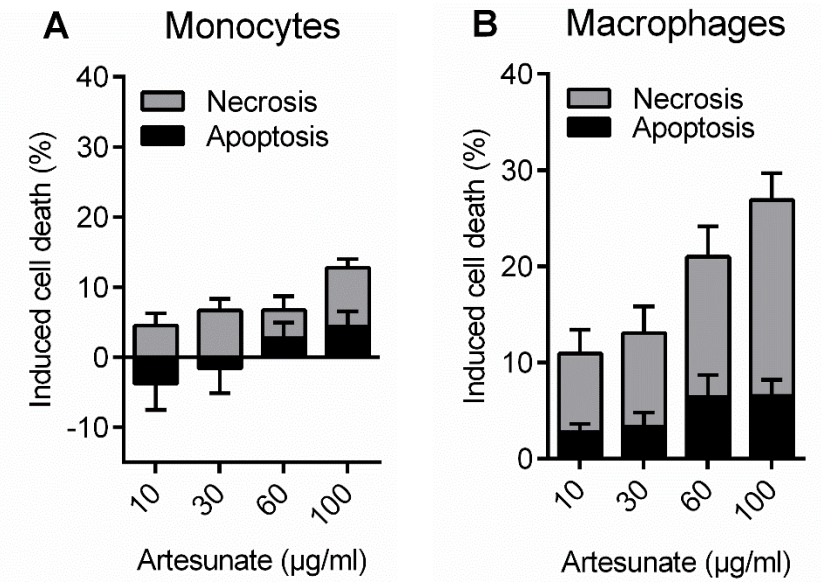

Fig. S5: Cell death of immune cells after 24 h ART treatment (high concentrations)
Induced cell death was measured with Annexin V / PI. Monocytes showed a slight increase in cell death at 100 µg/ml ART. Macrophages displayed a concentration-dependent increase in necrosis from 10 % at 10 µg/ml ART to ~25 % at 100 µg/ml ART. Data are the mean of four to eight independent experiments ± SEM. Some experiments were kindly performed by ..... under supervision.

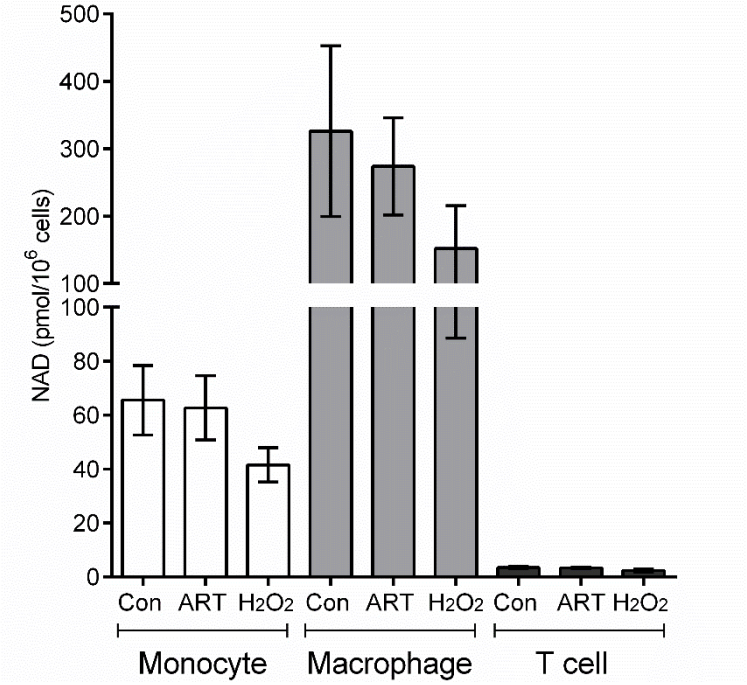

Fig. S6: Intracellular NAD^+ content in immune cells after artesunate treatment
Monocytes, macrophages and PBL were treated with 30 µg/ml ART for 24 h or 1 mM H_2O_2 for 5 min. Cells were harvested and subjected to the NAD^+ cycling assay. Data are the mean of five independent experiments ± SEM. The experiments were kindly performed by ..... under supervision.

7.3 Oxidative DNA damage and apoptosis in phagocytes

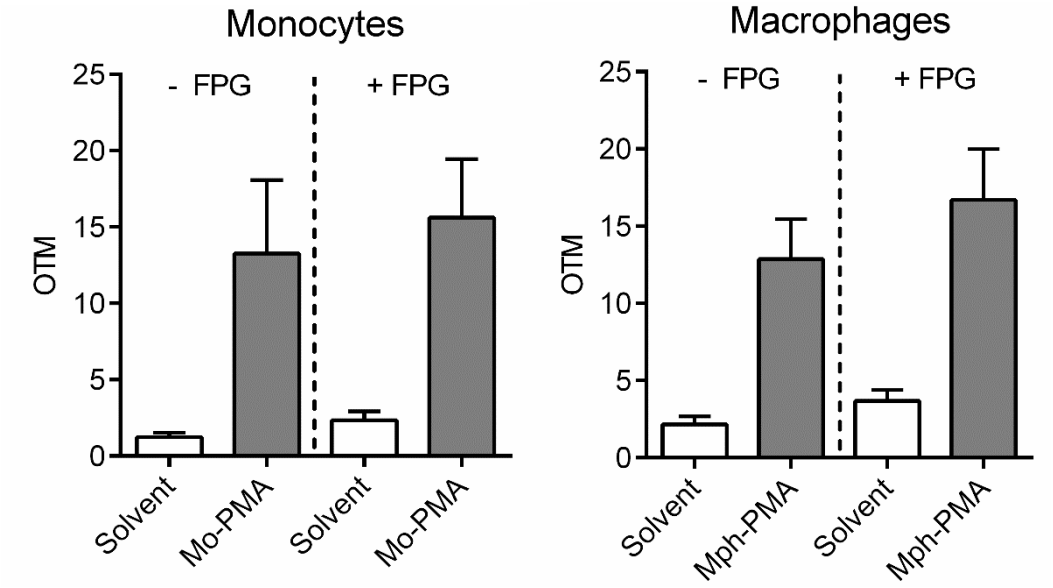

Fig. S7: FPG-modified alkaline Comet assay
Supplemented OTM data for Fig. 27. Cells were treated with PMA for 15 min (Mono-PMA and Mph-PMA) and were then incubated in PMA-free medium for 45 min. Initial DNA damage was assessed using the FPG-modified Comet assay. Without FPG, SSBs were measured. In the presence of FPG oxidative DNA lesions were converted to SSBs. Data are the mean of four-five independent experiments ± SEM

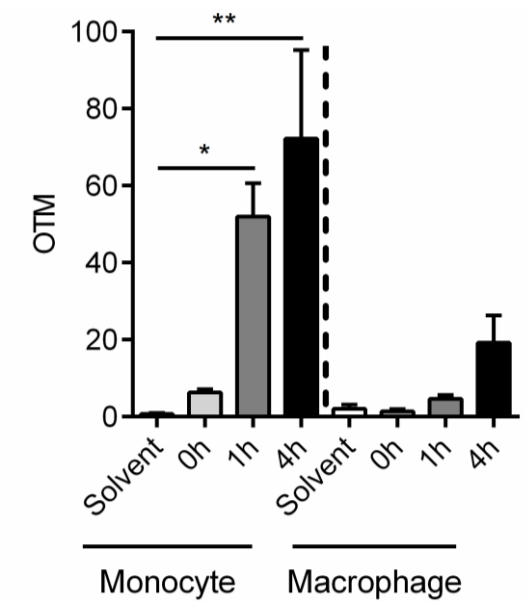

Fig. S8: Alkaline Comet assay
*Supplemented OTM data for Fig. 28. Cells were pulse-treated with PMA for 15 min to stimulate ROS production and then incubated for up to 4 h in fresh medium. SSB formation was measured in monocytes and macrophages over a period of 4 h. Data are the mean of at least three independent experiments ± SEM, 1-way ANOVA, Tukey's Multiple Comparison Test, *p < 0.05, **p < 0.01*

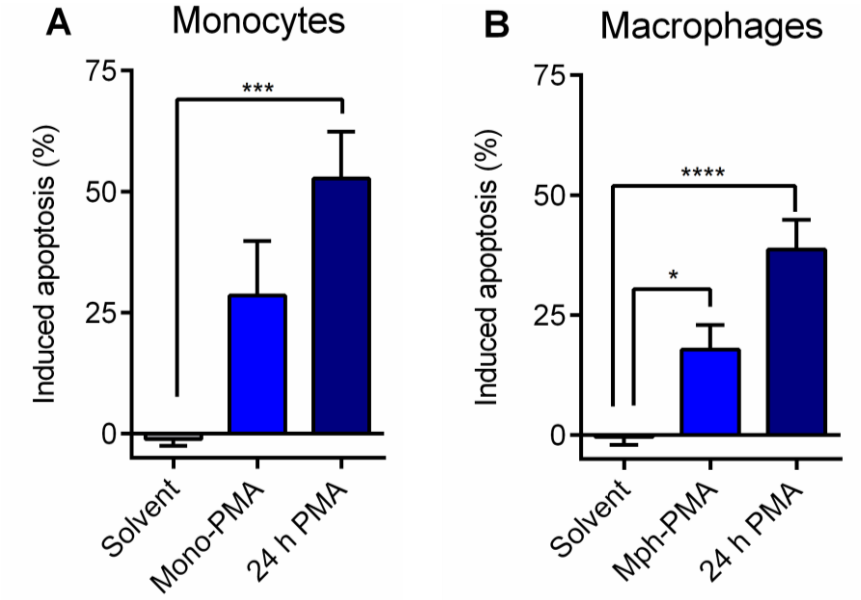

Fig. S9: Cell death of monocytes and macrophages after a ROS burst from PMA treatment
*Cells were either pulse-activated with 100 ng/ml PMA for 15 min (Mono-PMA and Mph-PMA) or continuously exposed to PMA for 24 h. Cell death of A) monocytes and B) macrophages was measured after 24 h using Annexin V. Data are the mean of three to nine independent experiments ± SEM, 1-way ANOVA, Tukey's Multiple Comparison Test, *p < 0.05, ***p < 0.001, ****p < 0.0001*

7.4 Co-culture of ROS-producing cells and non-stimulated cells

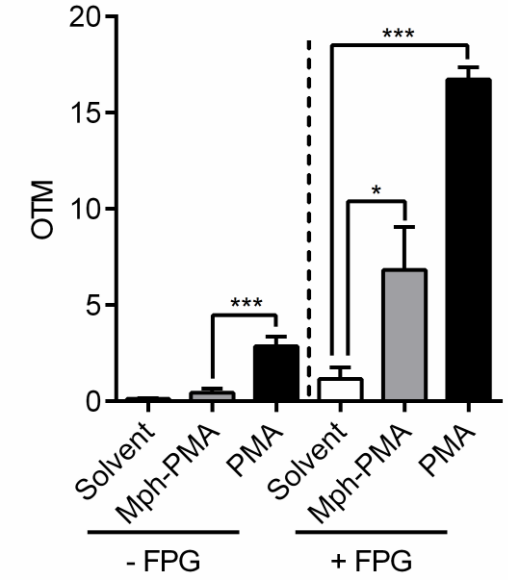

Fig. S10: FPG-modified alkaline Comet assay
*Supplemented OTM data for Fig. 31. Monocytes were co-cultured with PMA-activated macrophages for 45 min. Monocytes were harvested and subjected to the FPG-modified alkaline Comet assay to assess the SSB (-FPG) and oxidative DNA damage (+FPG). Data are the mean of four independent experiments ± SEM, 1-way ANOVA, Dunnett's Multiple Comparison Test, *p < 0.05, ***p < 0.001*

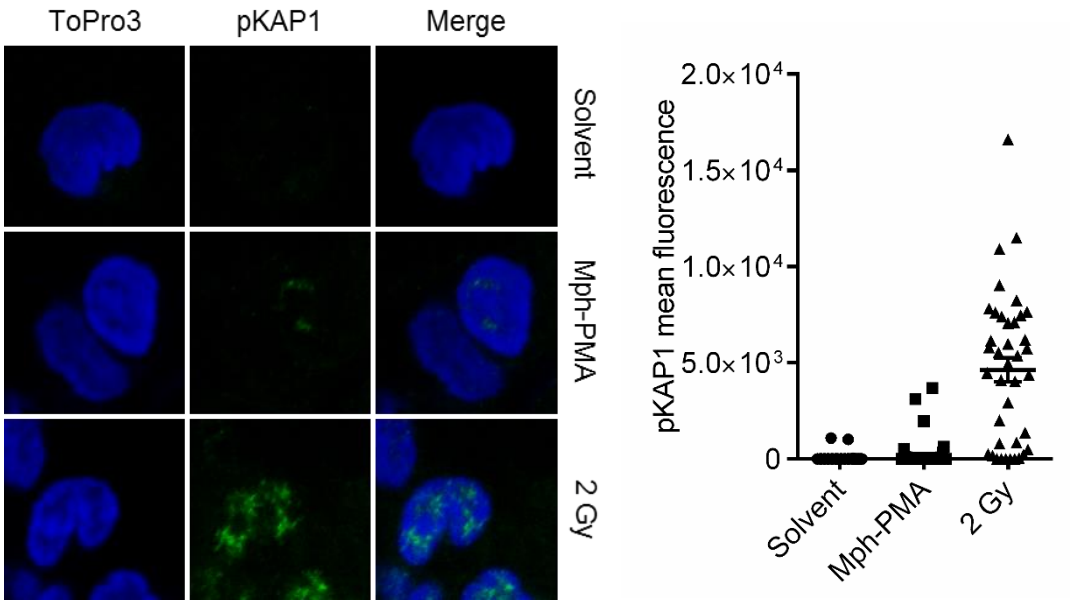

Fig. S11: DDR factor pKAP1 in co-cultured monocytes
Supplemented data for Fig. 32. Monocytes were co-cultured with PMA-activated (Mph-PMA) or solvent-treated macrophages (Mph-Solvent) for 24 h. As a positive control monocytes were irradiated with 2 Gy and incubated for 1 h. Monocytes were harvested and the DDR factor pKAP1 was detected via immunofluorescence staining. The mean fluorescence signal intensity of pKAP1 was quantified (right graph).

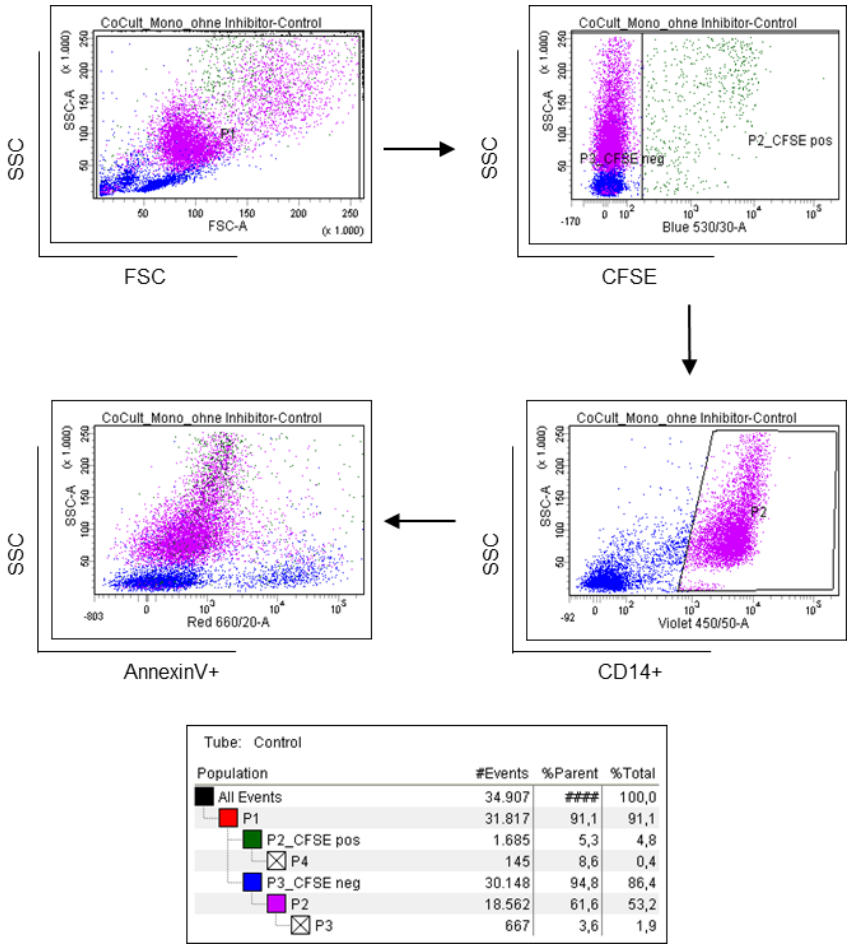

Tube: Control

Population	#Events	%Parent	%Total
All Events	34.907	####	100,0
P1	31.817	91,1	91,1
P2_CFSE pos	1.685	5,3	4,8
P4	145	8,6	0,4
P3_CFSE neg	30.148	94,8	86,4
P2	18.562	61,6	53,2
P3	667	3,6	1,9

Fig. S12. Gating strategy for co-cultured monocytes

Prior to the start of the co-culture experiment, macrophages were stained with 5 µM CFSE. Monocytes were gated by excluding CFSE+ cells (channel: Blue 530/30) and by including CD14+ cells (channel: Violet 450/50). Apoptotic cells were Annexin V+ in the Red 660/20 channel.

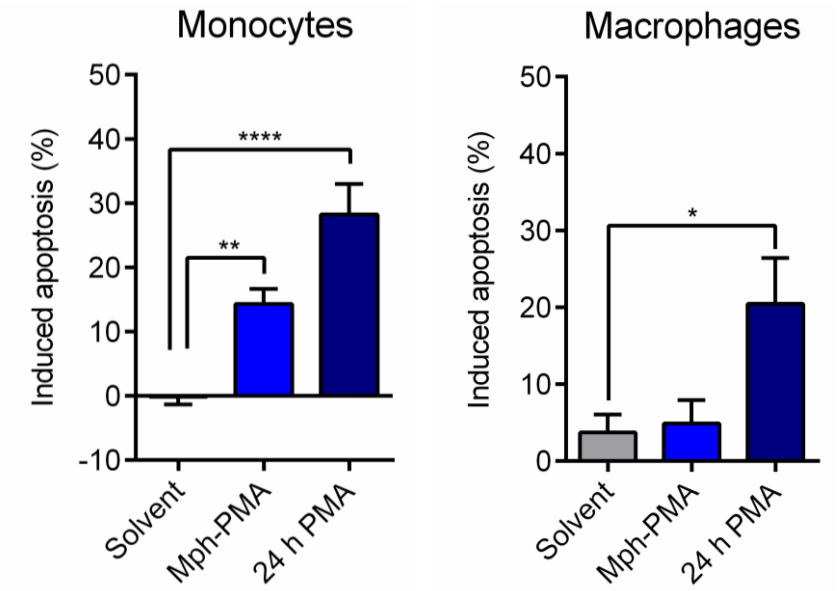

Fig. S13: Cell death of monocytes in co-culture with activated macrophages after 24 h
*Macrophages were pulse-activated with PMA for 15 min (Mph-PMA), washed with PBS and supplemented with fresh medium before monocytes were added. Alternatively, co-cultured cells were concomitantly exposed to PMA for 24 h (24 h PMA). Cell death of monocytes and macrophages was measured 24 h later using Annexin V. Data are the mean of five to eleven independent experiments ± SEM, 1-way ANOVA, Tukey's Multiple Comparison Test, *p < 0.05, **p < 0.01, ****p < 0.0001*

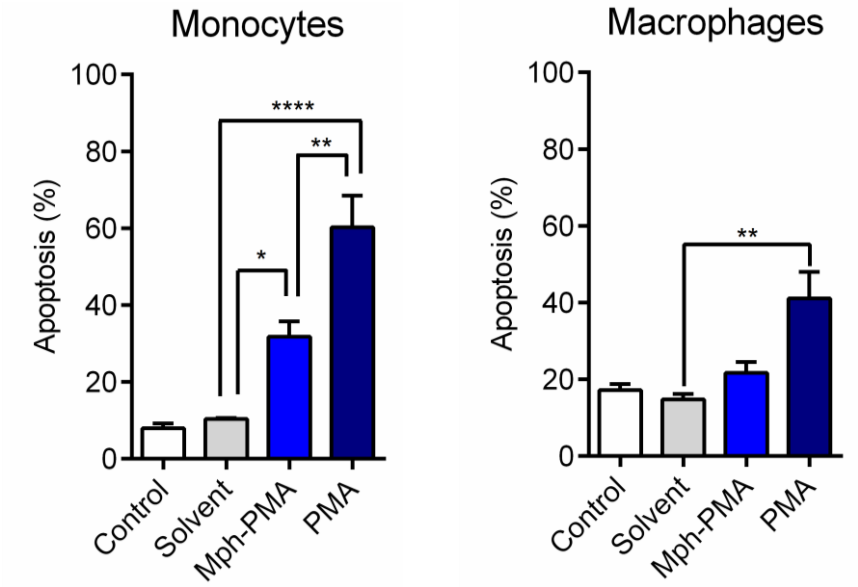

Fig. S14: Cell death of co-cultured monocytes with activated macrophages after 48 h
*Supplemented data for Fig. 33. Macrophages were pulse-activated with PMA for 15 min (Mph-PMA), washed with PBS and supplemented with fresh medium before monocytes were added. Alternatively, co-cultured cells were concomitantly exposed to PMA for 48 h (48 h PMA). Cell death of monocytes and macrophages was measured 48 h later using Annexin V. Data are the mean of five independent experiments ± SEM, 1-way ANOVA, Tukey's Multiple Comparison Test, *p < 0.05, **p < 0.01, ****p < 0.0001.*

7.5 Co-culture of monocytes and granulocytes

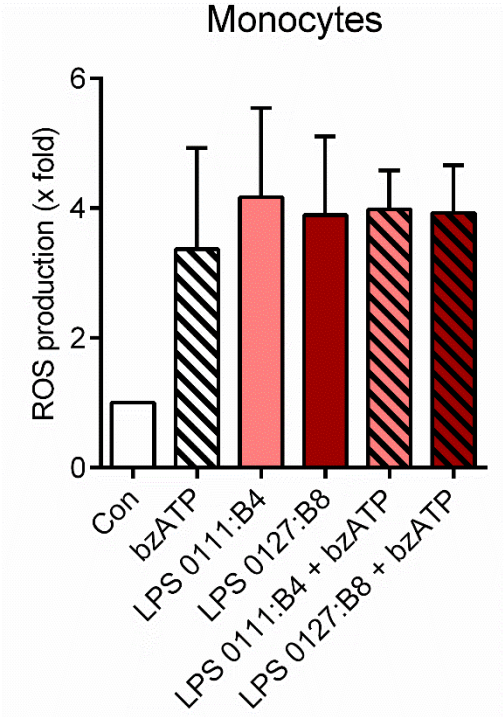

Fig. S15: Intracellular ROS production in monocytes after stimulation with LPS and bzATP
Cells were treated with two types of LPS (1 µg/ml) for 16 h. Then, they were stained with the ROS dye 2',7'-dichlorofluorescin diacetate (100 µM) and treated 250 µM bzATP for 30 min. Mean fluorescence was measured via flow cytometry. For co-culture experiments LPS 0127:B8 was used. Data are the mean of three independent experiments ± SEM

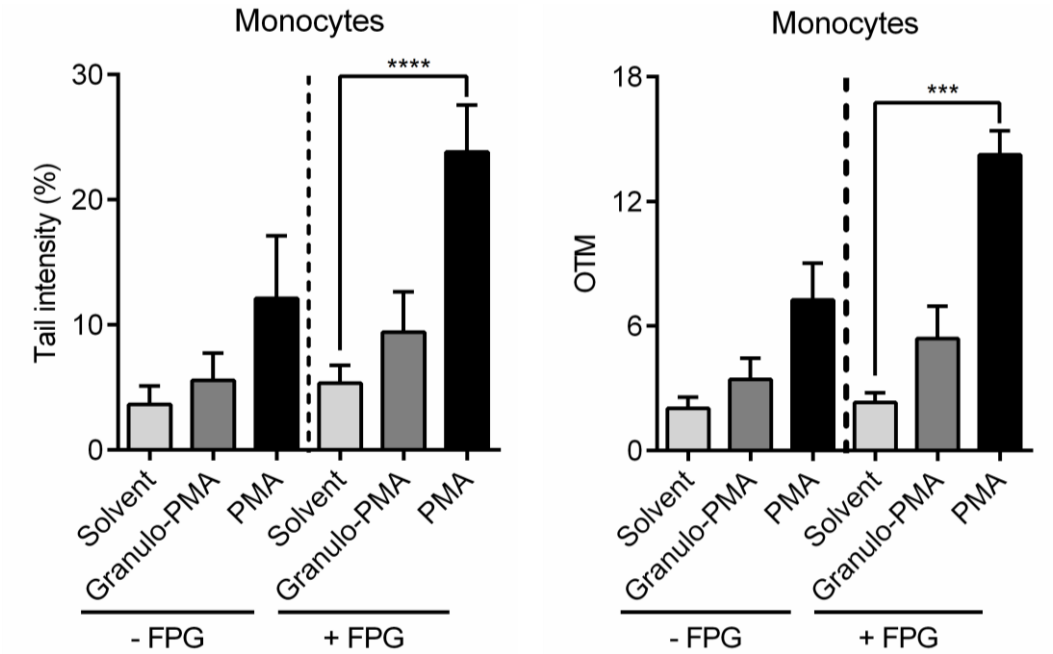

Fig. S16: FPG-modified alkaline Comet assay of monocytes co-cultured with granulocytes
Monocytes were co-cultured with PMA-activated granulocytes in trans-well plates. The cells were not incubated in one well as they are both suspension cells and could not be separated again for Comet assay analysis. The trans-well plates did not allow for the direct contact of both cell types. Granulocytes were PMA-activated for 8 min, washed and re-suspended in fresh medium before they were co-cultured with monocytes for 1 h. Monocytes were removed and DNA fragmentation was assessed. Monocytes showed a trend to increased oxidative DNA damage and SSB formation when

*exposed to pulse-activated granulocytes (Granulo-PMA). Concomitant PMA treatment for 1 h led to SSB formation and a significant increase in oxidative DNA damage. Data are the mean of four independent experiments ± SEM, 1-way ANOVA, Tukey's Multiple Comparison Test, ***p < 0.001, ****p < 0.0001*

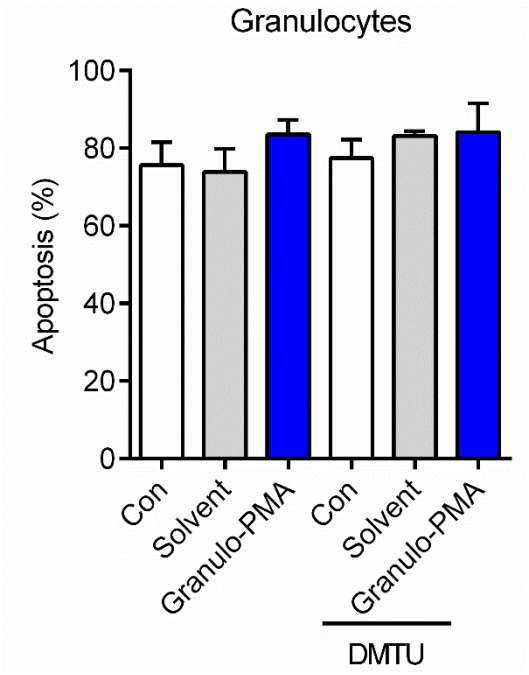

Fig. S17: Cell death in co-cultured granulocytes after 48 h
Granulocytes were pulse-activated with PMA for 10 min (Granulo-PMA), washed with PBS and supplemented with fresh medium before monocytes were added. Co-cultured cells were incubated in the presence or absence of the ROS scavenger DMTU (10 mM). Cell death of co-cultured granulocytes was measured after 48 h using Annexin V. Corresponding data of monocytes can be found in the results (Fig. 35). Data are the mean of six independent experiments ± SEM.

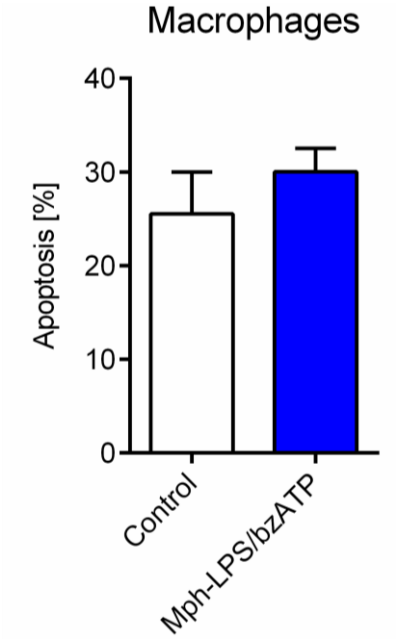

Fig. S18: Cell death of LPS/bzATP activated macrophages in co-culture with monocytes
Supplemented data for Fig. 36. Macrophages were primed with 1 µg/ml LPS for 16 h before they were pulse-activated with 250 µM bzATP for 15 min. Monocytes were co-cultured with macrophages

for 24 h and macrophages cell death was measured using Annexin V. Data are the mean of three independent experiments ± SEM

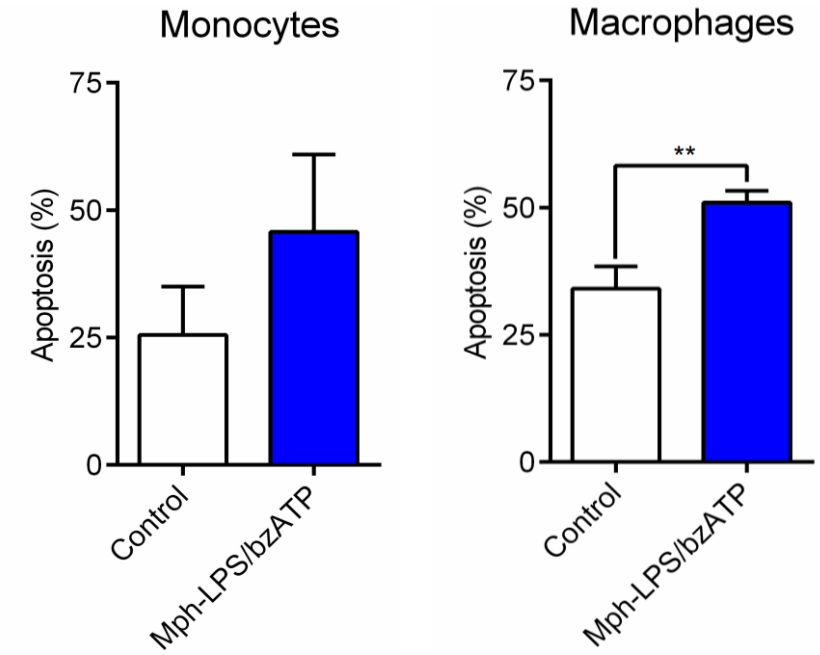

Fig. S19: Cell death of monocytes co-cultured with LPS/bzATP-activated macrophages
*Macrophages were primed with 1 µg/ml LPS for 16 h before they were pulse-activated with 250 µM bzATP for 15 min. Monocytes were co-cultured with macrophages for 48 h and cell death was measured using Annexin V. Data are the mean of five independent experiments ± SEM, Student's unpaired t-test (two-tailed), **p < 0.01*

7.6 Co-culture experiments with lymphoid cells

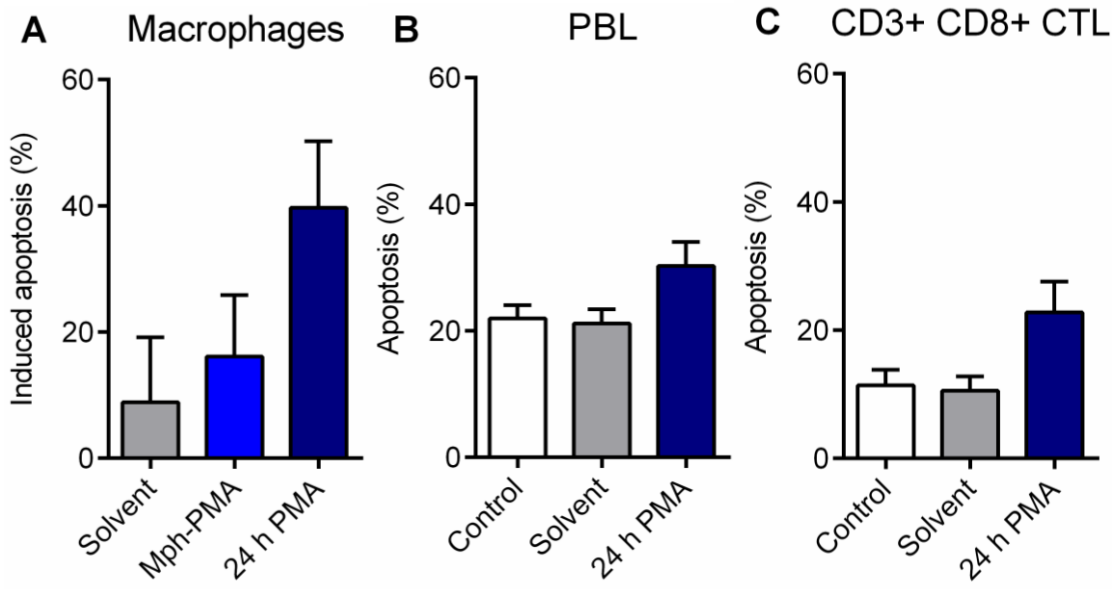

Fig. S20: Cell death of mono-cultured macrophages, PBL and CD3+ CD8+ cytotoxic T cells gated from the PBL pool
A) Macrophages were pulse-activated with 100 ng/ml PMA for 15 min (Mph-PMA) or continuously exposed to PMA (24 h PMA) and apoptosis was measured 24 h later using Annexin V. B) PBL were treated with PMA for 24 h before cell death was measured. C) Using CD3+ CD8+ markers, CTL were

gated from the PBL population and analysed for increases in apoptosis after treatment with PMA. Data are the mean of five independent experiments ± SEM

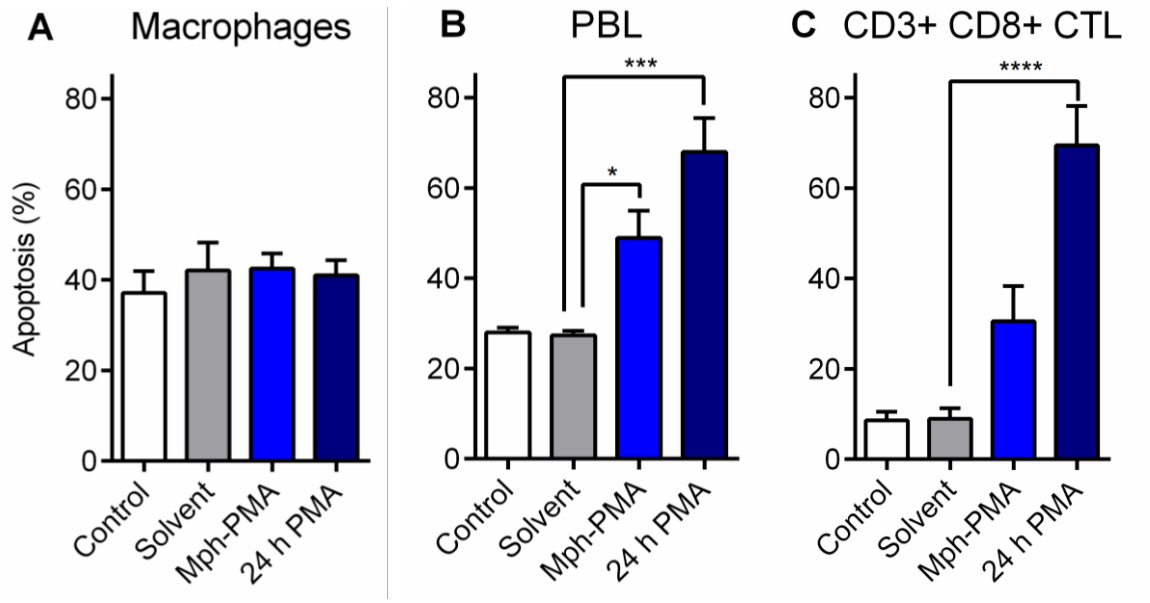

Fig. S21: Co-culture of activated macrophages and PBL / CD3+ CD8+ CTL
Corresponding data for Fig. ***38****. A) Macrophages were activated with PMA for 15 min (Mph-PMA), washed with PBS, supplemented with fresh medium and then incubated with PBL. Alternatively, co-cultured cells were concomitantly treated with PMA for 24 h (24 h PMA). Apoptosis was measured in A) macrophages, B) PBL and C) CD3+CD8 CTL gated from the PBL population after 24 h using Annexin V. Data are the mean of five independent experiments ± SEM, 1-way ANOVA, Tukey's Multiple Comparison Test, *p < 0.05, ***p < 0.001, ****p < 0.0001*

7.7 Attenuated XRCC1 expression in maturing macrophages in the presence of antimetabolite gemcitabine

The cytosine antimetabolite gemcitabine destabilises the DNA methyltransferase DNMT1 and can reactivate epigenetically silenced genes (Gray *et al.* 2012). Maturing macrophages were treated with two concentrations of gemcitabine (50 nM and 150 nM) (Schäfer *et al.* 2010) and XRCC1 expression was measured at days 4 and 6 of differentiation.

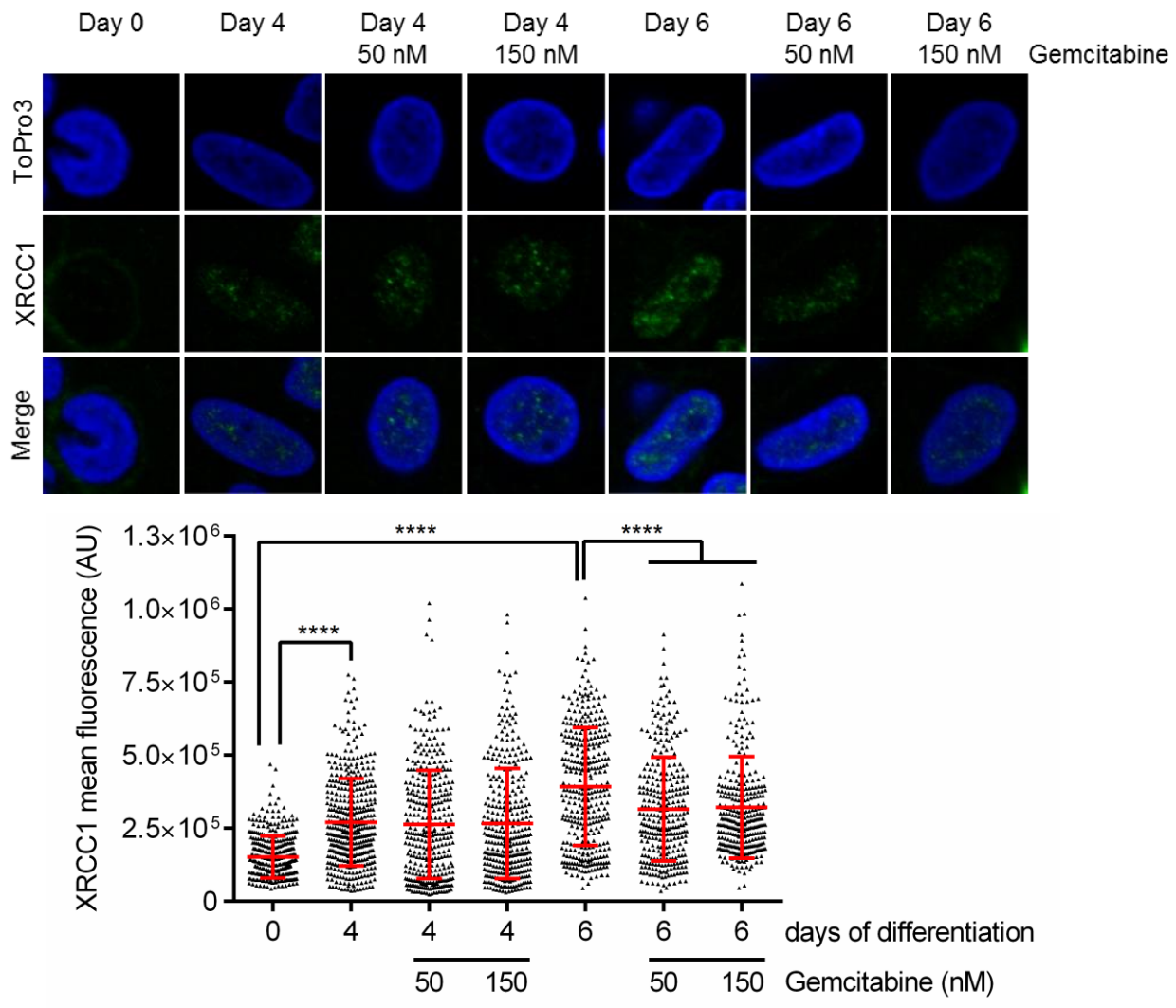

Fig. S22: XRCC1 expression in maturing macrophages ± gemcitabine

Representative images of XRCC1 expression in maturing macrophages at days 4 and six ± gemcitabine (top panel). Quantification of the XRCC1 signal intensity showed that gemcitabine treatment attenuated XRCC1 signal intensity in macrophages at day 6 (bottom panel). The data consists of five independent experiments ± SD. *For each condition 60 - 100 cells were counted, 1-Way ANOVA, Tukey's Multiple Comparison Test, ****p < 0.0001. Quantification of XRCC1 signal intensity was kindly performed by ..... under supervision.*

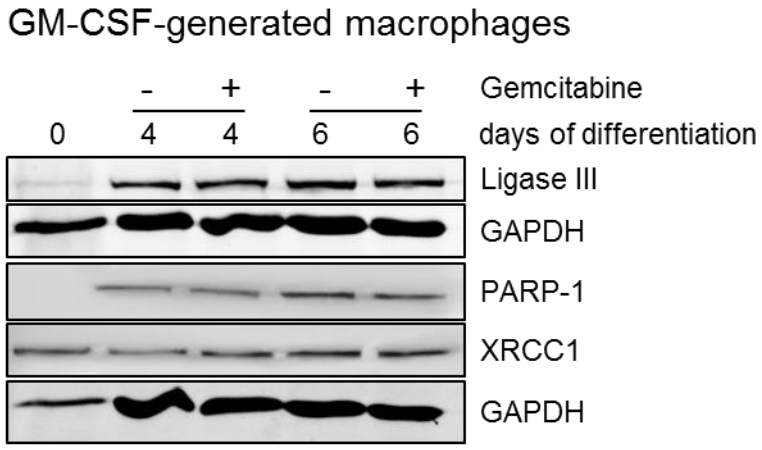

Fig. S23: BER protein expression in GM-CSF-maturing macrophages ± 150 nM gemcitabine

BER protein expression was analysed in maturing macrophages in the presence of 150 nM gemcitabine added a day 0 of differentiation. GAPDH was used as a loading control.

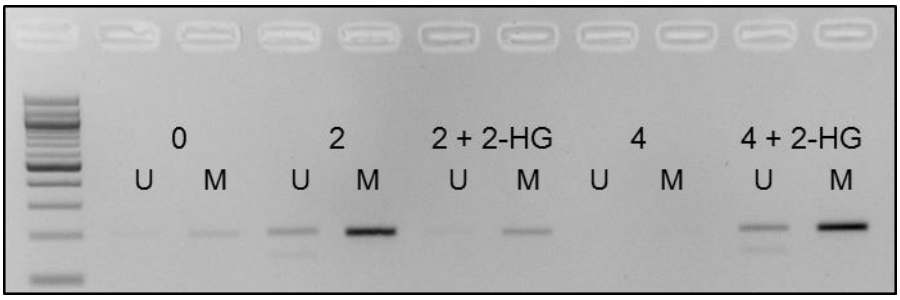

Fig. S24: XRCC1 promoter methylation at position -940 to -736 to the ATG start codon
MSP primers were taken from (Wang et al. 2010b). DNA of monocytes and GM-CSF-generated macrophages at days 2 and 4 ± 1 mM HG was isolated and bisulphite converted before MSP was performed according to the protocol by Wang et al. M = methylated products, U = unmethylated products

Fig. S25: Bisulphite converted XRCC1 promoter
Positions of primers for pyrosequencing regions Seq 1 (95 bp), 2a (212 bp), 2b (89 bp), 3a (269 bp) and 3b (124 bp).

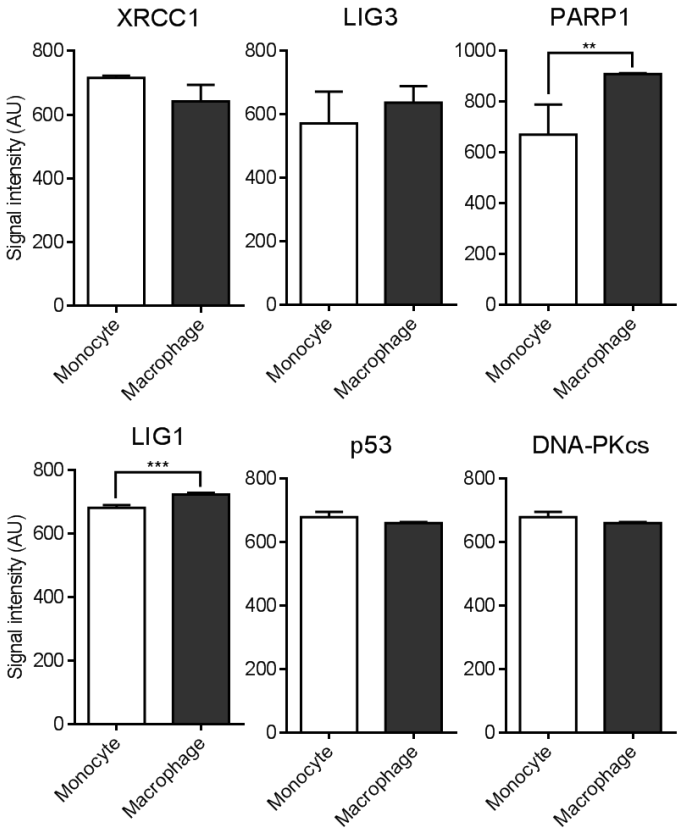

Fig. S26: Microarray data from Array E-GEOD-46903
The data were published as 'Transcriptome-based network analysis reveals a spectrum model of human macrophage activation by Joachim Schultze et al 2014. The data are stored at the Gene Expression Omnibus database of NCBI. The data were generated using Illumina HumanHT-12 v3.0 Expression Bead Chip A-MEXP-1171. The array was browsed for BER factors XRCC1, PARP-1, ligases I and III, transcription factor p53, and DSB factor DNA-PKcs. The gene expression profiles between monocytes and macrophages showed significantly increased expression for ligase I and PARP-1, but not for the other BER factors XRCC1 and ligase IIIα. Data are the mean of six monocyte samples and 17 macrophage samples (Xue et al. 2014).

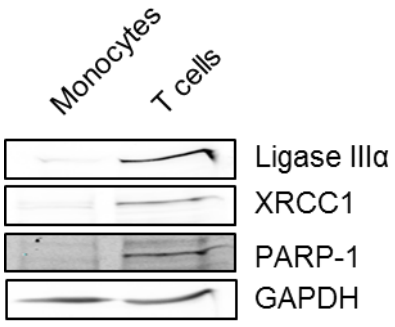

Fig. S27: BER protein expression in monocytes and T cells
The BER protein expression in monocytes and T cells was analysed using Western Blot technique. GAPDH was used as a loading control.

7.8 Promoter sequences of DNA repair factors

5‘
CCCAAGGAAGCACCCAGTGTGGGTAGGGCCCCACCTTGGAGCACCCAGCATGTCC
AGGCTGGTCCTGCGGGTGCGGGGTGCCTTGTCTCCCTTCCCCTCTCTTCATGTGCT
CGGCTCACACTCCTTGTGTGTTTGGGCTGTCTCCAGCTGCGACCCCACCCAGGGCT
GCACCCTTGGGTCTCCAAGGCACCGAATGAACAGAGGGATGTCTGTCGGCAGTCAT
AGGCGGGCGTAGTAAAAGACAGATGCCCACAGTCCACATATTGGGAAACTGAGGCT
TTTGTGGAAGAACTCCAGGATAGGGGTGTGTGTGTGTGTGTGTGGTGGGGGTTGG
GCACATGCTTTGTGTTATATTTAGGACGCAGAACCCTTCTCTTTTGGCCTCAGGCAT
AAGGCTGAAAGAGATCTGCTAATTTTTTTCGCGCGTGCGCGCGCGCGTATGTATGT
ATATGTGCGTGTGTGTGTGTGGCAAGGGGACAGAGAGAAGAGTGCAGCCGCCT
GAGCCATTTGAAGAGATCCTGTTGCGTAGAATCCAGGTTCCCTACGAAACTACGAAA
ATTCACTCAGATTTGCTGTCCTAGCCCAGCGCAGTCGCTCACGCCTGTAGTTCCAG
CACTTTGAGAGGCCGAGGCAGGTGGATCGCTTGAGCTGAGGAGTTCGAGACCAGT
CTGGGCAACATGGCAAGACCCGCCGCCCTCTCACCCCATGTCTCCACAAAAAATAC
AAAAATTAGCCGAATGTGGTGGCGCGTGCGTGTAATCCCAGCTACTTAGGAGGCTG
AAGTGGGAGGATCCCTTGGCCCCAGGAGACAGGGGTTGCAGAAAGCCGAGATCGT
GCCACTGCACTCCATCCTGGGTGAGAGAGCAAGACCCTGTCTCAACAAAAAATTTTT
AAAAAATAAAATAAATAATAATACAGCAAAAAGATTTGCTTTCTCGGCTTCAGTGTGG
GCGGTAACTCCATCGTGCAATGAGAAAGGCGAATTTCTTCCAGACACCAATCCCGG
AGGTCGCTTCTGTTGCTAGGCTCCCAGAAAGCAGGGTTCGGACGTCATTGGGAGG
CGAGGCTAGAGCGGGGTTGTGTGTGGCGGAGGGAGGCGGGGCTGGAGGAAACGC
TCGTTGCTAAGGAACGCAGCGCTCTTCCCGCTCTGGAGAGGCGCGACTGGGCTTG
CGCAGTGTCGACGCCGGCGCCGGCGCGCCGGGGTTTGAAAGGCCCGAGCCTCGC
GCGCTTGCGCACTTTAGCCAGCGCAGGGCGCACCCCGCCCCCTCCCACTCTCCCT
GCCCCTCGGACCCCATACTCTACCTCATCCTTCTGGCCAGGCGAAGCCCACGACGT
TGACATGCCGGAGATCCGCCTCCGCCATGTCGTGTCCTGCAGCAGCCAGGACTCG
GTGAGGG 3‘

Fig. S28: XRCC1 promoter sequence
The sequence was taken from the NCBI database (Gene ID: 7515, location NC_000019.10, NM_006297.2) and compared to a previous publication (Chen *et al.* 2008). In blue: additional DNA sequence not covered by Chen *et al.* The E2F1 binding site as stated by Chen *et al.* is shown in red. In yellow, the primer sequences used for cloning into a vector are shown. This DNA sequence was taken for the generation of a XRCC1 promoter plasmid and the amplification of XRCC1 PCR products for proteomics (Miriam Pons 2016).

5‘-
AGTGCTCGGAGTACCTGCGCGACAAGGACAAGCTCGGGCCGGGCCCGCCTCCCGG
CTTCCCTGCCCTGCTCCGCAGCGCGGACGTTCCCGTCGGCTCCGCGCCACGCCCT
CCCCGCCGGCGCGCGGTTACCGTGGAAAGGCGGCCGCTTGCCGACGACGCTCGCG
GACTCCGAGTCCACCTGGCGAGTAGCGCTCCCAAACCGCGAGACCCAGAGTTCCCG
CCGGCGGCAAGGTCGTCTCCGCCCCTGGCGGGGCCTCACCAATCACAGCGGCGCT
CGTACGTGGCTCCGCCTCCGGGAGGCGCCACTGCGCATCGGCAGGGGGGGACAGT
GCCGCTTCTTTCAGCGCCCGTGCGTAAACCAGAAGTAGGCCTCGCTCGGCCCCCCT
TGGTCCAGATGGTCTGACCCCCTGCGCGGCAGCGTTTTCGCGGGAAAACTGGGTCC
TACAGCACCAGCTCTCGGGGTGTGTTCCTCTAGCGTTGGCTAGGGAGCGTGTGCTT
CTTTATCCCTTAGGCGTTTTTGGTTAATAAGGACATTACAGATGCATTTCTCACTTAAA
GATTTTTTTTATTAAAAAAAATTAAGGACGGGAGGTGGTGGGGATGGTCTCATTATGT
TGCCCAGACTGGTCTCGAACTCCTGCGATCCCCCCGCCTCAGCTTCCTAAAGTGTTG

GGACTGCAGGCGGGCATCACCGCCCCCGACCGCGTTTGTCGTTTTTTATCGAGGAA
CAAACTTGGAACTCTTGACCTAGGCCCCTCGCTTGTTTTATCTGCCTCTGGTATTTAT
TTAGCCAAGTCCAACACCAAGTAGCCACCCAAACTACCTCCGCAGGTCAGACGTTTT
TCCTTAGGTTTCCATGTTGATTCGGGCCAAAGAGGCGCGCTTACTGGCCAGGCCTTC
CCGCAGGGGTCCCCGGGAAAGTTCCTGCCGCCGCGCCCCGCAGCCCCGCCTCCGC
GCGTAGGGGCATTTCCGGGTCCGGGCCGAGCGGGCGCACGCGCGGGAGCGGGAC
TCGGCGGCATG-3‘

Fig. S 29: PRKDC promoter sequence
The sequence was taken from the NCBI database (Gene ID: 5591, location NC_000008.11)

5‘-
CCTGACCTTAGGTGATCCACCCGCCTCAGATTCCCAAAGCGCTGGGATTACAGGCAT
GAGCCACTGCACCTGGCTAATATTGATATGTTTTCCCTCTCTCTGCCGCATCAGCCT
GTCCCACTGACAGAGTTGAGGATGCTCAAGGCGGCTCAACAGAGGGTACCTGGAGC
AACTCACACTGCACTATCAGAGAGACACAAGTGCAAGCACACTCAGCCACAGCTGCA
GCTCACCAATCAGCCTGCTGAACAGACCTGAACTTTAGCTGCATTTTTGGGGCAGAG
CATATGGGTGCCAGGATGGGACCATAATCTTATCACCAATGAGTGGCCATTTAGGGA
TGATATAGTTGTCAACCCAGAGATGGCATGATCATGCCTTTTGACTTGGTCATTCTCT
AAGTAAAACTTTTATTTGTTCCATCATATTTTCCACTTATTCTGTTTACCTTCAAAATAT
CTTTTTTTTTTTTTTTTGAGACAGGGTCACACTGTCACCCAGGCTAGAGTCCAGTGGC
ACTATCATGGCTCACCACAGCCTCAACCTTCAGGGCTCAGGTGATCCTCCCACTTCA
GCCTCCCGAGTAGATGGGACTACAGGCACCTGCCACCACCCCCAGCTAATTTTTGTA
GAGACAAGGTTTTGCCATGTTGTCCAGGCTGGTCTTGAACTCCTGGGCTCAAGGGAT
CCGGCCACCTCAGCCTCCCAAAGTGCTAGGATTATAGGCATGAGCCACTGTGCCCA
GCCTACCTTCAACGTATCTAACTGGTTACTAACTTTTAGGATTCGGCCTATGTCTCAC
AACCTTCTTGCTTACTCAACATCCTTGTCTCTTAAGCCACTAGCTTCTTCTCTATGGTT
AACACTTTTTATGAGTTTTATTCATCTGCTTATTTTTCTTATCCTCTATACCAGAATTGA
ATATTTTCAAATAAAGCACACTCATGTTACAATCTTTGAAATGAAAAAAAAAAATGCAT
AGGATTAGAAAAGAAACCAATTTTAATAAACTATATTTTGAAGTATAGTTCTATATTAAA
CAACAAGATCTAGGCCAGGTGCAGTGGCTCATGCCTGTAATCCCAGCAATTTGGGAA
GTCGAGGTGGGAGGATTGCTTGAGGCCAGGGGTTCAAGACCAGCCTGGGCAACAT
GGAGAGATTCCCCATCTCTTTCTTTACACACACACACACACACACACACAAAATATCT
GATAGCAACAGGTGCAGTCATTACCACAATTTCGAGTAGTGATGAGCTTAATAATATT
TCGAGTTATCACCAACAACTGTAAAGTAACATGAAAACGTCTGTGATGACTATTGCCC
ACAAAGTCACAGGTACTGCTAATACTCCTGGTATTTGTAGTCAAATTCATAATAAAGG
AAATGCTAGGTTTCAGTTGGTATTTTGTCCCGACGGTCTGTGGACGGCAGGTTAGAA
CGCCCGTCCAAGCCAGGAGGGTGGACCTAGCACTGCAGGGTCCACCTCGGGCCAA
TCAACTATATTCCCGAGGCGGGGGCCTGCGCTTCCCGGACCCAGCTGCCCTCAGGG
GAGAGAGGACACACTTAAGAGTTTGGGGCCGGCGTGGTAGCTCATGCCCCTGATCC
CAGCACTTCGGGAGGCTGAGGCGTGAAGATCACTTGTAGCAGGAGTTTGAGACCAG
TCTAGCCAACTTGGCGAGACCCTGTCCCTAAAAAAAATTTTTTTTTAATTAGCCAGTT
GTGGTGAGCGCCTGTAGTCCCAGCTACTCGGGAGGCTGAGGTGGGAGGATCGCTG
GGCTCAGGAGTTCCAGACTGCAGTGAGCCATGATGGCGGCACTGCACTCCAGCGCG
GTGAGACTCAGTCTCAAAAATAAAAGGGGGAGGGGTTGGGGGTAAAATTAGTTGTGA
AATCAAGTAAGACTTCCTGGGACAGAACAATCAAAGGGGTGGCGCCGGGTCCTCCA
AAGAGCTACTAGCTCAGCCCAAGCCCCGCCTCGGCCCCCAGGGCAGCGGCCCGCA
GAGCTCCACCCGGCAGGCGCCCGGGAAACTCCGCCCCCCGGCCGGCAGGGGGCG
CGCGCGCCGCCGGCCCCGCCCCGTGGACGCGGGTTCCGTGGGCGTTCCCGCGGC
CAGGCATCAGCAATCTATCAGGGAACGGCGGTGGCCGGTGCGGCGTGTTCGGTGG
CGGCTCTGGCCGCTCAGGCGCCTGCGGCTGGGTGAGCGCACGCGAGGCGGCGAG
GCGGCAGCGTGTTTCTAGGTCGTGGCGTCGGGCTTCCGGAGCTTTGGCGGCAGCTA
GGGGAGGATG-3’

Fig. S 30: PARP-1 promoter sequence

The sequence was taken from the NCBI database (Gene ID: 142, location NC_000001.11, NM_001618.3)

5'-

AGTTTGAGACCAGCCTGGCCAACATCGTGAAACCCCGTCTCTACTAAAAATACAAAA
ATTAGCCAGGCGTGGTGGCGGGTGCCTGTAATTCCAGCTACTCAGGAGGCTGAGGG
AGGAGAATTGCTTGAACCTAGGAGGCAGAGGTTGCAGTGAGCCAAAATCCTGCCAC
TGCACTCCAGCCTGGGCGACAAGAACAAAACTCTGTCGCAAAAAAAAAAAAAAAAAA
TTATTAGCCCATTGTGGTGGCAAGGGCCTGTAATCCCAGCTACTTGGGAGGCTGAG
GCAGGAGAATCACTTGAACCTGGGAGGCAGAGGTTGCAGTGAGCCAAGATCGTGGC
ACTGCACTCCAGCCTGGGCGACACAGCGAGACTCTGTCTCAAAAATAACTAAATTAA
TTAATTTAATTTAATGACAATAAAAGGTATAGTATACTAAATATATAAACCAGCAACATC
GTCCTTTATTATCATTATAAAGTTTTATATACTGTACATAATAGTGTGTGCTATGCTTTT
ATACAACTGGCAATGGAGTAGGTTCGTTTCCACCAGCATCTCCACAAACACATGAGT
AATGTGCTGTCACTATATGATAGGGATTTTTCAGCTCCATTATAATCTTATGGGACCA
CCCTCATATATTTGGTCCATTGTTGGCCTAAATGTCATTATGTGGTACATATTATTAAT
GAGATATTTTACTTTTTTTAGTATGAATTTTTTGGTGTGTATTTTCTTCACTTATAGCAC
ATCTCAATTCCATGCAACATTCAAGTGCTCAATAGTCACGTGTGGCTAGTGATTACAG
CATTGGAAAAAGACAGATACGGTTGAGGAAACTTAAAAAAATGTAGCAAATGTAGTTG
TAGAGACGTGCTCAAGATCACTCAATTATCATAGCTAGGACGTGAGTCTCCAGCGAC
CTTCCAATTGCCTGGTTGAACCAAAGCCCTGGTTCATTCTGCTGCGCATTAAAAGCA
GGCTTTACTCCCCTCCAAACAGTAGAATCGCAGTTAAACTTAGTCAAACAAACTTAAT
GTATCCAATACAAAACTCATCTTTCTAACCCTAACACCTCCTCTTCCTCTCTATTTTCT
ATTTCAGTTGATGGTACCATTATGTTTCTGCTCACTCAAATTATTATTATTTTATCCATA
AACGAGCACTTTATCTAGAAGATCATTTAAATTCTAAATGATCTTCAAAAACGCACTTT
ACTCTCCACCCTAACTAGCTGAATCATCTCCCACATGGGTCACTATGAGAGCCTTCT
GATTTGTTCCCTTGCCTCAGTCTCTCCCCACCCAGCTTCAGCAGTATTCCCTAAGACT
CTTCATGGCTCTCCGTCCTCTACAGAGTAAAGACGACACTCTTCATCACACAGCACA
GAATTCTCTCGGGAACCTGTTCTTTGCTTACCTAACAAGGCCCAGTTGTTTGCTCTTC
CTAGACTCTGAAGAGGTCACTTACCCTCAGGCTGCTACATTTGTAAAAATCGCCATCC
CAACTCTCAAAGAGCTGGCTTCAGATTTGAGATAATACACTTTGAATGATATACAATC
AAGGAGTTTCTCCTCCATCACTCCTTTACATTTTATATCTATCTGCTGTTTAGTGCCTC
GTCTCAATTCCATGAAAGCTACTGAATACAAACTATTTACTAGGGAGTCTGCGGGACA
CAAACAGAGGGATTATATTTAAAAAATAGATTGACGCGATCTTTGCCTTCCCCGACCT
CATTACAATATAGTTTCTCCACCAATATCTTTAAAAACAGATCCTCTCTAACAGTATGA
GAAAATCAAGGGGAGCCTCGGAAGTTCAGGCCAGGCTGCGTTCCGAGGAGCCGCC
ACGTCCCCCCACCTCCGCTTCCCGGGCCGCGATTGCAGGTTGAAAACTACTCCCAA
ACATCACAGGGCAGGCAGAATGCAACTACGACCCACGTGGCAGACGGGGGCGGGG
ACCGGTCGCGTGGCCGCGGCCTTGGCTCTTGCGCCTGCGCGCTGCCTCCCGCTCT
AGGACCCGGATTTAAAGAGACAGGCGCTCCAACCGTCGTGGGCTGCCCGCGGCCT
GTAATG-3'

Fig. S 31: Ligase III promoter sequence
The sequence was taken from the NCBI database (Gene ID: 3980, location NC_000017.11, NM_013975.3)

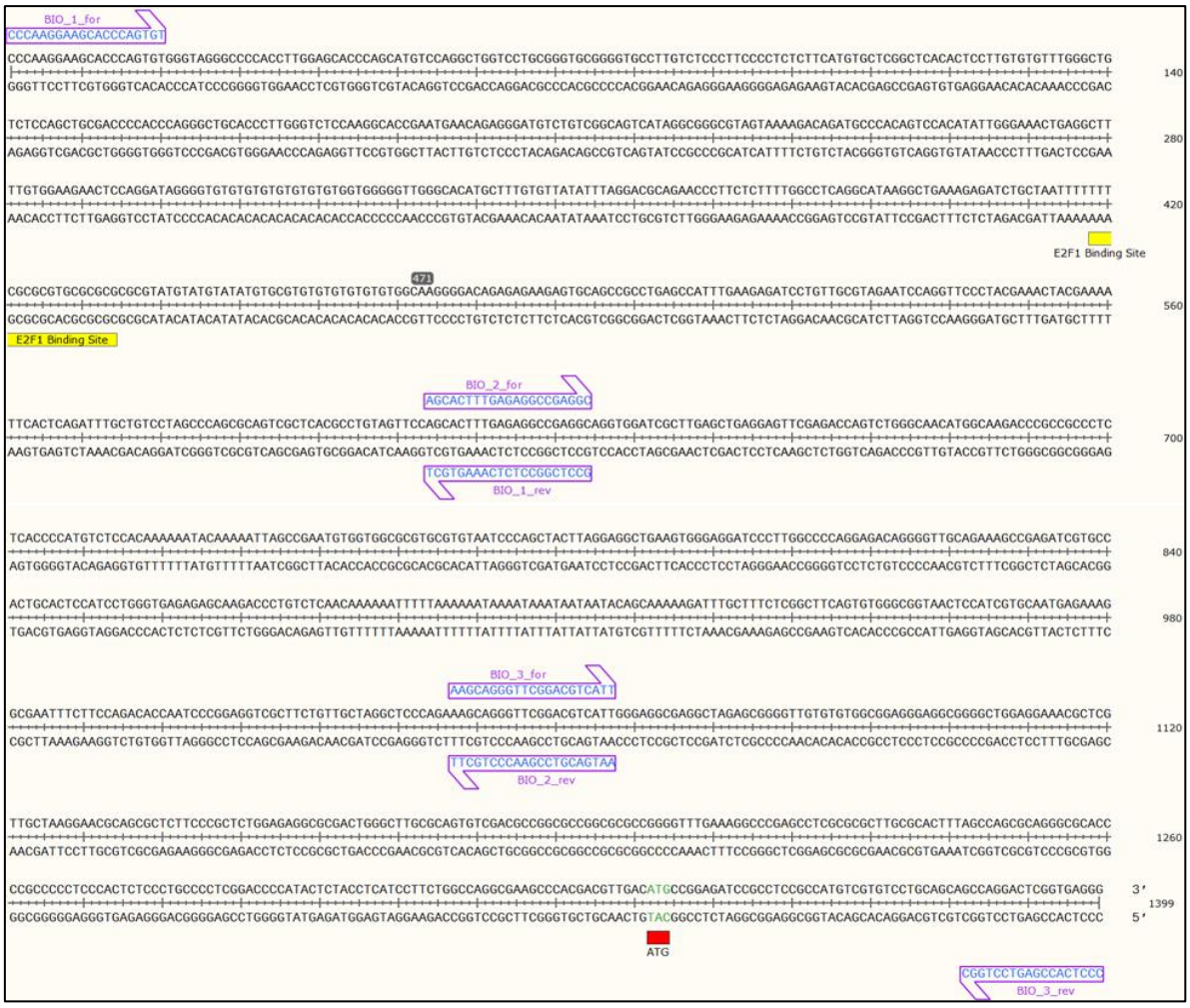

Fig. S32: XRCC1 promoter sequence with biotin-labelled primers
The XRCC1 promoter (1399 bp) was divided into three parts (product 634 bp, product 2 444 bp and product 3 363 bp). 5'-biotinylated primers were used for the amplification of the three products by endpoint PCR.

7.9 Proteomics data

Table 9: Transcription factors upregulated in macrophages

Protein	Gene	log2 of Ratio Heavy to Light Mph/Mono	log2 of Ratio Heavy to Light Mono/Mph
Microphthalmia-associated transcription factor	MITF	4.1706	-4.1325
Transcription factor AP-4	TFAP4	3.5334	-2.8665
Far upstream element-binding protein 1	FUBP1	3.1057	-2.7555
Bcl-2-associated transcription factor 1	BCLAF1	3.0327	-2.9563
Transcription factor EB	TFEB	2.8921	-2.9993
Upstream stimulatory factor 1	USF1	2.2858	-1.1759
SAFB-like transcription modulator	SLTM	1.7788	-0.4925
Myb-binding protein 1A	MYBBP1A	1.7758	-1.5553
Upstream stimulatory factor 2	USF2	1.6023	-1.2017
Transcription factor MafG; Transcription factor MafK	MAFG MAFK	1.2401	-2.2028
TATA-binding protein-associated factor 2N	TAF15	1.1568	-0.4517

Proteomics data – raw data

Table 10: Proteomics data – differentially expressed proteins, detected in both the Mph/Mono ratio and in the Mono/Mph ratio

Gene	log2 of Ratio Heavy to Light Mph/Mono	log2 of Ratio Heavy to Light Mono/Mph
RSL1D1	3.528	1.064
PRDX3	2.999	0.408
FBP1	8.198	-5.318
ATP6V1E1	3.789	-1.134
PSME2	2.181	0.079
TOP2A	4.223	-2.153
RTN4;NOGOC; Nbla00271	3.645	-1.702
NARS	4.468	-2.542
FTL;FTL variant	3.878	-2.029
CHERP	3.605	-1.769
CBX5	-0.837	2.626
SNRPG; SNRPGP15	0.549	1.185
DDX42	3.519	-1.786
ATP6V1H	4.915	-3.223
HLA-DRA; HLA-DQA1/DRA	4.085	-2.421
AZU1	-1.096	2.748
GPNMB	4.495	-2.846
SSRP1	0.705	0.830
ADAR	2.759	-1.269
HADHB	2.110	-0.651
FABP5	2.935	-1.512
SART1	3.077	-1.719
BLVRB	1.928	-0.576
RFX1	1.752	-0.400
SLTM	1.779	-0.492
DAZAP1; DAZAP1/MEF2D fusion	3.505	-2.242
SKP1	0.830	0.432
ATP1A1	2.905	-1.644
RAD23B; RAD23A	2.778	-1.584
GNS	2.756	-1.571
COPA	2.521	-1.363
MYL12A; MYL12B; MYL9	0.477	0.676
NPC2	3.404	-2.254
ACP5	5.097	-3.978
TRA2B	0.920	0.193
PABPN1	2.893	-1.781
USF1	2.286	-1.176
FTH1	1.943	-0.858
LRPPRC	3.562	-2.489
CCT7	2.941	-1.880
SSR4	2.568	-1.514
CIRBP	1.061	-0.007
PRTN3	-2.466	3.520
IFI30	3.476	-2.489
PSME1	2.234	-1.249
AIF1	2.557	-1.583
MANF	0.620	0.334
CYBA	2.260	-1.306
IDH1	3.746	-2.833
IGHG1	-1.857	2.755
ABCF1	1.609	-0.719
MAX	1.298	-0.415
TRIM25	2.265	-1.407
SFRS5; SRSF5	1.062	-0.204
SOD2	3.407	-2.552
RPL10A	0.471	0.384
SERBP1	2.529	-1.674
UNC84B; SUN2	0.172	0.672
ANPEP	2.331	-1.494
COX4I1	4.096	-3.263
AP2A1	1.796	-0.965
TAOK1	0.545	0.283
MATR3	3.207	-2.389
FUBP3	2.930	-2.115
ELF1;	3.726	-2.917
EL52; HSP90AA1	3.046	-2.237
MGST3	2.848	-2.040
CORO1B	3.761	-2.954
LGALS9	3.852	-3.054
SSR1	1.984	-1.187
GTF3C1	1.921	-1.131
TPM4	1.929	-1.148
TAGLN2	2.676	-1.897
SEC61A1	2.391	-1.618
TRIP12	1.674	-0.910
GTF3C2	1.825	-1.073
CORO1C	4.446	-3.694
DYNC1H1	1.151	-0.415
CTNNBL1	1.602	-0.869
STT3B	1.953	-1.221
SEPT9	0.886	-0.155

DOCK5	1.439	-0.710
TCP1	2.285	-1.558
HCLS1	3.925	-3.201
PNN	-0.458	1.175
PSMA4	2.105	-1.389
CALM1; CALM2; CALM3	0.558	0.158
ATP6V1B2	3.782	-3.068
PSMB2	2.615	-1.906
TAF15	1.157	-0.452
PADI4	-3.356	4.060
SPI1	3.352	-2.654
YARS	0.014	0.682
CTSD	3.872	-3.178
ZNF638	2.026	-1.335
PPIF	0.711	-0.028
ILF3	3.120	-2.438
PRPF40A	1.417	-0.735
RAB10	2.072	-1.402
LIG3	2.918	-2.249
PKM2	3.342	-2.673
LMNA	4.217	-3.548
TFAP4	3.533	-2.866
ATP5O	2.386	-1.720
FCN1	0.867	-0.201
VASP	3.197	-2.535
DDX46	1.724	-1.062
SRSF10; FUSIP1	0.360	0.292
FUS	1.611	-0.963
CSNK2A1; CSNK2A3	1.217	-0.570
CEBPA	3.229	-2.582
CETN2	1.565	-0.928
RFC1; LLDBP	3.198	-2.561
DLD	2.181	-1.545
PRPF4	1.883	-1.250
SF3B2	1.556	-0.923
RPN2	2.250	-1.619
RSU1	0.642	-0.011
NPM1	3.042	-2.411
PDIA4	1.854	-1.226
KIF2A	0.631	-0.010
EWSR1/ATF1 fusion; ATF1	2.540	-1.923
TRA1; HSP90B1	2.106	-1.492
DOCK2	0.319	0.295

PACSIN2	0.875	-0.266
S100A8	-0.556	1.163
RBM8; RBM8A	0.681	-0.073
RPS8	0.197	0.409
PPP2R1A	2.196	-1.593
VDAC2	3.530	-2.927
AHNAK	2.268	-1.667
BANF1	2.064	-1.467
DEK	-0.116	0.713
HADHA	0.932	-0.335
RCC1	1.039	-0.444
PARVG	0.675	-0.084
RPL23A	0.702	-0.111
PRPF31	1.294	-0.709
TARDBP	3.205	-2.623
HIST1H1B	-3.713	4.292
GPX1	1.955	-1.376
SF3A2	1.562	-0.983
SMARCC2	0.911	-0.333
SRBD1	1.175	-0.598
PNKP	1.661	-1.083
NCBP1	1.918	-1.343
TAOK3	0.721	-0.150
NOLA1; GAR1	-0.354	0.924
EIF5B	3.784	-3.213
VAT1	2.217	-1.648
KCTD12	2.917	-2.348
CANX	1.429	-0.860
EVL	3.151	-2.585
RPL17	1.570	-1.007
RPS28	0.543	0.018
RAB8A	1.556	-1.000
RPL13	-0.132	0.683
CYFIP1	1.470	-0.919
PTBP1	2.274	-1.725
EEF1B2	0.971	-0.425
PDCD11	1.165	-0.620
COPB2	2.256	-1.713
YTHDC1	0.245	0.298
ACO2; ACON	2.119	-1.577
HSPA9	2.407	-1.865
CAPZB	1.990	-1.451
SKIV2L2	2.861	-2.324
ZNF787	1.881	-1.348
CDC5L	1.322	-0.790

RPL21	0.562	-0.032
XRCC6	1.543	-1.014
DDB2	0.166	0.363
DDX18	1.276	-0.747
SAMHD1	0.930	-0.401
MTA2	0.658	-0.131
HIST1H1C	-3.548	4.072
EIF3B; EIF3S9	2.662	-2.140
MYST3; KAT6A	-2.379	2.902
NUMA1;NUMA1 variant protein	1.491	-0.971
HNRNPA0	3.340	-2.821
PTPN6	0.641	-0.123
RAP1B	1.765	-1.249
DHX15	1.537	-1.021
CPSF1	3.153	-2.640
YBX1	0.376	0.136
RNPC2	2.128	-1.616
NRF1	1.754	-1.243
DDX39A; DDX39	1.504	-0.993
ENO1	1.963	-1.453
SEPT2	1.115	-0.607
EEF2	2.232	-1.724
STK10	1.092	-0.586
ARID1A; ARID1A variant protein	1.170	-0.665
DDOST	2.059	-1.554
ARHGEF1	-0.012	0.516
PUF60	1.978	-1.476
TKT	1.517	-1.018
ALDH2	1.797	-1.299
SMC3	0.979	-0.482
PRPF6	1.689	-1.192
PDIA3	1.275	-0.779
HNRPDL; HNRNPDL	2.343	-1.846
RBPJ; RBPSUH	1.974	-1.479
CES1	1.847	-1.352
HNRNPA2B1; HNRPA2B1	2.912	-2.417
XRCC5	1.593	-1.099
TLN1	2.427	-1.936
RPL7A; RP-L7a	-0.063	0.550
CALR	2.255	-1.770
CAPZA1	1.853	-1.368

E2F3	-0.350	0.834
SLC25A24	3.186	-2.703
RPA3	1.626	-1.142
CNBP	3.623	-3.140
HIST1; H2BC; H2BK; H2BN; H2BD; H2BM; H2BL; H2BH; HIST2; H2BF; H2BFS	-1.196	1.677
PDS5B	1.132	-0.651
PRPF19	1.326	-0.846
SGPL1	0.987	-0.510
SQRDL	2.539	-2.063
RPS5	0.927	-0.452
KDM1A	2.047	-1.573
HNRNPA3	2.370	-1.897
ARF1; ARF3	2.337	-1.864
HIST1H4H; HIST1H4A	-1.430	1.902
YWHAQ	1.906	-1.435
POLB	0.473	-0.002
ERP29	0.907	-0.437
SH3BGRL3	2.328	-1.861
DHX9	1.612	-1.145
GTF3C4	1.938	-1.472
PABPC1; PABPC3	2.361	-1.897
CAT	1.114	-0.651
LMNB1	0.520	-0.059
YWHAZ	1.843	-1.383
LSP1	2.394	-1.934
NONO	1.342	-0.882
WDR1	2.736	-2.276
DDX48; EIF4A3	0.504	-0.046
EEF1G	1.300	-0.842
STAG2	0.390	0.068
CHMP2A	-2.321	2.775
PPIA	0.901	-0.447
RBM3	1.685	-1.231
EIF4A1; EIF4A2	2.331	-1.877
HSP90AB1	3.350	-2.898
UQCRC2	2.676	-2.224
G6PD	3.240	-2.790
S100A9	-0.975	1.424
PDXK	3.139	-2.690
SFPQ	1.230	-0.782

HNRNPUL2; HNRNPUL2-BSCL2	0.994	-0.549
SF3B5	1.037	-0.592
TPM3; TPM3-ROS1	2.161	-1.717
PFN1	1.952	-1.509
TFAM	1.133	-0.692
TCF7L2; TCF7; LEF1; TCF7L1	2.333	-1.892
PRPF8	1.209	-0.770
PBRM1	1.547	-1.109
HNRNPA1; RP11-78J21.1; HNRNPA1L2	2.930	-2.492
SND1	2.591	-2.154
HDGF	0.081	0.354
PGD	3.367	-2.932
SERPINB1	-0.754	1.188
CAP1	3.063	-2.630
DOCK8	1.546	-1.118
ARPC2	1.722	-1.294
HNRPD; HNRNPD	2.032	-1.604
TAF6	2.459	-2.032
EFHD2	2.063	-1.635
VPS35	2.280	-1.853
SNRPD1	1.285	-0.861
RAF1; RNASE3	-2.909	3.333
PLEK	0.786	-0.363
NCKAP1L	1.181	-0.759
RPL8	0.315	0.108
ABI1	1.288	-0.866
NOP58	0.299	0.123
PC	2.619	-2.198
HNRNPAB	2.285	-1.864
S100A10	0.638	-0.217
ANXA2; ANXA2P2	0.859	-0.438
DDX39B	1.475	-1.056
P4HB	1.848	-1.429
TALDO1	2.165	-1.746
VIM	-0.185	0.604
RPA1	1.697	-1.280
DDX21	1.452	-1.035
ANXA6	0.554	-0.138
MSN	0.445	-0.030
LCP1	2.752	-2.338
	1.985	-1.571
ACTN1	5.188	-4.776
SNRPA	0.877	-0.467
PSPC1	1.078	-0.668
ERH	1.210	-0.802
GNAI2; WUGSC:H_LUCA16.1	1.209	-0.804
TOP1	-0.411	0.815
SF3A3	1.337	-0.935
TYMP	2.496	-2.094
MPO	-1.286	1.687
CLPB	2.645	-2.244
USF2	1.602	-1.202
H2AFJ; HIST1H2AH; HIST1H2AK; HIST1H2AJ; HIST2H2AC; HIST2H2AA3; HIST1H2AD; HIST1H2AG; HIST1H2AB; HIST1H2AC; HIST3H2A; HIST1H2AA; H2AFX	-1.259	1.659
ARPC5	1.249	-0.849
CLTC	3.264	-2.864
HNRPF; HNRNPF	1.734	-1.334
NDUFB10	3.034	-2.635
TOR1AIP1	1.208	-0.809
H2AFY	-0.539	0.937
CTSS	2.741	-2.346
ARHGAP26	1.617	-1.222
NCL	1.871	-1.477
SF3B1	1.304	-0.910
VDAC1	3.883	-3.490
PDE6H; MYL6	0.400	-0.006
SUPT16H	0.368	0.022
PRAM1	1.449	-1.060
GANAB	1.940	-1.552
HSPD1	1.874	-1.487
SF3A1	1.185	-0.797
RPA2	1.759	-1.373
IFI16	2.413	-2.026
HNRNPH1	2.146	-1.760
FERMT3	0.334	0.051
RPS11	0.473	-0.089
APEX1	0.392	-0.009

MPG	0.567	-0.184
GIMAP4	-0.386	0.768
HSPA1A	0.747	-0.365
SRP9	-0.253	0.635
LDHA	2.189	-1.809
RPS24	0.001	0.377
LTA4H	3.350	-2.973
TFDP1	-0.585	0.962
DDB1	0.114	0.263
H1FX	-2.225	2.602
BAZ1A	0.219	0.155
ARHGDIA	1.884	-1.511
SSBP1	-0.250	0.622
HNRNPC	1.978	-1.606
TOMM70A	2.964	-2.594
UQCRC1	2.667	-2.297
SON	2.053	-1.684
RPN1	1.900	-1.532
RPL28	0.439	-0.072
EIF2S1	1.132	-0.766
PDIA6	1.814	-1.449
RNPS1	-0.297	0.660
SF1	2.710	-2.349
RPS20	0.791	-0.430
USP39	1.657	-1.300
RPL9	0.958	-0.602
COTL1	3.019	-2.662
S100A4	-0.332	0.688
HSD17B4	2.069	-1.714
RPL10; RPL10L	1.997	-1.642
SEPT7	0.819	-0.465
RCC2	0.190	0.163
DDX5	1.858	-1.504
ANXA1	1.313	-0.959
MYO1G	0.473	-0.120
RAN	1.296	-0.945
DDX17	1.096	-0.745
RBBP4	0.948	-0.598
FUBP1	3.106	-2.755
GRB2	1.673	-1.323
UBB; RPS27A; UBC; UBA52	0.504	-0.154
PSIP1	1.505	-1.157
RPS15A	0.641	-0.294
RRBP1	2.920	-2.572

GMIP	0.619	-0.273
UBE1;UBA1	2.465	-2.120
RPLP0; RPLP0P6	0.526	-0.182
RUNX1	0.864	-0.520
HSPA8	1.755	-1.412
PS1TP5BP1; ACTB	2.375	-2.034
SUPT5H	0.962	-0.621
ELAVL1	2.911	-2.571
TOP2B	0.971	-0.633
TCERG1	0.980	-0.643
CMAS	2.363	-2.027
ATP5A1	2.031	-1.695
TPI1	2.444	-2.109
DNAJC8	0.431	-0.097
HNRPH3; HNRNPH3	2.725	-2.391
CORO7	2.449	-2.116
SF3B3	1.044	-0.711
SNRPN; SNRPB	1.481	-1.151
SMU1	0.821	-0.492
U5-116KD; EFTUD2; SNRP116	1.006	-0.677
YWHAB	1.442	-1.114
SF3B6	1.173	-0.846
SMARCD2	0.491	-0.164
SLC25A5	3.690	-3.364
RPL23	1.028	-0.703
CKAP4	2.487	-2.163
NFKB1	1.268	-0.944
RANBP2; RGPD8; RGPD5	0.337	-0.014
ACTN4	4.135	-3.813
ATP5B	1.865	-1.543
SNRPD3	1.248	-0.927
ITGAM	1.336	-1.015
THOC1	1.305	-0.984
RUVBL1	1.569	-1.249
DNMT1	0.833	-0.513
H1F0	-0.800	1.120
RAB7A	2.088	-1.768
VDAC3	2.607	-2.289
RPS14	0.769	-0.451
ETF1	0.890	-0.573
MYH9	0.216	0.102

HMGB1; HMGB1P1	-2.658	2.976
RPL4	0.139	0.178
PARP1	0.195	0.121
HMGA1	2.364	-2.049
EWSR1	-0.041	0.355
APOBEC3C	1.310	-0.997
ILK	0.833	-0.521
CTSB	3.074	-2.763
RECQL	1.318	-1.013
HMGB3	-2.103	2.407
HK1	0.602	-0.298
HP1BP3	-0.913	1.217
UBE2N; UBE2NL	0.674	-0.372
SNRNP200	1.209	-0.908
ATP6V1G1	2.737	-2.437
SYK	0.361	-0.061
MSH2	0.191	0.108
ELMO1	0.038	0.261
IQGAP1	-0.896	1.193
ACTR2	1.589	-1.292
WARS	2.332	-2.039
SMC1A	0.876	-0.583
CYBB	2.847	-2.554
FLNA; FLJ00119	3.285	-2.994
SYNCRIP	3.417	-3.127
HNRNPR; HNRPR	2.827	-2.537
COX2; MT-CO2	3.305	-3.016
GAPDH	1.825	-1.536
ALDOA	2.574	-2.288
PSMA6	2.589	-2.306
RPS6	0.109	0.174
EEF1A1; EEF1A1P5; EEF1A1L14	0.288	-0.008
PPIB	0.206	0.072
HSPA5	1.820	-1.543
SRSF2; SFRS2	0.620	-0.345
RPL26; KRBA2	0.316	-0.042
HNRNPL	2.901	-2.628
KHDRBS1; KHDRBS2	1.042	-0.769
WDR5	1.090	-0.818
PLEC	0.258	0.012
CBFB	0.208	0.061

MAGT1	1.258	-0.991
API5	1.055	-0.788
C9orf142	1.973	-1.709
CORO1A	1.769	-1.508
NUDT21	1.755	-1.494
DDX3X	1.028	-0.768
PRKDC	1.861	-1.603
EEF1D	1.269	-1.011
RPSA	0.841	-0.585
TUBA1B; TUBA4A	3.608	-3.352
VRK1	0.327	-0.073
THYN1	1.389	-1.135
AP1B1	1.752	-1.498
CDC42	0.271	-0.018
ATP5H	1.939	-1.686
NAT10	1.758	-1.505
LGALS3	3.299	-3.047
TMPO	1.035	-0.783
DNAJB1	0.019	0.231
RPL22	1.038	-0.788
YWHAH	2.024	-1.774
CSTA	0.796	-0.546
FEN1	-0.981	1.229
RPL13A	0.273	-0.026
CTSG	-4.019	4.266
DECR1; DECR	1.388	-1.141
LDHB	2.153	-1.908
CDC37	2.969	-2.727
AIM1	1.140	-0.898
THRAP3	1.873	-1.631
RPS3	0.927	-0.688
RBMX	1.613	-1.374
BAZ1B	-1.328	1.566
PDIA5	-0.937	1.172
SRSF9	0.554	-0.319
SAFB	2.604	-2.373
LASP1	4.221	-3.990
ANXA5	3.161	-2.932
CLIC1	2.007	-1.778
RPS16	0.610	-0.382
CCT6A	2.184	-1.958
PC4;SUB1	-0.693	0.918
NAP1L1	0.876	-0.651
SMCHD1	-0.069	0.290

MYBBP1A	1.776	-1.555
LACTB	2.776	-2.557
SRRT	1.833	-1.614
EIF2S3; EIF2S3L	1.196	-0.977
TUBB2C; TUBB4B; TUBB4A	2.919	-2.700
FBL	-0.202	0.419
EHD4	0.495	-0.279
HNRNPM; ORF	2.598	-2.383
FKBP3	0.782	-0.567
MAGOH; MAGOHB	-0.044	0.258
BAF53A; ACTL6A	1.102	-0.887
XPC	1.666	-1.455
EZR; EZR-ROS1	-0.480	0.690
HEXB	2.198	-1.991
RPL12	0.221	-0.014
SRSF6	0.282	-0.075
CSRP1	2.861	-2.658
GDI2	1.501	-1.300
RPS23	0.293	-0.094
NCF2	0.342	-0.146
HNRNPU; HNRPU	2.199	-2.007
N-PAC; GLYR1	0.612	-0.420
PGK1	1.924	-1.735
EHD1	-0.255	0.443
RAB5C	1.737	-1.550
SEPT6	0.216	-0.030
SAP18	-0.663	0.847
CSTF3	2.503	-2.320
CDC40	-0.189	0.372
RPS7	0.929	-0.748
HMGB2	-1.370	1.548
VCP	2.075	-1.897
U2AF1	1.134	-0.956
RPS25	0.648	-0.474
U2AF2	1.253	-1.080
SRP14	-0.060	0.232
MNDA	-0.905	1.076
YWHAE/FAM22B fusion; YWHAE/FAM22A fusion; YWHAE	1.839	-1.668
RAB1A	2.389	-2.220

DKC1	-0.500	0.669
YWHAG	2.122	-1.954
PA2G4	1.829	-1.664
RPL15	-0.325	0.490
RPS2;rps2	0.774	-0.610
WDR76	0.396	-0.234
CSTB	3.683	-3.521
IQGAP2	1.437	-1.277
RPS4X	0.566	-0.407
CTCF	2.144	-1.984
NUP155	0.627	-0.467
GCS1; MOGS	0.652	-0.494
BUB3	1.148	-0.991
DMAP1	1.273	-1.116
HSPA4; HS24/p52	1.721	-1.566
RTCB	1.733	-1.579
VEZF1	-0.200	0.354
CKAP5	2.135	-1.982
ACIN1	0.401	-0.248
RUVBL2	1.424	-1.273
PURA	1.451	-1.302
RPL14	-0.465	0.612
LRRC59	1.521	-1.374
RPL7	-0.288	0.431
SRSF7	-1.018	1.161
IKZF1; ZNFN1A2; IKZF2;IKZF4; IKZF3	-0.748	0.8 90
MSH3	0.043	0.094
GNB2L1	1.278	-1.142
PLBD1	-0.871	1.004
NHP2L1	0.281	-0.149
KPNB1	1.889	-1.758
RFX5	1.774	-1.643
MAZ	-0.085	0.214
TBP; TBPL2	-0.744	0.871
EIF5A; EIF5AL1; EIF5A2	0.421	-0.295
DRAP1	-0.601	0.726
CCT2	2.275	-2.154
SMARCA2	0.744	-0.623
RPS18	0.812	-0.692
PRDX1	3.038	-2.918
RPS3A	0.539	-0.419
CHMP1B	-0.959	1.078

ATP6V1A	3.184	-3.066
KCNAB2	1.497	-1.380
TUFM	1.554	-1.438
EPFP1; HSPE1	1.409	-1.296
GLUD1; GLUD2	1.319	-1.206
NOP56	0.238	-0.125
ARPC4-TTLL3; ARPC4	1.452	-1.340
UBTF	0.390	-0.279
RBMS1	2.102	-1.994
WASF2	1.213	-1.106
CPVL	1.024	-0.917
SRSF1	-0.827	0.927
SMARCE1	0.569	-0.469
DPYSL2	1.623	-1.524
DNM2	1.353	-1.254
SNRP70; SNRNP70	1.126	-1.032
ANP32B	1.058	-0.964
SNRPD2	1.053	-0.961
DDX23	1.555	-1.464
DCD	0.692	-0.602
ELANE; ELA2	-1.602	1.689
EIF2S2	1.240	-1.153
RALY	1.639	-1.554
PPP1CA	1.749	-1.665
SLC25A3	3.171	-3.087
CCT8	2.578	-2.496
CYC1	3.004	-2.923
BCLAF1	3.033	-2.956
RPS12	0.970	-0.895
RPS9	-0.345	0.419
FLNB	3.222	-3.148
RPL30	0.813	-0.739
RBM14	1.317	-1.244
NHP2	-1.009	1.080
MECP2	1.795	-1.727
RPL6	-1.093	1.159
GNB2; GNB4	1.451	-1.387
CFL1	2.473	-2.408
PGAM1; PGAM2	2.234	-2.169
RNH1	1.115	-1.056
HDAC2	1.157	-1.098
TXN	2.511	-2.455
TRA2A	-0.024	0.077

CYCS	0.248	-0.198
CNN2	2.540	-2.494
LTF	-5.083	5.128
G3BP; G3BP1	2.074	-2.029
ARPC1B	1.713	-1.668
GSTP1	1.523	-1.478
SNRPF	0.790	-0.746
MAP1S	1.318	-1.274
HCFC1	0.248	-0.205
HCK; LYN	1.318	-1.275
SFRS3; SRSF3	0.113	-0.071
CREB1; CREM	1.564	-1.523
UQCRB	2.454	-2.414
PURB	2.256	-2.216
MITF	4.171	-4.133
SH3BP1	0.418	-0.380
IRF2	1.721	-1.691
HDAC1	0.721	-0.692
ILF2	2.765	-2.737
RPL35A	0.152	-0.125
PCCB	0.367	-0.340
PHB2	3.517	-3.492
MTDH	1.829	-1.808
XRCC1	3.033	-3.013
TSPO; PBR	2.564	-2.545
LYZ	-3.424	3.443
RPL5	0.422	-0.405
VCL	1.995	-1.978
RAC2; RAC1	1.152	-1.135
RPL11	0.739	-0.724
CROP; LUC7L3	1.528	-1.517
GRK6	-0.500	0.510
HIST1H1D	-4.078	4.088
RPS13	-0.127	0.135
WDR57; SNRNP40	0.860	-0.852
RPL18	-0.618	0.625
GLIPR2	1.031	-1.025
YY1	0.008	-0.003
SRPRB	1.530	-1.528
TPR	0.853	-0.851
ARPC3	1.583	-1.584
RPS19	0.517	-0.518
ASPH	2.205	-2.207
MLEC	1.090	-1.095

ATP6V0D1	2.799	-2.804
S100A11	1.314	-1.326
HNRNPK; HNRPK	2.631	-2.647
L27a; RPL27A	0.975	-0.995
HIST1H3A; HIST2H3A; HIST3H3; H3F3B; H3F3A; HIST2H3PS2	-1.469	1.447
RHOA; ARHA; RHOC	1.480	-1.509
KHSRP	3.912	-3.943
ACTR3	1.565	-1.597
LAMP1	2.642	-2.674
THOC2	2.057	-2.090
COPB1	2.191	-2.227
CCAR1	2.196	-2.234
CBX3	-1.428	1.371
ARHGDIB	1.177	-1.235
DOCK11	-0.404	0.344
TRIM28	1.970	-2.044
TECR	2.380	-2.458
MDH2	1.038	-1.123
LGALS1	0.950	-1.036
RPS17	-0.290	0.204
ATF7	1.420	-1.506
THOC6	1.800	-1.887
LUC7L2	0.227	-0.321
RAD21	0.999	-1.094
ATAD3A; ATAD3B	2.316	-2.420
RPL3	-0.073	-0.032
SNRPA1	1.226	-1.331
TFEB	2.892	-2.999
MDH1	2.511	-2.619
SEC23B	1.065	-1.177
RBM28	0.528	-0.643
TIAL1	3.189	-3.304
TREX1	-0.925	0.809
PIP	1.335	-1.455
FAM129B	1.955	-2.084
SMARCA5	-0.302	0.172
JUNB	1.090	-1.229
RPL27	0.388	-0.527
DBNL	2.167	-2.307
NME2; NME1-NME2; NME2P1	1.888	-2.035

VAPA	2.137	-2.289
PHF5A	0.994	-1.149
GTF2I	2.069	-2.232
SLC25A11	3.753	-3.918
NAGK	1.616	-1.783
LAP3	2.844	-3.017
FH	1.247	-1.430
TPT1	-0.073	-0.113
MAN2B1; MANB	1.320	-1.507
CCT3	1.916	-2.108
RPL24	2.922	-3.115
DRIP4; PDCD6IP	2.113	-2.309
NFIC	1.690	-1.900
RAB11A; RAB11B	1.354	-1.578
CAPG	2.600	-2.831
NNT	2.024	-2.257
RBM25	1.761	-1.995
RPL18A	-0.130	-0.114
SPTBN1	1.191	-1.448
PCBP1	2.161	-2.435
AP2M1	1.434	-1.709
PCBP2; PCBP3	2.254	-2.538
PSAP	2.198	-2.488
PICALM	1.598	-1.891
AHCY	1.972	-2.270
SERPINB2	3.658	-3.962
NOP2	0.839	-1.153
ZNF148; tb protein	2.488	-2.802
DNAJA2	1.040	-1.356
STT3A	1.980	-2.315
IGLC3; IGLC2; IGLC1; IGLC6; IGLL5	-2.178	1.835
EGR2; EGR3	2.040	-2.383
CHD4	0.704	-1.054
CPSF6	1.546	-1.900
ARHGAP10	2.614	-2.998
SPCS2	2.044	-2.432
TMEM113; WDR82	1.062	-1.457
SEPT11	1.139	-1.561
ZFHX1B; ZEB2; ZEB1	0.912	-1.336
SNX2;SNX1	1.554	-1.993
CEBPB	2.710	-3.153

HDLBP	3.703	-4.151
RPS15	0.396	-0.865
SNRPB2	1.421	-1.900
FASN	3.003	-3.493
CSK	0.097	-0.590
MTCH2	2.486	-3.004
SP3	0.850	-1.398
HK3	2.271	-2.826
TWF2	2.495	-3.077
CD14	1.744	-2.336
EIF3S6; EIF3E	3.105	-3.738
MRC1L1; MRC1	2.808	-3.454
FDPS	3.038	-3.695
RPL35	-0.987	0.308
PLIN3	1.899	-2.600
PHB	2.301	-3.012
SIPA1	1.386	-2.099
IMMT	1.576	-2.292
GSTO1	2.378	-3.122
Sp1;SP1	-0.343	-0.406
SDHA	1.372	-2.138
TBL2	2.311	-3.104
ACAT2	3.560	-4.423

ALYREF	0.481	-1.361
EIF3A; eIF3a	1.231	-2.158
KLF13	-0.459	-0.474
LBR	-1.951	1.015
MAFG; MAFK	1.240	-2.203
NDUFS3	1.892	-2.917
ARCN1	0.805	-1.854
TUBB; XTP3TPATP1	1.931	-2.983
NDUFS1	1.290	-2.399
HMGN2	1.769	-2.891
THBS1	-2.392	1.260
SMARCB1	0.095	-1.241
ZYX	2.064	-3.290
CECR1	-0.948	-0.444
PAK2;PAK3	0.655	-2.084
COPG;COPG1	1.223	-2.671
SLC25A1	1.374	-3.082
UGP2	0.300	-2.284
DEFA3; DEFA1	-5.357	3.127

9 Figures

10 Tables

11 Abbreviations

$^1O_2$	Singlet oxygen
2-HG	2-hydroxyglutarate
5'dRP	5'deoxyribose-5-phosphate
53BP1	p53-binding protein 1
5caC	5-carboxylcytosine
5fC	5-formylcytosine
5hmC	5-hydroxymethylcytosine
5mC	5-methylcytosine
8-oxoG	8-oxoguanine
alt-EJ	Alternative end-joining
AP site	Abasic site
AP-1	Activator protein-1
Apaf-1	Apoptotic protease activating factor 1
APC	Allophycocyanin
APC	Antigen-presenting cell
APE1	AP endonuclease 1. APEX1
APLF	Aprataxin and PNK-like factor
APTX	Aprataxin
ART	Artesunate
ATM	Ataxia-telangiectasia mutated
ATR	AT- and Rad3-related
AU	Arbitrary units
AUC	Area under the curve
Bak	Bcl-2 homologous antagonist killer
Bax	Bcl2-associated X protein
Bcl2	B-cell lymphoma 2
BER	Base excision repair
Bid	BH3-interacting death domain agonist
BP	Benzo(a)pyrene
BPDE	Benzo[a]pyrene-7.8-dihydrodiol-9.10-epoxide
BRCT	BRCA1 C-terminus
bzATP	2′(3′)-O-(4-Benzoylbenzoyl) ATP
CAD	Caspase-activated DNase
CCL	Chemokine ligand
CD	Cluster of differentiation
CEBPA	CCAAT/Enhancer binding protein alpha
CFSE	5(6)-carboxyfluorescein diacetate *N*-succinimidyl ester
CGD	Chronic granulomatous disease
ChIP	Chromatin immunoprecipitation
CHK	Checkpoint kinase
CLP	Common lymphoid progenitor
CMP	Common myeloid progenitor
c-NHEJ	Classical non-homologous end-joining
CSF	Colony-stimulating factor
CSF1R	Colony-stimulating factor 1 receptor. MCSFR. CD115
CSF2R	Colony-stimulating factor 2 receptor. GMCSFR. CD116
CSF3R	Colony-stimulating factor 3 receptor. GCSFR. CD114
CTL	Cytotoxic T lymphocytes
CXCL	Chemokine (C-X-C motif) ligand
CXCR4	CXC chemokine receptor 4
DAG	Diacylgycerol
DAMP	Danger-associated molecular pattern
DC	Dendritic cell
DDR	DNA damage response
DMR	Differential methylation region
DMTU	*N.N'*-dimethylthiourea

DNA-PKcs	DNA-dependent protein kinase catalytic subunit
DNMT	DNA-methyltransferase
DPI	Diphenyleneiodonium
DSB	DNA double-strand break
DTT	Dithiothreitol
ECS	Extracellular space
EGF	Epidermal growth factor
ELF1	E74 like ETS transcription factor 1
eNOS	Endothelial NOS
ETC	Electron transport chain
Etheno A	1.N6-ethenoadenine
Etheno C	3.N4-ethenocytosine
FACS	Fluorescence-activated cell sorting
Fapy	2.6-diamino-4-hydroxy-5-formamidopyrimidine
FasL	Fas Ligand
FasR	Fas Receptor. CD95. Apo1
FEN1	Flap endonuclease 1
fMLP	N-formyl-methionyl-leucyl-phenylalanine
FPG	Formamidopyrimidine DNA glycosylase
G-CSF	Granulocyte colony-stimulating factor
GM-CSF	Granulocyte/macrophage colony-stimulating factor
GMP	Granulocyte/macrophage progenitor
GPX	Glutathione peroxidase
GTF2I	General transcription factor II-I
Gy	Gray
HIF1-α	Hypoxia-inducible factor 1α
HIPK2	Homeodomain-interacting protein kinase 2
HOCl	Hypochlorous acid
HR	Homologous recombination
HRP	Horseradish peroxidase
HSC	Haematopoietic stem cell
iDC	Immature dendritic cell
IFN	Interferon
IL	Interleukin
iNOS	Induced NOS
IR	Ionising radiation
iTreg	Induced regulatory T cell
JAK	Janus tyrosine kinase
KAP1	KRAB-associated protein-1
LBP	LPS binding protein
LPS	Lipopolysaccharide
MAPK	Mitogen-activated protein kinase
MAPKK	Mitogen-activated protein kinase kinase. MAP2K
MAPKKK	Mitogen-activated protein kinase kinase kinase. MAP3K
MCP-1	Monocyte chemoattractant protein 1
M-CSF	Macrophage-colony stimulating factor
MHC	Major histocompatibility complex
Mono	Monocyte
MPG	N-methylpurine DNA glycosylase
Mph	Macrophage
MPO	Myeloperoxidase
NAC	N-acetyl cysteine
NAD^+/NADH	Nicotinamide adenine dinucleotide
NADPH	Nicotinamide adenine dinucleotide phosphate
NEIL	Nei Like DNA Glycosylase 1 Endonuclease VIII-like glycosylases 1
NET	Neutrophil extracellular trap
NFκB	Nuclear factor κB
$NO^{\cdot}$	Nitrogen oxide

NOS	NO synthase
NOX	NADPH oxidase
NTH	Endonuclease III
$O_2^{\cdot-}$	Superoxide anion
OGG1	8-Oxoguanine DNA Glycosylase
$OH^{\cdot}$	Hydroxyl radical
$ONOO^{\cdot-}$	Peroxynitrite anion
oxLDL	Oxidised low density lipoprotein
PAMP	Pattern-associated molecular pattern
PAR	Poly(ADP-ribose)
PARG	Poly(ADP-ribose)glycohydrolase
PARP-1	Poly(ADP-ribose)polymerase 1
PBL	Peripheral blood lymphocytes
PBMC	Peripheral blood mononuclear cells
PCNA	Proliferating cell nuclear antigen
PDGF	Platelet-derived growth factor
PI	Propidium iodide
PI3K	Phosphatidylinositol-3-kinase
PICD	Phagocytosis-induced cell death
PIKK	PI3K-related kinase
PKB	Protein kinase B
PKC	Protein kinase C
PMA	Phorbol 12-myristate 13-acetate
PMN	Polymorphonuclear neutrophils
PMSF	Phenylmethane sulfonyl fluoride
PNKP	5'-polynucleotide kinase 3'-phosphatase
Pol	Polymerase
PRR	Pattern recognition receptor
$PrxSS/Prx(SH)_2$	Peroxiredoxin
PS	Phosphatidylserine
RIPK	Receptor-interacting serine/threonine-protein kinase
RNS	Reactive nitrogen species
ROS	Reactive oxygen species
RT	Room temperature
RTK	Receptor tyrosine kinase
SAM	*S*-Adenosyl methionine
SDS-PAGE	Sodium dodecyl sulfate polyacrylamide gel electrophoresis
SOD	Superoxide dismutase
SSB	DNA single-strand break
STAT	Signal transducer and activator of transcription
TAF6	TATA-box binding protein associated factor 6
t-BOOH	*tert*-Butyl hydroperoxide
TCR	T cell receptor
TDG	Thymine DNA glycosylase
TET	Ten-eleven translocation methylcytosine dioxygenase
TFIID	Transcription factor II D
TGF-β	Transforming growth factor β
Th	T helper cell
TLR	Toll-Like Receptor
TMZ	Temozolomide
TNF	Tumour necrosis factor
TRIM28	Tripartite motif containing 28. KAP1
TSS	Transcription start site
VEGF	Vascular endothelial growth factor
XO	Xanthine oxidase
XP	Xeroderma Pigmentosum. Complementation Group
XRCC	X-ray repair complementing defective repair in Chinese hamster cells
γH2AX	γ histone H2A.X

12 Danksagung

13 Erklärung

Hiermit erkläre ich. dass ich die vorliegende Doktorarbeit mit dem Titel:

“The effect of reactive oxygen species on monocytes and macrophages“

selbstständig und ohne fremde Hilfe angefertigt habe. Ich habe dabei nur die in der Arbeit angegebenen Quellen und Hilfsmittel benutzt.

Die in der vorliegenden Arbeit vorgestellten Experimente wurden in der Zeit von Oktober 2013 bis August 2017 am Institut für Toxikologie an der Universitätsmedizin der Johannes Gutenberg-Universität Mainz unter der Betreuung des Institutsdirektors [redacted] durchgeführt.

Teilaspekte der Arbeit wurden bereits veröffentlicht. Die Publikation hierzu ist unter Kapitel 14, Publications aufgelistet.

Mainz, den

(Viviane Ponath)

14 Curriculum Vitae

Conferences

2017: 83rd Annual Meeting of the German Society for Experimental and Clinical Pharmacology and Toxicology (DGPT), Heidelberg. *DNA Repair Deficiency in Human Myeloid Immune Cells*. **oral presentation**

2017: Symposium “DNA damage response. genetic instability and cancer”, Mainz. *DNA repair deficiency in human myeloid immune cells*. **oral presentation → award**

2016: 19th Annual Meeting of the Society for Biological Radiation Research (GBS), Erlangen. *DNA repair deficiency in the myeloid lineage of the human immune system*. **short oral and poster presentation**

2016: 13th Biennial Conference of the German Society for Research on DNA Repair (DGDR), Essen. *Base Excision Repair defective monocytes are killed in trans by activated macrophages and granulocytes*. **oral presentation**

2016: 2nd Retreat of the Research Center for Immunotherapy (FZI) of the Johanes Gutenberg University Mainz, Bad Dürkheim. *Monocytes and neutrophils – DNA repair deficiency in the myeloid lineage*. **oral presentation**

2016: 82nd Annual Meeting of the German Society for Experimental and Clinical Pharmacology and Toxicology (DGPT), Berlin. *Crosstalk between macrophages and monocytes: killing in trans*. **oral presentation**

2015: 1st Retreat of the Research Center for Immunotherapy (FZI) of the Johanes Gutenberg University Mainz, Seeheim-Jugenheim. *BER deficient monocytes are sensitive to ROS produced by macrophages*. **poster presentation**

Publications

Manuscript in preparation: **Ponath V** & Heylmann D. Haak T. Woods K and Kaina B: Severe DNA repair defects in human granulocytes

1. Tomaszowski K-H. Hellmann N. **Ponath V**. Takatsu H. Shin H-W et al. (2017) Uptake of glucose-conjugated MGMT inhibitors in cancer cells. Role of flippases and type IV P-type ATPases. Sci Rep 7 (1): 48.
2. **Ponath V**. Kaina B (2017) Death of Monocytes through Oxidative Burst of Macrophages and Neutrophils. Killing in Trans. PloS one 12 (1): e0170347.
3. Mangerich A. Debiak M. Birtel M. **Ponath V**. Balszuweit F et al. (2016) Sulfur and nitrogen mustards induce characteristic poly(ADP-ribosyl)ation responses in HaCaT keratinocytes with distinctive cellular consequences. Toxicology letters 244: 56–71.
4. Debiak M. Lex K. **Ponath V**. Burckhardt-Boer W. Thiermann H et al. (2016) Immunochemical analysis of poly(ADP-ribosyl)ation in HaCaT keratinocytes induced by the mono-alkylating agent 2-chloroethyl ethyl sulfide (CEES). Impact of experimental conditions. Toxicology letters 244: 72–80.
5. Beneke S. Scherr A-L. **Ponath V**. Popp O. Bürkle A (2010) Enzyme characteristics of recombinant poly(ADP-ribose) polymerases-1 of rat and human origin mirror the correlation between cellular poly(ADP-ribosyl)ation capacity and species-specific life span. Mechanisms of ageing and development 131 (5): 366–369.